Iron-metabolising bacteria as a driving force in weathering of iron-bearing minerals

Dissertation

der Mathematisch-Naturwissenschaftlichen Fakultät

der Eberhard Karls Universität Tübingen

zur Erlangung des Grades eines

Doktors der Naturwissenschaften

(Dr. rer. nat.)

vorgelegt von

M.Sc. Christopher Schwerdhelm

aus Peine

Tübingen

2025

Gedruckt mit Genehmigung der Mathematisch-Naturwissenschaftlichen Fakultät der Eberhard Karls Universität Tübingen.

Tag der mündlichen Qualifikation:	24.09.2025
Dekan:	Prof. Dr. Thilo Stehle
1. Berichterstatter/-in:	Dr. Casey Bryce
2. Berichterstatter/-in:	Prof. Dr. Michaela Dippold

Declaration of Independence

I hereby declare that I have written the submitted thesis on my own. All references and resources used as well as passages that are taken literally or in terms of content from the works of other authors have been marked as such. I have made a detailed distinction between my own work and the contributions of my cooperation partners in the ”Statement of personal contribution” chapter.

Ich erkläre hiermit, dass ich die zur Promotion vorgelegte Arbeit selbstständig verfasst habe. Alle verwendeten Quellen und Hilfsmittel sowie Passagen, die wörtlich oder inhaltlich aus den Werken anderer Autoren entnommen sind, wurden als solche gekennzeichnet. Eine detaillierte Abgrenzung meiner eigenen Leistungen von den Beiträgen meiner Kooperationspartner habe ich im „Statement of personal contribution“ vorgenommen.

“Don’t worry about failure,

you only have to be right once.”

Drew Houston

Acknowledgements

First of all, I want to thank you, Casey, for giving me the opportunity to doing this PhD adventure with you! I am thankful that you gave me your trust and still do! You always had an open ear for me and answered all my questions. It was plenty of them. I enjoyed our shared fieldwork in Chile and trips to Potsdam a lot. May your passion for science ignite the fire for it in many!

Thank you, Andreas, in giving me the opportunity to doing my PhD in your group! I rejoice my time in Tübingen a lot! I have always enjoyed talking about science with you, because there are many things I could learn from you. I value your clear mind and focus on things, which matter. Thanks a lot for showing me the world of iron!

I also would like to thank you Muammar. You stepped in when Casey moved to Bristol and supported me to progress in my PhD. Discussing and formulating thermodynamic calculations was great fun! I also remember our Dungeons and Dragon sessions. Thank you for your time!

My next big thank you goes to you, Lea! When I was new in the group, you were the one, who helped me so much in the laboratory and in getting used to the big world of geomicrobiology. You always had an open ear for me. I will always remember our field trip to Pan de Azúcar.

I have been told by many that there would be times in my PhD, in which it might get rough and the next steps hard. Toby, I want to express you my uttermost respect and thankfulness for helping me in the way you did! Your quality of seeing the potential in people and things is so precious, a true driving force! Thank you for everything!

Next, I would like to thank you, Ferdinand! I value your friendship and unique way of looking at things! No rock is too hard to crack for you! When I started my project I was wondering, who my project partner would be, and can definitely say that it was a great pleasure to spending time with you in the field, laboratory and all other places we have been. Thank you also, Laura, for the amazing time we spent together. Your good vibes and help made some unforgettable memories!

I would also like to thank you, Friedhelm and Todd, who made this PhD project possible in the first place, driven by your curiosity and fascination for geo-bio interactions! Thank you Carolina and Francisco for being valuable colleagues and making this Chilean-German collaboration a great experience! A big thank you also goes to all people involved in the fieldwork, among others Kerstin, Dixie, Axel, Oli, Lars, Ròmulo, Nicole, James, Marie and Caro and many more! Thank you all, dear EarthShape PhD students on the way, especially Lucas, Nestor, Charlotte, Kristina and Trichandi!

Next, I want to thank the whole Geomicrobiology group, especially you, Ellen, Franzi and Lars, for lifting the heavy weights in the lab in Tübingen! Your great experience and help in the laboratory was valuable! I felt like I could always come to you. Thank you Kari, Sarah and Ruchen for helping me with numerous experimental setups, Fe extractions, sampling and ferrozine plates in the lab! I also enjoyed the time of your master thesis a lot, Ruchen! It was a pleasure to co-supervise you and seeing you grow!

I am convinced that one can only do a PhD with great friends and colleagues on the way. Hence, I want to thank you all for the shared time spend in the lab and in private, Timm, Natalia, Michal, Anh, Lea, Hanna, Lars, Nora, Caro, Eva, Ulf, Markus, Benny, Hrvoje, Monique, Verena, Manuel, Yuge, Julian, Martina, Martina, Sören, Marie, Alex, Katrin, Ankita, Constantin and Steffi!

Finally, I want to thank my family and friends for their support! Talking about non-scientific topics let me reset and recharge my battery for the days ahead. Good company and vibes made me pursue my way. I want to thank my friends Hannah and Ole for their inspiration and view! My special thanks go to you, dear Sonja! You have always supported me, no matter how joyful or challenging the PhD time was.

Summary

Microbial rock weathering takes place in Earth´s crust, in which the fourth most abundant element is iron (Fe). Iron occurs during all stages of rock-soil transformation such as primary rock colonisation, rock breakdown, saprolite formation and element cycling. Microorganisms weather rocks and minerals via alteration of pH, metal chelation, breakdown of organic matter and redox reactions and thereby physiochemically alter their surrounding environment. Redox reactions are the key process of biota to gain energy in all major biogeochemical cycles (i.e. those centred around C, Fe, Mn, N, P and S) via electron transfer between a redox couple, consisting of an electron donor and an electron acceptor. Fe-metabolising bacteria are agents of redox reactions, which allow them to adapt and survive in oligotrophic (i.e. nutrient depleted) environments.

Field and laboratory studies are a valuable tool to decipher microbial rock weathering at different special and temporal scales. So far, field studies mainly focused on (a) deep subsurface mineral weathering of granitoid weathering profiles and (b) microbial weathering of Fe-bearing minerals in shallow depths and humid climate. However, there is barely any studies on microbial weathering of Fe-bearing minerals in the deep subsurface of granitoid lithology in arid and semi-arid environments. Moreover, it is also poorly constrained how microbial weathering activity of Fe-metabolising microorganisms in the deep subsurface is linked to different climatic conditions. Even more, due to the lack of microbial weathering studies in the deep subsurface of more arid climates we probably underestimate how quantitatively important and widespread microbial weathering may be. Hence, it is key to understand which factors control microbial weathering activity in the deep subsurface along climate gradients. This thesis addresses these issues by investigating drill core and soil samples from four weathering profiles of felsic plutonic rock along a climate gradient from North to South. The climate gradient ranges from arid (Pan de Azúcar, PdA), to semi-arid (Santa Gracia, SG), Mediterranean (La Campana, LC) and humid (Nahuelbuta, NA) climate zones of the Chilean Coastal Cordillera.

The first part of this dissertation addresses the role of Fe-metabolising bacteria in the weathering of hydrothermally altered, granitoid rock in semi-arid climate. Applying geochemical, mineralogical and cultivation-based methods fractured and hydrothermally altered zones were found to not be hot spots for microbial Fe(III)-reducing activity, but rather hamper microbial activity. To thrive, Fe-metabolising microorganisms require increased concentrations of accessible, bioavailable Fe, independent from the alteration degree. The data indicates that Fe-metabolising microorganisms probably do not contribute to the weathering of Fe(II)-bearing silicate minerals, but reveal their importance for reductive dissolution of secondary Fe(III) (oxyhydr)oxides. The successful cultivation of a robust Fe(III)-

reducing enrichment culture (culture SG) from the deepest weathering zone in 77 m depth, dominated by the spore-forming *Desulfotomaculum ruminis*, underpins this statement. Culture SG is capable of Fe(III) and sulfate reduction using lactate or dihydrogen. Hence, there is the possibility of microbial sulfate reduction-driven weathering of Fe-bearing minerals. However, the low amount of quantified S in this zone suggests a minor role of S in the process.

In the second part of this dissertation, controlling factors of microbial weathering of Fe-bearing minerals along the climate gradient are elucidated. Geochemical and petrophysical data are combined with statistics to identify locations of potential microbial *in situ* weathering of Fe-bearing minerals within the four weathering profiles. The four field sites are characterised by an increase in precipitation from North to South. However, the bedrock of the study sites differs in terms of fracturing and hydrothermal alteration. The two Northern field sites (PdA and SG) are characterised by a high fracture intensity, hydrothermal alteration and high inorganic carbon (IC) concentrations. In contrast, weathering profiles of the two Southern field sites (LC and NA) show a low fracture intensity, absence of hydrothermal alteration and low IC concentrations. We identified an increase in the amount of extractable, adsorbed and crystalline Fe with depth in LC and NA. Furthermore, high Fe(II)/Fe(tot)-ratios were found to positively correlate with low and medium fracture intensity zones. Fractures were identified as locations of more poorly crystalline Fe-bearing minerals compared to unfractured zones in all four sites. Finally, there is less bioavailable organic carbon in fractures compared to unfractured zones in SG, LC and NA, while the opposite is the case for PdA. In short, the highest probability of microbial *in situ* weathering of Fe-bearing minerals is linked to open fractures.

In summary, this work has expanded our knowledge on the role of Fe-metabolising bacteria in weathering of Fe-bearing minerals. It underlines that we are currently underestimating how important and widespread microbial weathering may be. Investigating a hydrothermally altered granitoid weathering profile in semi-arid climate demonstrated that Fe-metabolising microorganisms are rather important for reductive dissolution of secondary Fe(III) (oxyhydr)oxides but probably do not contribute to the weathering of Fe(II)-bearing silicate minerals. Along the climate gradient, open fractures were found to have the highest probability of hosting active Fe-metabolising microorganisms. The complex interplay of minerals, geochemistry, fracturing and hydrothermal alteration and water supply with microbes highlights that more interdisciplinary research is necessary to get an in-depth understand of microbial weathering processes in the deep subsurface.

Zusammenfassung

Mikrobielle Gesteinsverwitterung findet in der Erdkruste statt, in der Eisen (Fe) das am vierthäufigsten vorkommende Element ist. Eisen kommt in allen Stadien der Umwandlung von Gestein in Boden vor, z. B. bei der Besiedlung von Primärgestein, dem Abbau von Gestein, der Saprolitbildung und den Elementkreisläufen. Mikroorganismen verwittern Gestein und Minerale durch Veränderung des pH-Werts, Metallchelatbildung, Abbau von organischem Material und Redoxreaktionen und verändern dadurch physiochemisch ihre Umgebung. Redoxreaktionen sind der Schlüsselprozess der Biota zur Energiegewinnung in allen wichtigen biogeochemischen Kreisläufen (d. h. denjenigen, die sich um C, Fe, Mn, N, P und S drehen) durch Elektronenübertragung zwischen einem Redoxpaar, bestehend aus einem Elektronendonor und einem Elektronenakzeptor. Fe-metabolisierende Bakterien nutzen Redoxreaktionen, um sich an oligotrophe (d. h. nährstoffarme) Umgebungen anzupassen und dort zu überleben.

Feld- und Laborstudien sind ein wertvolles Instrument zur Entschlüsselung der mikrobiellen Gesteinsverwitterung auf verschiedenen räumlichen und zeitlichen Ebenen. Bisher konzentrierten sich Feldstudien hauptsächlich auf (a) die Mineralverwitterung im tiefen Untergrund (von granitoiden Verwitterungsprofilen) und (b) die mikrobielle Verwitterung von Fe-haltigen Mineralen in geringer Tiefe und feuchtem Klima. Es gibt jedoch kaum Studien über die mikrobielle Verwitterung von Fe-haltigen Mineralen im tiefen Untergrund von granitoiden Gesteinen in ariden und semiariden Umgebungen. Darüber hinaus ist nur unzureichend geklärt, wie die mikrobielle Verwitterungsaktivität von Fe-metabolisierenden Mikroorganismen im tiefen Untergrund mit den unterschiedlichen klimatischen Bedingungen zusammenhängt. Mehr noch, aufgrund des Mangels an Studien zur mikrobiellen Verwitterung im tiefen Untergrund ariderer Klimazonen unterschätzen wir wahrscheinlich, wie wichtig und weit verbreitet die mikrobielle Verwitterung quantitativ ist. Daher ist es wichtig zu verstehen, welche Faktoren die mikrobielle Verwitterungsaktivität im tiefen Untergrund entlang von Klimagradienten steuern. Die vorliegende Arbeit befasst sich mit diesen Fragen, indem sie Bohrkerne und Bodenproben von vier Verwitterungsprofilen aus felsischem plutonischem Gestein entlang eines Klimagradienten von Norden nach Süden untersucht. Der Klimagradient reicht von ariden (Pan de Azúcar, PdA) über semiaride (Santa Gracia, SG) und mediterrane (La Campana, LC) bis hin zu feuchten (Nahuelbuta, NA) Klimazonen der chilenischen Küstenkordillere.

Der erste Teil dieser Dissertation befasst sich mit der Rolle Fe-metabolisierender Bakterien bei der Verwitterung von hydrothermal verändertem, granitoiden Gestein in semiaridem Klima. Unter Anwendung geochemischer, mineralogischer und kultivierungsbasierter Methoden wurde festgestellt, dass zerklüftete und hydrothermal veränderte Zonen keine Hot Spots für

mikrobielle Fe(III)-reduzierende Aktivität sind, sondern die mikrobielle Aktivität eher behindern. Um zu wachsen, benötigen Fe-metabolisierende Mikroorganismen höhere Konzentrationen an zugänglichem, bioverfügbarem Fe, unabhängig vom Grad der hydrothermalen Überprägung. Die Daten deuten darauf hin, dass Fe-metabolisierende Mikroorganismen wahrscheinlich nicht zur Verwitterung von Fe(II)-haltigen Silikatmineralen beitragen, sondern ihre Bedeutung in der reduktiven Auflösung von sekundären Fe(III)-(Oxyhydr)oxiden liegt. Die erfolgreiche Kultivierung einer robusten Fe(III)-reduzierenden Anreicherungskultur (Kultur SG) aus der tiefsten Verwitterungszone in 77 m Tiefe, die von dem sporenbildenden Taxon *Desulfotomaculum ruminis* dominiert wird, untermauert diese Aussage. Kultur SG ist in der Lage, Fe(III) und Sulfat unter Verwendung von Laktat oder Wasserstoff zu reduzieren. Daher besteht die Möglichkeit einer durch mikrobielle Sulfatreduktion angetriebenen Verwitterung von Fe-haltigen Mineralen.

Im zweiten Teil dieser Dissertation werden die Einflussfaktoren der mikrobiellen Verwitterung von Fe-haltigen Minerale entlang des Klimagradienten untersucht. Geochemische und petrophysikalische Daten werden mit statistischen Daten kombiniert, um die Orte potenzieller mikrobieller *In situ*-Verwitterung von Fe-haltigen Mineralen innerhalb der vier Verwitterungsprofile zu ermitteln. Die vier Feldstandorte sind durch eine Zunahme der Niederschläge von Norden nach Süden gekennzeichnet. Das Grundgestein der untersuchten Standorte unterscheidet sich jedoch in Bezug auf die Frakturierung und hydrothermale Alteration. Die beiden nördlichen Feldstandorte (PdA und SG) sind durch eine hohe Bruchintensität, hydrothermale Alteration und hohe Konzentrationen anorganischen Kohlenstoffs (IC) gekennzeichnet. Im Gegensatz dazu zeigen die Verwitterungsprofile der beiden südlichen Feldstandorte (LC und NA) eine geringe Bruchintensität, keine hydrothermale Alteration und niedrige IC-Konzentrationen. Wir stellten fest, dass die Menge an extrahierbarem, adsorbiertem und kristallinem Fe mit der Tiefe in LC und NA zunimmt. Außerdem wurde festgestellt, dass hohe Fe(II)/Fe(tot)-Verhältnisse positiv mit Zonen geringer und mittlerer Bruchintensität korrelieren. An allen vier Standorten wurden Brüche als Orte identifiziert, an denen mehr gering kristalline Fe-haltige Minerale im Vergleich zu nicht-frakturierten Zonen vorkommen. Schließlich gibt es in SG, LC und NA weniger bioverfügbaren organischen Kohlenstoff in Frakturen im Vergleich zu nicht geklüfteten Zonen, während in PdA das Gegenteil der Fall ist. Kurz gesagt, die höchste Wahrscheinlichkeit einer mikrobiellen *In situ*-Verwitterung von Fe-haltigen Mineralen ist mit offenen Frakturen verbunden.

Zusammenfassend lässt sich sagen, dass diese Arbeit unser Wissen über die Rolle von Fe-metabolisierenden Bakterien bei der Verwitterung von Fe-haltigen Mineralen erweitert hat. Sie unterstreicht, dass wir derzeit unterschätzen, wie wichtig und weit verbreitet die mikrobielle

Verwitterung sein kann. Die Untersuchung eines hydrothermal veränderten Granitoid-Verwitterungsprofils in semiaridem Klima zeigte, dass Fe-metabolisierende Mikroorganismen eher für die reduktive Auflösung sekundärer Fe(III)-(Oxyhydr)oxide wichtig sind, aber wahrscheinlich nicht zur Verwitterung von Fe(II)-haltigen Silikatmineralen beitragen. Entlang des Klimagradienten wurde festgestellt, dass offene Klüfte die höchste Wahrscheinlichkeit aufweisen, aktive Fe-metabolisierende Mikroorganismen zu beherbergen. Das komplexe Zusammenspiel von Mineralen, Geochemie, Kluftbildung, hydrothermaler Umwandlung und Wasserversorgung mit Mikroben macht deutlich, dass mehr interdisziplinäre Forschung notwendig ist, um ein tieferes Verständnis der mikrobiellen Verwitterungsprozesse im tiefen Untergrund zu erlangen.

Table of Contents

List of Abbreviations

16S rRNA	16S ribosomal ribonucleic acid
AFM	Atomic force microscopy
AIC	Akaike Information Criterion
AICc	Corrected Akaike Information Criterion
alt	Alteration
AOM	Anaerobic oxidation of methane
ASV	Amplicon sequencing variant
ATP	Adenosine triphosphate
Bt	Biotite
C	Carbon
C_{org}	Organic carbon
Ca	Calcium
CBD	Citrate-bicarbonate dithionite
CH_4	Methane
Chl	Chlorite
CO_2	Carbon dioxide
Cu	Copper
CZ	Critical Zone
df	degrees of freedom
DNA	Desoxyribonucleic acid
DOC	Dissolved organic carbon
DSMZ	German Collection of Microorganisms and Cell Cultures GmbH
e^-	Electron
EPS	Exopolymeric substance
Fe	Iron
Fe_3S_4	Greigite
Fe_{bio}	Bioavailable Iron
Fe_{cryst}	Crystalline Iron
FeOx	Iron(II) oxidation
FeRed	Iron(III) reduction
FeS	(Iron(III)-)mackinawite
FeS_2	Pyrite

Fhy	Ferrihydrite
FIA	Flow-injection analyser
GW	Groundwater
H_2	Dihydrogen
H_2S	Dihydrogen sulfide
H_2-SR	Sulfate reduction coupled with dihydrogen oxidation
Hbl	Hornblende
HCl	Hydrochloric acid
Hem	Hematite
Het	Heterotrophy
HPLC	High pressure liquid chromatography
HS-AFM	High-speed atomic force microscopy
IC	Inorganic carbon
K	Potassium
LC	La Campana
LGM	Last Glacial Maximum
LM	Linear model
LMWOA	Low molecular weight organic acid
Mag	Magnetite
MAP	Mean annual precipitation
MAT	Mean annual temperature
Mg	Magnesium
Mkw	Mackinawite
Mn	Manganese
MnO_2	Manganese oxide
MWMM	MW mineral medium
N	Nitrogen
N_2	Nitrogen gas
N/A	Not available
NA	Nahuelbuta
N_2O	Nitrous oxide
NaAc	Sodium acetate
NH_4	Ammonium
NO	Nitric Oxide

NO_2^-	Nitrite
NO_3^-	Nitrate
NPP	Net primary production
NRFeOx	Nitrate-reducing, Fe(II)-oxidising
O_2	Oxygen
O_2^-	Superoxide
OC	Organic carbon
OM	Organic matter
P	Phosphorus
PCR	Polymerase chain reaction
PdA	Pan de Azúcar
pH	pondus hydrogenii (lat.), “weight of hydrogen”
R^2	Coefficient of determination
ROC	Residual organic carbon
ROS	Residual organic sulfur
rpm	Rotations per minute
rxn	Redox reaction
S	Sulfur
S^0	Elemental sulfur
S_x^-	Other intermediate sulfur species
SEM	Scanning electron microscope
SG	Santa Gracia
SI	Supplementary information
Si	Silicium
Sme	Smectite
SO_4^{2-}	Sulfate
SR	Sulfate reduction
SRDTC	Single-run dual temperature combustion
TOC	Total organic carbon
TOC400	Bioavailable organic carbon
vol	Volume
WGS84	World Geodetic System 1984
WIF	Weathering-induced fracturing
XPS	X-ray photoelectron spectroscopy

XRD	X-ray diffraction
ZVI	Zero valent iron

Chapter 1: Introduction

1.1 Microbial weathering of minerals and rocks

Microorganisms are active agents shaping Earth`s surface (Ehrlich, 1996). Microbial activity physiochemically alters their surrounding environment and thus makes essential elements such as carbon, iron, phosphorus and sulfur available for biogeochemical cycles (Falkowski et al., 2008; Samuels et al., 2020). This microbial activity is also known as microbial weathering of minerals and rocks (Ehrlich, 1998). Microbial weathering contributes to biological weathering and comprises activity and growth of both prokaryotes and eukaryotes (Brantley et al., 2012; Ehrlich et al., 2015). It is a key process for microorganisms to adapt and survive in oligotrophic (i.e. nutrient depleted) environments such as caves and the deep biosphere, since it facilitates nutrient access and energy production (autolithotrophy) (Tebo et al., 2015). From a geological perspective, microbial weathering occurs during all stages of rock-soil transformation such as primary rock colonisation, rock breakdown, saprolite formation, and element cycling (Melton et al., 2014; Banwart et al., 2019).

Microorganisms have a variety of mechanisms to weather rocks and minerals at their disposal (Fig. 1). These mechanisms can be divided into four major categories for a better understanding of the microbe-mineral/rock interactions (Uroz et al., 2009; Gadd, 2010). (1) Firstly, microbes can alter the pH surrounding the mineral via release of organic and inorganic acids on a microscopic to bulk-solution scale (Drever and Stillings, 1997; Konhauser, 2009). (2) Secondly, they can use organic acids acting as chelators of (heavy) metals to remove elements from within a mineral matrix or bulk rock (Liermann et al., 2000; Włodarczyk et al., 2015). (3) Thirdly, they can transform or degrade geological organic matter (Petsch et al., 2001; Berlendis et al., 2014). (4) Fourthly, microbes can oxidise and reduce specific elements (Fe, Mn and S) within a mineral via redox reactions resulting in mineral transformations (Barker et al., 1998; Gadd, 2010).

(1) Alteration of pH. Microorganisms dissolve minerals and weather rocks by increasing or decreasing the pH of their surrounding environment. The pH increase is caused by photosynthetic microbes producing carbonate anions leading to enhanced release rates of Ca, K, Mg and Si from rocks (Olsson-Francis et al., 2012). The pH decrease, on the other hand, is created by protons released from inorganic and organic acids (Konhauser, 2009). Organic acids are either actively synthesised (e.g. amino acids) or passively produced as by-products of cellular metabolism when producing organic acids such as citrate or oxalate (e.g. LMWOAs) (Thorley et al., 2015). This proton-promoted dissolution, also known as acidolysis, occurs via

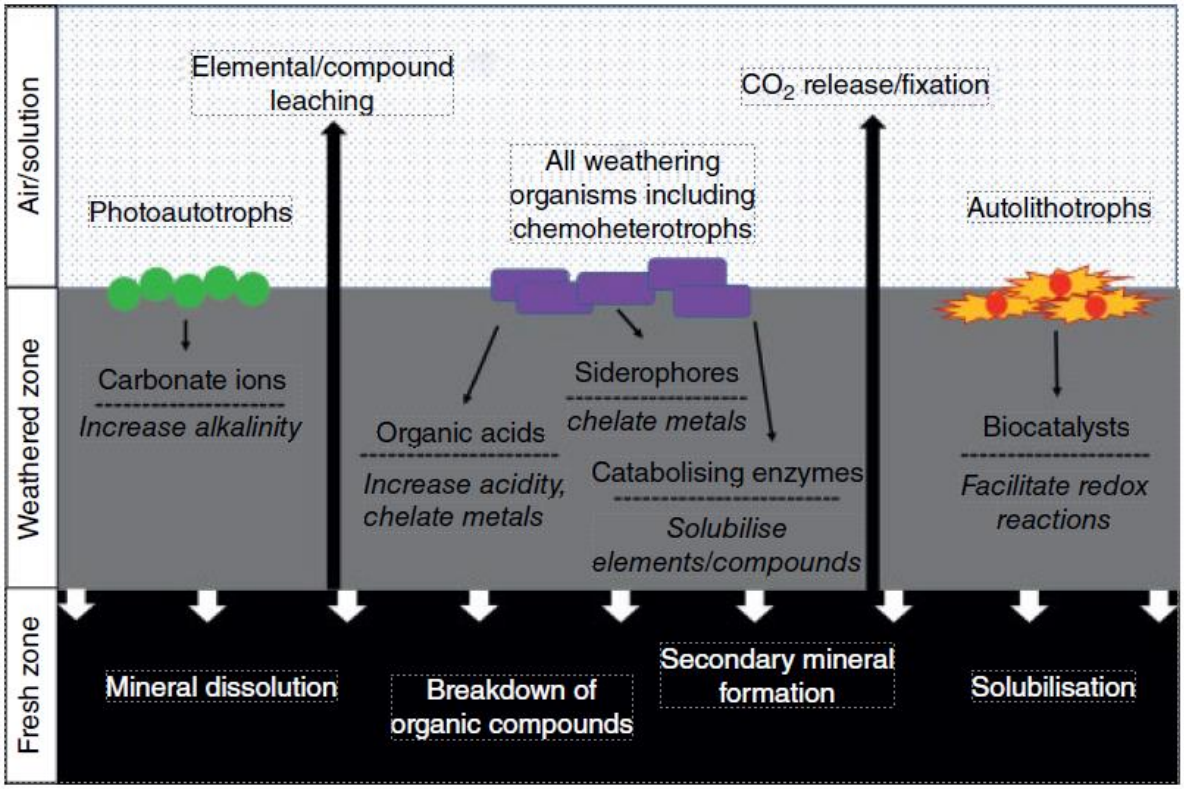

Figure 1.1. Summary of major microbial weathering mechanisms and their impact on geological substrates. The sketch shows three zones, which represent fresh bedrock ("Fresh zone"), the weathering front ("Weathered zone") and the interface between water or air and a substrate ("Air/solution") (from bottom to top). Weathering processes displayed in the Fresh zone are mineral dissolution, breakdown of organic compounds, secondary mineral formation and solubilisation. Above in the weathered zone, microbial weathering mechanisms such as metal chelation and redox reactions are listed. In the interface (uppermost zone), microorganisms facilitating weathering and weathering products are shown. (Figure re-published with permission of the author; Samuels et al. (2020))

two mechanisms. Protons can cleave aluminosilicate (Al-O-Si) and siloxane (Si-O-Si) bonds in silicate minerals, which weakens the mineral structure and promotes dissolution (Gadd, 2010). Alternatively, protons create gaps within aluminosilicate mineral lattices by metal cation displacement (e.g. Al, Fe, K), are subsequentially oxidised and diffuse out of the structure (Bennett, 1991; Bennett et al., 2001). Besides organic acids, there are more sources of biogenically derived acidity such as the (a) release of respiratory CO_2 and subsequent carbonic acid formation (Xiao et al., 2014; Thorley et al., 2015), (b) formation of exopolymeric substances (EPS) (Welch et al., 1999; Hall-Stoodley et al., 2004; Pokrovsky et al., 2009), and (c) release of inorganic acids from redox reactions (Nordstrom and Southam, 1997; Li et al., 2014).

(2) Metal chelation. Organic acids can not only alter the pH (proton-promoted dissolution) but can also function as effective chelators of heavy metals (ligand-promoted dissolution) (Bennett et al., 2001). Chelation is defined as binding and immobilisation of organic acids to heavy metal

cations via complexation leading to potential mineral precipitation (Konhauser, 2009). Microbes utilise the release of organic ligands to obtain metals from minerals and rocks (Ahmed and Holmström, 2014; Bray et al., 2015; Saad et al., 2017). The effectivity of organic ligands depends on the amount of their hydroxyl groups (tridentate > bidentate > monodentate) (Welch and Ullman, 1993). If deprotonated, organic ligands withdraw dissolved metals from solution. This metal withdrawal decreases the amount of freely available cations in solution (i.e. decrease in saturation state), which fosters even more metal release from the mineral. Siderophores are a specific group of organic molecules that have a very high affinity for Fe^{3+}. These molecules are tetra- or hexadentates and their oxygen-bearing moieties directly bind to the complexed metal (Akafia et al., 2014). The release of siderophores by microorganisms is key to make ferric Fe at circumneutral pH bioavailable (Liermann et al., 2000; Kalinowski et al., 2006). On top of that, numerous studies have demonstrated that siderophores enhance dissolution rates of Fe-bearing minerals (Akafia et al., 2014; Bray et al., 2015; X Liu et al., 2015; Saad et al., 2017).

(3) Organic matter breakdown. Microorganisms also transform and degrade organic matter (OM), which can be found in all rock types in different amounts (Wengel et al., 2006; Nichols, 2009; Kulkarni et al., 2022). OM degradation depends on several factors such as environmental conditions, OM composition, and microorganisms participating in the process. Microbial processes involved are among others anaerobic methanogenesis, aerobic oxidative breakdown and enzymatic degradation of recalcitrant OM (Petsch et al., 2001; Meslé et al., 2013; Berlendis et al., 2014).

(4) Redox reactions. Redox reactions are the key process of biota to gain energy in all major biogeochemical cycles (i.e. C, Fe, Mn, N, P and S) via electron transfer between a redox couple consisting of an electron donor and electron acceptor (Hayes and Waldbauer, 2006; Pasek et al., 2014; Keiluweit et al., 2015; Stüeken et al., 2016; Jørgensen et al., 2019; Kappler et al., 2021). By electron transfer between a redox couple the gained energy is utilised to generate adenosine triphosphate (ATP), which is needed by microorganisms to perform their metabolic processes (Shen et al., 2024). Examples of weathering of minerals and rocks via redox reactions are desert rock varnish, carbonate cave wall weathering or pyrite dissolution and subsequent sulfur oxidation (Kuhlman et al., 2006; Carmichael et al., 2013; Jakus et al., 2021a).

1.2 Environmental relevance of iron

Microbial rock weathering takes place in Earth`s crust, in which the fourth most abundant element is iron (Fe) (Taylor, 1964; Kappler et al., 2015). Iron is a very reactive element and has two relevant oxidation states regarding environmental processes and biogeochemical cycling: ferrous Fe (Fe(II)) and ferric Fe (Fe(III)) (Becker et al., 2021). Within Earth`s crust, Fe

occurs in Fe(II) minerals, Fe(III) minerals and mixed Fe(II)/Fe(III) minerals of varying crystallinity and bioavailability (Table 1.1).

Table 1.1. Relevant Fe-bearing minerals that can be found in (hydrothermally altered) granitoid soil and rocks. Table modified from Ehrlich`s Geomicrobiology, Sixth Edition, Chapter 17, Table 17.1 (2015). Added minerals are highlighted in italic.

Fe(II)(-bearing) minerals	Fe(III) minerals	Mixed Fe(II)/Fe(III) minerals
Ferrous sulfide (FeS)	Goethite (α-FeO(OH))	Magnetite (Fe_3O_4)
Pyrite, marcasite (FeS_2)	Akageneite (β-FeO(OH,Cl))	Greigite (Fe_3S_4)
Illite ($(K,H_3O)(Al,Mg,Fe)_2(Si,Al)_4O_{10}[(OH)_2,(H_2O)]$)	Lepidocrocite (γ-FeO(OH))	
Biotite ($KFe_3AlSi_3O_{10}(OH)_2$)	Hematite (α-Fe_2O_3)	
Chlorite ($Fe_5Al_2Si_3O_{10}(OH)_8$)	Maghemite (γ-Fe_2O_3)	
Hornblende ($Fe_7Si_8O_{22}(OH)_2$)	Ferrihydrite ($Fe(OH)_3$)	
	Smectite ($Na_{0.3}Fe^{3+}{}_2Si_3AlO_{10}(OH)_2 \cdot 4(H_2O)$)	

At circumneutral pH (pH 5-8), Fe(II) is quite soluble and hence bioavailable, while Fe(III) is poorly soluble as expressed by the low solubility products of Fe(III) minerals (K_{sp} = 10^{-38}-10^{-42}) (Cornell and Schwertmann, 2003). This contrast of Fe minerals in solubility is reflected in its environmental concentrations of dissolved Fe(II) ranging from high µM to low mM, while concentrations of dissolved Fe(III) are in the low nM range. The solubility of Fe(II), though, is negatively impacted by abiotic Fe(II) oxidation in the presence of oxygen forcing microorganisms to adapt their growth (Emerson, 2012). Likewise, Fe(III)-reducing microorganisms have to adapt to the low solubility of Fe(III) minerals by producing and secreting Fe(III)-complexing ligands and siderophores (see Chapter 1.1) (Ahmed and Holmström, 2014; Akafia et al., 2014). Together, abiotic and biotic (here microbial) oxidation of Fe(II)-bearing minerals and reduction of Fe(III)-bearing minerals in the environment are connected by the Fe cycle (Fig. 1.2).

1.3 Microbial rock weathering studies

Field and laboratory studies are a valuable tool to decipher microbial rock weathering at different spacial and temporal scales as demonstrated by previous weathering studies (Table 1.2). Table 1.2 lists field studies on (deep) subsurface weathering of Fe-bearing minerals and rocks with and without Fe-metabolising microorganisms. As this compilation shows, studies explore microbial rock weathering either on a “whole-environment” scale (Li et al., 2014; Olsson-Francis et al., 2016) or a “reduced-complexity” scale (Matlakowska et al., 2012; Bryce et al., 2016) – a terminology introduced by Samuels et al. (2020). The idea of “whole-environ-

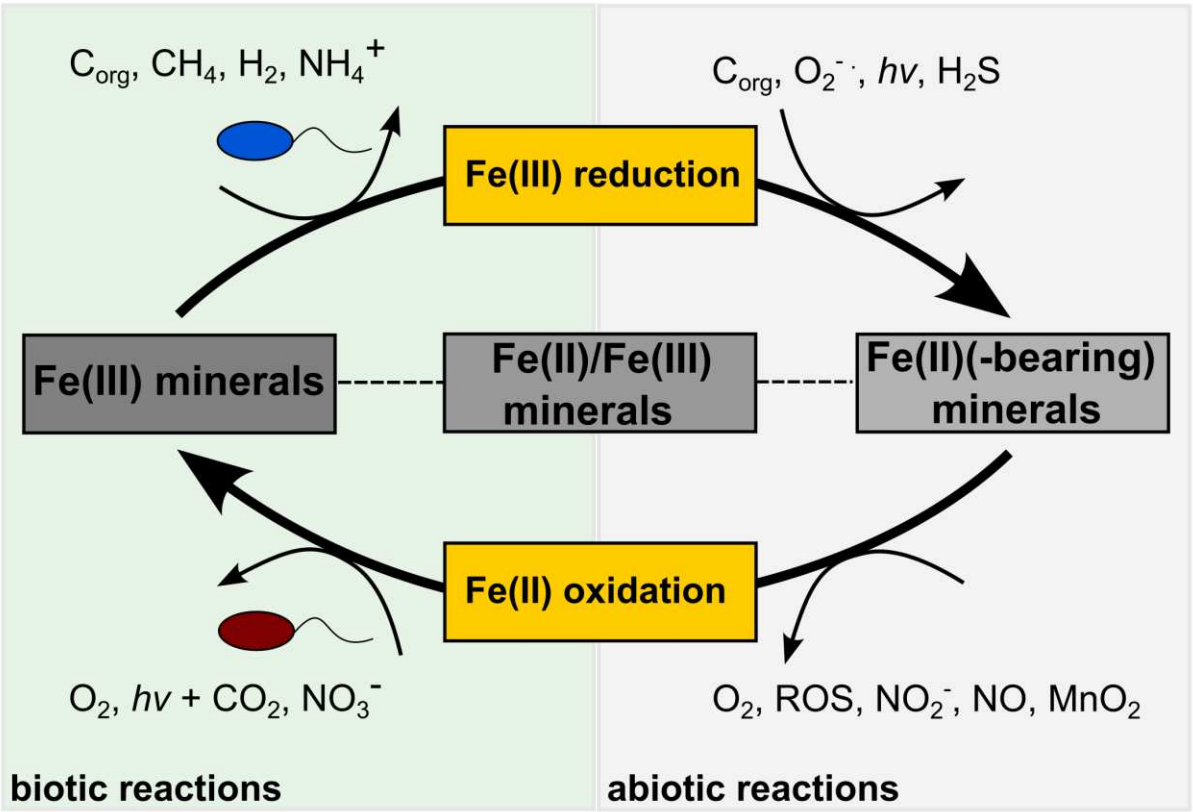

Figure 1.2. Fe cycling in the environment. Under anoxic conditions Fe(III) can be biotically reduced to Fe(II) by microorganisms, if coupled to electron donors such as organic carbon (C_{org}), methane (CH_4), dihydrogen (H_2) or ammonium (NH_4^+) (i.e. electron donors). Abiotic Fe(III) reduction can occur with help of reduced organic carbon (C_{org}), superoxide ($O_2^{-\cdot}$), light (*hv*) while Fe is organically complexed and hydrogen sulfide (H_2S). Under oxic conditions, Fe(II) can be biotically oxidised to Fe(III) by microorganisms, if coupled to electron acceptors such as oxygen (O_2, microaerophiles), light and carbon dioxide (*hv* + CO_2, photoferrotrophs), or nitrate (NO_3^-, nitrate-reducing Fe(II) oxidisers). Abiotic Fe(II) oxidation can happen in the presence of oxygen (O_2), residual organic sulfur (ROS), nitrite (NO_2^-), nitric oxide (NO) and manganese oxide (MnO_2). The Fe cycle overlaps with other biogeochemical cycles relevant for Fe-metabolising microorganisms such as C, Mn, N, P and S cycles.

ment" scale studies is to demonstrate various effects microorganisms have on a specific rock type or weathering profile. However, it can be challenging to proof their *in situ* activity. Studies have approached this challenge by showing the potential of microorganisms to performing weathering activity via involved key genes or enzyme assays (Berlendis et al., 2014; Liermann et al., 2015). Alternatively, "reduced-complexity" studies have the advantage of being experimentally easier to constrain due to less microbe-rock interactions investigated (Uroz and Frey-Klett, 2011; Gerrits et al., 2020). However, their findings` application within the natural environment must be interpretated more cautiously. To this end, studies have focused on microbial weathering in temperate and humid climate conditions.

Table 1.2. Summary of field studies on (deep) subsurface weathering of Fe-bearing minerals and rocks with/without Fe-metabolising microorganisms. Features as fractures, groundwater, hydrothermal alteration and microorganisms involved in the studies are highlighted. Studies are listed in chronological order. Abbreviations used: *N/A = not available, + = presence, - = absence, +* = implication for presence, FeOx = Fe(II) oxidation, FeR = Fe(III) reduction, H_2-SR = sulfate-reduction coupled with H_2 oxidation, AOM = anaerobic oxidation of methane, Het = heterotrophy*.

No.	Field site	Environment	Lithology	Depth (m)	Climate	Fractures	Aquifer	Alteration	Microbes	Reference
1	Mineral Park mine, Kingman, Arizona (USA)	mine, desert	biotite-quartz-monzonite	120	dry, arid	+	+	+	FeOx	(Lehman et al., 2001)
2	Rio Icacos watershed, Luquillo Mountains (Puerto Rico)	watershed, tropical forest	quartz diorite	7.5	humid, tropical	+	-	+	FeOx	(Buss et al., 2005)
3	Gold mine, Ventersgroup Supergroup metabasalt (SA)	saline fracture water	metabasalt	2800	subtropical, semi-arid	+	+	+	H_2-SR	(Lin et al., 2006; Chivian et al., 2008)
4	Simpewarp area, Swedish East Coast (SWE)	drill cores	granite, quartz monzodiorite	900 - 1000	temperate	+	+	+	-	(Drake et al., 2008)
5	Damma Glacier Forefield, Central Swiss Alps (SUI)	glacier forefield	granite	< 1	polar	N/A	-	-	Het	(Frey et al., 2010)
6	South Ice Cave, Oregon Cascades (USA)	lava tube	basalt	a few	polar	N/A	-	-	FeOx	(Popa et al., 2012)
7	Shovelers Sink, Madison, Wisconsin (USA)	wetland soil	illite, smectite	1.5	humid	-	+	-	FeOx, FeR	(E Shelobolina et al., 2012)
8	Outokumpu Deep Drill Hole (FIN)	groundwater, fracture zones	gneiss, schist, granite	2500	cold, subarctic	+	+	+	H_2-SR	(Purkamo et al., 2013; 2016)
9	Sanford Underground Research Facility (USA)	former gold mine	basalt, metasediment	1500	semiarid	+	N/A	+	FeOx, FeR, SR	(Osburn et al., 2014; 2019; Casar et al., 2020; 2021b)
10	Laxemar site (SWE)	drill core, biofilm	granite	740	temperate	+	+	+	H_2-SR, AOM	(Drake et al., 2017)
11	North Yorkshire coastline (UK)	cliff surface	pyrite-bearing shale	< 1	humid	-	-	N/A	FeOx, Het	(Samuels et al., 2019)
12	Guaba Ridge, Luquillo Mountains (Puerto Rico)	ridge, tropical forest	quartz diorite	8	wet, tropical	+	-	+	FeOx	(Napieralski et al., 2019; Napieralski and Roden, 2020)
13	Lysina catchment, Slavkov Forest CZO (CZE)	drill core	leucogranite	30	cold, humid	+	+	+	-	(Hayes et al., 2020)
14	Guidel, Ploemeur CZO (FR)	fractured rock aquifer	granite, micaschist	130	mild, temperate	+	+	-	FeOx	(Bethencourt et al., 2020; Bochet et al., 2020)
15	Ammer catchment, Altingen (GER)	artesian well	pyrite-bearing limestone	29-35	mild, temperate	+	+	-	FeOx, Het	(Jakus et al., 2021a; 2021b)
16	Santa Gracia, La Serena (CL)	drill cores	quartz monzodiorite	87.2	semi-arid	+	N/A	+	-	(Krone et al., 2021b; Hampl et al., 2022)
17	Susquehanna Shale Hills CZO (USA)	fractured subsurface shale	organic poor grey shale	30	temperate	+	+	N/A	FeOx	(Napieralski et al., 2022)
18	Kermadoye and Guidel, Ploemeur CZO (FR)	fractured rock aquifer	granite, micaschist	50-150	mild, temperate	+	+	-	-	(Osorio-Leon et al., 2023)
19	Pan de Azúcar, Santa Gracia, La Campana, Nahuelbuta (CL)	drill cores	granitoid	41-94	arid - temperate	+/+/ +/+	+*/+*/ -/+*	+/+/ -/-	FeOx, FeR	this study; (Schwerdhelm et al., 2025)

1.4 Research objectives and hypotheses

There is a fine collection of field studies investigating (a) deep subsurface mineral weathering of Fe-bearing weathering profiles (in granitoid lithology) and (b) microbial weathering of Fe-bearing minerals in shallow depths and humid climate (Table 1.2). However, there is barely any study on microbial weathering of Fe-bearing minerals in the deep subsurface of granitoid lithology in arid and semi-arid environments, in which the availability of water and energy sources for microbial metabolisms is limited. Additionally, it is also poorly constrained how microbial weathering activity in the deep subsurface varies in different climate zones. Hence, the aim of this study was to:

- Investigate the suitability of Fe-bearing minerals for microbial metabolism in the deep subsurface of granitoid lithology in semi-arid climate, i.e. in a water- and nutrient deprived system (**Chapter 2**).

- Identify mineralogical and geochemical conditions in the deep subsurface of a semi-arid climate, in which Fe-metabolising microorganisms would thrive (**Chapter 2**).

- Elucidate the role and impact of Fe-metabolising bacteria in weathering of Fe-bearing minerals in a semi-arid climate by assessing their presence, activity and identity (**Chapter 2**).

- Identify controlling factors of microbial deep subsurface weathering of Fe-bearing minerals along a climate gradient (**Chapter 3**).

- Evaluate the relative importance of controlling factors for microbial deep subsurface weathering of Fe-bearing minerals along a climate gradient (**Chapter 3**).

1.5 The Deep EarthShape study sites

The aim of the present thesis is to elucidate the effect of climate on subsurface weathering processes by investigating the impact of Fe-metabolising microorganisms on subsurface weathering of Fe-bearing minerals and rocks. “EarthShape - Earth`s surface shaping by Biota” is a German-Chilean priority programme funded by the German Research Foundation (DFG-SPP 1803) and offers ideal conditions to approach the aims of this dissertation. The goal of the programme is to investigate the role of biota, i.e. animals, fungi, plants and microorganisms, in shaping the Earth`s surface in short (days - months) to geological (Ma) time scales. “Deep EarthShape” is a subproject and aimed at deciphering subsurface (< 100m) weathering processes by combining mineralogical, geochemical, geophysical and

geomicrobiological techniques. To do so, four granitoid weathering profiles along the Chilean Coastal Cordillera were investigated (Fig. 1.3).

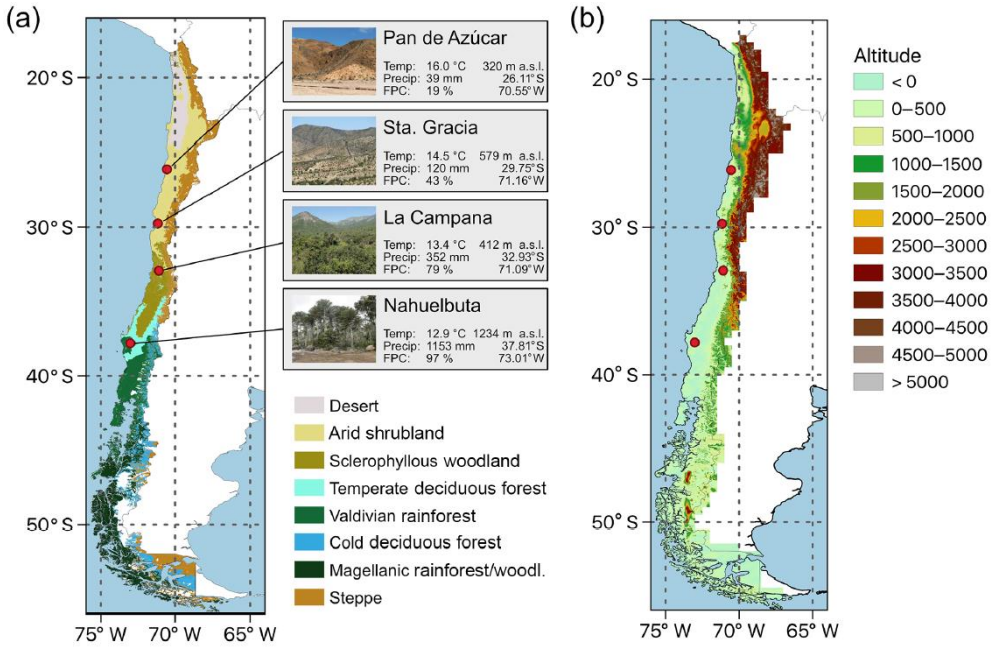

Figure 1.3. Deep EarthShape study sites. Drill cores have been retrieved from the four field sites Pan de Azúcar (PdA), Santa Gracia (SG), La Campana (LC) and Nahuelbuta (NA). The figure shows (a) a map of the vegetation zones in Chile with climate data and (b) a map of the altitude zonation within Chile. (Figure reproduced from Werner et al. (2018))

The four field sites span an extreme climate gradient from arid climate in the North to humid climate in the South between 26° and 38° S, which is caused by the Humboldt Current and Pacific High-pressure Zone (Garreaud et al., 2009). The climate gradient (from North to South) includes an increase in mean annual precipitation (MAP) (PdA: 39 mm, SG: 120 mm, LC: 352 mm, NA: 1153 mm) and vegetation cover, and a decrease in mean annual temperature (MAT) (PdA: 16.0 °C, SG: 14.5 °C, LC: 13.4 °C, NA: 12.9 °C) (Übernickel et al., 2020). These four locations are suitable study sites to answer the research questions of this thesis as they are characterised by (a) a similar rock type (felsic plutonic rock) (Oeser et al., 2018), (b) the absence of glaciation during the Last Glacial Maximum (LGM) (Hulton et al., 2002) and (c) the absence of volcanic influence. Until now, there has been a plethora of studies conducted on studying subsurface weathering processes using the four study sites (Krone et al., 2021b, 2024; Hampl et al., 2022, 2023; Scheibe and Spohn, 2022; Trichandi et al., 2022, 2023, 2024; Scheibe et al., 2023).

1.6 References

Ahmed E. and Holmström S.J. (2014) Siderophores in environmental research: roles and applications. *Microbial biotechnology* **7**(3)**,** 196-208.

Akafia M.M., Harrington J.M., Bargar J.R. and Duckworth O.W. (2014) Metal oxyhydroxide dissolution as promoted by structurally diverse siderophores and oxalate. *Geochimica et Cosmochimica Acta* **141,** 258-269.

Banwart S.A., Nikolaidis N.P., Zhu Y.-G., Peacock C.L. and Sparks D.L. (2019) Soil Functions: Connecting Earth's Critical Zone. *Annual Review of Earth and Planetary Sciences* **47,** 333-359.

Barker W., Welch S., Chu S. and Banfield J. (1998) Experimental observations of the effects of bacteria on aluminosilicate weathering. *American Mineralogist* **83**(11)**,** 1551-1563.

Becker S., Enright A.M.L. and Kappler A. (2021) Living on Iron. In *Metals, Microbes, and Minerals-The Biogeochemical Side of Life.* De Gruyter, 185-228.

Bennett P.C. (1991) Quartz dissolution in organic-rich aqueous systems. *Geochimica et Cosmochimica Acta* **55**(7)**,** 1781-1797.

Bennett P.C., Rogers J., Choi W. and Hiebert F. (2001) Silicates, silicate weathering, and microbial ecology. *Geomicrobiology Journal* **18**(1)**,** 3-19.

Berlendis S., Beyssac O., Derenne S., Benzerara K., Anquetil C., Guillaumet M., Estève I. and Capelle B. (2014) Comparative mineralogy, organic geochemistry and microbial diversity of the Autun black shale and Graissessac coal (France). *International journal of coal geology* **132,** 147-157.

Bethencourt L., Bochet O., Farasin J., Aquilina L., Borgne T.L., Quaiser A., Biget M., Michon-Coudouel S., Labasque T. and Dufresne A. (2020) Genome reconstruction reveals distinct assemblages of Gallionellaceae in surface and subsurface redox transition zones. *FEMS Microbiology Ecology*. https://doi.org/10.1093/femsec/fiaa036.

Bochet O., Bethencourt L., Dufresne A., Farasin J., Pédrot M., Labasque T., Chatton E., Lavenant N., Petton C., Abbott B.W., Aquilina L. and Le Borgne T. (2020) Iron-oxidizer hotspots formed by intermittent oxic–anoxic fluid mixing in fractured rocks. *Nature Geoscience*. https://doi.org/10.1038/s41561-019-0509-1.

Brantley S.L., Lebedeva M. and Hausrath E.M. (2012) A geobiological view of weathering and erosion. *Fundamentals of geobiology***,** 205-227.

Bray A.W., Oelkers E.H., Bonneville S., Wolff-Boenisch D., Potts N.J., Fones G. and Benning L.G. (2015) The effect of pH, grain size, and organic ligands on biotite weathering rates. *Geochimica et Cosmochimica Acta* **164,** 127-145.

Bryce C.C., Le Bihan T., Martin S.F., Harrison J.P., Bush T., Spears B., Moore A., Leys N., Byloos B. and Cockell C.S. (2016) Rock geochemistry induces stress and starvation responses in the bacterial proteome. *Environmental microbiology* **18**(4)**,** 1110-1121.

Buss H., Bruns M., Schultz M., Moore J., Mathur C. and Brantley S. (2005) The coupling of biological iron cycling and mineral weathering during saprolite formation, Luquillo Mountains, Puerto Rico. *Geobiology* **3**(4)**,** 247-260.

Carmichael M.J., Carmichael S.K., Santelli C.M., Strom A. and Bräuer S.L. (2013) Mn (II)-oxidizing bacteria are abundant and environmentally relevant members of ferromanganese deposits in caves of the upper Tennessee River Basin. *Geomicrobiology Journal* **30**(9)**,** 779-800.

Casar C.P., Kruger B.R., Flynn T.M., Masterson A.L., Momper L.M. and Osburn M.R. (2020) Mineral-hosted biofilm communities in the continental deep subsurface, Deep Mine Microbial Observatory, SD, USA. *Geobiology* **18**(4)**,** 508-522. https://doi.org/https://doi.org/10.1111/gbi.12391.

Casar C.P., Momper L.M., Kruger B.R. and Osburn M.R. (2021b) Iron-Fueled Life in the Continental Subsurface: Deep Mine Microbial Observatory, South Dakota, USA. *Appl Environ Microbiol* **87**(20)**,** e0083221. https://doi.org/10.1128/aem.00832-21.

Cavicchioli R., Ripple W.J., Timmis K.N., Azam F., Bakken L.R., Baylis M., Behrenfeld M.J., Boetius A., Boyd P.W. and Classen A.T. (2019) Scientists' warning to humanity: microorganisms and climate change. *Nature Reviews Microbiology* **17**(9)**,** 569-586.

Chivian D., Brodie E.L., Alm E.J., Culley D.E., Dehal P.S., DeSantis T.Z., Gihring T.M., Lapidus A., Lin L.-H., Lowry S.R., Moser D.P., Richardson P.M., Southam G., Wanger G., Pratt L.M., Andersen G.L., Hazen T.C., Brockman F.J., Arkin A.P. and Onstott T.C. (2008) Environmental Genomics Reveals a Single-Species Ecosystem Deep Within Earth. *Science* **322**(5899)**,** 275-278. https://doi.org/doi:10.1126/science.1155495.

Cornell R.M. and Schwertmann U. (2003) *The iron oxides: structure, properties, reactions, occurrences, and uses*. Wiley-vch Verlag GmbH & Co. KGaA.

Drake H., Ivarsson M., Bengtson S., Heim C., Siljeström S., Whitehouse M.J., Broman C., Belivanova V. and Åström M.E. (2017) Anaerobic consortia of fungi and sulfate reducing bacteria in deep granite fractures. *Nature Communications* **8**(1)**,** 55. https://doi.org/10.1038/s41467-017-00094-6.

Drake H., Tullborg E.-L. and Annersten H. (2008) Red-staining of the wall rock and its influence on the reducing capacity around water conducting fractures. *Applied Geochemistry* **23**(7)**,** 1898-1920. https://doi.org/https://doi.org/10.1016/j.apgeochem.2008.02.017.

Drever J. and Stillings L. (1997) The role of organic acids in mineral weathering. *Colloids and Surfaces A: physicochemical and engineering aspects* **120**(1-3)**,** 167-181.

Ehrlich H.L. (1996) How microbes influence mineral growth and dissolution. *Chemical Geology* **132**(1-4)**,** 5-9.

Ehrlich H.L. (1998) Geomicrobiology: its significance for geology. *Earth-Science Reviews* **45**(1-2)**,** 45-60.

Ehrlich H.L., Newman D.K. and Kappler A. (2015) *Ehrlich's Geomicrobiology*, 6th Edition edn.: CRC Press.

Emerson D. (2012) Biogeochemistry and microbiology of microaerobic Fe (II) oxidation. In.: Portland Press Ltd.

Falkowski P.G., Fenchel T. and Delong E.F. (2008) The microbial engines that drive Earth's biogeochemical cycles. *Science* **320**(5879)**,** 1034-1039.

Frey B., Rieder S.R., Brunner I., Plötze M., Koetzsch S., Lapanje A., Brandl H. and Furrer G. (2010) Weathering-associated bacteria from the Damma glacier forefield: physiological capabilities and impact on granite dissolution. *Applied and Environmental Microbiology* **76**(14)**,** 4788-4796.

Gadd G.M. (2010) Metals, minerals and microbes: geomicrobiology and bioremediation. *Microbiology* **156**(3)**,** 609-643.

Garreaud R.D., Vuille M., Compagnucci R. and Marengo J. (2009) Present-day south american climate. *Palaeogeography, Palaeoclimatology, Palaeoecology* **281**(3-4)**,** 180-195.

Gerrits R., Pokharel R., Breitenbach R., Radnik J., Feldmann I., Schuessler J., Von Blanckenburg F., Gorbushina A. and Schott J. (2020) How the rock-inhabiting fungus K. petricola A95 enhances olivine dissolution through attachment. *Geochimica et Cosmochimica Acta* **282,** 76-97.

Hall-Stoodley L., Costerton J.W. and Stoodley P. (2004) Bacterial biofilms: from the natural environment to infectious diseases. *Nature Reviews Microbiology* **2**(2)**,** 95-108.

Hampl F.J., Schiperski F., Byrne J.M., Schwerdhelm C., Kappler A., Bryce C., von Blanckenburg F. and Neumann T. (2022) The role of iron-bearing minerals for the deep weathering of a hydrothermally altered plutonic rock in semi-arid climate (Chilean Coastal Cordillera). *Chemical Geology* **604,** 120922. https://doi.org/https://doi.org/10.1016/j.chemgeo.2022.120922.

Hampl F.J., Schiperski F., Schwerdhelm C., Stroncik N., Bryce C., von Blanckenburg F. and Neumann T. (2023) Feedbacks between the formation of secondary minerals and the infiltration of fluids into the regolith of granitic rocks in different climatic zones (Chilean Coastal Cordillera). *Earth Surf. Dynam.* **11**(3)**,** 511-528. https://doi.org/10.5194/esurf-11-511-2023.

Hayes J.M. and Waldbauer J.R. (2006) The carbon cycle and associated redox processes through time. *Philosophical Transactions of the Royal Society B: Biological Sciences* **361**(1470)**,** 931-950.

Hayes N.R., Buss H.L., Moore O.W., Krám P. and Pancost R.D. (2020) Controls on granitic weathering fronts in contrasting climates. *Chemical Geology* **535,** 119450. https://doi.org/https://doi.org/10.1016/j.chemgeo.2019.119450.

Hulton N.R., Purves R., McCulloch R., Sugden D.E. and Bentley M.J. (2002) The last glacial maximum and deglaciation in southern South America. *Quaternary Science Reviews* **21**(1-3)**,** 233-241.

Jakus N., Blackwell N., Osenbrück K., Straub D., Byrne J.M., Wang Z., Glöckler D., Elsner M., Lueders T., Grathwohl P., Kleindienst S. and Kappler A. (2021a) Nitrate Removal by a Novel Lithoautotrophic Nitrate-Reducing, Iron(II)-Oxidizing Culture Enriched from a Pyrite-Rich Limestone Aquifer. *Applied and Environmental Microbiology* **87**(16)**,** e00460-00421. https://doi.org/doi:10.1128/AEM.00460-21.

Jakus N., Blackwell N., Straub D., Kappler A. and Kleindienst S. (2021b) Presence of Fe(II) and nitrate shapes aquifer-originating communities leading to an autotrophic enrichment dominated by an Fe(II)-oxidizing Gallionellaceae sp. *FEMS Microbiology Ecology* **97**(11). https://doi.org/10.1093/femsec/fiab145.

Jørgensen B.B., Findlay A.J. and Pellerin A. (2019) The Biogeochemical Sulfur Cycle of Marine Sediments. *Frontiers in Microbiology* **10**. https://doi.org/10.3389/fmicb.2019.00849.

Kalinowski B.E., Johnsson A., Arlinger J., Pedersen K., Ödegaard-Jensen A. and Edberg F. (2006) Microbial mobilization of uranium from shale mine waste. *Geomicrobiology Journal* **23**(3-4)**,** 157-164.

Kappler A., Bryce C., Mansor M., Lueder U., Byrne J.M. and Swanner E.D. (2021) An evolving view on biogeochemical cycling of iron. *Nature Reviews Microbiology* **19**(6)**,** 360-374.

Kappler A., Emerson D., Gralnick J.A., Roden E.E. and Muehe E.M. (2015) Geomicrobiology of iron. *Ehrlich's geomicrobiology* **6,** 635.

Keiluweit M., Nico P., Harmon M.E., Mao J., Pett-Ridge J. and Kleber M. (2015) Long-term litter decomposition controlled by manganese redox cycling. *Proceedings of the National Academy of Sciences* **112**(38)**,** E5253-E5260.

Konhauser K.O. (2009) *Introduction to geomicrobiology*. John Wiley & Sons.

Krone L.V., Hampl F.J., Schwerdhelm C., Bryce C., Ganzert L., Kitte A., Übernickel K., Dielforder A., Aldaz S., Oses-Pedraza R., Perez J.P.H., Sanchez-Alfaro P., Wagner D., Weckmann U. and von Blanckenburg F. (2021b) Deep weathering in the semi-arid Coastal Cordillera, Chile. *Scientific Reports* **11**(1)**,** 13057. https://doi.org/10.1038/s41598-021-90267-7.

Krone L.V., Wittmann H. and von Blanckenburg F. (2024) Precipitation Control on Weathering Intensity and Depositional Flux of Meteoric 10Be Revealed From Soil Profiles Along a Climate Gradient (Chile). *Geophysical Research Letters* **51**(15)**,** e2024GL108825. https://doi.org/https://doi.org/10.1029/2024GL108825.

Kuhlman K., Fusco W., La Duc M., Allenbach L., Ball C., Kuhlman G., Anderson R., Erickson I., Stuecker T. and Benardini J. (2006) Diversity of microorganisms within rock varnish in the Whipple Mountains, California. *Applied and Environmental Microbiology* **72**(2)**,** 1708-1715.

Kulkarni H.V., Ford J., Blank J.G., Park M. and Datta S. (2022) Geochemical interactions among water, minerals, microbes, and organic matter in formation of speleothems in volcanic (lava tube) caves. *Chemical Geology* **594,** 120759.

Lehman R.M., Roberto F.F., Earley D., Bruhn D.F., Brink S.E., O'Connell S.P., Delwiche M.E. and Colwell F.S. (2001) Attached and unattached bacterial communities in a 120-meter corehole in an acidic, crystalline rock aquifer. *Applied and Environmental Microbiology* **67**(5)**,** 2095-2106.

Li J., Sun W., Wang S., Sun Z., Lin S. and Peng X. (2014) Bacteria diversity, distribution and insight into their role in S and F e biogeochemical cycling during black shale weathering. *Environmental microbiology* **16**(11)**,** 3533-3547.

Liermann L.J., Albert I., Buss H.L., Minyard M. and Brantley S.L. (2015) Relating microbial community structure and geochemistry in deep regolith developed on volcaniclastic rock in the Luquillo Mountains, Puerto Rico. *Geomicrobiology Journal* **32**(6)**,** 494-510.

Liermann L.J., Kalinowski B.E., Brantley S.L. and Ferry J.G. (2000) Role of bacterial siderophores in dissolution of hornblende. *Geochimica et Cosmochimica Acta* **64**(4)**,** 587-602.

Lin L.-H., Wang P.-L., Rumble D., Lippmann-Pipke J., Boice E., Pratt L.M., Lollar B.S., Brodie E.L., Hazen T.C., Andersen G.L., DeSantis T.Z., Moser D.P., Kershaw D. and Onstott T.C. (2006) Long-Term Sustainability of a High-Energy, Low-Diversity Crustal Biome. *Science* **314**(5798)**,** 479-482. https://doi.org/doi:10.1126/science.1127376.

Liu X., Yang G.-M., Guan D.-X., Ghosh P. and Ma L.Q. (2015) Catecholate-siderophore produced by As-resistant bacterium effectively dissolved FeAsO4 and promoted Pteris vittata growth. *Environmental Pollution* **206,** 376-381.

Matlakowska R., Skłodowska A. and Nejbert K. (2012) Bioweathering of Kupferschiefer black shale (Fore-Sudetic Monocline, SW Poland) by indigenous bacteria: implication for dissolution and precipitation of minerals in deep underground mine. *FEMS Microbiology Ecology* **81**(1)**,** 99-110.

Melton E.D., Swanner E.D., Behrens S., Schmidt C. and Kappler A. (2014) The interplay of microbially mediated and abiotic reactions in the biogeochemical Fe cycle. *Nature Reviews Microbiology* **12**(12)**,** 797.

Meslé M., Dromart G. and Oger P. (2013) Microbial methanogenesis in subsurface oil and coal. *Research in Microbiology* **164**(9)**,** 959-972.

Napieralski S.A., Buss H.L., Brantley S.L., Lee S., Xu H. and Roden E.E. (2019) Microbial chemolithotrophy mediates oxidative weathering of granitic bedrock. *Proceedings of the National Academy of Sciences* **116**(52)**,** 26394-26401.

Napieralski S.A., Fang Y., Marcon V., Forsythe B., Brantley S.L., Xu H. and Roden E.E. (2022) Microbial chemolithotrophic oxidation of pyrite in a subsurface shale weathering environment: Geologic considerations and potential mechanisms. *Geobiology* **20**(2)**,** 271-291.

Napieralski S.A. and Roden E.E. (2020) The weathering microbiome of an outcropping granodiorite. *Frontiers in Microbiology* **11,** 601907.

Nichols G. (2009) *Sedimentology and stratigraphy*. John Wiley & Sons.

Nordstrom D.K. and Southam G. (1997) Geomicrobiology of sulfide mineral oxidation. *Reviews in mineralogy* **35,** 361-390.

Oeser R.A., Stroncik N., Moskwa L.-M., Bernhard N., Schaller M., Canessa R., van den Brink L., Köster M., Brucker E. and Stock S. (2018) Chemistry and microbiology of the Critical Zone along a steep climate and vegetation gradient in the Chilean Coastal Cordillera. *Catena* **170,** 183-203.

Olsson-Francis K., Pearson V.K., Schofield P.F., Oliver A. and Summers S. (2016) A study of the microbial community at the interface between granite bedrock and soil using a culture-independent and culture-dependent approach. *Advances in Microbiology* **6**(3)**,** 233-245.

Olsson-Francis K., Simpson A., Wolff-Boenisch D. and Cockell C. (2012) The effect of rock composition on cyanobacterial weathering of crystalline basalt and rhyolite. *Geobiology* **10**(5)**,** 434-444.

Osburn M.R., Kruger B., Masterson A.L., Casar C.P. and Amend J.P. (2019) Establishment of the Deep Mine Microbial Observatory (DeMMO), South Dakota, USA, a Geochemically Stable Portal Into the Deep Subsurface. *Frontiers in Earth Science* **7**. https://doi.org/10.3389/feart.2019.00196.

Osburn M.R., LaRowe D.E., Momper L.M. and Amend J.P. (2014) Chemolithotrophy in the continental deep subsurface: Sanford Underground Research Facility (SURF), USA. *Frontiers in Microbiology* **5**(610). https://doi.org/10.3389/fmicb.2014.00610.

Osorio-Leon I., Bouchez C., Chatton E., Lavenant N., Longuevergne L. and Le Borgne T. (2023) Hydrological and geological controls for the depth distribution of dissolved oxygen and iron in silicate catchments. *Water Resources Research* **59**(8)**,** e2023WR034986.

Pasek M.A., Sampson J.M. and Atlas Z. (2014) Redox chemistry in the phosphorus biogeochemical cycle. *Proceedings of the National Academy of Sciences* **111**(43)**,** 15468-15473.

Petsch S., Eglinton T. and Edwards K. (2001) 14C-dead living biomass: evidence for microbial assimilation of ancient organic carbon during shale weathering. *Science* **292**(5519)**,** 1127-1131.

Pokrovsky O., Shirokova L., Bénézeth P., Schott J. and Golubev S. (2009) Effect of organic ligands and heterotrophic bacteria on wollastonite dissolution kinetics. *American Journal of Science* **309**(8)**,** 731-772.

Popa R., Smith A.R., Popa R., Boone J. and Fisk M. (2012) Olivine-respiring bacteria isolated from the rock-ice interface in a lava-tube cave, a Mars analog environment. *Astrobiology* **12**(1)**,** 9-18.

Purkamo L., Bomberg M., Kietäväinen R., Salavirta H., Nyyssönen M., Nuppunen-Puputti M., Ahonen L., Kukkonen I. and Itävaara M. (2016) Microbial co-occurrence patterns in deep Precambrian bedrock fracture fluids. *Biogeosciences* **13**(10)**,** 3091-3108.

Purkamo L., Bomberg M., Nyyssönen M., Kukkonen I., Ahonen L., Kietäväinen R. and Itävaara M. (2013) Dissecting the deep biosphere: retrieving authentic microbial communities from packer-isolated deep crystalline bedrock fracture zones. *FEMS Microbiology Ecology* **85**(2)**,** 324-337.

Saad E.M., Sun J., Chen S., Borkiewicz O.J., Zhu M., Duckworth O.W. and Tang Y. (2017) Siderophore and organic acid promoted dissolution and transformation of Cr (III)-Fe (III)-(oxy) hydroxides. *Environmental science & technology* **51**(6)**,** 3223-3232.

Samuels T., Bryce C., Landenmark H., Marie-Loudon C., Nicholson N., Stevens A.H. and Cockell C. (2020) Microbial weathering of minerals and rocks in natural environments. In *Biogeochemical cycles: Ecological drivers and environmental impact.* 59-79.

Samuels T., Pybus D., Wilkinson M. and Cockell C.S. (2019) pH Influences the Distribution of Microbial Rock-Weathering Phenotypes in Weathered Shale Environments. *Geomicrobiology Journal* **36**(8)**,** 752-763. https://doi.org/10.1080/01490451.2019.1620381.

Scheibe A., Sierra C.A. and Spohn M. (2023) Recently fixed carbon fuels microbial activity several meters below the soil surface. *Biogeosciences* **20**(4)**,** 827-838. https://doi.org/10.5194/bg-20-827-2023.

Scheibe A. and Spohn M. (2022) N2 fixation per unit microbial biomass increases with aridity. *Soil Biology and Biochemistry* **172,** 108733.

Schwerdhelm C., Hampl F.J., Krone L.V., Sauter L., Kaphegyi K., Horstmann L., Straub D., Samuels T., Mansor M., Merino C., Matus F., v. Blanckenburg F., Wagner D., Neumann T., Kappler A. and Bryce C. (2025) Microbial weathering of iron-bearing minerals in deep hydrothermally altered granitic rock of a semi-arid environment (Chilean Coastal Cordillera). *Geo-Bio Interfaces* **2,** e8. https://doi.org/10.1180/gbi.2025.2.

Shelobolina E., Konishi H., Xu H., Benzine J., Xiong M.Y., Wu T., Blöthe M. and Roden E. (2012) Isolation of Phyllosilicate–Iron Redox Cycling Microorganisms from an Illite–Smectite Rich Hydromorphic Soil. *Frontiers in Microbiology* **3**. https://doi.org/10.3389/fmicb.2012.00134.

Shen Y., Dinh H.V., Cruz E.R., Chen Z., Bartman C.R., Xiao T., Call C.M., Ryseck R.-P., Pratas J. and Weilandt D. (2024) Mitochondrial ATP generation is more proteome efficient than glycolysis. *Nature chemical biology***,** 1-10.

Stüeken E.E., Kipp M.A., Koehler M.C. and Buick R. (2016) The evolution of Earth's biogeochemical nitrogen cycle. *Earth-Science Reviews* **160,** 220-239.

Taylor S. (1964) Abundance of chemical elements in the continental crust: a new table. *Geochimica et Cosmochimica Acta* **28**(8)**,** 1273-1285.

Tebo B.M., Davis R.E., Anitori R.P., Connell L.B., Schiffman P. and Staudigel H. (2015) Microbial communities in dark oligotrophic volcanic ice cave ecosystems of Mt. Erebus, Antarctica. *Frontiers in Microbiology* **6,** 179.

Thorley R.M., Taylor L.L., Banwart S.A., Leake J.R. and Beerling D.J. (2015) The role of forest trees and their mycorrhizal fungi in carbonate rock weathering and its significance for global carbon cycling. *Plant, cell & environment* **38**(9)**,** 1947-1961.

Trichandi R., Bauer K., Ryberg T., Heit B., Araya Vargas J., von Blanckenburg F. and Krawczyk C.M. (2024) 3D shear wave velocity imaging of the subsurface structure of

granite rocks in the arid climate of Pan de Azúcar, Chile, revealed by Bayesian inversion of HVSR curves. *Earth Surf. Dynam.* **12**(3)**,** 747-763. https://doi.org/10.5194/esurf-12-747-2024.

Trichandi R., Bauer K., Ryberg T., Scherler D., Bataille K. and Krawczyk C.M. (2022) Combined seismic and borehole investigation of the deep granite weathering structure—Santa Gracia Reserve case in Chile. *Earth Surface Processes and Landforms* **n/a**(n/a). https://doi.org/https://doi.org/10.1002/esp.5457.

Trichandi R., Bauer K., Ryberg T., Wawerzinek B., Araya Vargas J., von Blanckenburg F. and Krawczyk C.M. (2023) Shear-wave velocity imaging of weathered granite in La Campana (Chile) from Bayesian inversion of micro-tremor H/V spectral ratios. *Journal of Applied Geophysics* **217,** 105191. https://doi.org/https://doi.org/10.1016/j.jappgeo.2023.105191.

Uroz S., Calvaruso C., Turpault M.-P. and Frey-Klett P. (2009) Mineral weathering by bacteria: ecology, actors and mechanisms. *Trends in microbiology* **17**(8)**,** 378-387.

Uroz S. and Frey-Klett P. (2011) Linking diversity to function: highlight on the mineral weathering bacteria. *Open Life Sciences* **6**(5)**,** 817-820.

Welch S., Barker W. and Banfield J. (1999) Microbial extracellular polysaccharides and plagioclase dissolution. *Geochimica et Cosmochimica Acta* **63**(9)**,** 1405-1419.

Welch S.A. and Ullman W.J. (1993) The effect of organic acids on plagioclase dissolution rates and stoichiometry. *Geochimica et Cosmochimica Acta* **57**(12)**,** 2725-2736.

Wengel M., Kothe E., Schmidt C.M., Heide K. and Gleixner G. (2006) Degradation of organic matter from black shales and charcoal by the wood-rotting fungus Schizophyllum commune and release of DOC and heavy metals in the aqueous phase. *Science of The Total Environment* **367**(1)**,** 383-393.

Werner C., Schmid M., Ehlers T.A., Fuentes-Espoz J.P., Steinkamp J., Forrest M., Liakka J., Maldonado A. and Hickler T. (2018) Effect of changing vegetation and precipitation on denudation – Part 1: Predicted vegetation composition and cover over the last 21 thousand years along the Coastal Cordillera of Chile. *Earth Surf. Dynam.* **6**(4)**,** 829-858. https://doi.org/10.5194/esurf-6-829-2018.

Włodarczyk A., Stasiuk R., Skłodowska A. and Matlakowska R. (2015) Extracellular compounds produced by bacterial consortium promoting elements mobilization from polymetallic Kupferschiefer black shale (Fore-Sudetic Monocline, Poland). *Chemosphere* **122,** 273-279.

Xiao L., Hao J., Wang W., Lian B., Shang G., Yang Y., Liu C. and Wang S. (2014) The up-regulation of carbonic anhydrase genes of Bacillus mucilaginosus under soluble Ca2+ deficiency and the heterologously expressed enzyme promotes calcite dissolution. *Geomicrobiology Journal* **31**(7)**,** 632-641.

Chapter 2: Microbial weathering of iron-bearing minerals in deep hydrothermally altered granitic rock of a semi-arid environment (Chilean Coastal Cordillera)

C. Schwerdhelm[a], *F. J. Hampl*[b], *L. V. Krone*[c], *L. Sauter*[a], *K. Kaphegyi*[a], *L. Horstmann*[d], *D. Straub*[e], *T. Samuels*[a], *M. Mansor*[a], *C. Merino*[f,g], *F. Matus*[g,h], *F. v. Blanckenburg*[c], *D. Wagner*[d,i], *T. Neumann*[j], *A. Kappler*[a,k], *C. Bryce*[l,*]

[a] Geomicrobiology, Department of Geosciences, University of Tuebingen, Schnarrenbergstrasse 94-96, 72076 Tuebingen, Germany

[b] Department of Applied Geochemistry, Technische Universität Berlin, Ernst-Reuter-Platz 1, 10587 Berlin, Germany; now: Chair of Resource Mineralogy, Montanuniversität Leoben, Peter-Tunner-Straße 5, 8700 Leoben, Austria

[c] Institute of Geological Sciences, Freie Universität Berlin, Malteserstrasse 74-100, 12249 Berlin, Germany

[d] GFZ German Research Centre for Geosciences, Section Geomicrobiology, 14473 Potsdam, Germany

[e] Quantitative Biology Center (QBiC), University of Tuebingen, 72076 Tuebingen, Germany

[f] Center of Plant, Soil Interaction and Natural Resources Biotechnology Scientific and Technological Bioresource Nucleus (BIOREN), Temuco, Chile

[g] Network for Extreme Environmental Research (NEXER), Universidad de la Frontera, Temuco, Chile

[h] Laboratory of Conservation and Dynamics of Volcanic Soils, Department of Chemical Sciences and Natural Resources, Universidad de La Frontera, Temuco, Chile

[i] University of Potsdam, Institute of Geosciences, Karl-Liebknecht-Str. 24-25, 14476 Potsdam, Germany

[j] Department of Applied Geochemistry, Technische Universität Berlin, Ernst-Reuter-Platz 1, 10587 Berlin, Germany

[k] Cluster of Excellence: EXC 2124: Controlling Microbes to Fight Infection, Tübingen, Germany

[l] School of Earth Sciences, University of Bristol, Wills Memorial Building, Queens Road, Bristol BS15N 1RJ, United Kingdom

*To whom correspondence should be sent:

Dr. Casey Bryce

Published in Geo-Bio Interfaces

Schwerdhelm, C., Hampl, F. J., Krone, L. V., Sauter, L., Kaphegyi, K., Horstmann, L., … Bryce, C. (2025). Microbial weathering of iron-bearing minerals in deep hydrothermally altered granitic rock of a semi-arid environment (Chilean Coastal Cordillera). Geo-Bio Interfaces, 2, e8. https://doi.org/10.1180/gbi.2025.2

2.1 Abstract

Microbial mineral weathering has been predominantly investigated at shallow depths in humid and tropical environments. Much less is understood about its role in the deeper subsurface of arid and semi-arid environments where microbial weathering is limited by the availability of water and energy sources for microbial metabolism. However, the deep subsurface in these climate zones may host a microbial community that thrives on weathering of iron (Fe)-bearing minerals, that serve as electron donor or acceptor.

To investigate the role of microorganisms in weathering of Fe-bearing minerals in a dry climate, we recovered a >80 m deep weathering profile in a semi-arid region of the Chilean Coastal Cordillera. The bedrock is rich in Fe-bearing minerals (hornblende, biotite, chlorite, magnetite, and hematite) but lacks detectable organic carbon. We evaluated the bioavailability of Fe(III)-bearing minerals that may serve as an electron acceptor for Fe(III)-reducing microorganisms. Using geochemical, mineralogical and cultivation-based methods, we found enhanced Fe bioavailability and more *in vitro* microbial Fe(III) reduction at increased depth. We obtained an Fe(III)-reducing enrichment culture from the deepest weathered rock found at 77 m depth. This enrichment culture is capable of reducing ferrihydrite (up to 0.6 mM d^{-1}) using lactate or dihydrogen as an electron donor and grows at circumneutral pH. The main organism in the enrichment culture is the spore-forming *Desulfotomaculum ruminis* (abundance of 98.5%) as revealed by 16S rRNA gene amplicon sequencing.

Our findings provide evidence for a microbial contribution to the weathering of Fe-bearing minerals in semi-arid environments. While microorganisms are probably not contributing to the weathering of Fe(II)-bearing silicate minerals, they are most likely of importance regarding reductive dissolution of secondary weathering products. The Fe(III) reduction quantified in this weathering profile by the *in situ* microbial community suggests that microorganisms are active weathering agents in semi-arid climates.

Keywords

Critical Zone, deep weathering, hydrothermal alteration, semi-arid, Fe-metabolising bacteria, Fe(II) oxidation, Fe(III) reduction, sulfate reduction

2.2 Introduction

Microbes are active agents in mineral weathering and contribute to the transformation of hard rock to soil in the Critical Zone (CZ) (Ehrlich, 1998; Riebe et al., 2017; Holbrook et al., 2019; Krone et al., 2021b; Hampl et al., 2022). The CZ is defined as Earth's near surface environment, which regulates life by the interplay of biological, chemical, physical and geological processes (Brantley et al., 2007). Microbial weathering occurs during all stages of rock-soil transformation from primary rock colonization to rock breakdown, and saprolite formation, whereby it also contributes to elemental cycling in the regolith (Banwart et al., 2019; Samuels et al., 2020). Most studies on microbial weathering focus on shallow and humid tropical soils and saprolites, or on transects across corestones (Buss et al., 2008; Minyard et al., 2012; Barcellos et al., 2018; Gu et al., 2020b). However, much less is understood about the role of microorganisms in weathering processes occurring in the deep (10s to 100s of metres) CZ especially in (semi-)arid climates where rocks are less intensely weathered (Moser et al., 2003; Fredrickson and Balkwill, 2006; Onstott et al., 2019; Bochet et al., 2020; Takamiya et al., 2021). Furthermore, unlike sedimentary rocks, granitic rocks are a particularly challenging environment for microbial growth, as after solidification of hot magma the rocks formed contain neither organic carbon nor cells. Even more, due to the lack of microbial weathering studies in the deep subsurface and more arid climates it is possible that we are currently underestimating how quantitatively important and widespread microbial weathering may be.

In such environments fracturing of rocks is the first process that may enable conditions to form microbial habitats (Pedersen, 1997). Tectonic activity creates fractures on different spatial scales (µm to km) that serve as pathways for meteoric water infiltration into the subsurface (Mitchell and Faulkner, 2009). The availability of water throughout all stages of rock-soil transformation is key, as water acts as a transport medium for gases such as dissolved O_2 and CO_2 that alter or dissolve soluble minerals, transport organic carbon from the surface to the subsurface and regulates bacterial activity (Brantley et al., 2017). Bacterial activity is not only regulated by the availability of water but also by the presence of elements essential for life (e.g., C, N, P, S) and elements functioning as electron sources and electron acceptors for microbial metabolisms, such as Fe and S of various oxidation states (Napieralski et al., 2019; Gu et al., 2020b; Napieralski et al., 2022).

In dry climatic settings, the supply of meteoric water and thus the O_2, CO_2 and nutrients that are contained in it is limited. Moreover, the available O_2 is readily consumed by abiotic oxidation of Fe(II)-bearing silicates in the upper zone of weathering profiles (White and Yee, 1985; Perez et al., 2005). This weathering process transforms Fe(II)-bearing silicates into secondary phases such as Fe(III) (oxyhydr)oxides and clay minerals. The ensuing volume

expansion caused by this transformation generates weathering-induced fractures (Isherwood and Street, 1976; Buss et al., 2005; Bazilevskaya et al., 2015; Kim et al., 2017; Hampl et al., 2022).

The aim of this study was to investigate the role of Fe-metabolising bacteria in the promotion of weathering in a water- and nutrient-deprived system. We investigated an 87.2 m deep weathering profile in granitoid (quartz monzodiorite) rock in a semi-arid region of the Chilean Coastal Cordillera (Santa Gracia (SG)). More specifically, we (1) identified the presence of Fe(II)-oxidising and Fe(III)-reducing microbes via microbial enrichments, (2) identified the mineralogical and geochemical conditions in which they thrive via Fe extractions and thermodynamic calculations, (3) explored whether they actively induce major weathering by fostering alteration of solids (i.e. via demonstrating active Fe(III) reduction by the *in situ* community), and (4) investigated the *in situ* microbial community composition in the deepest weathering zone via 16S rRNA sequencing. Weathering profile-specific thermodynamic calculations of Gibbs free energy and energy density for chemolithotrophic and organoheterotrophic microbial redox reactions provide constraints for the most favourable metabolic processes (i.e. electron sources) in this deep, arid system.

2.3 Materials and methods

2.3.1 Study site

The study was conducted in a semi-arid climate zone of the Coastal Cordillera in Chile, ca. 18 km northeast of La Serena (Coquimbo) within the Santa Gracia National Reserve. The bedrock of the drilling location (-29.759414°N, -71.160322°E [WGS84]) is a quartz monzodiorite containing biotite ($KFe_3AlSi_3O_{10}(OH)_2$), chlorite ($Fe_5Al_2Si_3O_{10}(OH)_8$), hornblende ($Fe_7Si_8O_{22}(OH)_2$), magnetite (Fe_3O_4) and hematite (Fe_2O_3) (see Table 2.1) (Krone et al., 2021b). The bedrock is part of granitic to dioritic intrusions of the early Cretaceous (144-124 Ma), fractured by the Atacama Fault Zone and hydrothermally overprinted (Cembrano et al., 2005; Hampl et al., 2022; Trichandi et al., 2022). The study area is characterised by gently dipping hillslopes, mean annual precipitation of <100 mm yr^{-1}, mean annual temperature of 16°C, and a sparse vegetation coverage of 30-40%, dominated by shrubs and cacti (Ministerio de Obras Públicas de Chile, 2016; Bernhard et al., 2018; Oeser et al., 2018; Oeser and von Blanckenburg, 2020; Übernickel et al., 2020). This semi-arid study site was intensively investigated by geochemical, geophysical and mineralogical methods (Weckmann et al., 2020; Krone et al., 2021b; Hampl et al., 2022; Trichandi et al., 2022) and thus serves as an ideal model site to study microbial contributions to weathering of Fe-bearing minerals from a terrestrial hydrothermally overprinted setting under water- and nutrient-limiting conditions. There are indications of a possible water table in about 68-70 m depth in the form of poor core recovery, a low amplitude zone (acoustic televiewer) and enhanced porosity (up to 9.5%) (Krone et al., 2021b; Hampl et al., 2022), but this is not conclusive evidence due to the lack of *in situ* fluid data. In this study, the term “weathering” in the context of microbial activity includes both the chemical breakdown of primary minerals and the turnover of secondary mineral products, which have been generated by previous hydrothermal events or meteoric weathering.

2.3.2 Drilling procedure and sample preparation

The weathering profile comprises 87.2 m of drilled core, i.e. soil, saprolite and rock. The uppermost 2 m are additionally recovered by a manually sampled soil pit adjacent to the drill hole. Drill core material was obtained by wireline diamond drilling, using a PQ3-sized crown and potable water as drill fluid (including contamination control) (Friese et al., 2017; Krone et al., 2021b). After retrieving the drill cores (up to 1.5 m length), bulk core sample intervals with a length of ca. 20 cm were aseptically taken using a hammer, a chisel and an angle grinder in the field. Afterwards, the samples were anoxically stored at 4°C. For microbial cultivation, the samples were aseptically split with a rock trimmer and separated into an outer and an inner part in the laboratory. The outer part was further milled to a grain size of <10 µm with a planetary ball mill (used for selective Fe extractions in this study) while the inner part was

processed with a disk mill to obtain a grain size of <2 mm (used for all geomicrobiological investigations in this study; i.e. microbial enrichments, ferrihydrite reduction experiments and microbial community sequencing). Samples for geochemical and mineralogical analyses were further ground to a grain size of <63 µm, and an aliquot of both the outer and inner part was taken for contamination control (Hampl et al., 2021; Krone et al., 2021a). Strict contamination control protocols were applied to all samples which included the use of a tracer in the drill fluid, strict sample handling conditions and the retrieval of inner core samples that had not been in contact with the drill casing, the core liners or the drill fluid (Krone et al., 2021b). Additionally, fracture covers/fillings of five drill core samples were removed with corundum drill bits to examine their mineralogy in hydrothermally altered zones.

2.3.3 Selective extractions

Selective Fe extractions using hydrochloric acid (0.5 M HCl) and citrate-bicarbonate dithionite (CBD) were performed on samples of the entire weathering profile to quantify Fe pools available for microbial Fe redox reactions (N = 59, technical extraction triplicates). After extraction, Fe(II) and total Fe (Fe(tot)) were spectrophotometrically quantified using the ferrozine assay (Hegler et al., 2008). Furthermore, water soluble organic carbon and nitrate were extracted to quantify the potentially available amount of these compounds as electron donors and acceptors for microbial Fe(II) oxidation and Fe(III) reduction. Reported dissolved organic carbon and nitrate values were blank corrected. Details of the extractions were as follows:

0.5 M HCl. 0.5 M HCl is considered to extract bioavailable Fe-bearing phases such as ferrihydrite, lepidocrocite, siderite and partly magnetite, maghemite, hematite, goethite, biotite and chlorite via dissolution by protonation (Sidhu et al., 1981; Raiswell et al., 1994; Voelz et al., 2019). We extracted the bioavailable Fe with 0.5 M HCl at room temperature under anoxic conditions in the dark for 24 h, while shaking at 10 rpm (solid:liquid = 1:60) (Roden and Zachara, 1996).

Citrate bicarbonate dithionite. CBD targets reactive Fe minerals such as ferrihydrite, lepidocrocite, akageneite, goethite and hematite via reductive dissolution (Voelz et al., 2019). Extractions were conducted using a solution of 0.27 M trisodium citrate, 0.11 M sodium bicarbonate, and 0.1 M sodium dithionite (Lalonde et al., 2012). Samples were extracted in the dark under oxic conditions for 15 min, and in a water bath at 75-80°C (solid:liquid = 1:60). The pH of the CBD solution was circumneutral to obtain maximum reduction potential and to avoid precipitation of sulfides.

Water extractions. 10 mL MilliQ water was added to 0.25 g crushed rock to target water extractable organic carbon and nitrate. The extract was analysed with a multi N/C 2100S elemental analyser for organic carbon concentrations (Analytik Jena GmbH, Germany) via

combustion (detection limit = 0.022 mg C g^{-1} rock). Nitrate in the extracts was analysed with a Flow-injection analyser (FIA) using an AA3 HR AutoAnalyser System (Seal Analytical, Germany) (detection limit = 0.0002 mg N g^{-1} rock). Extractions were performed under oxic conditions at room temperature in the dark, for 24 h on a shaker (shaking frequency f = 180 s^{-1}) (solid:liquid = 1:40).

pH. Potential and active pH of drill core samples were measured as follows: 2 g of milled drill core samples or air-dried soil (<63 µm) were weighed into 15 mL Falcon tubes and either 10 mL of 0.01 M $CaCl_2$ (potential pH) or 10 mL MilliQ water (active pH) were added. Falcon tubes were shaken, and the slurries left untouched for 1 h. Thereafter, Falcon tubes were shaken again and the pH was measured in the supernatant. The procedure was repeated after 24 h to exclude a major shift in pH (*N* = 10, technical extraction triplicates).

2.3.4 Thermodynamic calculations

Based on Fe-bearing silicates and Fe minerals identified in the SG weathering profile (Krone et al., 2021b; Hampl et al., 2022) we calculated the Gibbs energy yields for 38 potential *in situ* chemolithotrophic and organoheterotrophic microbial redox reactions to identify potentially favourable metabolisms (cf. Kappler et al., 2021). Energetic yields are controlled by various factors such as mineral species, electron donor, electron acceptor, temperature, pH, and solute ion concentrations. Oxygen and nitrate served as electron acceptors for microbial Fe(II) oxidation reactions, while dihydrogen or organic carbon (acetate or lactate) served as electron donor for Fe(III) reduction (Table 2.1) (see Kappler et al., 2021). Calculations were performed using fixed dissolved ion and gas concentrations, with pH ranging from 6 to 9 based on *in situ* pH values of powdered drill core samples. We compared these Gibbs energy yields with energy density yields (molar vs. volumetric Gibbs energy) (Fig. 2.S1), as the latter scales Gibbs energy calculations by the limiting reactant and has been shown to be a more accurate measure for biomass abundance (Kallmeyer and Wagner, 2014; Osburn et al., 2014). Gibbs energy yields were calculated by using Eq. 1.

$$\Delta G_r = \Delta G_r^0 + RT \ln Q_r \quad (1)$$

where ΔG_r represents the Gibbs energy of a reaction, R and T represent the gas constant and temperature (in K), respectively, and Q_r represents the activity product. The activity product Q_r can be evaluated from Eq. 2.

$$Q_r = \prod a_i^{v_i} \quad (2)$$

where a_i represents the activity of species i and v_i its stoichiometric reaction coefficient.

Thermodynamic calculations are based on geochemical and mineralogical data of the drill core investigated in this study as well as previous studies (Hampl et al., 2021; Krone et al., 2021a). Due to the aridity, the sampling depths, and the wireline drilling procedure, it was not possible to collect *in situ* fluid data. Hence, we also estimated the Gibbs free energy assuming an *in*

Table 2.1. Metabolic reactions with minerals investigated in this study. The redox reactions (# 1-38) represent 14 oxidation and 24 reduction reactions for major Fe minerals identified in the Santa Gracia drill core profile (see Krone et al., 2021b; Hampl et al., 2022). Oxygen or nitrate serve as electron acceptors for microbial Fe(II) oxidation, while dihydrogen or organic carbon (acetate and lactate) serve as electron donors for microbial Fe(III) reduction. The amount of electrons (e^-) transferred per redox reaction (rxn) is listed on the right.

No.	Mineral	Reaction	e^-/rxn ( )
Fe(II) oxidation with oxygen as electron acceptor			
1	Magnetite	$4Fe_3O_4 + 6H_2O + O_2 \leftrightarrow 12FeOOH$	4
2	Biotite *1	$0.1KFe_3AlSi_3O_{10}(OH)_2 + 3.01Mg^{2+} + 0.755Al^{3+} + 2.845H_4SiO_4 + 0.05875O_2 \leftrightarrow 1(Mg_{3.01}Fe^{2+}_{0.065}Fe^{3+}_{0.235})(Si_{3.145}Al_{0.855})O_{10}(OH)_2 + 0.1K^+ + 0.695H_2O + 8.185H^+$	188
3	Biotite *2	$4KFe_3AlSi_3O_{10}(OH)_2 + 12H_2O + 16H^+ + 3O_2 \leftrightarrow 12FeOOH + 4K^+ + 12H_4SiO_4 + 4Al^{3+}$	12
4	Chlorite *1	$0.08Fe_5Al_2Si_3O_{10}(OH)_8 + 0.3K^+ + 1.34Al^{3+} + 3.76H_4SiO_4 + 0.1O_2 \leftrightarrow 1K_{0.3}Al_{1.5}Fe^{3+}_{0.4}Si_4O_{10}(OH)_2 + 2.44H_2O + 1.96H^+$	20
5	Chlorite *2	$4Fe_5Al_2Si_3O_{10}(OH)_8 + 24H^+ + 6H_2O + 5O_2 \leftrightarrow 20FeOOH + 8Al^{3+} + 12H_4SiO_4$	20
6	Hornblende	$4Fe_7Si_8O_{22}(OH)_2 + 74H_2O + 7O_2 \leftrightarrow 28FeOOH + 32H_4SiO_4$	28
7	$Fe^{2+}_{(aq)}$	$4Fe^{2+} + 6H_2O + O_2 \leftrightarrow 4FeOOH + 8H^+$	4
Fe(II) oxidation with nitrate as electron acceptor			
8	Magnetite	$10Fe_3O_4 + 2NO_3^- + 2H^+ \rightarrow 30FeOOH + N_2$	10
9	Biotite *1	$0.1KFe_3AlSi_3O_{10}(OH)_2 + 3.01Mg^{2+} + 0.755Al^{3+} + 2.845H_4SiO_4 + 0.047NO_3^- \leftrightarrow 1Mg_{3.01}Fe^{2+}_{0.065}Fe^{3+}_{0.235}Si_{3.145}Al_{0.855}O_{10}(OH)_2 + 0.1K^+ + 0.721H_2O + 8.138H^+ + 0.0235N_{2(aq)}$	47
10	Biotite *2	$10KFe_3AlSi_3O_{10}(OH)_2 + 42H_2O + 46H^+ + 6NO_3^- \leftrightarrow 30FeOOH + 10K^+ + 10Al^{3+} + 30H_4SiO_4 + 3N_{2(aq)}$	30
11	Chlorite *1	$2Fe_5Al_2Si_3O_{10}(OH)_8 + 7.5K^+ + 33.5Al^{3+} + 94H_4SiO_4 + 2NO_3^- \leftrightarrow 25K_{0.3}Al_{1.5}Fe^{3+}_{0.4}Si_4O_{10}(OH)_2 + 118H_2O + 106H^+ + N_2$	10
12	Chlorite *2	$2Fe_5Al_2Si_3O_{10}(OH)_8 + 14H^+ + 2H_2O + 2NO_3^- \leftrightarrow 10FeOOH + 6H_4SiO_4 + 4Al^{3+} + N_2$	10
13	Hornblende	$10Fe_7Si_8O_{22}(OH)_2 + 178H_2O + 14NO_3^- + 14H^+ \leftrightarrow 70FeOOH + 80H_4SiO_4 + 7N_2$	70
14	$Fe^{2+}_{(aq)}$	$10Fe^{2+} + 14H_2O + 2NO_3^- \leftrightarrow 10FeOOH + 18H^+ + N_2$	10
Fe(III) reduction with dihydrogen as electron donor			
15	Magnetite	$Fe_3O_4 + 6H^+ + H_2 \leftrightarrow 3Fe^{2+} + 4H_2O$	2
16	Goethite	$2FeOOH + 4H^+ + H_2 \leftrightarrow 2Fe^{2+} + 4H_2O$	2
17	Hematite	$Fe_2O_3 + 4H^+ + H_2 \leftrightarrow 2Fe^{2+} + 3H_2O$	2
18	Ferrihydrite	$2Fe(OH)_3 + 5H^+ + H_2 \leftrightarrow 2Fe^{2+} + 6H_2O$	2
19	Biotite *3	$2KFe^{2+}Fe^{3+}Si_4O_{10}(OH)_2 + 8H_2O + 10H^+ + H_2 \leftrightarrow 4Fe^{2+} + 2K^+ + 8H_4SiO_4$	2
20	Biotite *2	$2KFe^{2+}Fe^{3+}Si_4O_{10}(OH)_2 + 2K^+ + H_2 \leftrightarrow K_2Fe^{2+}{}_2Si_4O_{10}(OH)_2 + 2H^+$	2
21	Chlorite *3	$9.09Mg_{2.89}Fe^{2+}_{1.78}Fe^{3+}_{0.22}Al_{2.49}Ca_{0.01}Si_{2.63}O_{10}(OH)_8 + 156.91H^+ + H_2 \leftrightarrow 18.18Fe^{2+} + 26.27Mg^+ + 0.09Ca^{2+} + 22.64Al^{3+} + 23.91H_4SiO_4 + 68H_2O$	9.09
22	Chlorite *2	$9.09Mg_{2.89}Fe^{2+}_{1.78}Fe^{3+}_{0.22}Al_{2.49}Ca_{0.01}Si_{2.63}O_{10}(OH)_8 + 0.64Al^{3+} + H_2 \leftrightarrow 9.09Mg_{2.89}Fe^{2+}{}_2Al_{2.56}Ca_{0.01}Si_{2.63}O_{10}(OH)_8 + 2H^+$	9.09
Fe(III) reduction with acetate as electron donor			
23	Magnetite	$4Fe_3O_4 + 23H^+ + C_2H_3O_2^- \leftrightarrow 12Fe^{2+} + 12H_2O + 2HCO_3^-$	8
24	Goethite	$8FeOOH + 15H^+ + C_2H_3O_2^- \leftrightarrow 8Fe^{2+} + 12H_2O + 2HCO_3^-$	8
25	Hematite	$4Fe_2O_3 + 15H^+ + C_2H_3O_2^- \leftrightarrow 8Fe^{2+} + 8H_2O + 2HCO_3^-$	8
26	Ferrihydrite	$8Fe(OH)_3 + 15H^+ + C_2H_3O_2^- \leftrightarrow 8Fe^{2+} + 20H_2O + 2HCO_3^-$	8
27	Biotite *3	$8KFe^{2+}Fe^{3+}Si_4O_{10}(OH)_2 + 36H_2O + 39H^+ + C_2H_3O_2^- \leftrightarrow 16Fe^{2+} + 8K^+ + 32H_4SiO_4 + 2HCO_3^-$	8
28	Biotite *2	$8KFe^{2+}Fe^{3+}Si_4O_{10}(OH)_2 + 8K^+ + C_2H_3O_2^- + 4H_2O \leftrightarrow 8K_2Fe^{2+}{}_2Si_4O_{10}(OH)_2 + 9H^+ + 2HCO_3^-$	8
29	Chlorite *3	$72.73Mg_{2.89}Fe^{2+}_{1.78}Fe^{3+}_{0.22}Al_{2.49}Ca_{0.01}Si_{2.63}O_{10}(OH)_8 + 626.64H^+ + C_2H_3O_2^- \leftrightarrow 72.73Fe^{2+} + 105.19Mg^{2+} + 0.36Ca^{2+} + 90.55Al^{3+} + 95.64H_4SiO_4 + 268H_2O + 2HCO_3^-$	8
30	Chlorite *2	$36.36Mg_{2.89}Fe^{2+}_{1.78}Fe^{3+}_{0.22}Al_{2.49}Ca_{0.01}Si_{2.63}O_{10}(OH)_8 + 2.55Al^{3+} + C_2H_3O_2^- + 4H_2O \leftrightarrow 36.36Mg_{2.89}Fe^{2+}{}_2Al_{2.56}Ca_{0.01}Si_{2.63}O_{10}(OH)_8 + 9H^+ + 2HCO_3^-$	8
Fe(III) reduction with lactate as electron donor			
31	Magnetite	$6Fe_3O_4 + 34H^+ + C_3H_5O_3^- \leftrightarrow 18Fe^{2+} + 18H_2O + 3HCO_3^-$	12
32	Goethite	$12FeOOH + 22H^+ + C_3H_5O_3^- \leftrightarrow 12Fe^{2+} + 18H_2O + 3HCO_3^-$	12
33	Hematite	$6Fe_2O_3 + 22H^+ + C_3H_5O_3^- \leftrightarrow 12Fe^{2+} + 12H_2O + 3HCO_3^-$	12
34	Ferrihydrite	$12Fe(OH)_3 + 22H^+ + C_3H_5O_3^- \leftrightarrow 12Fe^{2+} + 30H_2O + 3HCO_3^-$	12
35	Biotite *3	$12KFe^{2+}Fe^{3+}Si_4O_{10}(OH)_2 + 54H_2O + 58H^+ + C_3H_5O_3^- \leftrightarrow 24Fe^{2+} + 12K^+ + 48H_4SiO_4 + 3HCO_3^-$	12
36	Biotite *2	$12KFe^{2+}Fe^{3+}Si_4O_{10}(OH)_2 + 12K^+ + C_3H_5O_3^- + 6H_2O \leftrightarrow 12K_2Fe^{2+}{}_2Si_4O_{10}(OH)_2 + 14H^+ + 3HCO_3^-$	12
37	Chlorite *3	$54.55Mg_{2.89}Fe^{2+}_{1.78}Fe^{3+}_{0.22}Al_{2.49}Ca_{0.01}Si_{2.63}O_{10}(OH)_8 + 939.45H^+ + C_3H_5O_3^- \leftrightarrow 109.09Fe^{2+} + 157.64Mg^{2+} + 0.55Ca^{2+} + 135.82Al^{3+} + 143.45H_4SiO_4 + 402H_2O + 3HCO_3^-$	12
38	Chlorite *2	$54.55Mg_{2.89}Fe^{2+}_{1.78}Fe^{3+}_{0.22}Al_{2.49}Ca_{0.01}Si_{2.63}O_{10}(OH)_8 + 3.82Al^{3+} + C_3H_5O_3^- + 6H_2O \leftrightarrow 54.55Mg_{2.89}Fe^{2+}{}_2Al_{2.56}Ca_{0.01}Si_{2.63}O_{10}(OH)_8 + 14H^+ + 3HCO_3^-$	12

*1 = biotite(bt)/chlorite(chl) → Fe(III) oxides, *2 = bt/chl → Fe(III) silicates, *3 = bt/chl → Fe^{2+}

situ pH of 8 for a range of dissolved ion and gas concentrations. This range included either (i) those typically found in comparable deep biosphere systems (i.e. lower end of ion and gas concentration range), or (ii) those that are typically used in lab studies and are thus experimentally relevant (Fig. 2.S2) (Bach and Edwards, 2003; Boettger et al., 2013; Heidari et al., 2017; Jones et al., 2018; Xiao et al., 2021). The latter higher concentration condition ((ii)) may also be relevant to a drying period after a rain event, as drying increases the concentrations of elements within a microbial biofilm (Table S1).

2.3.5 Microbial enrichments and incubation conditions

Cultivation of microorganisms. Aseptically crushed soil/rock samples were used as inoculum to identify zones of active microbial Fe(II) oxidation and/or Fe(III) reduction (N = 59). Fe(II) was provided as an FeS layer in gradient tubes for microaerophilic Fe(II)-oxidising bacteria (3 replicates per depth interval). Additionally, Fe(III) was added as synthesized 2-line ferrihydrite (Fhy) (as described in Straub et al., 2005) in 96 deep-well plates to test for Fe(III) reduction coupled to acetate/lactate or dihydrogen oxidation (6 replicates per depth interval). Under lab conditions, the Fe minerals provided were assumed to be bioavailable in addition to the Fe already present in the environmental samples. For inoculation of the native microbial community, crushed core samples were mixed with anoxic mineral medium and added to each setup.

Microaerophilic Fe(II)-oxidising bacteria were grown in gradient tubes following the protocol of Emerson and Floyd (2005), in which we established opposing gradients of oxygen and Fe^{2+} prior to sample injection. Positive growth was indicated by the formation of an orange band (compared to an abiotic control tube = negative control), as exemplified in Lueder et al. (2018). As positive control, a microaerophilic Fe(II)-oxidising enrichment culture from a mine (Segen Gottes Mine, SW Germany) dominated by *Curvibacter* sp. (Picard et al., 2015) from the laboratory culture collection (Geomicrobiology Group, Department of Geosciences, University of Tuebingen, Germany) was used.

To enrich Fe(III)-reducing bacteria, an anoxic mineral medium (N_2:CO_2 90:10; see SI for media composition details) was amended with Fhy as an Fe(III) source and either a mix of 5 mM sodium acetate and 5 mM sodium lactate, or H_2 in excess were provided as an electron donor for Fe(III) reduction. Thereafter, the soil/rock slurry was added into 96 deep-well plates which were anoxically incubated for 8 weeks at room temperature in the dark. Positive growth evaluation was based on the formation of black-coloured, reduced Fe(II) minerals in comparison to rusty-orange coloured control wells (Fig. 2.S3). A detailed analysis of the black-coloured minerals can be found in the Supplementary Discussion Section. As positive control, the Fe(III)-reducing culture *Geobacter sulfurreducens* (Caccavo et al., 1994) from the laboratory culture collection (Geomicrobiology Group, Department of Geosciences, University

of Tuebingen, Germany) was used. As Fhy was added as an electron source in addition to the Fe species already present in the environmental samples, control experiments without Fhy were carried out. These control setups included 11 powdered drill core samples to account for background Fe mineral dissolution from the Fe pool of the environmental samples, i.e. by dissolution or microbial Fe(III) reduction. In these control experiments, powdered drill core samples were added into the 96 deep-well plates using the same media components as for the cultivation experiments, but in contrast did not contain 2-line ferrihydrite as an additional Fe(III) source. In this study, *in situ* Fe(III) reduction is defined as the activation of Fe(III)-reducing microbial activity within core samples inoculated into media, as described above.

Fe(III)-reducing enrichments from the eight most promising depth intervals (i.e. which showed most Fe(III) reduction) were transferred four times each into Hungate tubes (N = 8, four biological replicates each) to obtain a robust Fe(III)-reducing enrichment culture. One robust (i.e. healthy and reproducible) Fe(III)-reducing culture was obtained and further characterised as outlined below. For convenience, this Fe(III)-reducing culture is referred to as “culture SG”.

2.3.6 Ferrihydrite reduction by an enrichment culture

Batch ferrihydrite reduction experiments were conducted to determine which electron donors are used by enrichment culture SG to reduce Fe(III). Experiments were carried out in 58 mL serum bottles filled with 22.5 mL anoxic 30 mM mineral medium (N_2:CO_2 90:10). Biotic setups were amended with 5 mM Fhy as an electron acceptor and either (1) 5 mM sodium acetate, (2) 5 mM sodium lactate, (3) a 5 mM sodium acetate/lactate mix, or (4) dihydrogen in excess as an electron donor. The mix of sodium acetate/lactate was used to determine, if culture SG can (i) use both electron donors, and (ii) prefers one over the other. Since we opted not to add inhibitors for sulfate reduction such as molybdate, the sulfate contained in the growth medium could also have served as an alternative electron acceptor. All biotic setups were inoculated with 10% (vol/vol) pre-grown enrichment culture SG. Abiotic setups were identical to biotic setups except for addition of cells, in order to quantify abiotic ferrihydrite dissolution over time. An additional biotic control was set up with Fhy and cells, but without the addition of an electron donor. By doing so, we assessed how much Fe(III) reduction occurs based on the amount of organics carried over from the inoculum. Both biotic and abiotic setups were conducted in triplicates.

Sampling and chemical analysis

For the ferrihydrite reduction experiments, sampling was performed in an anoxic glovebox (100% N_2) by taking an aliquot of 0.6 mL with a needle and syringe (0.55 mm) into a 2 mL Eppendorf tube.

Fe quantification. The sample slurries were anoxically extracted with 6 M HCl for 24 h to target crystalline Fe phases. Fe quantification was conducted via a ferrozine assay (Hegler et al., 2008).

High pressure liquid chromatography (HPLC). Lactate and acetate were quantified by using a HPLC device (Shimadzu, Kyoto, Japan) equipped with an Aminex HPX 87H column (BioRad, Hercules, USA), using a refractive index detector for lactate and a diode array detector for acetate analysis.

Ion chromatography (IC). We quantified water extractable sulfate of the rock sample, from which the enrichment culture was obtained, as well as dissolved sulfate in the batch ferrihydrite reduction experiment samples using a Dionex DX-120 ion chromatograph (Thermo, USA).

Raman spectroscopy. Raman spectra of Fe-S minerals within the Fhy microcosms were acquired with an alpha 500R confocal Raman microscope (WITec GmbH, Ulm, Germany). The microscope was equipped with a 532 nm excitation laser, UHTS 300 spectrometer and DV401-BV CCD camera. Optical grating was 600 g mm^{-1} for spectra recording in the range of 0 to 3790 cm^{-1}, while using a 40× objective with a numerical aperture of 0.6 (EC Epiplan-neofluor, Carl Zeiss, Germany). The laser power was adjusted to 0.1 mW using an optical power meter (PM100D, Thorlabs GmbH, Dachau, Germany). Three spots of each sample were analysed using 10 integrations for 20 s respectively and combined to create a composite spectrum. Relative intensities were normalised to 100.

2.3.7 Microbial community sequencing

Fe(III)-reducing enrichment culture community compositions

In order to assess the adaptation of the enrichment culture to different electron donors provided and its effect on the microbial community composition, DNA was extracted from the cultures after termination of the Fhy microcosms with the DNeasy® PowerSoil® Pro" Kit (QIAGEN®). DNA was amplified by using forward primer 16S-515F and reverse primer 16S-806R (Caporaso et al., 2011) targeting the V4 region. Library preparation steps (Nextera, Illumina) and 250 bp paired-end sequencing with MiSeq (Illumina, San Diego, CA, USA) using v2 chemistry were performed by Microsynth AG (Switzerland). Between 1,309 and 86,992 read pairs were obtained for each sample (in total 580,028). Samples treated with ferrihydrite and acetate had the lowest read counts (1,309, 1,312, and 1,974), all other samples had more than 45,000. Sequencing data was analysed with nf-core/ampliseq v2.3.1, which includes all analysis steps and software and is publicly available (Ewels et al., 2020; Straub et al., 2020), with Nextflow v21.10.3 (Di Tommaso et al., 2017) and singularity v3.8.7 (Kurtzer et al., 2017). Primers were trimmed, and untrimmed sequences were discarded (<30% per sample) with

Cutadapt version 3.4 (Martin, 2011). Adapter and primer-free sequences were processed with DADA2 v1.22.0 (Callahan et al., 2016) to eliminate PhiX contamination, trim reads (before median quality drops below 35; forward reads were trimmed at 181 bp and reverse reads at 206 bp), correct errors, merge read pairs, and remove polymerase chain reaction (PCR) chimeras; ultimately, 48 amplicon sequencing variants (ASVs) were obtained across all samples. Taxonomic classification was performed with DADA2 and the SILVA v138 database (Quast et al., 2012). Intermediate results were imported into QIIME2 version 2021.8.0 (Bolyen et al., 2019). 5 ASVs classified as chloroplasts or mitochondria were removed, totaling <1.7% relative abundance per sample, and retaining 43 ASVs across all samples. Alpha rarefaction curves were produced with the QIIME2 diversity alpha-rarefaction plugin, which indicated that the richness of the samples had been fully observed, except for samples treated with ferrihydrite and acetate.

Native microbial community composition

The community composition of the enrichment was compared to the native (*in situ)* microbial community. Total DNA was extracted from the uncontaminated inner rock core sample (76.5 m depth, IGSN: https://doi.org/10.60510/GFCHS009N) using the “DNeasy® PowerSoil® Pro” Kit (QIAGEN®). Therefore, three replicates containing 1 g of rock powder were weighed into PowerBead Pro Tubes and extracted according to the protocol of the kit manufacturer. During the silica binding step of the extraction, replicates were pooled together to increase DNA concentration. An extraction control was run during all extraction steps in order to identify potential lab and kit contaminants. Microbial community composition was assessed using 16S-rRNA amplicon sequencing with MiSeq (Illumina, San Diego, CA, USA) with 2x300 bp. Library preparation, including polymerase chain reaction and DNA clean-up was done in the GFZ Potsdam laboratories (Section 3.7 Geomicrobiology). The V4 region of bacterial and archaeal DNA was targeted using the universal primer pair 16S-515F and 16S-806R (Caporaso et al., 2011). During PCR an additional control containing PCR grade water instead of DNA template was performed to identify PCR contaminants. Barcoded versions of the primers were used to later distinguish between sample, extraction control and PCR control. After successful amplification, the products were purified using the Agencourt AMPure XP PCR Purification Kit (Beckman Coulter) and send to Eurofins Genomics Germany GmbH (Konstanz, Germany) for sequencing on a MiSeq System. After recovery of the raw data, libraries were demultiplexed using Cutadapt (Martin, 2011). Taxonomic classification was performed using the DADA2 pipeline (Callahan et al., 2016). Reads were truncated (250 - forward, 200 - reverse) and quality-filtered before the error model was generated. The amplicon sequence variants (ASVs) were assigned to the SILVA taxonomy (Quast et al., 2012). Chloroplast, mitochondria, and singletons were removed. The contamination was assessed using the negative controls of the

extraction and the PCR run. Potential contaminant sequences were completely removed from the data set resulting in a total of 25878 sequences for the investigated rock sample.

2.3.8 Data and statistical analysis

Data analyses were performed in the R statistical environment (R Core Team, 2024) and plots were produced with the package ggplot2 (Wickham, 2016). Fe(III) reduction by *in situ* microbial communities along the SG weathering profile was analysed using a general linear model (LM). We tested the combined effect of electron donor and setup type treatments on Fe(III) reduction (response variable) in a multipredictor model. Setting up the model we included six predictor variables, which can be classified into two experimental variables (electron donor and setup type), two simple environmental variables (bioavailable and crystalline Fe) and two complex environmental variables (depth and alteration). We further added all significant interactions between predictor variables to maximise the variance in Fe(III) reduction values explained by the model. Model assumptions were checked for all selected models and found not to have been violated. For statistical analyses of Fe(III) reduction, all reasonable models were explored and selection based upon comparison of differences in the Akaike Information Criterion (ΔAIC) (Zuur et al., 2009). In order to include all significant interactions while ensuring model parsimony, the best model fit was determined by the dredge() function in the MuMIn package (Barton and Barton, 2015). However, we excluded alteration as predictor variable from our model during the model building process to avoid collinearity (Figs 2.S4-2.S8). The role of alteration in Fe(III) reduction is still addressed in the discussion. As the general linear model was found to be significant, we ran *post hoc* paired-samples t-tests, corrected with Holm's sequential Bonferroni procedure (Holm, 1979), to assess whether the compared pairs of setup type and electron donor type showed significant differences in mean Fe(III) reduction.

2.4 Results

2.4.1 Drill core mineralogy and geochemistry of SG weathering profile

Extractions were performed to quantify the amounts of poorly crystalline and crystalline Fe phases in the drill core samples. Extractions targeted (1) the Fe that is poorly crystalline and prone to be more "bioavailable" to Fe-metabolising microorganisms (via 0.5 M HCl) and (2) the crystalline Fe that is present as Fe(III) (oxyhydr)oxides (via CBD). These complement total Fe(II) and Fe(III) data reported in Krone et al. (2021b). Higher amounts (>7.6 mg Fe g^{-1} rock) of bioavailable Fe are associated with unaltered zones (Fig. 2.1a), while altered zones positively correlate with the presence of crystalline Fe (2.5-9.5 mg Fe g^{-1} rock) (Fig. 2.1b). The Fe(III) (oxyhydr)oxide depth profile (Fig. 2.1b) mirrors the pattern of the bulk Fe(III)/Fe(total)-ratio profile (Fig. 2.1c) (see Krone et al., 2021b). The Fe extraction data also complements

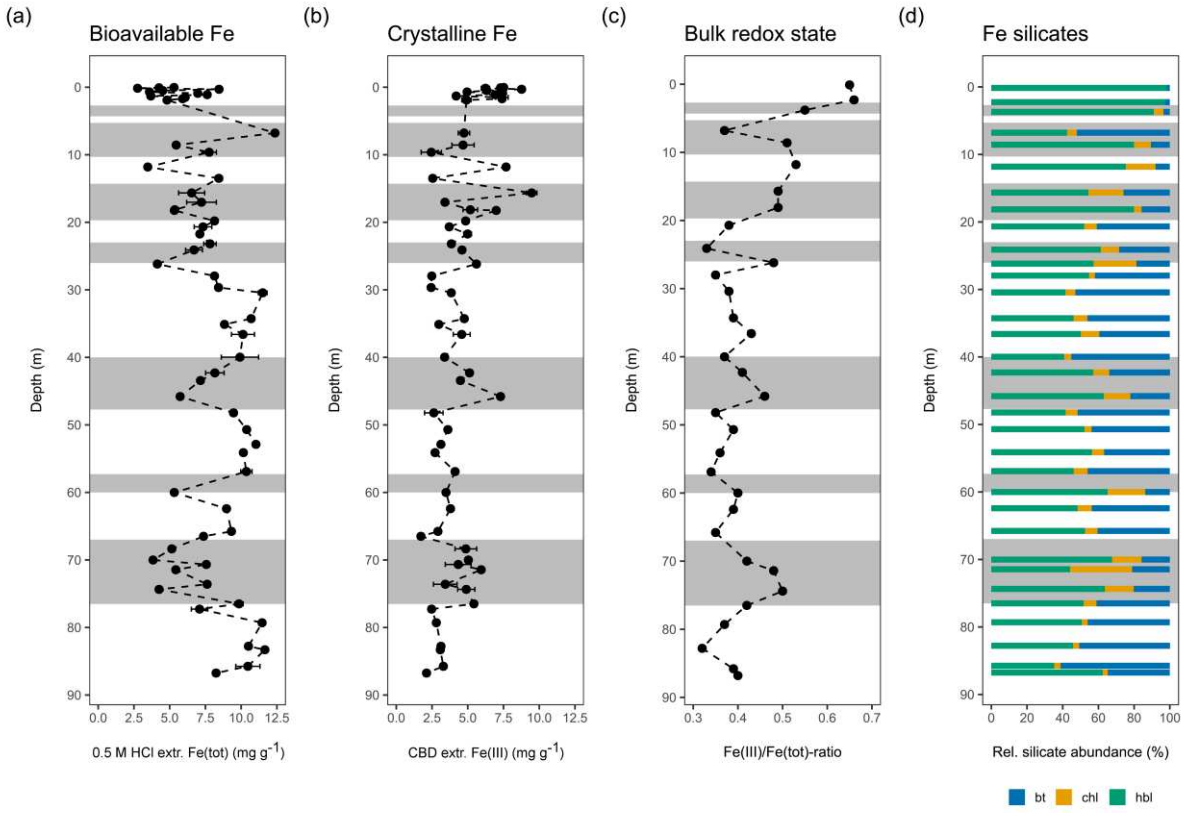

Fig. 2.1. Geochemical, mineralogical, and geophysical data of the Santa Gracia drill core. (a) 0.5 M HCl extractable Fe(tot) represents the bioavailable Fe pool, while (b) citrate-bicarbonate-dithionite (CBD) extractable Fe(III) is indicative for the amount of present Fe(III) (oxyhydr)oxides (crystalline Fe). Data points in (a) and (b) represent the average of technical extraction replicates. Error bars denote standard error of the technical extraction replicates. (c) Redox state of bulk drill core samples displayed as Fe(III)/Fe(total)-ratios (replotted after Krone et al., 2021b; Hampl et al., 2022). (d) Relative abundances of Fe-bearing silicates biotite (bt), chlorite (chl) and hornblende (hbl) (modified after Hampl et al., 2022). Grey boxes display the presence of prominent reddish zones, fracture (zones) and zones of correlating mineral abundances (see Weckmann et al., 2020). Hampl et al. (2022) provides a more detailed overview of the connections between fracture zones, hydrothermal alteration and mineral abundances (see Figs. 2-4).

previous analysis of the bulk mineralogy of the core samples (Fig. 2.1d) (Hampl et al., 2022). This highlights a zone of particularly intense weathering and hydrothermal alteration in the deepest weathering zone (67-77 m depth) rich in Fe(III).

Furthermore, high resolution water extractable organic carbon (DOC) and nitrate data were obtained for the whole SG weathering profile (Fig. 2.S9). DOC and nitrate potentially serve as electron donors and acceptors for microbial Fe(III) reduction and Fe(II) oxidation, respectively. The amount of DOC in the deep (<2 m) subsurface (0.17 mg g^{-1} rock) on average was lower compared to the uppermost soil horizon (0-2 m; 0.25 mg g^{-1} soil), as it was for nitrate (<2 m vs. 0-2 m: 0.0008 vs. 0.0035 mg g^{-1} rock). The mean pH of SG weathering profile was 8.20 ± 0.02 (potential pH) and 9.31 ± 0.04 (active pH) (N = 10, technical extraction triplicates) (Fig. 2.S10).

2.4.2 Gibbs free energy of metabolic reactions with Fe-bearing minerals

We calculated Gibbs free energy yields for 38 Fe redox reactions based on the previously reported primary Fe-bearing minerals (Krone et al., 2021b; Hampl et al., 2022) and secondary minerals formed by weathering (Fig. 2.2, Tables 2.1,2.S4). Overall, there is a wide range from highly exergonic (i.e. release of energy) to highly endergonic (i.e. requires energy supply) yields depending on the electron donor and acceptor chosen. Of 14 Fe(II) oxidation reactions listed (Table 2.1), 10 reactions are exergonic when coupled to either oxygen or nitrate reduction (Fig. 2.2a,b). With regard to primary Fe(II)-bearing minerals, there is a clear energetic benefit for microbial Fe(II) oxidation in biotite and hornblende with either oxygen or nitrate as an electron acceptor. Magnetite and free Fe(II) in solution could also fuel microaerophilic and/or nitrate-dependent Fe(II) oxidation, while chlorite oxidation would not provide enough energy to be energetically feasible. Moreover, reactions with nitrate as an electron acceptor could provide more energy than oxygen, e.g. in case of magnetite being the electron donor.

In stark contrast to the situation for microbial Fe(II) oxidation, microbial Fe(III) reduction always requires the availability of Fe(III) (oxyhydr)oxides as an electron acceptor (Fig. 2.2c-e), while assuming free Fe^{2+} to be the Fe(II) product (Table 2.1). Of 24 Fe(III) reduction reactions listed, only 12 reactions are exergonic when coupled to either dihydrogen, acetate or lactate. Reduction of Fe(III)-bearing silicates are all endergonic meaning there is no energetic advantage for microorganisms to use these minerals as an Fe(III) source. Reduction of Fe(III) (oxyhydr)oxides showed the strongest dependence on pH, specifically decreasing in energy yield with increasing pH but still being feasible up to pH 9.

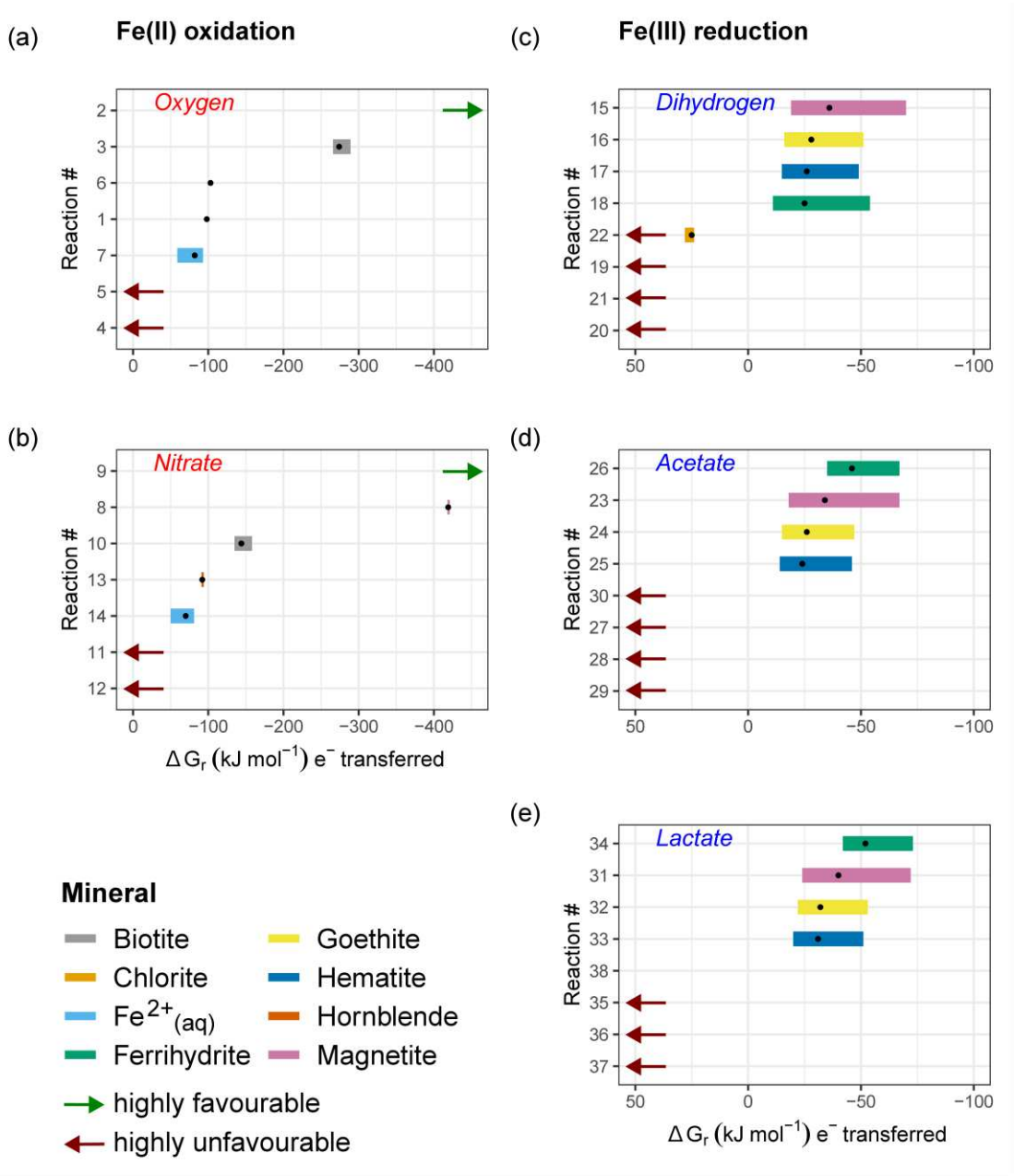

Fig. 2.2. Gibbs free energy of Fe(II) oxidation and Fe(III) reduction redox reactions per electron transferred for *in situ* conditions. The 38 redox reactions (# 1-38) represent 14 oxidation (left column) and 24 reduction (right column) reactions for major Fe-bearing minerals present in the Santa Gracia depth profile (Table 1). Gibbs free energy per mole of electron transferred is shown for Fe(II) oxidation coupled to (a) O_2 reduction; (b) nitrate reduction (electron acceptors indicated in red letters); as well as for Fe(III) reduction coupled to (c) dihydrogen oxidation; (d) acetate oxidation; and (e) lactate oxidation (electron donors indicated in blue letters). Gibbs free energy values of redox reactions are shown for fixed concentrations and a pH range of 6-9. Black dots represent Gibbs free energy values of redox reactions for pH 8, which is about the potential *in situ* pH of SG bulk drill core samples (Fig. 2.S10). Gibbs free energy values of Fe(II) oxidation reactions #4, 5, 11, and 12 are not displayed, because they are highly positive and hence not thermodynamically favourable, or in the case of reactions #2 and 9, unrealistically favourable (potentially due to unreliable ΔG_r^0 database for Fe-bearing silicates). Energetic yields for reactions #1 and 8 (= magnetite) and #6 and 13 (= hornblende) show narrow to no ranges, as they are marginally to non-dependent from pH. Energetic yields for Fe(III) reduction reactions #19-21, 27-30, and 35-38 are not shown as they are highly unfavourable.

2.4.3 Fe(III) reduction by in situ microbial communities

As Fe(III) (oxyhydr)oxides are abundant in fracture zones marked by weathering and/or hydrothermal alteration, and thermodynamic calculations demonstrated their potential as prevalent Fe(III) sources, Fe(III) reduction enrichments were set up to identify depths in which the *in situ* community could be activated to perform Fe(III) reduction. Microbial Fe(III) reduction could be observed in screening/enrichment setups with ground rock powder (amended with ferrihydrite) throughout the whole weathering profile (Fig. 2.3), independent of the provided electron donor. In contrast, enrichments of Fe(II)-oxidisers were successful for 8 depths.

In order to determine whether altered zones act as hot spots for Fe(III)-reducing microbial activity, we investigated the effect of alteration on the concentrations of bioavailable Fe, crystalline Fe and Fe(III) reduction (Figs 2.S6-2.S8). In the presence of alteration, we found a significant decrease in bioavailable Fe by 2.1 mg g^{-1} rock (+alt = -2.06, t = -4.9, df = 92, P < 0.001) and a significant increase in crystalline Fe by 1.4 mg g^{-1} rock (+alt = 1.371, t = 4.7, df = 92, P < 0.001). However, once the effect of depth is considered, Fe(III) reduction in altered and unaltered zones does not appear to be substantially different (Fig. 2.3), which is supported by Fig. 2.S8 showing no significant effect of alteration on Fe(III) reduction. Contrastingly, depth (t = 5.0, df = 92, P < 0.001) and increased bioavailable Fe concentrations (t = 5.1, df = 92, P < 0.001) did both significantly increase the amount of Fe(III) reduction (Figs 2.S11,2.S12), unlike crystalline Fe (Fig. 2.13). It is noteworthy that the deepest unaltered zone sampled did have substantially greater Fe(III) reduction than the altered zone above it (H_2: 47.5 vs 28.6%; organics: 46.1 vs 37.3%) (Supplementary Table 2.1).

To better understand Fe(III) reduction by *in situ* microbial communities along the SG weathering profile, we analysed the data using a linear model (LM). We used Akaike Information Criterion (AIC) model selection to distinguish among a set of possible statistical models describing the relationship between setup type (control "-Fhy" vs. experiment "+Fhy"), electron donor (H_2 vs. organics), depth, bioavailable (poorly crystalline) Fe (Fe_{bio}), crystalline Fe (Fe_{cryst}) and Fe(III) reduction (Supplementary Table 2.2). The best-fit model, carrying 94% of the cumulative model weight, included every parameter with three interaction effects (AIC = 907.2). It explains 50.4% of the variation in Fe(III) reduction (= adjusted R^2) (Supplementary Table 2.3), and has a significant fit to the data (F =15.59, df = 8, 107, P < 0.001), leaving a residual standard error of 11.54 with 107 degrees of freedom. The LM identified the setup type, electron donor, depth, Fe_{bio} and the interaction depth:Fe_{bio} to be highly significant (P < 0.001), while the term Fe_{cryst} and the interactions setup:Fe_{bio} and depth:Fe_{cryst} were found to be significant (P < 0.05). Six *post hoc* paired-samples t-tests, corrected with Holm's sequential Bonferroni procedure (Supplementary Table 2.S4), indicated that the extent of Fe(III) reduction is (1) significantly larger in the experimental setups than in the control setups, and (2) signifi-

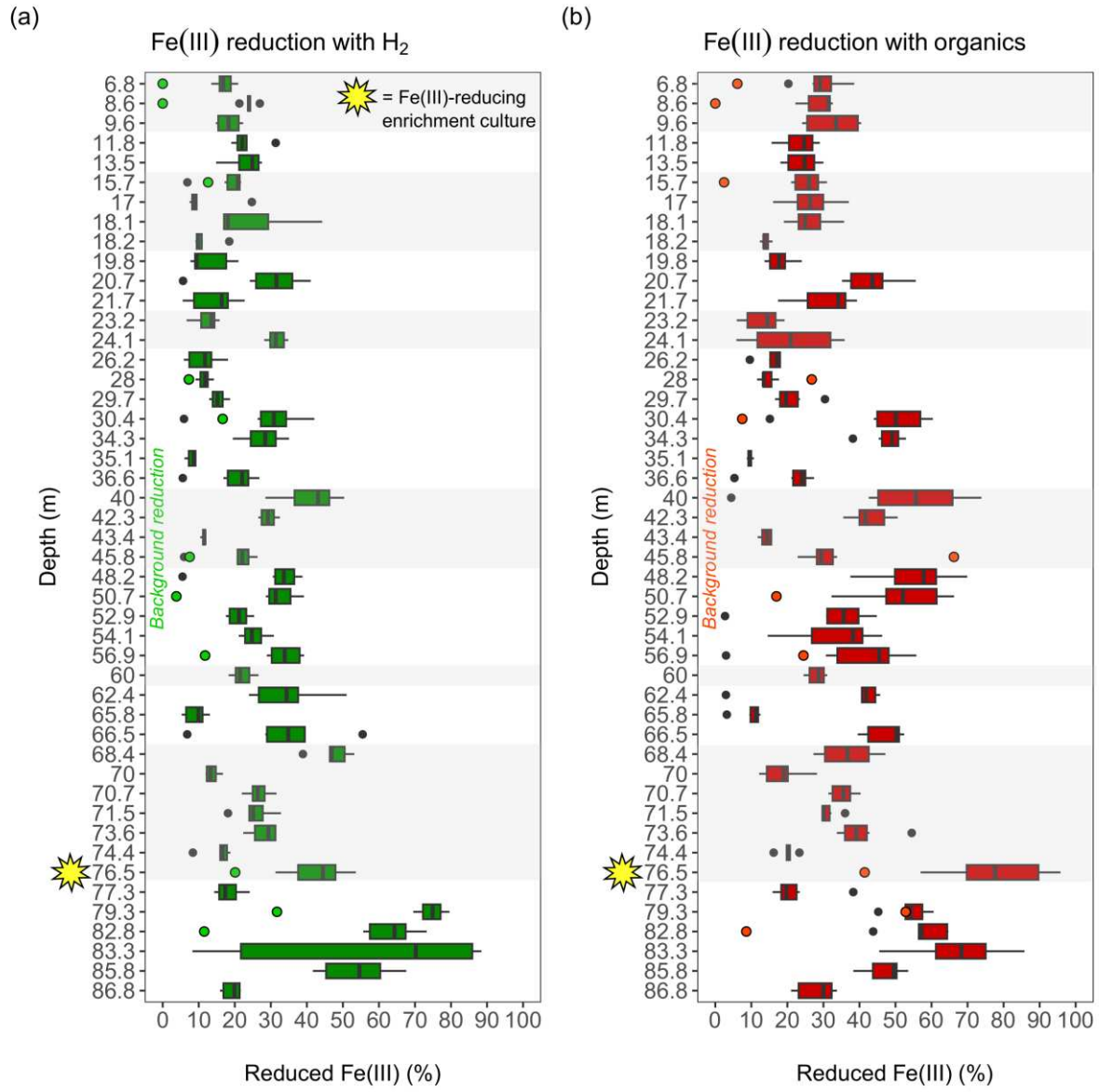

Fig. 2.3. Fe(III) Reduction by the *in situ* microbial community in the weathering profile of Santa Gracia. Drill core samples were amended with 5 mM ferrihydrite (Fhy) (= electron acceptor) and either (a) dihydrogen (H_2) in excess; or (b) 5 mM acetate and lactate (= electron donor). Relative amount of microbially reduced Fe(III) in the experimental setups (= Fe from mineral powder with Fhy addition "+Fhy"; boxplots) is compared to Fe(III) reduction in the control setups (= Fe from mineral powder without Fhy addition "-Fhy", identical to background reduction; filled, light-coloured circles). Fe concentrations were determined after 6 - 8 weeks of incubation. Boxplots show the variance of six biological replicates for each depth. Black dots represent boxplots outliers. Grey boxes display the presence of prominent reddish zones and fracture (zones).

cantly larger in the organics setups than in the H_2 setups (Figs 2.S14,2.S15). The mean Fe(III) reduction extent between the two electron donor treatments differed by 6.8% (H_2 vs. organics: 32.8 to 26.0%).

2.4.4 Fe(II) oxidation by in situ microbial communities

Enrichments of Fe(II)-oxidisers were successful for 8 out of 47 samples (~17%) from 30.4, 34.3, 35.1, 40.0, 43.3, 50.7, 70.7 and 73.6 m depth. We identified growth in FeS tubes by the formation of distinct orange Fe(III) mineral accumulations within or below the orange coloured top layer. Subsequent cultivation and isolation attempts were not successful.

2.4.5 Ferrihydrite microcosms with enrichment culture SG from the deep subsurface

Growth of Fe(III)-reducing enrichment culture. While microbial Fe(III) reduction could be observed in screening (i.e. positive enrichment) setups with ground rock powder throughout the whole weathering profile, a robust Fe(III)-reducing enrichment culture could only be obtained from crushed rock sample of a single depth interval located within the deepest identified weathering zone at ~77 m depth. The obligately anaerobic culture can grow chemoheterotrophically with lactate as well as autotrophically with dihydrogen as an electron donor but cannot oxidise acetate. Prior to its usage in batch ferrihydrite reduction experiments, the culture was pre-grown on 30 mM bicarbonate-buffered anoxic mineral medium (see SI methods for medium composition) and had been transferred six times. The dominant sequence (relative abundance of ~98.5%) in the enrichment culture community composition analysis was found to be 100% identical to the spore-forming sulfate-reducing *Desulfotomaculum ruminis* (Coleman, 1960; Spring et al., 2012). It is noteworthy, that the crushed rock powder sample contains about 9 µM MQ-water extractable sulfate per g powder while 2 mM sodium sulfate is included in the growth medium.

Batch ferrihydrite reduction experiments were conducted to determine which electron donors are used by the enrichment culture to reduce Fe(III). Ferrihydrite reduction was observed in setups with the addition of acetate/lactate, lactate and dihydrogen, but not in setups with acetate addition alone (Figs 2.4, 2.S16). Generally, 4-5 mM added Fe(III) was completely reduced within 11-14 days in both acetate/lactate and dihydrogen setups. The main difference between these was the lag-phase observed in the acetate/lactate setup (11 days), which was not observed in the dihydrogen setup (Fig. 2.4). Additionally, we observed that the Fe(II) concentration in solution rose during ferrihydrite reduction but quickly decreased again once the major part of Fe(III) (~85 %) had been reduced. This might be due to interaction of dissolved Fe(II) with reduced sulfur species. As this strain is closely related to a known sulfate-reducing microorganism and there is some sulfate present in the growth medium, we also measured sulfate concentrations during the incubations which decreased from ~1.8 to 0 mM (Fig. 2.S16). Together these observations suggest a complex interplay of processes is occurring in the batch reactors driven by (i) Fe(III) reduction by Fe(III)-reducing microorganisms, (ii) sulfate reduction by sulfate-reducing microorganisms, and (iii) further reaction between the products of these two processes (Fe(II) and sulfide) in the solution.

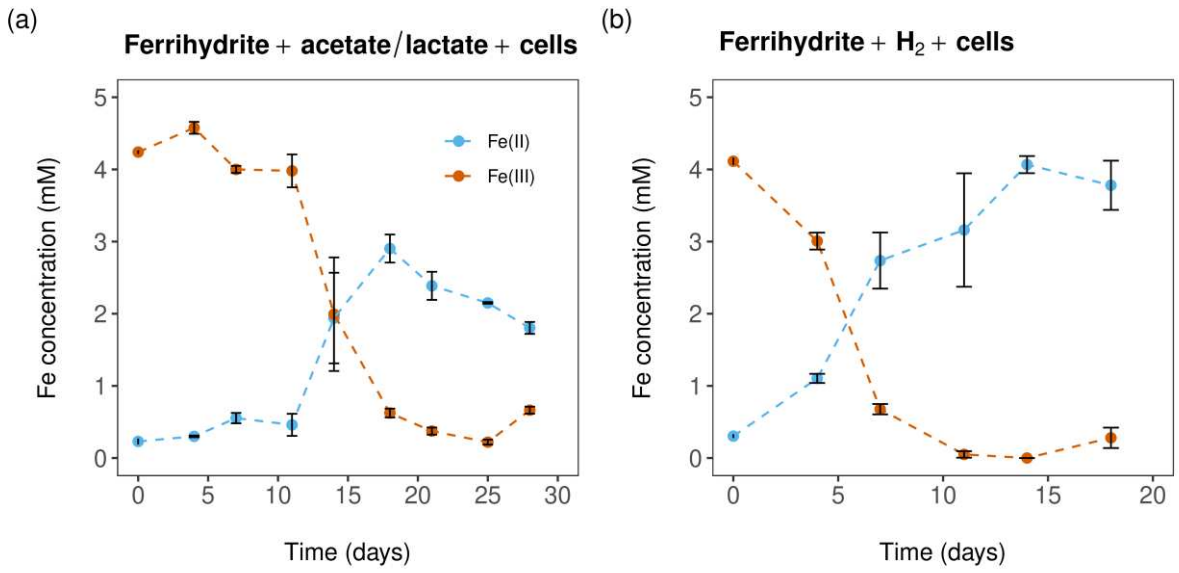

Fig. 2.4. Ferrihydrite reduction by the enrichment culture obtained from the deepest weathering zone (~ 77 m depth) of the Santa Gracia weathering profile. An Fe(III)-reducing enrichment culture (culture SG) obtained from this zone was inoculated into microcosms (6th transfer, 10 % (v/v)) to identify the preferential substrate condition. Microcosms were set up with 5 mM ferrihydrite (Fhy) (= electron acceptor) and either (a) 5 mM acetate and lactate; or (b) dihydrogen (H_2) in excess (= electron donor). Further treatments with acetate or lactate addition as sole electron donor as well as control setups can be found in the SI (Fig. 2.S16). Microbially driven Fe(III) reduction is shown over time. Data points in (a) and (b) represent the average of three biological replicates. Error bars denote standard error of the biological replicates.

2.4.6 Microbial community sequencing

In situ and enrichment culture samples were independently sequenced and analysed. 16S-rRNA sequencing was conducted based on total DNA extracted from the uncontaminated inner rock core as well as from the final timepoint of Fhy microcosms for comparison (Fig. 2.5). Figure 2.5 shows enrichment culture community compositions of ferrihydrite microcosms amended with substrates culture SG can grow with, i.e. dihydrogen ("+H_2") or lactate ("+Lactate"). Overall, *in situ* and enrichment culture compositions clearly differ, although it should be highlighted that separate sequencing and analysis for each composition could lead to batch effects. The *in situ* community composition displays a variety of ASVs typical for extreme environments. Only the two low abundant ASVs (genus level) *Sideroxydans* (0.04%) and *CL500_29_marine_group* (0.15%) can be attributed to the Fe cycle, here in the form of microaerophilic Fe(II)-oxidising microorganisms. The two enrichment culture communities are dominated by a single ASV (species level) related to *Desulfotomaculum ruminis*, a sulfate-reducing strain.

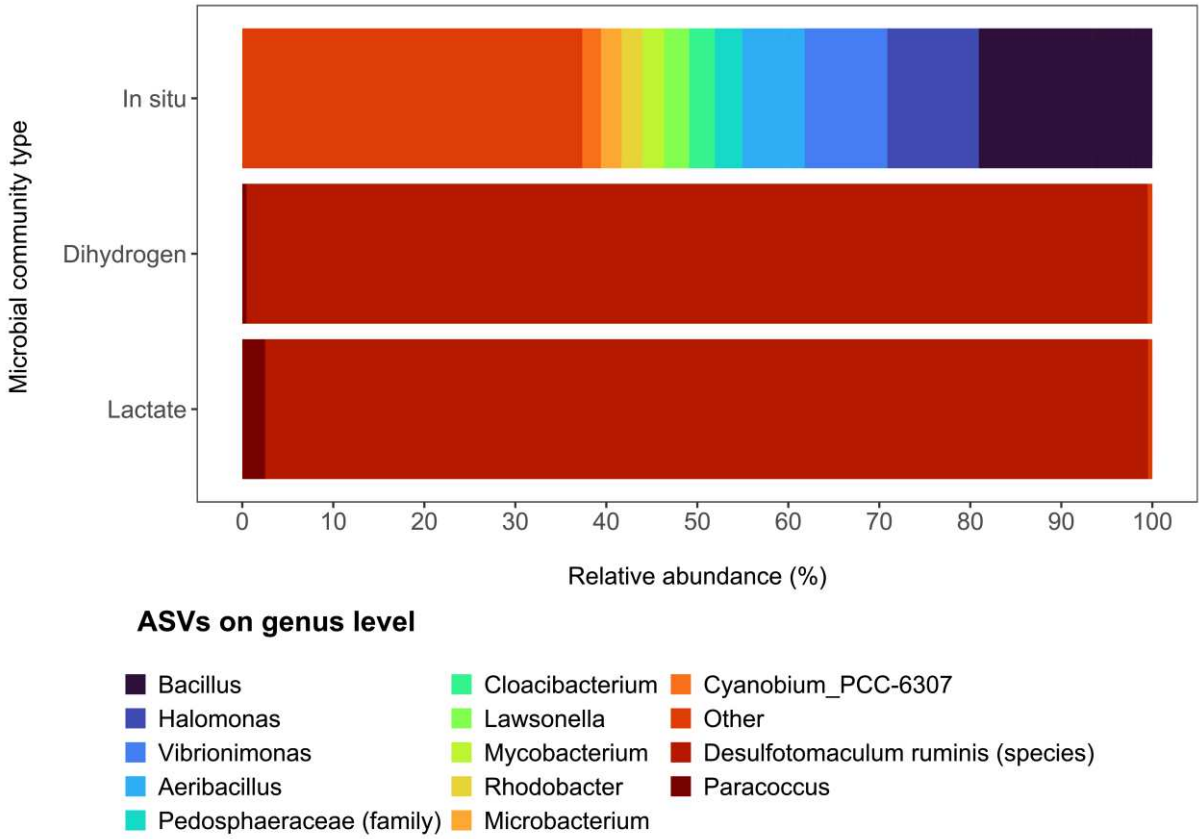

Fig. 2.5. Comparison of *in situ* (= native) community composition versus enrichment culture community composition retrieved from identical drill core sample from ~77 m depth. *In situ* and enrichment culture samples were independently sequenced and analysed. The *in situ* community composition ("In situ") reflects the relative amplicon sequence variants (ASV) abundance pre-enrichment (top panel). Enrichment culture compositions reflect shifted community compositions after substrate addition of ferrihydrite and dihydrogen (H_2) ("Dihydrogen") or ferrihydrite and lactate ("Lactate") (shown ASVs represent average abundances of three biological replicates; mid and bottom panel). In the top panel ("In situ"), relative abundances of the 15 most abundant ASVs ("top15") are shown. The remaining genera ≤2.0 % are summarised in "Other". In the middle ("Dihydrogen") and bottom ("Lactate") panels, only two ASVs with a cumulative abundance of 99.5 % are displayed. Genera <0.2 % are summarised in "Other".

2.5 Discussion

2.5.1 Potential for Fe-cycling in the deep biosphere of a semi-arid region

Localisation of relevant depth intervals for microbial weathering of Fe-bearing minerals

The SG weathering profile comprises multiple weathering zones that are partly situated in Fe-rich hydrothermally overprinted intervals of the profile (Krone et al., 2021b; Hampl et al., 2022). However, it is unknown if these locations represent hotspots for microbial activity and if microbial metabolisms contribute to subsurface weathering processes at the study site. We found that unaltered zones are locations of enhanced Fe bioavailability with poorly crystalline Fe serving as potential electron acceptor for microbial Fe metabolisms. In contrast, hydrothermally overprinted fractures and fracture zones were found to be comprised of more crystalline Fe(III) (oxyhydr)oxides, which hampers microbial Fe(III) reduction. However, a particularly intense hydrothermal alteration in the deepest identified weathering zone (67-77 m depth) hosts a microbial community which is probably contributing to weathering processes at depth (Fig. 2.1). The presence of highly abundant bioavailable Fe(II) (Fig. 2.1a) indicates the potential of this environment to act as a habitat for Fe(II)-oxidising microbes, which is supported by the positive results of microaerophilic Fe(II)-oxidising enrichment cultures from numerous rock samples taken throughout the depth profile.

To facilitate microbial Fe(II) oxidation / Fe(III) reduction, Fe species also need to be accessible (Figs. 2.2,2.3). Abiotic processes like weathering-induced fracturing (WIF) make mineral surfaces more accessible for microbial Fe(II) oxidation, but also consume O_2 (Isherwood and Street, 1976; Kim et al., 2017). Despite this enhanced mineral surface accessibility, it could be argued that microbial Fe(II) oxidation is outcompeted by abiotic Fe(II) oxidation at an *in situ* pH ~8 (Fig. 2.S1) (see Peiffer et al., 2024). However, the measured pH of ground bulk core samples might be biased towards higher values by carbonates such as calcite, which were identified in hydrothermally altered fractures and fracture zones (Fig. 2.S17) (see Krone et al., 2021b; Hampl et al., 2022). Our results suggest that there is potential for both Fe(II) oxidation and Fe(III) reduction (Figs 2.1,2.2,2.S1,2.S2). While microbial Fe(II) oxidation is relevant in parts of the weathering profile, microbial Fe(III) reduction was identified over the entire depth profile (Fig 2.3).

Thermodynamic constraints on microbial weathering of Fe-bearing minerals

To study the potential impact of Fe-metabolising microbes on the weathering of primary and secondary Fe-bearing minerals within the SG weathering profile, energetically favourable Fe redox reactions were identified. Gibbs free energy yields for microbial Fe(II) oxidation were found to be favourable if the Fe source was magnetite or free Fe(II) in solution, and, to a lesser extent, biotite and hornblende (Fig. 2.2). However, because Fe(II) is strongly bound in the crystal structure of poorly soluble, highly crystalline biotite and hornblende, it is less accessible

for microbial redox reactions (Shelobolina et al., 2012; Napieralski et al., 2019; Fan et al., 2023). Fe(II) oxidation in pure biotite has been demonstrated previously, but only under lab conditions using very fine-grained (<5 µm) biotite (stock suspension concentration of 15 to 20 g L^{-1}) (Shelobolina et al., 2012). These conditions and characteristics do not match the natural samples we were analysing. Thermodynamic calculations and the incorporation of Fe as structural Fe(II) in Fe(II)-bearing silicates, suggest that primary Fe(II) minerals are probably not suitable as a main Fe source for Fe(II) oxidisers at our study site. Nonetheless, initial cultivation success of Fe(II)-oxidising microorganisms demonstrates their *in situ* existence, while not providing information on how active they are in *in situ* weathering of Fe(II)-bearing minerals. Hence, we can conclude that Fe-metabolising microorganisms are likely not the main driving force for weathering of primary Fe(II)-bearing silicates. In contrast, Fe(III) reduction is energetically feasible for microbes with magnetite and Fe(III) (oxyhydr)oxides like hematite, goethite or ferrihydrite (Crosby et al., 1983). Based on our calculation results and building upon the minerals identified in the rock samples, we conclude that the deep biosphere at our study site is preferentially using secondary Fe(III) (oxyhydr)oxides for their metabolism.

Importance of semi-arid climatic setting on microbial weathering

The semi-arid nature of the climatic setting at our field site SG is of importance when evaluating the potential for microbial Fe-cycling in the deep subsurface. Unlike for weathering profiles situated in more humid climate, the supply of meteoric water into the subsurface of SG via fractures and hence the transport of O_2, CO_2 and nutrients essential for microbial Fe redox reactions are limited (Napieralski et al., 2019; 2022). Even more, organoheterotrophic based subsurface microbial activity in (semi-)arid climates heavily feeds on the input of young organic C (Scheibe et al., 2023). These limitations in available amounts of water and nutrients force Fe-metabolising microorganisms towards most energy efficient redox reactions to ensure survival (Figs 2.2,2.S1,2.S2). Alternatively, microorganisms can form endospores or minimise their genome size (to reduce the cost of replication) to facilitate survival under water and nutrient deprivation (Lin et al., 2006; Chivian et al., 2008; Suzuki et al., 2017; Fones et al., 2019). In short, microbial weathering activity in our semi-arid deep weathering profile will only occur, where environmental conditions allow for Fe redox reactions.

2.5.2 Fe-metabolising microorganisms are weathering agents

In our *in situ* Fe(III) reduction enrichments, we demonstrated that microbial Fe(III) reduction occurs with both H_2 and organics as electron donor (Figs 2.3,2.S14,2.S15). Overall, on average 6.8% more Fe(III) was reduced in the “+Fhy” setups with organic carbon added compared to setups with dihydrogen. This has two plausible explanations. Firstly, bicarbonate was the only previously identified C source in the dihydrogen setups and thus the differences in Fe reduction extent may be related to different efficiencies of autotrophic vs heterotrophic carbon metabolism. Secondly, the observation might be a result of the higher energetic yield

of Fe(III) reduction coupled to acetate/lactate oxidation over dihydrogen oxidation (see energy densities of reactions #18, 26 and 34; Fig. 2.S1). Fe(III) reduction extent in unaltered versus altered zones in the setup with organics added (Fig. 2.3b) does not seem to be strongly influenced by the *in situ* DOC concentrations (Fig. 2.S9). Organic carbon is most probably transported from the surface via the fracture network (Krumholz et al., 1997). Zones of hydrothermal alteration did not show significantly more Fe(III) reduction (Fig. 2.S8), thus partially ruling out our initial hypothesis that hydrothermally altered zones function as hot spots for Fe(III)-reducing microbial activity.

Regarding microbial Fe(II) oxidation, the failure to subsequently cultivate microaerophilic Fe(II)-oxidising microorganisms does not invalidate the fact that they grew initially. As abiotic Fe(II) oxidation can be ruled out based on the conducted control experiments, observed growth suggests that gradient tubes were an accurate measure of microbial Fe(II)-oxidising activity. In summary, these results suggest that microbial Fe(III) reduction is relatively more important than microbial Fe(II) oxidation with regard to transformation of Fe-bearing minerals in the subsurface.

2.5.3 Evidence for microbial weathering of Fe-bearing minerals from community sequencing

We were able to enrich a robust Fe(III)-reducing culture (Fig. 2.4) and we can rule out that the obtained enrichment culture has entered the subsurface via a contamination, a common risk when retrieving subsurface samples. This leads us to be confident that the detected taxon *Desulfotomaculum* in the enrichment culture (abundance of 98.5%) is part of the *in situ* community (Fig. 2.5), even though it is not abundant (<0.01%) in the detected *in situ* ASVs. The taxon has also been found in other subsurface environments including uranium/heavy metal-contaminated aquifers, freshwater and marine sediments, mines, and oil reservoirs (Magot et al., 2000; Chang et al., 2001; Kaksonen et al., 2006; Ollivier et al., 2007; Wang et al., 2008; Aullo et al., 2013).

Desulfotomaculum ruminis is capable of Fe(III) and sulfate reduction (Figs 2.4,2.S16), while it is unclear if Fe(III) reduction was driven directly (i.e. direct Fe(III) reduction), or indirectly by the oxidation of sulfide produced by this culture. Given that culture SG is able to reduce Fe(III) and sulfate, genera related to Fe(III) and sulfate reduction, as well as Fe(II) and sulfur oxidation are expected. Genera and species confirming this assumption are *Thiomonas*, *Pseudomonas kujiense*, *Chlorobium*, *Thiodictyon*, *Rhodoferax*, *Flavobacterium*, *Paludibacter blasticus*, *Gallionella capsiferriformans*, *Sulfuricurvum kujiense* and *Thiodictyon ruminis* (Widdel et al., 1993; Ehrenreich and Widdel, 1994; Heising et al., 1999; Finneran et al., 2003; Croal et al., 2004; Harris et al., 2004; Kodama and Watanabe, 2004; Hegler et al., 2008; Gregersen et al., 2009; Hegler et al., 2010; Zhuang et al., 2011; Walter et al., 2014; Fabisch et al., 2016; Gauger

et al., 2016; Ghosh et al., 2018; Akob et al., 2020; Ross et al., 2022). They could also be quantified in minor (<0.01%) to larger (up to 8.5%) amounts in the enrichments in this study (Fig. 2.5). In summary, this suggests a potential interconnection between microbial Fe and S cycles in the culture (Fig. 2.6; SI discussion section). There is the possibility of microbial sulfate reduction-driven weathering of Fe-bearing minerals, but the low amount of quantified S in the rock suggests the impact of S *in situ* is limited.

The *in situ* community composition in the deepest weathering zone is not dominated by ASVs related to microbial Fe(III) and sulfate reduction. Most abundant ASVs are related to microorganisms living in the rhizosphere (*Bacillus* [12.5%]), saline (*Halomonas* [10.1%]) or hot environments (*Aeribacillus* [4.6%], *Mycobacterium* [2.4%] and *Rhodobacter* [2.3%]), metabolizing complex hydrocarbon compounds (*Lawsonella* [2.8%] and *Vibrionimonas* [9.1%]), or fixing N_2 (*Pedosphaeraceae* [3.0%]) (Fig. 2.5) (see Schröder et al., 1997; Cruz-Martínez et al., 2009; Yasawong et al., 2011; Filippidou et al., 2015; Khan et al., 2019; Xian et al., 2020; Campbell et al., 2021; Mahmoud et al., 2023). Moreover, *in situ* ASVs of minor relative abundance (≤2%) can be assigned to genera related to microorganisms oxidising Fe(II), sulfur and H_2 (*Sideroxydans* [<0.01%]) and utilising carbohydrates (*CL500_29_marine_group* [0.2%]) (see Warnecke et al., 2004; Lüdecke et al., 2010; J Liu et al., 2015; McIlroy et al., 2017; Chen et al., 2020; Cooper et al., 2023). Natural abiotic H_2 gas can originate from biotite hydration in granite (Murray et al., 2020) or rock comminution (i.e. fracture-induced water reduction) (Sato et al., 1984; Klein et al., 2020). Overall, the sequencing results of the *in situ* community might be explained by the low cell abundance of specific strains and high degree of adaptation and specialisation in such a water- and nutrient-deprived subsurface system. In summary, the ASVs identified from the deep subsurface of our study site paired with the geochemical/mineralogical setting most probably indicate microbial involvement in (1) Fe(II), sulfur and H_2 oxidation; (2) Fe(III) and sulfate reduction; and (3) complex hydrocarbon compound metabolism. To account for the possibility of cryptic sulfur cycling in this context, we considered the stoichiometry of probable Fe-S redox reactions (SI discussion section).

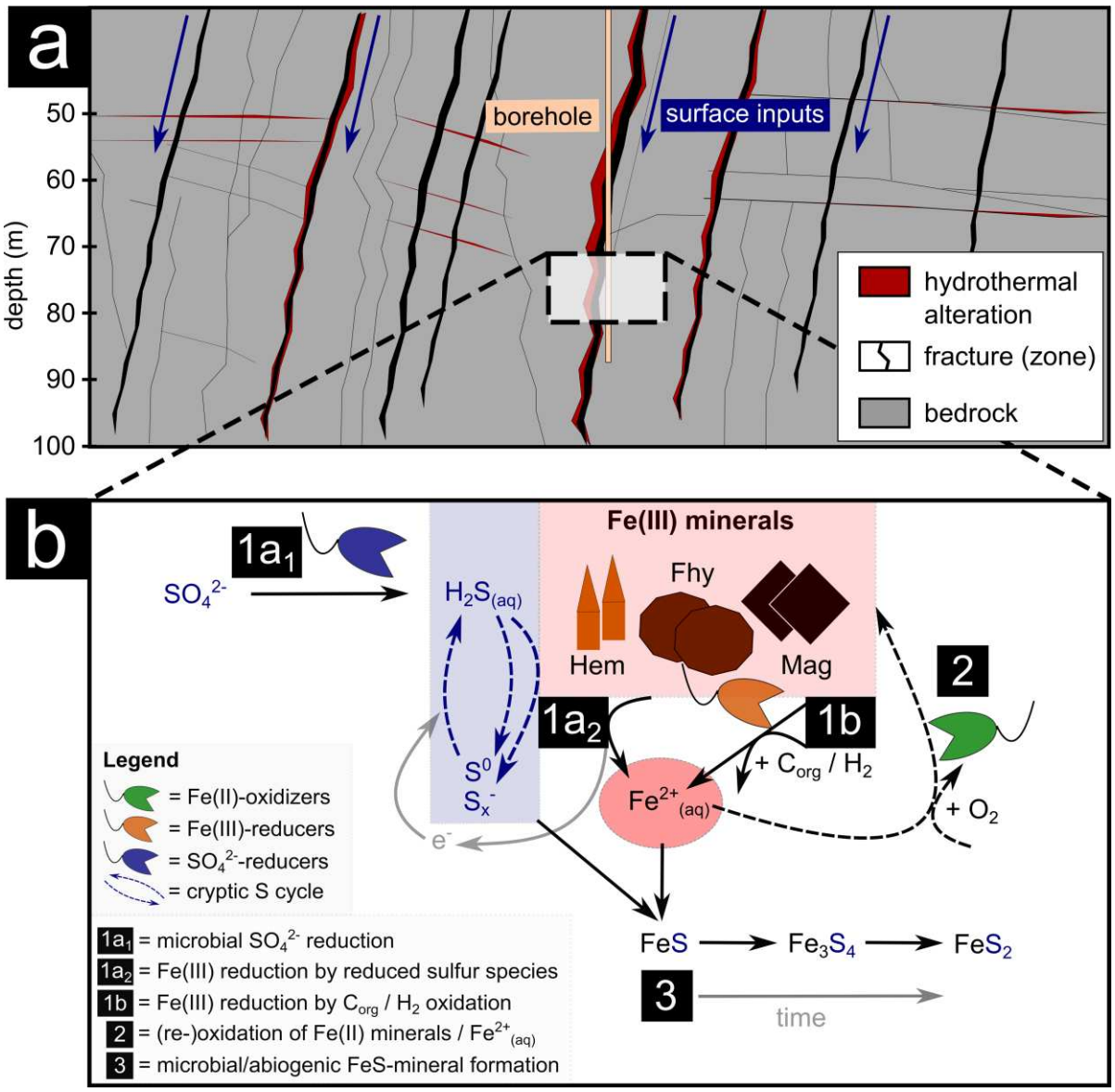

Fig. 2.6. Summary of potential, microbially driven weathering scenario in the deepest weathering zone of the SG weathering profile. (a) The subsurface is characterised by (tectonic) fracturing, hydrothermal alteration and weathering. Hydrothermal alteration and weathering are often superimposed. (b) Cartoon of a proposed microbially-driven Fe cycle, interlinked with a S cycle in the deepest, hydrothermally altered SG weathering zone (~77 m depth, cf. Fig. 2.1). Sulfate-reducing microorganisms reduce sulfate with help of a non-organic energy source as Fe(III) to reduced sulfur species (step $1a_1$). Subsequently, Fe(III) minerals can be reduced to Fe(II) when (a) reacting with highly reactive sulfur species (e.g. H_2S) (step $1a_2$), or (b) coupled to oxidation of organic carbon or dihydrogen (H_2) (step 1b). Formed Fe(II) species are reoxidised by Fe(II)-oxidising microorganisms (step 2), and/or react with reduced sulfur species and form FeS-minerals such as mackinawite or Fe(III)-mackinawite (step 3, Fig. 2.S18). Over time, FeS minerals become more crystalline (Fe_3S_4, FeS_2 formation). Reduced sulfur species can be reoxidised, fueling a cryptic S cycle and by that further amplifying Fe(III) reduction. The cryptic sulfur cycle component is probably more important in the enrichment culture than *in situ*. Abbreviations: *SO_4^{2-} = sulfate, H_2S = dihydrogen sulfide, S^0 = elemental sulfur, S_x^- = other intermediate sulfur species, Hem = hematite, Fhy = ferrihydrite, Mag = magnetite, $Fe^{2+}_{(aq)}$ = aqueous iron, FeS = (Fe(III)-)mackinawite, Fe_3S_4 = greigite, FeS_2 = pyrite, C_{org} = organic carbon, H_2 = dihydrogen, and O_2 = oxygen.*

2.6 Conclusions and environmental implications

This study has revealed the potential of microorganisms in weathering of Fe-bearing minerals in the deep subsurface of a semi-arid environment. We underpin its existence with a comprehensive cultivation approach of Fe(II)-oxidising and Fe(III)-reducing microorganisms under quasi-environmental conditions (growth conditions as close to the environment as possible). To comprehensively consider the potential for microbial Fe cycling, we included all Fe-bearing minerals in our approach, including Fe-bearing silicates.

Our main conclusions are as follows:

1. Zones of unaltered and altered rock with increased concentration of bioavailable Fe provide an Fe pool that is accessible to microorganisms.
2. Fe present in fractured and hydrothermally altered zones are not hot spots for microbial Fe(III)-reducing activity, as the minerals are probably less accessible due to their more crystalline nature.
3. Microorganisms are probably not contributing to the weathering of Fe(II)-bearing silicate minerals.
4. Secondary Fe(III) (oxyhydr)oxides are required for microbial Fe(III) reduction and hence microbial weathering activity.
5. Fe and S cycles are potentially interconnected in the deepest, hydrothermally altered weathering zone of the Santa Gracia weathering profile.
6. The microbiome of deep weathering zones has adapted towards most energy efficient redox reactions (organoheterotrophy and chemolithotrophy) to ensure survival in a water- and nutrient-deprived system.

In the deep subsurface, Fe-metabolising microorganisms contribute to weathering in both unfractured and fractured, altered rock and need to be considered when investigating deep subsurface weathering processes, even within semi-arid environments.

2.7 Author notes

Supplemental Material. Supplementary figures (Figs 2.S1-2.S18), tables (ST 2.1-2.4), methods and discussion have been deposited with the Principal Editors of Geo-Bio Interfaces and are available as Supplementary material.

Data availability. Additional supplementary tables (S1-S12, ST1-5) including raw data and thermodynamic calculations are available in the data publication Schwerdhelm et al. (2025), https://doi.org/10.5880/fidgeo.2024.027. The data publication is hosted by the GFZ data services. The raw sequencing data has been deposited at the Sequence Read Archive (SRA) under BioProject accession number PRJNA1072308 (https://www.ncbi.nlm.nih.gov/bioproject/PRJNA1072308).

Sample availability. The metadata of all the IGSN-registered samples used for this study (samples in SI tables) can be accessed via https://doi.org/10.60510/(IGSN of sample).

Author contributions.
Christopher Schwerdhelm: conceptualisation, methodology, investigation, writing – original draft preparation, writing – review & editing
Ferdinand J. Hampl: investigation, writing – review & editing
Laura V. Krone: investigation, writing – review & editing
Lea Sauter: investigation, writing – review & editing
Kari Kaphegyi: investigation, writing – review & editing
Lucas Horstmann: investigation, writing – review & editing
Daniel Straub: investigation, writing – review & editing
Toby S. Samuels: supervision, methodology, writing – review & editing
Muammar Mansor: supervision, methodology, writing – review & editing
Carolina Merino: writing – review & editing
Francisco Matus: writing – review & editing
Friedhelm von Blanckenburg: writing – review & editing
Dirk Wagner: writing – review & editing
Thomas Neumann: funding acquisition, writing – review & editing
Andreas Kappler: funding acquisition, supervision, writing – review & editing
Casey Bryce: funding acquisition, conceptualisation, supervision, writing – review & editing

Competing interests. None of the authors has any competing interests.

Acknowledgements. This study was funded by the German science foundation (DFG) priority research program EarthShape: “Earth Surface Shaping by Biota” (grant no. BR 5927/2-1; KA 1736/54-1) and the EarthShape Coordination (EH 329/17-2, BL562/20-1). We are grateful to Dixie Rivera, Kirstin Übernickel, Lars Ganzert, Axel Kitte and Ròmulo Oses for their support during the drilling campaign. We also thank the national park service of Chile (CONAF) for access to the study areas during field excursions. We further thank Monika Hertel and Björn Spranglewski for their help with IC measurements, Hanna Grimm for her help with DOC measurements, Verena Nikeleit for her help with HPLC measurements and culture maintenance/transfer, Franziska Schädler for her help with molecular microbiology sample preparation, Natalia Jakus for her help with µXRD measurements, and Eric Runge for his help with Raman spectroscopy measurements.

2.8 References

Akob D.M., Hallenbeck M., Beulig F., Fabisch M., Küsel K., Keffer J.L., Woyke T., Shapiro N., Lapidus A., Klenk H.-P. and Chan C.S. (2020) Mixotrophic Iron-Oxidizing *Thiomonas* Isolates from an Acid Mine Drainage-Affected Creek. *Applied and Environmental Microbiology* **86**(24), e01424-01420. https://doi.org/doi:10.1128/AEM.01424-20.

Aullo T., Ranchou-Peyruse A., Ollivier B. and Magot M. (2013) Desulfotomaculum spp. and related gram-positive sulfate-reducing bacteria in deep subsurface environments. *Frontiers in Microbiology* **4**. https://doi.org/10.3389/fmicb.2013.00362.

Bach W. and Edwards K.J. (2003) Iron and sulfide oxidation within the basaltic ocean crust: implications for chemolithoautotrophic microbial biomass production. *Geochimica et Cosmochimica Acta* **67**(20), 3871-3887. https://doi.org/https://doi.org/10.1016/S0016-7037(03)00304-1.

Banwart S.A., Nikolaidis N.P., Zhu Y.-G., Peacock C.L. and Sparks D.L. (2019) Soil Functions: Connecting Earth's Critical Zone. *Annual Review of Earth and Planetary Sciences* **47**, 333-359.

Barcellos D., O'Connell C., Silver W., Meile C. and Thompson A. (2018) Hot spots and hot moments of soil moisture explain fluctuations in iron and carbon cycling in a humid tropical forest soil. *Soil Systems* **2**(4), 59.

Barton K. and Barton M. (2015) Package 'mumin'. Version, 1, 18. *R Foundation for Statistical Computing: Vienna, Austria*.

Bazilevskaya E., Rother G., Mildner D.F., Pavich M., Cole D., Bhatt M.P., Jin L., Steefel C.I. and Brantley S.L. (2015) How oxidation and dissolution in diabase and granite control porosity during weathering. *Soil Science Society of America Journal* **79**(1), 55-73.

Bell E., Lamminmäki T., Alneberg J., Andersson A.F., Qian C., Xiong W., Hettich R.L., Frutschi M. and Bernier-Latmani R. (2020) Active sulfur cycling in the terrestrial deep subsurface. *The ISME Journal* **14**(5), 1260-1272.

Bernhard N., Moskwa L.-M., Schmidt K., Oeser R.A., Aburto F., Bader M.Y., Baumann K., von Blanckenburg F., Boy J. and van den Brink L. (2018) Pedogenic and microbial interrelations to regional climate and local topography: new insights from a climate gradient (arid to humid) along the Coastal Cordillera of Chile. *Catena* **170**, 335-355.

Bochet O., Bethencourt L., Dufresne A., Farasin J., Pédrot M., Labasque T., Chatton E., Lavenant N., Petton C., Abbott B.W., Aquilina L. and Le Borgne T. (2020) Iron-oxidizer hotspots formed by intermittent oxic–anoxic fluid mixing in fractured rocks. *Nature Geoscience*. https://doi.org/10.1038/s41561-019-0509-1.

Boettger J., Lin H.-T., Cowen J.P., Hentscher M. and Amend J.P. (2013) Energy yields from chemolithotrophic metabolisms in igneous basement of the Juan de Fuca ridge flank system. *Chemical Geology* **337-338**, 11-19. https://doi.org/https://doi.org/10.1016/j.chemgeo.2012.10.053.

Bolyen E., Rideout J.R., Dillon M.R., Bokulich N.A., Abnet C.C., Al-Ghalith G.A., Alexander H., Alm E.J., Arumugam M. and Asnicar F. (2019) Reproducible, interactive, scalable and extensible microbiome data science using QIIME 2. *Nature biotechnology* **37**(8), 852-857.

Brantley S.L., Goldhaber M.B. and Ragnarsdottir K.V. (2007) Crossing disciplines and scales to understand the critical zone. *Elements* **3**(5), 307-314.

Brantley S.L., Lebedeva M.I., Balashov V.N., Singha K., Sullivan P.L. and Stinchcomb G. (2017) Toward a conceptual model relating chemical reaction fronts to water flow paths in hills. *Geomorphology* **277**, 100-117.

Buss H., Bruns M., Schultz M., Moore J., Mathur C. and Brantley S. (2005) The coupling of biological iron cycling and mineral weathering during saprolite formation, Luquillo Mountains, Puerto Rico. *Geobiology* **3**(4), 247-260.

Buss H.L., Sak P.B., Webb S.M. and Brantley S.L. (2008) Weathering of the Rio Blanco quartz diorite, Luquillo Mountains, Puerto Rico: Coupling oxidation, dissolution, and fracturing. *Geochimica et Cosmochimica Acta* **72**(18), 4488-4507.

Caccavo F., Lonergan D.J., Lovley D.R., Davis M., Stolz J.F. and McInerney M.J. (1994) Geobacter sulfurreducens sp. nov., a hydrogen- and acetate-oxidizing dissimilatory metal-reducing microorganism. *Applied and Environmental Microbiology* **60**(10), 3752-3759. https://doi.org/doi:10.1128/aem.60.10.3752-3759.1994.

Callahan B.J., McMurdie P.J., Rosen M.J., Han A.W., Johnson A.J.A. and Holmes S.P. (2016) DADA2: High-resolution sample inference from Illumina amplicon data. *Nature methods* **13**(7), 581-583.

Campbell B.C., Gong S., Greenfield P., Midgley D.J., Paulsen I.T. and George S.C. (2021) Aromatic compound-degrading taxa in an anoxic coal seam microbiome from the Surat Basin, Australia. *FEMS Microbiology Ecology* **97**(5). https://doi.org/10.1093/femsec/fiab053.

Caporaso J.G., Lauber C.L., Walters W.A., Berg-Lyons D., Lozupone C.A., Turnbaugh P.J., Fierer N. and Knight R. (2011) Global patterns of 16S rRNA diversity at a depth of millions of sequences per sample. *Proceedings of the National Academy of Sciences* **108**(supplement_1), 4516-4522.

Cembrano J., González G., Arancibia G., Ahumada I., Olivares V. and Herrera V. (2005) Fault zone development and strain partitioning in an extensional strike-slip duplex: A case study from the Mesozoic Atacama fault system, Northern Chile. *Tectonophysics* **400**(1), 105-125. https://doi.org/https://doi.org/10.1016/j.tecto.2005.02.012.

Chang Y.-J., Peacock A.D., Long P.E., Stephen J.R., McKinley J.P., Macnaughton S.J., Hussain A.K.M.A., Saxton A.M. and White D.C. (2001) Diversity and Characterization of Sulfate-Reducing Bacteria in Groundwater at a Uranium Mill Tailings Site. *Applied and Environmental Microbiology* **67**(7), 3149-3160. https://doi.org/doi:10.1128/AEM.67.7.3149-3160.2001.

Chen Y., Shao Z., Kong Z., Gu L., Fang J. and Chai H. (2020) Study of pyrite based autotrophic denitrification system for low-carbon source stormwater treatment. *Journal of Water Process Engineering* **37**, 101414. https://doi.org/https://doi.org/10.1016/j.jwpe.2020.101414.

Chivian D., Brodie E.L., Alm E.J., Culley D.E., Dehal P.S., DeSantis T.Z., Gihring T.M., Lapidus A., Lin L.-H., Lowry S.R., Moser D.P., Richardson P.M., Southam G., Wanger G., Pratt L.M., Andersen G.L., Hazen T.C., Brockman F.J., Arkin A.P. and Onstott T.C. (2008) Environmental Genomics Reveals a Single-Species Ecosystem Deep Within Earth. *Science* **322**(5899), 275-278. https://doi.org/doi:10.1126/science.1155495.

Coleman G. (1960) A sulphate-reducing bacterium from the sheep rumen. *Microbiology* **22**(2), 423-436.

Cooper R.E., Finck J., Chan C. and Küsel K. (2023) Mixotrophy broadens the ecological niche range of the iron oxidizer Sideroxydans sp. CL21 isolated from an iron-rich peatland. *FEMS Microbiology Ecology* **99**(2). https://doi.org/10.1093/femsec/fiac156.

Croal L.R., Johnson C.M., Beard B.L. and Newman D.K. (2004) Iron isotope fractionation by Fe (II)-oxidizing photoautotrophic bacteria. *Geochimica et Cosmochimica Acta* **68**(6), 1227-1242.

Crosby S.A., Glasson D.R., Cuttler A.H., Butler I., Turner D.R., Whitfield M. and Millward G.E. (1983) Surface areas and porosities of iron(III)- and iron(II)-derived oxyhydroxides. *Environmental science & technology* **17**(12), 709-713. https://doi.org/10.1021/es00118a004.

Cruz-Martínez K., Suttle K.B., Brodie E.L., Power M.E., Andersen G.L. and Banfield J.F. (2009) Despite strong seasonal responses, soil microbial consortia are more resilient to long-term changes in rainfall than overlying grassland. *The ISME Journal* **3**(6), 738-744. https://doi.org/10.1038/ismej.2009.16.

Di Tommaso P., Chatzou M., Floden E.W., Barja P.P., Palumbo E. and Notredame C. (2017) Nextflow enables reproducible computational workflows. *Nature biotechnology* **35**(4), 316-319.

Ehrenreich A. and Widdel F. (1994) Anaerobic oxidation of ferrous iron by purple bacteria, a new type of phototrophic metabolism. *Applied and Environmental Microbiology* **60**(12), 4517-4526.

Ehrlich H.L. (1998) Geomicrobiology: its significance for geology. *Earth-Science Reviews* **45**(1-2)**,** 45-60.

Emerson D. and Floyd M.M. (2005) Enrichment and Isolation of Iron-Oxidizing Bacteria at Neutral pH. In *Methods in enzymology.* Academic Press, 112-123.

Ewels P.A., Peltzer A., Fillinger S., Patel H., Alneberg J., Wilm A., Garcia M.U., Di Tommaso P. and Nahnsen S. (2020) The nf-core framework for community-curated bioinformatics pipelines. *Nature biotechnology* **38**(3)**,** 276-278.

Fabisch M., Freyer G., Johnson C.A., Büchel G., Akob D.M., Neu T.R. and Küsel K. (2016) Dominance of 'Gallionella capsiferriformans' and heavy metal association with Gallionella-like stalks in metal-rich pH 6 mine water discharge. *Geobiology* **14**(1)**,** 68-90. https://doi.org/10.1111/gbi.12162.

Fan Q., Wang L., Fu Y., Li Q., Liu Y., Wang Z. and Zhu H. (2023) Iron redox cycling in layered clay minerals and its impact on contaminant dynamics: A review. *Science of The Total Environment* **855,** 159003. https://doi.org/https://doi.org/10.1016/j.scitotenv.2022.159003.

Filippidou S., Jaussi M., Junier T., Wunderlin T., Jeanneret N., Regenspurg S., Li P.-E., Lo C.-C., Johnson S. and McMurry K. (2015) Genome sequence of Aeribacillus pallidus strain GS3372, an endospore-forming bacterium isolated in a deep geothermal reservoir. *Genome announcements* **3**(4)**,** 10.1128/genomea. 00981-00915.

Finneran K.T., Johnsen C.V. and Lovley D.R. (2003) Rhodoferax ferrireducens sp. nov., a psychrotolerant, facultatively anaerobic bacterium that oxidizes acetate with the reduction of Fe(III). *International Journal of Systematic and Evolutionary Microbiology* **53**(3)**,** 669-673. https://doi.org/https://doi.org/10.1099/ijs.0.02298-0.

Fisher B.J., Moore O.W., Faust J.C., Peacock C.L. and März C. (2020) Experimental evaluation of the extractability of iron bound organic carbon in sediments as a function of carboxyl content. *Chemical Geology* **556,** 119853.

Fones E.M., Colman D.R., Kraus E.A., Nothaft D.B., Poudel S., Rempfert K.R., Spear J.R., Templeton A.S. and Boyd E.S. (2019) Physiological adaptations to serpentinization in the Samail Ophiolite, Oman. *The ISME Journal* **13**(7)**,** 1750-1762.

Fredrickson J.K. and Balkwill D.L. (2006) Geomicrobial Processes and Biodiversity in the Deep Terrestrial Subsurface. *Geomicrobiology Journal* **23**(6)**,** 345-356. https://doi.org/10.1080/01490450600875571.

Friese A., Kallmeyer J., Axel Kitte J., Montaño Martínez I., Bijaksana S., Wagner D., Team I.L.C.D.S. and Team t.I.T.D.S. (2017) A simple and inexpensive technique for assessing contamination during drilling operations. *Limnology and Oceanography: Methods* **15**(2)**,** 200-211.

Gauger T., Byrne J.M., Konhauser K.O., Obst M., Crowe S. and Kappler A. (2016) Influence of organics and silica on Fe (II) oxidation rates and cell–mineral aggregate formation by the green-sulfur Fe (II)-oxidizing bacterium Chlorobium ferrooxidans KoFox–Implications for Fe (II) oxidation in ancient oceans. *Earth and Planetary Science Letters* **443,** 81-89.

Ghosh D., Bhadury P. and Routh J. (2018) Coping with arsenic stress: Adaptations of arsenite-oxidizing bacterial membrane lipids to increasing arsenic levels. *MicrobiologyOpen* **7**(5)**,** e00594.

Gregersen L.H., Habicht K.S., Peduzzi S., Tonolla M., Canfield D.E., Miller M., Cox R.P. and Frigaard N.-U. (2009) Dominance of a clonal green sulfur bacterial population in a stratified lake. *FEMS Microbiology Ecology* **70**(1)**,** 30-41. https://doi.org/10.1111/j.1574-6941.2009.00737.x.

Gu X., Heaney P.J., Reis F.D.A.A. and Brantley S.L. (2020) Deep abiotic weathering of pyrite. *Science* **370**(6515)**,** eabb8092. https://doi.org/doi:10.1126/science.abb8092.

Hampl F.J., Schiperski F., Byrne J.M., Schwerdhelm C., Kappler A., Bryce C., von Blanckenburg F. and Neumann T. (2021) Mineralogical, geochemical and magnetic susceptibility data from a deep hydrothermally altered profile in a semi-arid region (Chilean Coastal Cordillera).

Hampl F.J., Schiperski F., Byrne J.M., Schwerdhelm C., Kappler A., Bryce C., von Blanckenburg F. and Neumann T. (2022) The role of iron-bearing minerals for the

deep weathering of a hydrothermally altered plutonic rock in semi-arid climate (Chilean Coastal Cordillera). *Chemical Geology* **604,** 120922. https://doi.org/https://doi.org/10.1016/j.chemgeo.2022.120922.

Hansel C.M., Lentini C.J., Tang Y., Johnston D.T., Wankel S.D. and Jardine P.M. (2015) Dominance of sulfur-fueled iron oxide reduction in low-sulfate freshwater sediments. *The ISME Journal* **9**(11)**,** 2400-2412.

Harris J.K., Kelley S.T. and Pace N.R. (2004) New Perspective on Uncultured Bacterial Phylogenetic Division OP11. *Applied and Environmental Microbiology* **70**(2)**,** 845-849. https://doi.org/doi:10.1128/AEM.70.2.845-849.2004.

Hegler F., Posth N.R., Jiang J. and Kappler A. (2008) Physiology of phototrophic iron (II)-oxidizing bacteria: implications for modern and ancient environments. *FEMS Microbiology Ecology* **66**(2)**,** 250-260.

Hegler F., Schmidt C., Schwarz H. and Kappler A. (2010) Does a low-pH microenvironment around phototrophic FeII-oxidizing bacteria prevent cell encrustation by FeIII minerals? *FEMS Microbiology Ecology* **74**(3)**,** 592-600.

Heidari P., Li L., Jin L., Williams J.Z. and Brantley S.L. (2017) A reactive transport model for Marcellus shale weathering. *Geochimica et Cosmochimica Acta* **217,** 421-440. https://doi.org/https://doi.org/10.1016/j.gca.2017.08.011.

Heising S., Richter L., Ludwig W. and Schink B. (1999) Chlorobium ferrooxidans sp. nov., a phototrophic green sulfur bacterium that oxidizes ferrous iron in coculture with a "Geospirillum" sp. strain. *Archives of Microbiology* **172**(2)**,** 116-124. https://doi.org/10.1007/s002030050748.

Hellige K., Pollok K., Larese-Casanova P., Behrends T. and Peiffer S. (2012) Pathways of ferrous iron mineral formation upon sulfidation of lepidocrocite surfaces. *Geochimica et Cosmochimica Acta* **81,** 69-81. https://doi.org/https://doi.org/10.1016/j.gca.2011.12.014.

Holbrook W.S., Marcon V., Bacon A.R., Brantley S.L., Carr B.J., Flinchum B.A., Richter D.D. and Riebe C.S. (2019) Links between physical and chemical weathering inferred from a 65-m-deep borehole through Earth's critical zone. *Scientific Reports* **9**(1)**,** 4495. https://doi.org/10.1038/s41598-019-40819-9.

Holm S. (1979) A Simple Sequentially Rejective Multiple Test Procedure. *Scandinavian Journal of Statistics* **6**(2)**,** 65-70.

Isherwood D. and Street A. (1976) Biotite-induced grussification of the Boulder Creek Granodiorite, Boulder County, Colorado. *GSA Bulletin* **87**(3)**,** 366-370.

Jones R.M., Goordial J.M. and Orcutt B.N. (2018) Low Energy Subsurface Environments as Extraterrestrial Analogs. *Frontiers in Microbiology* **9**(1605). https://doi.org/10.3389/fmicb.2018.01605.

Jørgensen B.B., Findlay A.J. and Pellerin A. (2019) The Biogeochemical Sulfur Cycle of Marine Sediments. *Frontiers in Microbiology* **10**. https://doi.org/10.3389/fmicb.2019.00849.

Jørgensen B.B. and Nelson D.C. (2004) Sulfide oxidation in marine sediments: geochemistry meets microbiology.

Kaksonen A.H., Spring S., Schumann P., Kroppenstedt R.M. and Puhakka J.A. (2006) Desulfotomaculum thermosubterraneum sp. nov., a thermophilic sulfate-reducer isolated from an underground mine located in a geothermally active area. *International Journal of Systematic and Evolutionary Microbiology* **56**(11)**,** 2603-2608. https://doi.org/https://doi.org/10.1099/ijs.0.64439-0.

Kallmeyer J. and Wagner D. (2014) *Microbial Life of the Deep Biosphere*. Microbial Life of the Deep Biosphere. Berlin, Boston: De Gruyter.

Kappler A., Bryce C., Mansor M., Lueder U., Byrne J.M. and Swanner E.D. (2021) An evolving view on biogeochemical cycling of iron. *Nature Reviews Microbiology* **19**(6)**,** 360-374.

Khan I.U., Habib N., Xiao M., Li M.-M., Xian W.-D., Hejazi M.S., Tarhriz V., Zhi X.-Y. and Li W.-J. (2019) Rhodobacter thermarum sp. nov., a novel phototrophic bacterium isolated from sediment of a hot spring. *Antonie van Leeuwenhoek* **112**(6)**,** 867-875. https://doi.org/10.1007/s10482-018-01219-7.

Kim H., Stinchcomb G. and Brantley S.L. (2017) Feedbacks among O2 and CO2 in deep soil gas, oxidation of ferrous minerals, and fractures: A hypothesis for steady-state regolith thickness. *Earth and Planetary Science Letters* **460,** 29-40.

Klein F., Tarnas J.D. and Bach W. (2020) Abiotic sources of molecular hydrogen on Earth. *Elements: An International Magazine of Mineralogy, Geochemistry, and Petrology* **16**(1)**,** 19-24.

Kodama Y. and Watanabe K. (2004) Sulfuricurvum kujiense gen. nov., sp. nov., a facultatively anaerobic, chemolithoautotrophic, sulfur-oxidizing bacterium isolated from an underground crude-oil storage cavity. *International Journal of Systematic and Evolutionary Microbiology* **54**(6)**,** 2297-2300.

Krone L.V., Hampl F.J., Schwerdhelm C., Bryce C., Ganzert L., Kitte A., Übernickel K., Dielforder A., Aldaz Cifuentes S.R. and Oses-Pedraza R. (2021a) Physical and geochemical data on a drill core from the semi-arid Coastal Cordillera, Chile.

Krone L.V., Hampl F.J., Schwerdhelm C., Bryce C., Ganzert L., Kitte A., Übernickel K., Dielforder A., Aldaz S., Oses-Pedraza R., Perez J.P.H., Sanchez-Alfaro P., Wagner D., Weckmann U. and von Blanckenburg F. (2021b) Deep weathering in the semi-arid Coastal Cordillera, Chile. *Scientific Reports* **11**(1)**,** 13057. https://doi.org/10.1038/s41598-021-90267-7.

Krumholz L.R., McKinley J.P., Ulrich G.A. and Suflita J.M. (1997) Confined subsurface microbial communities in Cretaceous rock. *Nature* **386**(6620)**,** 64-66. https://doi.org/10.1038/386064a0.

Kurtzer G.M., Sochat V. and Bauer M.W. (2017) Singularity: Scientific containers for mobility of compute. *PLOS ONE* **12**(5)**,** e0177459.

Lalonde K., Mucci A., Ouellet A. and Gélinas Y. (2012) Preservation of organic matter in sediments promoted by iron. *Nature* **483,** 198. https://doi.org/https://doi.org/10.1038/nature10855.

Lin L.-H., Wang P.-L., Rumble D., Lippmann-Pipke J., Boice E., Pratt L.M., Lollar B.S., Brodie E.L., Hazen T.C., Andersen G.L., DeSantis T.Z., Moser D.P., Kershaw D. and Onstott T.C. (2006) Long-Term Sustainability of a High-Energy, Low-Diversity Crustal Biome. *Science* **314**(5798)**,** 479-482. https://doi.org/doi:10.1126/science.1127376.

Liu J., Fu B., Yang H., Zhao M., He B. and Zhang X.-H. (2015) Phylogenetic shifts of bacterioplankton community composition along the Pearl Estuary: the potential impact of hypoxia and nutrients. *Frontiers in Microbiology* **6,** 64.

Lüdecke C., Reiche M., Eusterhues K., Nietzsche S. and Küsel K. (2010) Acid-tolerant microaerophilic Fe (II)-oxidizing bacteria promote Fe (III)-accumulation in a fen. *Environmental microbiology* **12**(10)**,** 2814-2825.

Lueder U., Druschel G., Emerson D., Kappler A. and Schmidt C. (2018) Quantitative analysis of O2 and Fe2+ profiles in gradient tubes for cultivation of microaerophilic Iron (II)-oxidizing bacteria. *FEMS Microbiology Ecology* **94**(2)**,** fix177.

Magot M., Ollivier B. and Patel B.K.C. (2000) Microbiology of petroleum reservoirs. *Antonie van Leeuwenhoek* **77**(2)**,** 103-116. https://doi.org/10.1023/A:1002434330514.

Mahmoud F.M., Kusari S., Kublik S.B., Siani R., Zühlke S., Radl V., Mahnkopp-Dirks F. and Schloter M. (2023) Draft Genome Sequence of the Bacterial Endophyte *Priestia megaterium* B1, Isolated from Roots of Apple (*Malus domestica*). *Microbiology Resource Announcements* **12**(6)**,** e01172-01122. https://doi.org/doi:10.1128/mra.01172-22.

Martin M. (2011) Cutadapt removes adapter sequences from high-throughput sequencing reads. *EMBnet. journal* **17**(1)**,** 10-12.

McIlroy S.J., Kirkegaard R.H., McIlroy B., Nierychlo M., Kristensen J.M., Karst S.M., Albertsen M. and Nielsen P.H. (2017) MiDAS 2.0: an ecosystem-specific taxonomy and online database for the organisms of wastewater treatment systems expanded for anaerobic digester groups. *Database* **2017,** bax016.

Ministerio de Obras Públicas de Chile D. (2016) Información oficial hidrometeorológica y de calidad de aguas en línea. In.: DGA (Dirección General de Aguas), Ministerio de Obras Públicas de Chile.

Minyard M.L., Bruns M.A., Liermann L.J., Buss H.L. and Brantley S.L. (2012) Bacterial associations with weathering minerals at the regolith-bedrock interface, Luquillo Experimental Forest, Puerto Rico. *Geomicrobiology Journal* **29**(9)**,** 792-803.

Mitchell T.M. and Faulkner D.R. (2009) The nature and origin of off-fault damage surrounding strike-slip fault zones with a wide range of displacements: A field study from the Atacama fault system, northern Chile. *Journal of Structural Geology* **31**(8)**,** 802-816. https://doi.org/https://doi.org/10.1016/j.jsg.2009.05.002.

Moser D.P., Onstott T.C., Fredrickson J.K., Brockman F.J., Balkwill D.L., Drake G.R., Pfiffner S.M., White D.C., Takai K., Pratt L.M., Fong J., Lollar B.S., Slater G., Phelps T.J., Spoelstra N., Deflaun M., Southam G., Welty A.T., Baker B.J. and Hoek J. (2003) Temporal Shifts in the Geochemistry and Microbial Community Structure of an Ultradeep Mine Borehole Following Isolation. *Geomicrobiology Journal* **20**(6)**,** 517-548. https://doi.org/10.1080/713851170.

Murray J., Clément A., Fritz B., Schmittbuhl J., Bordmann V. and Fleury J.M. (2020) Abiotic hydrogen generation from biotite-rich granite: A case study of the Soultz-sous-Forêts geothermal site, France. *Applied Geochemistry* **119,** 104631.

Napieralski S.A., Buss H.L., Brantley S.L., Lee S., Xu H. and Roden E.E. (2019) Microbial chemolithotrophy mediates oxidative weathering of granitic bedrock. *Proceedings of the National Academy of Sciences* **116**(52)**,** 26394-26401.

Napieralski S.A., Fang Y., Marcon V., Forsythe B., Brantley S.L., Xu H. and Roden E.E. (2022) Microbial chemolithotrophic oxidation of pyrite in a subsurface shale weathering environment: Geologic considerations and potential mechanisms. *Geobiology* **20**(2)**,** 271-291.

Oeser R.A., Stroncik N., Moskwa L.-M., Bernhard N., Schaller M., Canessa R., van den Brink L., Köster M., Brucker E. and Stock S. (2018) Chemistry and microbiology of the Critical Zone along a steep climate and vegetation gradient in the Chilean Coastal Cordillera. *Catena* **170,** 183-203.

Oeser R.A. and von Blanckenburg F. (2020) Do degree and rate of silicate weathering depend on plant productivity? *Biogeosciences* **17**(19)**,** 4883-4917. https://doi.org/10.5194/bg-17-4883-2020.

Ollivier B., Cayol J.-L. and Fauque G. (2007) Sulphate-reducing bacteria from oil field environments and deep-sea hydrothermal vents. In Barton L.L. and Hamilton W.A. (eds.), *Sulphate-Reducing Bacteria: Environmental and Engineered Systems.* Cambridge: Cambridge University Press, 305-328.

Onstott T.C., Ehlmann B.L., Sapers H., Coleman M., Ivarsson M., Marlow J.J., Neubeck A. and Niles P. (2019) Paleo-rock-hosted life on Earth and the search on Mars: a review and strategy for exploration. *Astrobiology* **19**(10)**,** 1230-1262.

Osburn M.R., LaRowe D.E., Momper L.M. and Amend J.P. (2014) Chemolithotrophy in the continental deep subsurface: Sanford Underground Research Facility (SURF), USA. *Frontiers in Microbiology* **5**(610). https://doi.org/10.3389/fmicb.2014.00610.

Pedersen K. (1997) Microbial life in deep granitic rock. *FEMS microbiology reviews* **20**(3-4)**,** 399-414.

Peiffer S., Behrends T., Hellige K., Larese-Casanova P., Wan M. and Pollok K. (2015) Pyrite formation and mineral transformation pathways upon sulfidation of ferric hydroxides depend on mineral type and sulfide concentration. *Chemical Geology* **400,** 44-55. https://doi.org/https://doi.org/10.1016/j.chemgeo.2015.01.023.

Peiffer S., Maisch M., Kappler A., Schmidt C., Mansor M., Obst M. and Frei S. (2024) Kinetic constraints for the formation of microniches for microaerophilic Fe(II) oxidation. *Geochimica et Cosmochimica Acta* **364,** 211-223. https://doi.org/https://doi.org/10.1016/j.gca.2023.11.006.

Perez J.R., Banwart S.A. and Puigdomenech I. (2005) The kinetics of O2 (aq) reduction by structural ferrous iron in naturally occurring ferrous silicate minerals. *Applied Geochemistry* **20**(11)**,** 2003-2016.

Pester M., Knorr K.-H., Friedrich M., Wagner M. and Loy A. (2012) Sulfate-reducing microorganisms in wetlands – fameless actors in carbon cycling and climate change. *Frontiers in Microbiology* **3**. https://doi.org/10.3389/fmicb.2012.00072.

Picard A., Kappler A., Schmid G., Quaroni L. and Obst M. (2015) Experimental diagenesis of organo-mineral structures formed by microaerophilic Fe (II)-oxidizing bacteria. *Nature Communications* **6**(1), 6277.

Poulton S.W., Krom M.D. and Raiswell R. (2004) A revised scheme for the reactivity of iron (oxyhydr) oxide minerals towards dissolved sulfide. *Geochimica et Cosmochimica Acta* **68**(18), 3703-3715.

Quast C., Pruesse E., Yilmaz P., Gerken J., Schweer T., Yarza P., Peplies J. and Glöckner F.O. (2012) The SILVA ribosomal RNA gene database project: improved data processing and web-based tools. *Nucleic acids research* **41**(D1), D590-D596.

Raiswell R., Canfield D.E. and Berner R.A. (1994) A comparison of iron extraction methods for the determination of degree of pyritisation and the recognition of iron-limited pyrite formation. *Chemical Geology* **111**(1), 101-110. https://doi.org/https://doi.org/10.1016/0009-2541(94)90084-1.

Riebe C.S., Hahm W.J. and Brantley S.L. (2017) Controls on deep critical zone architecture: a historical review and four testable hypotheses. *Earth Surface Processes and Landforms* **42**(1), 128-156. https://doi.org/10.1002/esp.4052.

Roden E.E. and Zachara J.M. (1996) Microbial Reduction of Crystalline Iron(III) Oxides: Influence of Oxide Surface Area and Potential for Cell Growth. *Environmental science & technology* **30**(5), 1618-1628. https://doi.org/10.1021/es9506216.

Ross A.M., Peoples L.M., Bilbrey E.M. and Church M.J. (2022) Draft Metagenome-Assembled Genomes from Methane-Rich Echo Lake, Montana. *Microbiol Resour Announc* **11**(2), e0111221. https://doi.org/10.1128/mra.01112-21.

Samuels T., Bryce C., Landenmark H., Marie-Loudon C., Nicholson N., Stevens A.H. and Cockell C. (2020) Microbial weathering of minerals and rocks in natural environments. In *Biogeochemical cycles: Ecological drivers and environmental impact.* 59-79.

Sato M., Sutton A.J. and McGee K.A. (1984) Anomalous hydrogen emissions from the San Andreas fault observed at the Cienega Winery, central California. *pure and applied geophysics* **122**(2), 376-391. https://doi.org/10.1007/BF00874606.

Scheibe A., Sierra C.A. and Spohn M. (2023) Recently fixed carbon fuels microbial activity several meters below the soil surface. *Biogeosciences* **20**(4), 827-838. https://doi.org/10.5194/bg-20-827-2023.

Schröder K.-H., Naumann L., Kroppenstedt R. and Reischl U. (1997) Mycobacterium hassiacum sp. nov., a new rapidly growing thermophilic mycobacterium. *International journal of systematic bacteriology* **47**(1), 86-91.

Shelobolina E., Xu H., Konishi H., Kukkadapu R., Wu T., Blöthe M. and Roden E. (2012) Microbial Lithotrophic Oxidation of Structural Fe(II) in Biotite. *Applied and Environmental Microbiology* **78**(16), 5746-5752. https://doi.org/10.1128/aem.01034-12.

Sidhu P., Gilkes R., Cornell R., Posner A. and Quirk J. (1981) Dissolution of iron oxides and oxyhydroxides in hydrochloric and perchloric acids. *Clays and Clay Minerals* **29**, 269-276.

Spring S., Visser M., Lu M., Copeland A., Lapidus A., Lucas S., Cheng J.-F., Han C., Tapia R., Goodwin L.A., Pitluck S., Ivanova N., Land M., Hauser L., Larimer F., Rohde M., Göker M., Detter J.C., Kyrpides N.C., Woyke T., Schaap P.J., Plugge C.M., Muyzer G., Kuever J., Pereira I.A.C., Parshina S.N., Bernier-Latmani R., Stams A.J.M. and Klenk H.-P. (2012) Complete genome sequence of the sulfate-reducing firmicute Desulfotomaculum ruminis type strain (DLT). *Standards in Genomic Sciences* **7**(2), 304-319. https://doi.org/10.4056/sigs.3226659.

Straub D., Blackwell N., Langarica-Fuentes A., Peltzer A., Nahnsen S. and Kleindienst S. (2020) Interpretations of environmental microbial community studies are biased by the selected 16S rRNA (gene) amplicon sequencing pipeline. *Frontiers in Microbiology* **11**, 550420.

Straub K.L., Kappler A. and Schink B. (2005) Enrichment and isolation of ferric-iron-and humic-acid-reducing bacteria. *Methods in enzymology* **397**, 58-77.

Suzuki S., Ishii S.i., Hoshino T., Rietze A., Tenney A., Morrill P.L., Inagaki F., Kuenen J.G. and Nealson K.H. (2017) Unusual metabolic diversity of hyperalkaliphilic microbial

communities associated with subterranean serpentinization at The Cedars. *The ISME Journal* **11**(11)**,** 2584-2598.
Takamiya H., Kouduka M. and Suzuki Y. (2021) The deep rocky biosphere: new geomicrobiological insights and prospects. *Frontiers in Microbiology* **12,** 785743.
Team R.C. (2024) R: A language and environment for statistical computing. R Foundation for Statistical Computing. *(No Title)*.
Trichandi R., Bauer K., Ryberg T., Scherler D., Bataille K. and Krawczyk C.M. (2022) Combined seismic and borehole investigation of the deep granite weathering structure—Santa Gracia Reserve case in Chile. *Earth Surface Processes and Landforms* **n/a**(n/a). https://doi.org/https://doi.org/10.1002/esp.5457.
Übernickel K., Ehlers T.A., Ershadi M.R., Paulino L., Fuentes Espoz J.-P., Maldonado A., Oses-Pedraza R. and von Blanckenburg F. (2020) Time series of meteorological station data in the EarthShape study areas in the Coastal Cordillera, Chile.
Voelz J.L., Johnson N.W., Chun C.L., Arnold W.A. and Penn R.L. (2019) Quantitative Dissolution of Environmentally Accessible Iron Residing in Iron-Rich Minerals: A Review. *ACS Earth and Space Chemistry* **3**(8)**,** 1371-1392.
Walter X.A., Picazo A., Miracle M.R., Vicente E., Camacho A., Aragno M. and Zopfi J. (2014) Phototrophic Fe (II)-oxidation in the chemocline of a ferruginous meromictic lake. *Frontiers in Microbiology* **5,** 713.
Wang P., Xiao X., Zhang H. and Wang F. (2008) Molecular survey of sulphate-reducing bacteria in the deep-sea sediments of the west Pacific Warm Pool. *Journal of Ocean University of China* **7**(3)**,** 269-275. https://doi.org/10.1007/s11802-008-0269-9.
Warnecke F., Amann R. and Pernthaler J. (2004) Actinobacterial 16S rRNA genes from freshwater habitats cluster in four distinct lineages. *Environmental microbiology* **6**(3)**,** 242-253.
Weckmann U., Bauer K., Krawczyk C., Kück J., Übernickel K. and von Blanckenburg F. (2020) Geophysical borehole logging data from Santa Gracia, Chile.
White A.F. and Yee A. (1985) Aqueous oxidation-reduction kinetics associated with coupled electron-cation transfer from iron-containing silicates at 25 C. *Geochimica et Cosmochimica Acta* **49**(5)**,** 1263-1275.
Wickham H. (2016) Programming with ggplot2. In Wickham H. (ed.), *ggplot2: Elegant Graphics for Data Analysis.* Cham: Springer International Publishing, 241-253.
Widdel F. (1980) Anaerober Abbau von Fettsauren and Benzosaure durch neu isolierte Arten sulfat-reduzierender Bakterien.(Anaerobic Degradation of Fatty Acids and Benzoic Acid by Newly Isolated Types of Sulfate-Reducing Bacteria). Doctoral Dissertation, Georg-August-Universität, Gottingen.
Widdel F., Kohring G.-W. and Mayer F. (1983) Studies on dissimilatory sulfate-reducing bacteria that decompose fatty acids. *Archives of Microbiology* **134**(4)**,** 286-294.
Widdel F. and Pfennig N. (1981) Studies on dissimilatory sulfate-reducing bacteria that decompose fatty acids. *Archives of Microbiology* **129**(5)**,** 395-400.
Widdel F., Schnell S., Heising S., Ehrenreich A., Assmus B. and Schink B. (1993) Ferrous iron oxidation by anoxygenic phototrophic bacteria. *Nature* **362**(6423)**,** 834-836. https://doi.org/10.1038/362834a0.
Xian W.-D., Liu Z.-T., Li M.-M., Liu L., Ming Y.-Z., Xiao M., Salam N. and Li W.-J. (2020) Rhodobacter flagellatus sp. nov., a thermophilic bacterium isolated from a hot spring. *International Journal of Systematic and Evolutionary Microbiology* **70**(3)**,** 1541-1546. https://doi.org/https://doi.org/10.1099/ijsem.0.003929.
Xiao D., Brantley S.L. and Li L. (2021) Vertical Connectivity Regulates Water Transit Time and Chemical Weathering at the Hillslope Scale. *Water Resources Research* **57**(8)**,** e2020WR029207. https://doi.org/https://doi.org/10.1029/2020WR029207.
Yao W. and Millero F.J. (1996) Oxidation of hydrogen sulfide by hydrous Fe (III) oxides in seawater. *Marine Chemistry* **52**(1)**,** 1-16.
Yasawong M., Areekit S., Pakpitchareon A., Santiwatanakul S. and Chansiri K. (2011) Characterization of thermophilic halotolerant Aeribacillus pallidus TD1 from Tao dam hot spring, Thailand. *International journal of molecular sciences* **12**(8)**,** 5294-5303.

Zhuang K., Izallalen M., Mouser P., Richter H., Risso C., Mahadevan R. and Lovley D.R. (2011) Genome-scale dynamic modeling of the competition between Rhodoferax and Geobacter in anoxic subsurface environments. *The ISME Journal* **5**(2)**,** 305-316. https://doi.org/10.1038/ismej.2010.117.

Zuur A.F., Ieno E.N., Walker N.J., Saveliev A.A. and Smith G.M. (2009) *Mixed effects models and extensions in ecology with R*. Springer.

2.9 Supplementary Information

Microbial weathering of Fe-bearing minerals in deep hydrothermally altered granitic rock of a semi-arid environment (Chilean Coastal Cordillera): Supplementary Files

C. Schwerdhelm, F. J. Hampl, L. V. Krone, L. Sauter, K. Kaphegyi, L. Horstmann, D. Straub, T. Samuels, M. Mansor, C. Merino, F. Matus, F. v. Blanckenburg, D. Wagner, T. Neumann, A. Kappler, C. Bryce*

*Correspondence: Dr. Casey Bryce

Supplementary Material and Methods (Detailed and extended version)

Selective extractions

Selective Fe extractions using hydrochloric acid (0.5 M HCl) and citrate-bicarbonate dithionite (CBD) were performed on samples of the entire weathering profile to quantify Fe pools available for microbial redox reactions (*N* = 59, technical extraction triplicates). 20 mL glass vials were treated with 1 M HCl for 15 min, washed three times with DI water, and sterilized at 180°C in the oven for 4.5 h. 0.25 g of soil / rock powder were weighed into headspaces vial with 15 mL extractant. Each sample was extracted in triplicates as described in detail below. The extractions were carried out in the dark, under anoxic conditions with N_2 headspace for 0.5 M HCl extractions and under oxic conditions for CBD extractions. An aliquot of 2 mL of the well-mixed extraction solution was taken into a fresh 2 mL Eppendorf tube and centrifuged at room temperature for 10 min at 12,100 g. After centrifugation, the supernatant was diluted in anoxic 1 M HCl for Fe quantification via ferrozine assay (Hegler et al., 2008). Furthermore, water extractable organic carbon (DOC) and nitrate were extracted to quantify the potentially available amount of these as electron sources for microbial Fe(III) reduction and Fe(II) oxidation. 0.25 g of soil / rock powder were weighed into Falcon tubes with 10 mL extractant. After 24 h of extraction, Falcon tubes were centrifuged for 15 min at 7000 g. Supernatants were stored at 4°C to avoid organic carbon precipitation. DOC concentrations of the water extracts were quantified with a carbon analyser (Multi N/C 2100 s, Analytik Jena, Germany). Water extractable nitrate was quantified by using a continuous flow analyser (CFA, AA3 HR System, SEAL Analytical). Both reported dissolved organic carbon and nitrate values were blank corrected. Details of the extractions are as follows:

0.5 M HCl. 0.5 M HCl is considered to extract operationally defined bioavailable Fe-bearing phases such as ferrihydrite and lepidocrocite. We extracted the bioavailable Fe with

0.5 M HCl at room temperature under anoxic conditions in the dark for 24 h, while shaking at 10 rpm (solid:liquid = 1:60) (Raiswell et al., 1994; Roden and Zachara, 1996).

Citrate bicarbonate dithionite*.* CBD targets reactive Fe minerals such as ferrihydrite, lepidocrocite, akageneite, goethite and hematite via reductive dissolution (Voelz et al., 2019). Extractions were done using a solution of 0.27 M trisodium citrate, 0.11 M sodium bicarbonate, and 0.1 M sodium dithionite (Lalonde et al., 2012). Samples were extracted in the dark under oxic conditions for 15 min, and in a water bath at 75-80°C (solid:liquid = 1:60). Extraction time was kept short and not extended to 24 hours as done for the HCl extraction, since % extractable Fe is primarily a function of added dithionite amount (Fisher et al., 2020). The pH of the CBD solution was circumneutral to obtain maximal reduction potential and to avoid precipitation of sulfides.

Water extractions*. 10 mL* MilliQ water was added to 0.25 g crushed rock to target water extractable organic carbon and nitrate. The extract was analysed with a multi N/C 2100S elemental analyser for organic carbon concentrations (Analytik Jena GmbH, Germany) via combustion (detection limit = 0.022 mg C g^{-1} rock). Nitrate in the extracts was analysed with a Flow-injection analyser (FIA) using an AA3 HR AutoAnalyser System (Seal Analytical, Germany) (detection limit = 0.0002 mg N g^{-1} rock). Extractions were performed under oxic conditions at room temperature in the dark, for 24 h on a shaker (shaking frequency f = 180 s^{-1}) (solid:liquid = 1:40).

X-ray diffraction (XRD)

X-ray diffraction on five representative fine-powered (<10 µM) fracture surface samples of Santa Gracia drill core profile was conducted to identify Fe mineral phases present in the deep subsurface. The identified phases were later used for thermodynamic calculations. A Bruker D2 Phaser XRD device with Bragg-Brentano geometry and Cu anode (Department of Applied Geochemistry, Technische Universität Berlin, Germany) was employed to record diffraction data in the range of 3–80° 2θ at a step width of 0.01° 2θ and a time per step of 0.5 s (detector opening angle: 4°, lower/upper discriminator of detector: 0.180/0.280, airscatter 1.0 mm, divergence aperture: 1.0 mm, Ni-filter, Soller slit 2.5◦, sample rotation: 20/min, voltage: 30 kV, current: 10 mA, scantype: Coupled TwoTheta/Theta). The samples were mounted on a silicon single crystal holder (Bruker).

pH

Potential and active pH of drill core samples taken for microbiological investigations and thermodynamic calculations was quantified. Mean potential and active pH provide estimates for the exchangeable activity and active activity of rock water solutions. While exchangeable activity refers to the amount of hydrogen, aluminum and acid cations present in rock water solution, active activity only comprises hydrogen ions. Potential pH was determined by addition

of 0.01 M $CaCl_2$, while MilliQ water was added to quantify active pH according to the European Norm of International Organization for Standardisation (EN ISO 10390:2022-08). More specifically, 2 g or air-dried soil (< 63 µm grain size) were weighed into 15 mL Falcon tubes and either 10 mL 0.01 M $CaCl_2$ or 10 mL MilliQ water were added Falcon tubes were shaken, and the slurries left untouched for 1 h. Thereafter, Falcon tubes were shaken again and the pH was measured in the overlying solution. The procedure was repeated after 24 h to exclude a major shift in pH (*N* = 10, technical extraction triplicates).

Cultivation of microorganisms

Aseptically crushed soil/rock samples were used as inoculum to identify zones of active microbial Fe(II) oxidation and/or Fe(III) reduction (*N* = 59). Fe was provided as an FeS layer in gradient tubes for microaerophilic Fe(II)-oxidising bacteria (3 replicates per depth interval), and as (b) synthesized 2-line ferrihydrite (Fhy) (as described in Straub et al., 2005) in 96 deep-well plates for Fe(III) reduction coupled to acetate/lactate or dihydrogen gas oxidation (6 replicates per depth interval). Under lab conditions, the Fe minerals provided were assumed to be bioavailable in addition to the Fe already present in the environmental samples. For inoculation, crushed core samples were mixed with anoxic mineral medium and added to each setup.

Microaerophilic Fe(II)-oxidising bacteria were grown in gradient tubes following the protocol of Emerson and Floyd (2005), in which we established opposing gradients of oxygen and Fe^{2+} in 8 mL screw cap vials containing MWMM (recipe according to Emerson and Floyd, 2005) by addition of a 760 µL FeS plug (bottom layer) containing 1 % (wt./vol) high-melt agarose. Thereafter, 10 µL of diluted sample from the hungate tubes were injected into the gradient tubes. Positive growth was indicated by formation of an orange band (compared to an abiotic control tube = negative control), as exemplified in Lueder et al. (2018). As positive control, a microaerophilic Fe(II)-oxidising enrichment culture from a mine (Segen Gottes Mine, SW Germany) dominated by *Curvibacter* sp. (Picard et al., 2015) from the laboratory culture collection was used.

In order to enrich Fe(III)-reducing bacteria, an anoxic (N_2:CO_2 90:10) mineral medium (0.6 g/L KH_2PO_4, 0.3 g/L NH_4Cl, 0.5 g/L $MgSO_4$ x 7 H_2O, 0.1 $CaCl_2$ x 2 H_2O, 2.5 g/L $NaHCO_3$, 1 mL trace elements SL10 (Widdel et al., 1983), 1 mL/L 7 vitamin solution (Widdel and Pfennig, 1981), and 1 mL/L selenite/tungstate solution (Widdel, 1980) was amended with Fhy as an Fe source and either a mix of 5 mM sodium acetate and 5 mM sodium lactate, or H_2 gas in excess as an electron donor for Fe(III) reduction. After media preparation, we dispensed 900 µL of the respective media mix into each well of the 96 deep-well plate in an anoxic glovebox (N_2 atmosphere), and added 100 µL soil/rock slurry. The 96 deep-well plates contained 12 samples (first six rows = biological replicates), a negative control (seventh row, 12 replicates) and a

positive control (eighth row, 12 replicates). The negative control consisted of mineral medium amended with Fhy, while the positive control consisted of mineral medium amended with Fh and addition of *Geobacter sulfurreducens* (see Caccavo et al., 1994) from the laboratory culture collection. 96 deep-well plates were anoxically incubated with an Anaerocult System and O_2 indicator stick (Merck, Germany) for 8 weeks at room temperature in the dark. Positive growth evaluation was based on the formation of black-coloured, reduced Fe(II) minerals in comparison to rusty-orange coloured control wells (Fig. 2.S3).

Since Fhy was added as an electron source in addition to the Fe species already present in the environmental samples, control experiments without Fhy were carried out. These experiments included 11 powdered drill core samples to account for background Fe mineral dissolution from the Fe pool of the environmental samples. In these control experiments, powdered drill core samples were added in the 96 deep-well plates using the same media components as for the cultivation experiments, but in contrast did not contain 2-line ferrihydrite as an additional Fe(III) source.

Fe(III)-reducing enrichments from the eight most promising depth intervals were transferred four times each into Hungate tubes (N = 8, four biological replicates each) to obtain a robust Fe(III)-reducing enrichment culture. One robust Fe(III)-reducing culture was obtained and further characterised as outlined below. For convenience, the robust Fe(III)-reducing culture is referred to as “culture SG”.

Sampling and chemical analysis

For the ferrihydrite reduction experiments, sampling was performed in an anoxic glovebox (100% N_2) by taking an aliquot of 0.6 mL with a needle and syringe (0.55 mm) into a 2 mL Eppendorf tube.

Fe quantification. 0.1 mL of well mixed, resuspended slurry was diluted in 0.9 mL of 6 M HCl, vortexed and anoxically extracted for 24 h to target crystalline Fe phases. Extracts were centrifuged at room temperature for 10 min at 12100 g, and supernatant diluted in anoxic 1 M HCl to avoid abiotic Fe(II) oxidation and quantify Fe(II) and Fe(tot) via a ferrozine assay (Hegler et al., 2008).

High pressure liquid chromatography (HPLC). Prior to transfer into HPLC vials, Eppendorf tubes were stored oxically on the lab bench to support Fe mineral precipitation. Subsequently, the Eppendorf tubes were centrifuged and 150 µL of supernatant transferred into HPLC vials. HPLC vials were stored cold at 4°C until measurement. Lactate and acetate were quantified by using a HPLC device (Shimadzu, Kyoto, Japan) equipped with an Aminex HPX 87H column (BioRad, Hercules, USA), a refractive index detector for lactate and a diode array detector for acetate analysis.

Supplementary Discussion Section

Potential interconnections of the Fe and S cycles

As sulfate is a part of our growth medium, the observed Fe(III) reduction in ferrihydrite microcosms could also be driven by microbial sulfate reduction and subsequent reaction of reactive reduced S species with poorly crystalline and hence highly reactive Fhy (Figs 2.4,2.S16,2.S18). This “cryptic sulfur cycling” occurs in marine and terrestrial environmental systems (Pester et al., 2012; Hansel et al., 2015; Jørgensen et al., 2019; Bell et al., 2020), and our results suggest that Fe and S cycles are probably interconnected in our enrichment culture. Sequencing data (Fig. 2.5) and 9 µM of water extractable sulfate from the deepest weathering zone in 77 m depth suggest this is possible *in situ*. However, it is important to note the low amount of S quantified in the rock which suggests that the overall impact of S cycling on weathering is probably limited.

To assess how much Fhy (mM) in the microcosms could have been reduced by reactive reduced S species, we considered the stoichiometry of probable Fe-S redox reactions:

Step 1: Microbially driven sulfate reduction

$$SO_4^{2-} + 2C_3H_5O_3^- \Rightarrow H_2S + 2C_2H_3O_2^- + 2HCO_3^- \quad (1)$$

Step 2: Ferrihydrite reduction coupled with sulfide oxidation (e.g. H_2S)

$$H_2S + 2Fe(OH)_3 + 4H^+ \Rightarrow S^0 + Fe^{2+} + 6H_2O \quad (2)$$

Step 3: Re-reduction of oxidised sulfur species S^0 through reduction coupled to (a) H_2, (b_1, b_2) organics (Hansel et al., 2015) or (c) disproportionation (Jørgensen and Nelson, 2004)

$$(a)\ S^0 + H_2 \Rightarrow H_2S \quad (3)$$

$$(b_1)\ 2S^0 + C_3H_5O_3^- + 2H_2O \Rightarrow 2HS^- + C_2H_3O_2^- + HCO_3^- + 3H^+ \quad (4)$$

$$(b_2)\ 4S^0 + C_2H_3O_2^- + 4H_2O \Rightarrow 4HS^- + 2HCO_3^- + 5H^+ \quad (5)$$

$$(c)\ 4S^0 + 4H_2O \Rightarrow 3H_2S + SO_4^{2-} + 2H^+ \quad (6)$$

In essence, this means that 1 mM of sulfate results in the formation of 1 mM dihydrogen sulfide (1). This amount of produced dihydrogen sulfide is enough to reduce 2 mM of ferrihydrite, while forming 1 mM of elemental sulfur (2). The elemental sulfur could be reduced to H_2S again, via S^0 reduction or S^0 disproportionation (reactions (3) - (6)) (Jørgensen et al., 2019). Since all three reactions are possible, we cannot eliminate one or the other without further investigations. Thus, repeated microbial cycling of S species could in theory reduce all ferrihydrite in the enrichment culture without any necessity for direct microbial Fe(III) reduction. This argument assumes that S^0 is the sole S-containing product when H_2S reacts with Fe(III), which is possible as shown in previous studies (Yao and Millero, 1996; Poulton et al., 2004). However, a portion of the H_2S could react with Fe^{2+} to form the mineral mackinawite (FeS),

which was detected by Raman spectroscopy (Fig. 2.S18). The balance between S^0 and FeS formation depends on the electron transfer rate from Fe(II) to Fe(III) (oxyhydr)oxides, which is controlled by the ratio between dissolved sulfide, available mineral surface sites and pH (Hellige et al., 2012; Peiffer et al., 2015). Thus, microbial S cycling could be a mediator of abiotic Fe(III) reduction in our system while not excluding the contribution from direct microbial Fe(III) reduction.

Supplementary Tables and Figures

Supplementary Tables

Supplementary Table 2.1. Fe(III) reduction done by the *in situ* microbial community *in vitro* from samples taken from the SG weathering profile. The extent of Fe(III) reduction is compared between altered and non-altered zones as well as between the electron donors H_2 and organics. *N* denotes the sample size for each zone. This summary table is complementary to Figure 2.3.

Zone	Depth (m)	Alteration	Fe(III) reduction (%)		*N*
			H_2	organics	
#1	5.3 - 10.3	yes	19.8	30.4	3
#2	10.3 - 14.3	no	23.2	23.8	2
#3	14.3 - 19.7	yes	16.3	23.1	4
#4	19.7 - 23.0	no	18.5	30.7	3
#5	23.0 - 26.0	yes	22.0	17.2	2
#6	26.0 - 40.0	no	17.5	25.2	7
#7	40.0 - 47.7	yes	25.5	34.2	4
#8	47.7 - 57.3	no	28.6	42.2	5
#9	57.3 - 60.0	yes	22.1	28.1	1
#10	60.0 - 67.0	no	25.6	31.1	3
#11	67.0 - 76.5	yes	28.6	37.3	7
#12	76.5 - 90.0	no	47.5	46.1	6

Supplementary Table 2.2. Terms within the general linear model used to explain *in situ* microbial Fe(III) reduction. Model terms used in the R statistical environment are the Akaike Information criterion (AIC), degrees of freedom (df), log likelihood of the model (logLik), corrected Akaike information criterion (AICc), difference in AICc score (delta) and the predictive model power (weight). Best-fit model is listed first, indicated by the lowest AIC and AICc values. The best-fit model formula is fe.red_4 <- lm(fe_red ~ E_donor + depth + setup + Fe_bio + Fe_cryst + Fe_bio*depth + Fe_bio*setup + Fe_cryst*depth, data=Fe3). For the sake of completeness of information: fe.red_3 <- lm(fe_red ~ E_donor + depth + setup + Fe_bio + Fe_cryst + Fe_bio*depth, data=Fe3); fe.red_2 <- lm(fe_red ~ E_donor * setup * depth * Fe_bio * Fe_cryst, data=Fe3); fe.red_1 <- lm(fe_red ~ E_donor + setup + depth + Fe_bio + Fe_cryst, data=Fe3).

Model	AIC	df	logLik	AICc	delta	weight
fe.red_4	907.2	10	-443.605	909.3	0.00	0.939
fe.red_3	913.4	8	-448.718	914.8	5.48	0.061
fe.red_1	923.4	7	-454.705	924.4	15.14	0.000
fe.red_2	918.0	33	-425.991	945.3	36.04	0.000

Supplementary Table 2.3. Analysis of Variance Table for best-fit model. Model terms, degrees of freedom (df), sum of squares (Sum Sq), mean of squares (Mean Sq), effect sizes (F values), significance (*P* values) and percent variance explained by terms (Var. (%)) within the statistical model (fe.red_4) to explain variation in Fe(III) reduction. Terms in bold were statistically significant at $P < 0.05$.

Model term	df	Sum Sq	Mean Sq	F value	*P* value	Var. (%)
E_donor	1	1740.26	1740.26	13.07	**0.000459**	5.3
depth	1	6480.52	6480.52	48.68	**< 0.0001**	19.7
setup	1	2471.30	2471.30	18.56	**< 0.0001**	7.5
Fe_bio	1	2158.69	2158.69	16.22	**0.000106**	6.6
Fe_cryst	1	750.12	750.12	5.63	**0.019389**	2.3
depth:Fe_bio	1	1691.80	1691.80	12.71	**0.000545**	5.1
setup:Fe_cryst	1	578.17	578.17	4.34	**0.039537**	1.8
depth:Fe_cryst	1	734.50	734.50	5.52	**0.020662**	2.2
Residuals	107	14243.67	133.12	NA	NA	49.6

Supplementary Table 2.4. *post hoc* paired-samples t-tests, corrected with Holm's sequential Bonferroni procedure, were run for comparing within-group means of the two factorial variables 'E_donor' and 'setup'. Note that negative estimate values indicate that the extent of Fe(III) reduction is greater for the second eda/setup-term within the pair. SE denotes standard error. Pairwise comparisons that were significant at $P < 0.05$ are highlighted in bold. Scientifically relevant comparisons are marked with an asterisk (*).

E_donor/setup comparison	Estimate	SE	df	T ratio	*P* value
H_2 ctrl - org ctrl*	-7.75	2.14	107	-3.616	**0.0014**
H_2 ctrl - H_2 exp*	-14.91	3.09	107	-4.821	**< 0.0001**
H_2 ctrl - org exp	-22.66	3.76	107	-6.022	**< 0.0001**
org ctrl - H_2 exp	-7.17	3.76	107	-1.904	0.0596
org ctrl - org exp*	-14.91	3.09	107	-4.821	**< 0.0001**
H_2 exp - org exp*	-7.75	2.14	107	-3.616	**0.0014**

Supplementary Figures

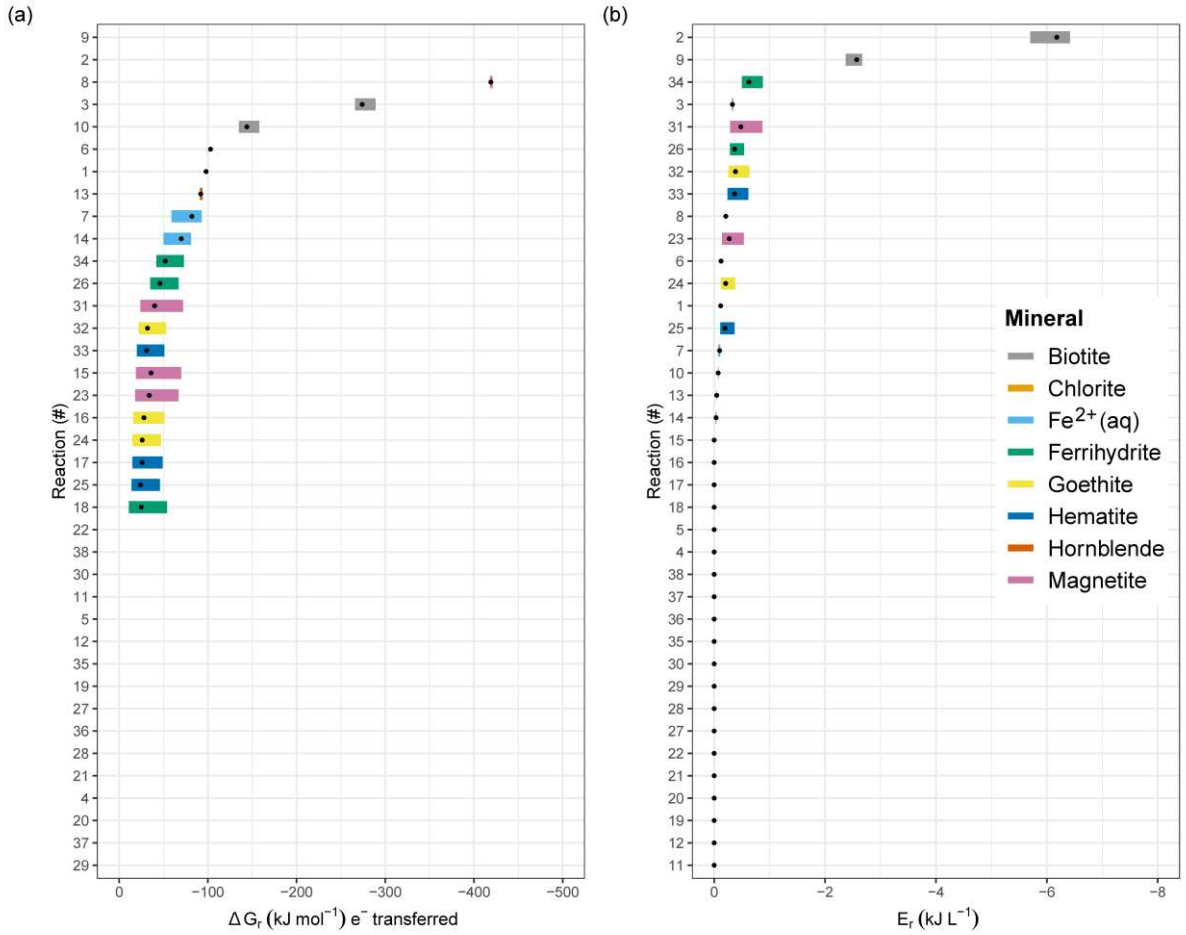

Fig. 2.S1. Gibbs free energy of Fe(II) oxidation and Fe(III) reduction redox reactions per electron transferred (left) versus energy density of identical redox reactions (right) for *in situ* conditions. The redox reactions (# 1-38) represent 14 oxidation and 24 reduction reactions for major Fe minerals present in Santa Gracia drill core profile (Table 2.1). (a) Gibbs free energy per mole of electron transferred and (b) energy density as kilojoule per litre are shown for Fe(II) oxidation coupled to electron acceptors oxygen and nitrate as well as for Fe(III) reduction coupled to dihydrogen, acetate, and lactate. Gibbs free energy and energy density values of redox reactions are shown for fixed concentrations and a pH range of 6-9. Black dots represent Gibbs free energy values of redox reactions for pH 8, which is about the potential *in situ* pH of SG drill core samples (Fig. 2.S3). Positive Gibbs free energy values are not shown as they are not thermodynamically favourable, which is also true for positive energy densities values set to “0”.

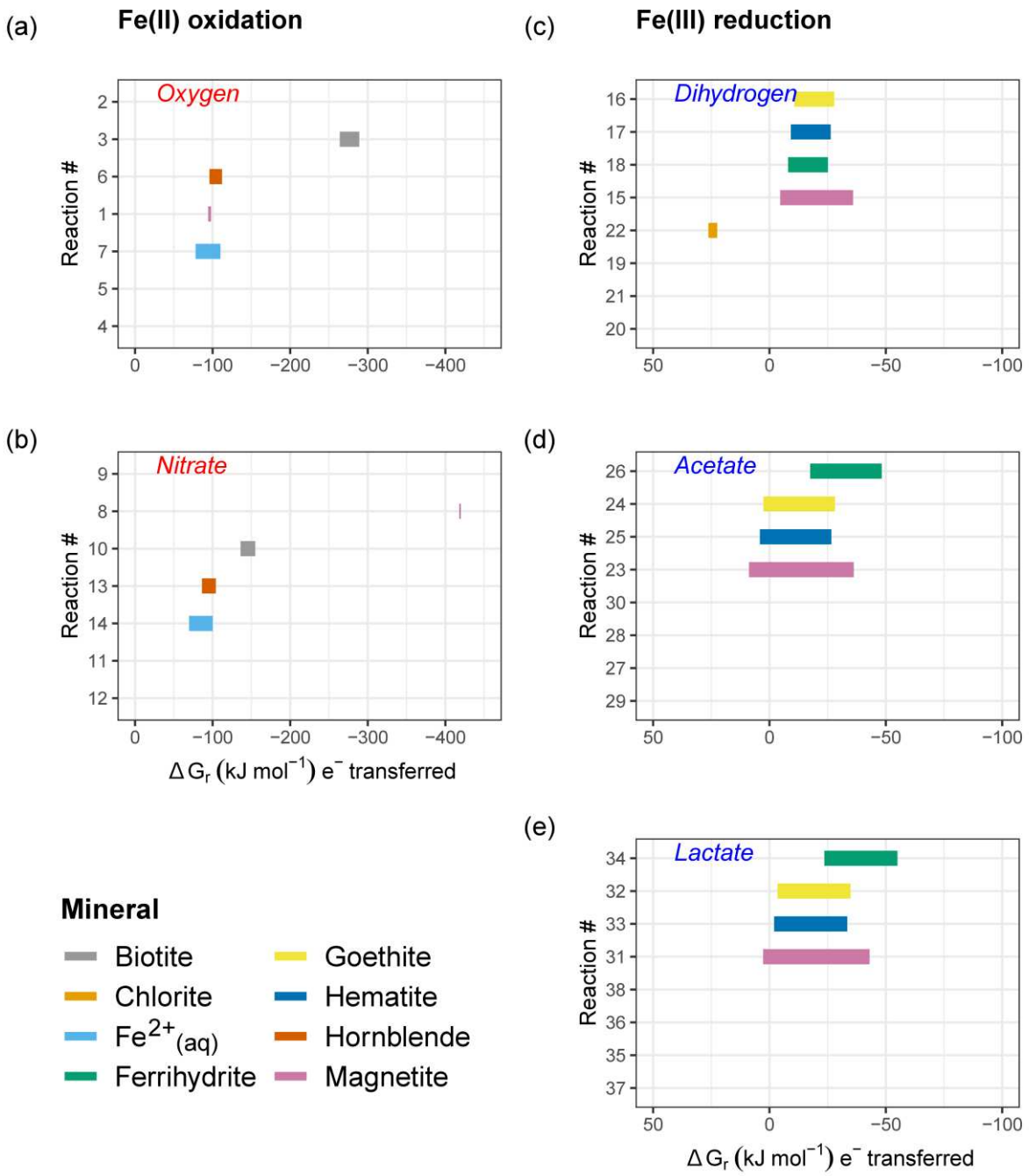

Fig. 2.S2. Gibbs free energy of Fe(II) oxidation and Fe(III) reduction redox reactions per electron transferred for *in situ* conditions. The redox reactions (# 1-38) represent 14 oxidation and 24 reduction reactions for major Fe minerals present in Santa Gracia drill core profile (Table 2.1). Gibbs free energy per mole of electron transferred is shown for Fe(II) oxidation (left) coupled to (a) O_2 reduction; (b) nitrate reduction; as well as for Fe(III) reduction (right) coupled to (c) dihydrogen oxidation; (d) acetate oxidation; and (e) lactate oxidation. Gibbs free energy values of redox reactions are shown for a concentration range and a fixed pH of 8. Gibbs free energy of Fe(II) oxidation reactions #4, 5, 11, and 12 are not displayed, because they are highly positive and hence not thermodynamically favourable, or in the case of reactions #2 and 9, unrealistically favourable. Energetic yields for Fe(III) reduction reactions #19-21, 27-30, and 35-38 are not shown as they are highly unfavourable.

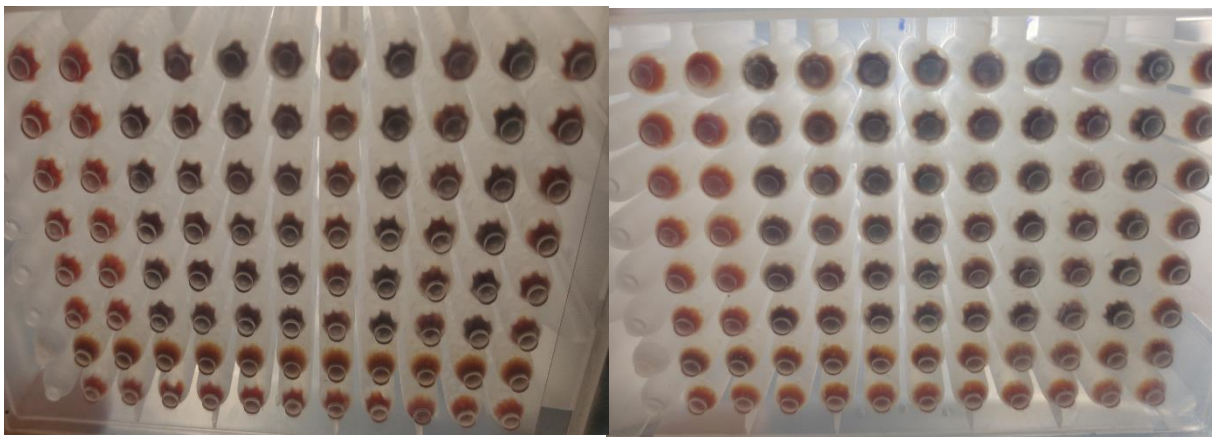

Fig. 2.S3. Fe(III)-reducing enrichments in anoxic 96 deep-well plates. Fe(III)-reducers within powdered drill core samples were enriched with ferrihydrite as an Fe source (electron acceptor) and either (a) dihydrogen (left side) or (b) organic carbon (right side) (electron donor). Incubations were set up under anoxic conditions, in the dark, at room temperature. Brown reddish colour at the bottom and left hand side is indicative for negative controls with ferrihydrite but no cell addition, while blackish colour shows microbially driven Fe(III) reduction by the respective *in situ* communities (N = 6, biological replicates / depth).

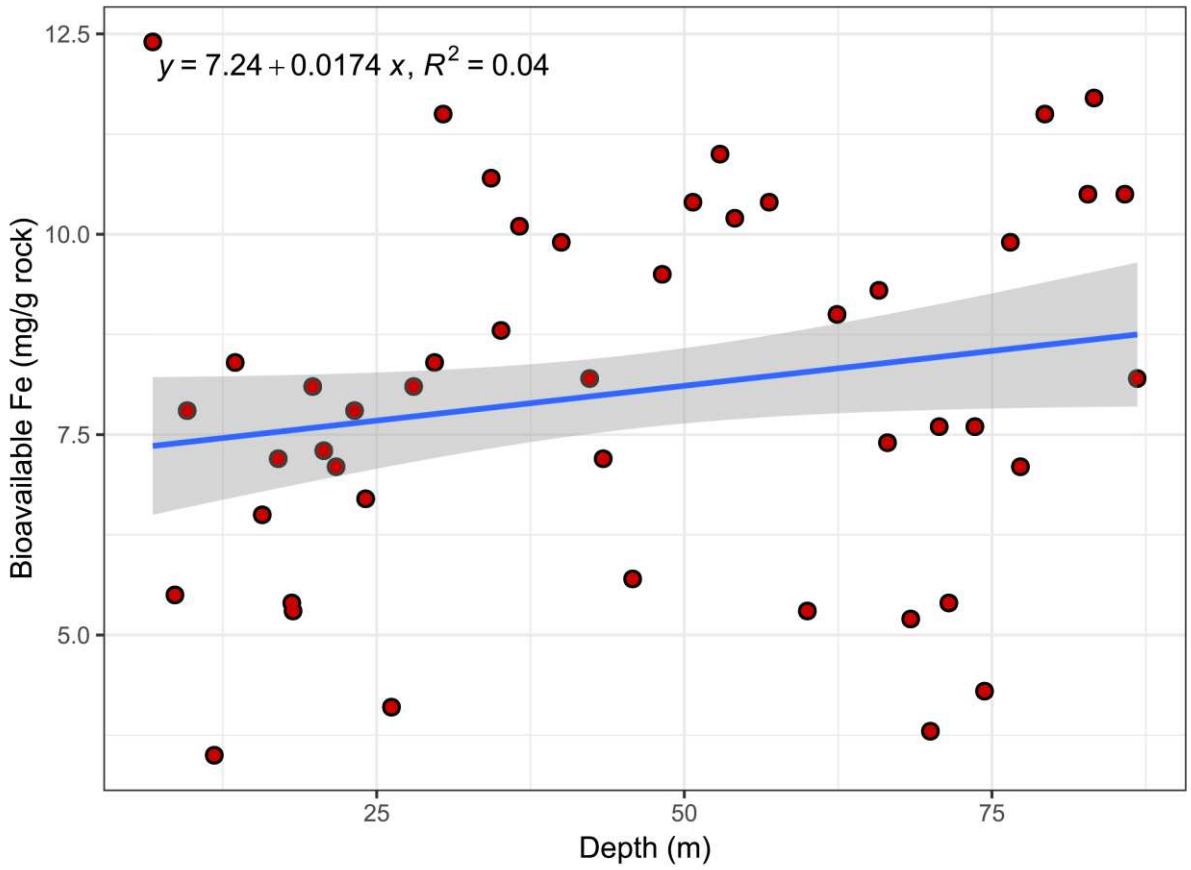

Fig. 2.S4. Linear regression plot of bioavailable Fe versus depth. The amount of "bioavailable" (amorphous) Fe (mg/g rock) does not significantly increase with depth (m), while having a very weak correlation (R^2 = 0.04). For each unit increase in depth, bioavailable Fe increased by 0.017 (mg/g rock) (slope = 0.017, t = 1.8, df = 92, *P* = 0.07). The blue line shows the regression line, while its equation is shown in the top left corner. The grey area surrounding the regression line denotes the 95% confidence interval of the linear model fit.

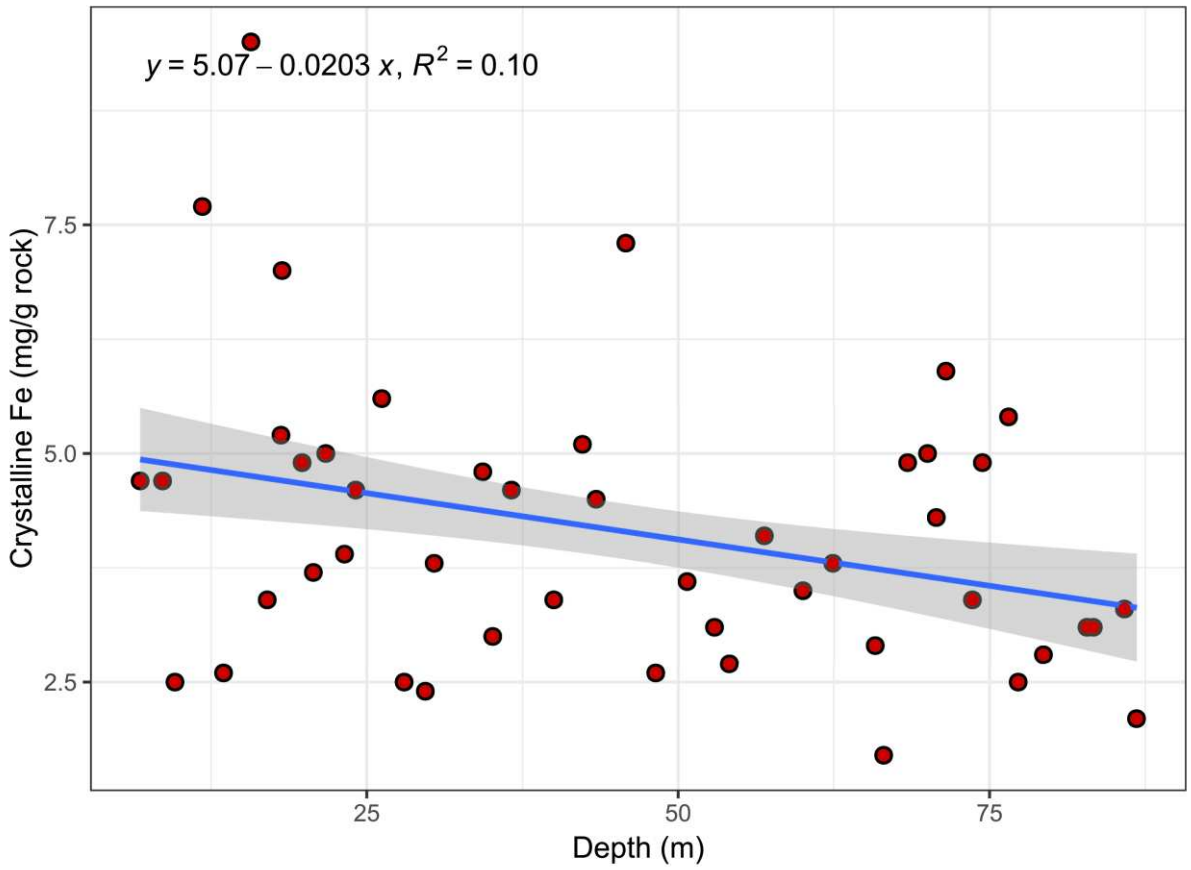

Fig. 2.S5. Linear regression plot of crystalline Fe versus depth. The amount of crystalline Fe (mg/g rock) does significantly decrease with depth (m), while having a very weak correlation (R^2 = 0.10). For each unit increase in depth, crystalline Fe decreased by 0.02 (mg/g rock) (slope = -0.02, t = -3.3, df = 92, P < 0.01). The blue line shows the regression line, while its equation is shown in the top left corner. The grey area surrounding the regression line denotes the 95% confidence interval of the linear model fit.

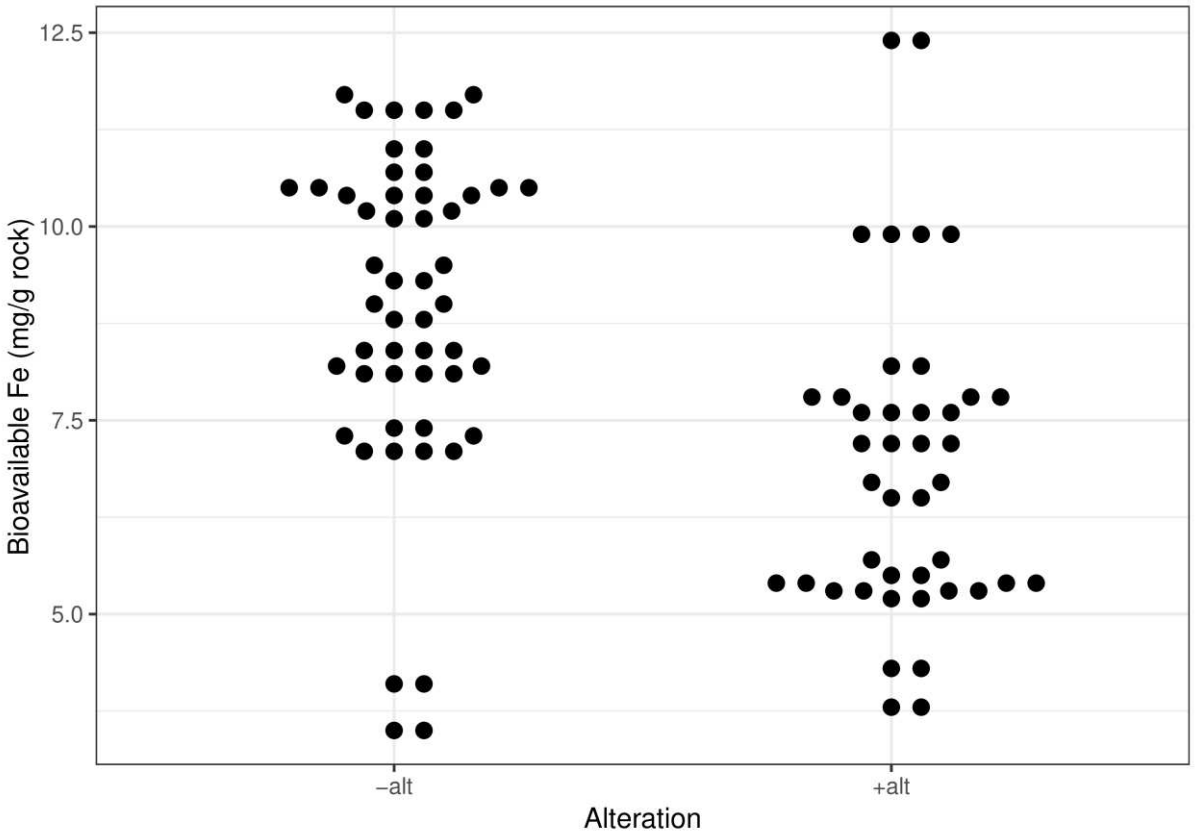

Fig. 2.S6. Beeswarm plot of bioavailable Fe versus alteration. The beeswarm plot (= swarmplot) compares the effect of alteration on the amount of bioavailable Fe, while the graph presents individual data points without overlap. The presence of alteration ("+alt") does significantly decrease the amount of bioavailable Fe (mg/g rock) compared to the absence of alteration ("-alt"). Alteration decreased the amount of bioavailable Fe on average by 2.06 (mg/g rock) (+alt = -2.06, t = -4.9, df = 92, $P < 0.001$).

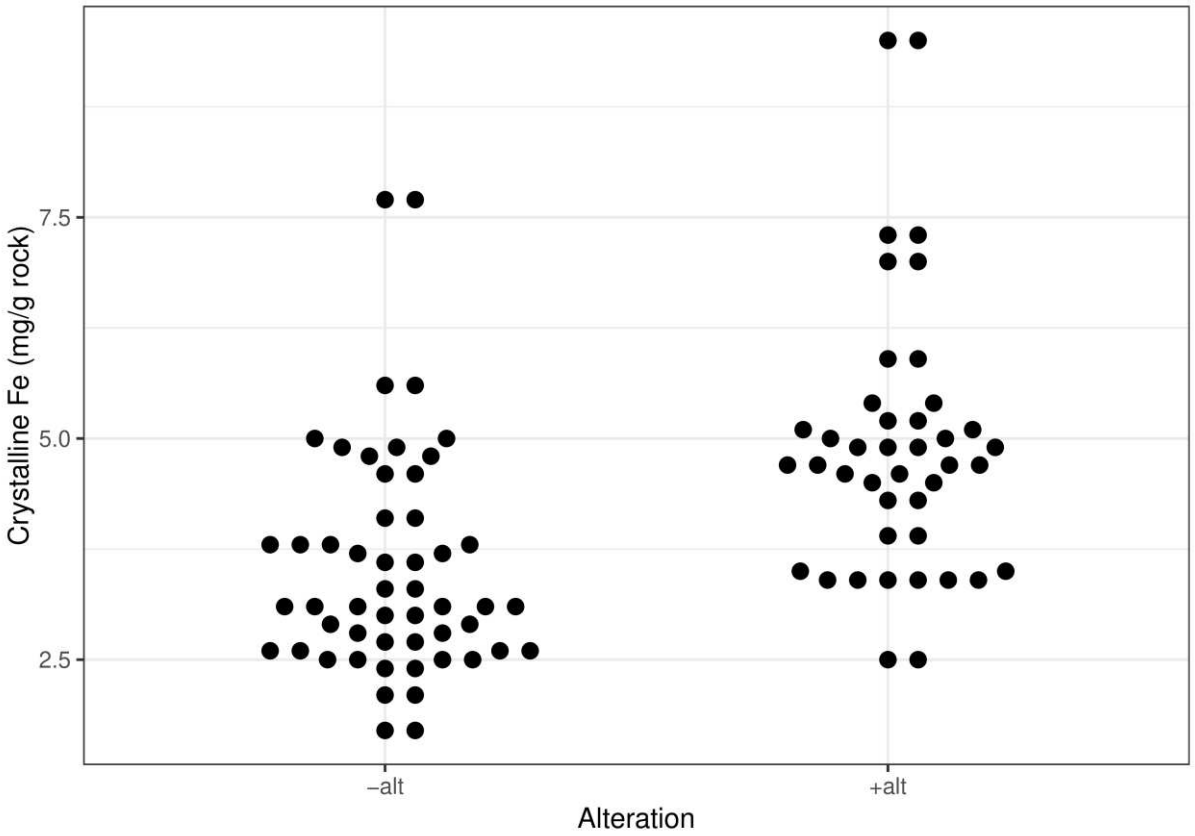

Fig. 2.S7. Beeswarm plot of crystalline Fe versus alteration. The beeswarm plot (= swarmplot) compares the effect of alteration on the amount of crystalline Fe, while the graph presents individual data points without overlap. The presence of alteration ("+alt") does significantly increase the amount of crystalline Fe (mg/g rock) compared to the absence of alteration ("-alt"). Alteration increased the amount of crystalline Fe on average by 1.37 (mg/g rock) (+alt = 1.371, t = 4.7, df = 92, $P < 0.001$).

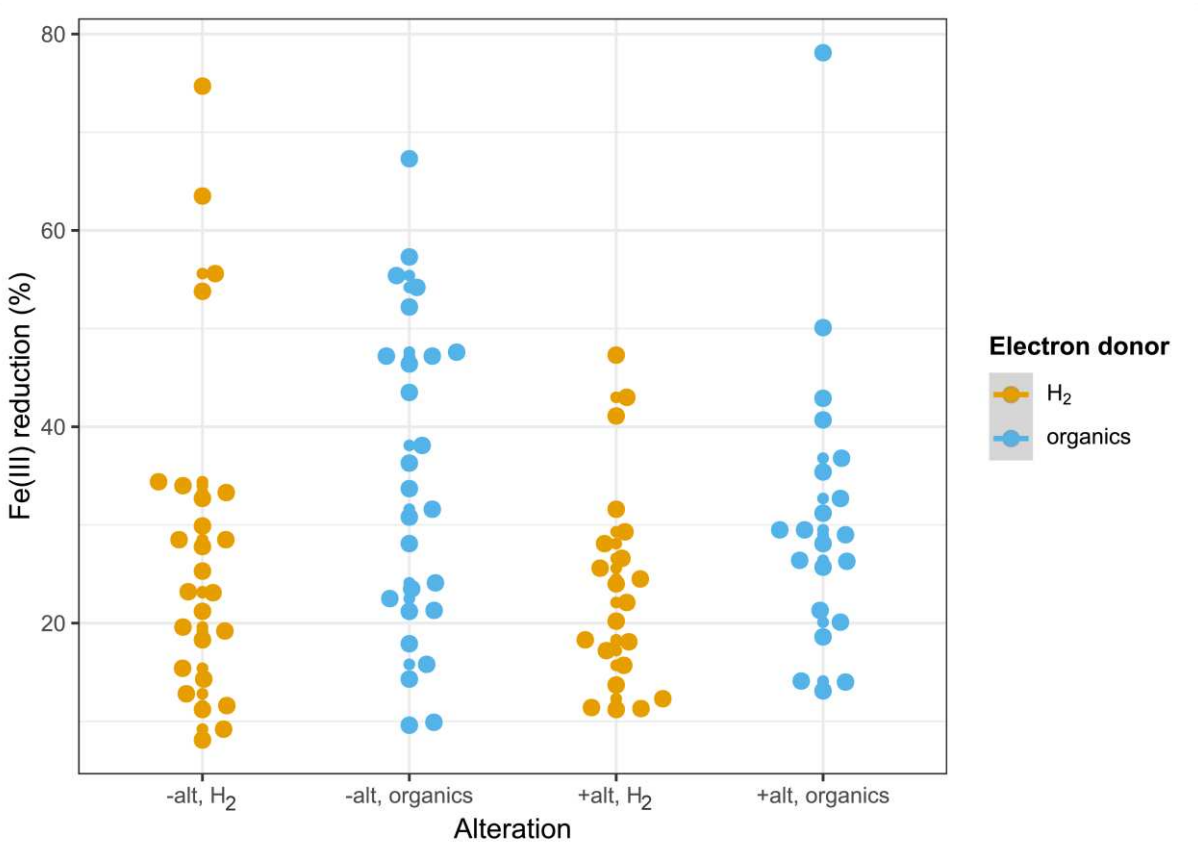

Fig. 2.S8. Beeswarm plot of Fe(III) reduction versus alteration. The beeswarm plot compares the effect of alteration on the amount of Fe(III) reduction for H_2 and organics as electron donors. The presence of alteration ("+alt") does not significantly decrease the amount of Fe(III) reduction (%) compared to the absence of alteration ("-alt"). Alteration decreased the amount of Fe(III) reduction by 4.59 % for H_2 (t = 1.6, df = 90, *P* = 0.12) and by 3.85 % for organics (t = 0.6, df = 90, *P* = 0.56). The interaction between alteration and electron donor was not significant either (t = 0.1, df = 90, *P* = 0.91). Electron donors H_2 and organics are displayed in orange and blue colour.

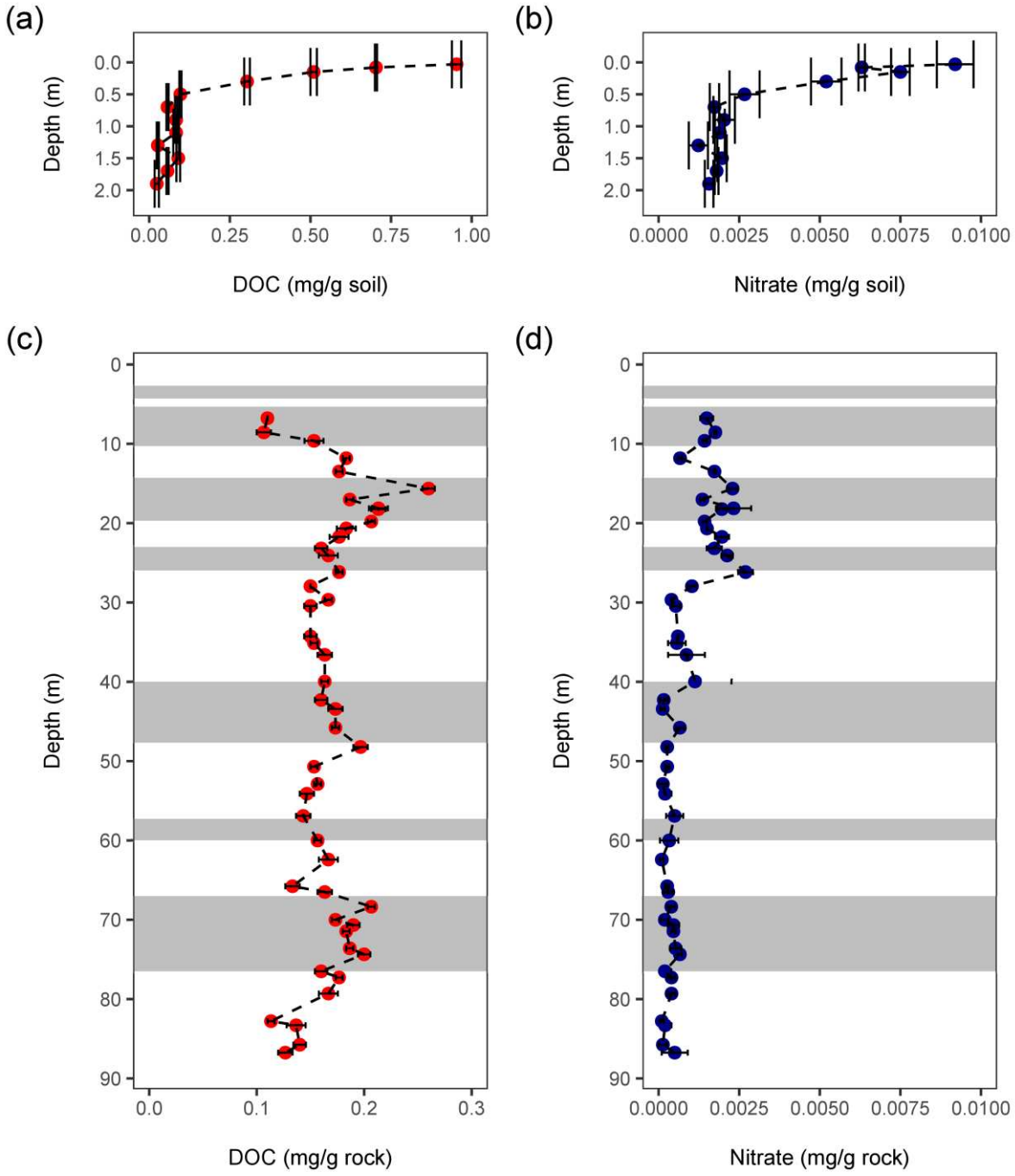

Fig. 2.S9. Water extractable organic carbon (DOC) and nitrate of Santa Gracia bulk drill core samples. Water extractable organic carbon and nitrate (mg/g powder) of soil (a,b) and rock (c,d) samples respectively are plotted versus depth (m) ($N = 59$). They could serve as potential electron sources for microbial Fe redox reactions. Data points represent the average of three technical extraction replicates. Error bars denote standard error of the technical extraction replicates. Note the x-scale differences for the individual subplots. Grey boxes denote the presence of prominent red zones and fracture (zones) (cf. Fig. 2.1).

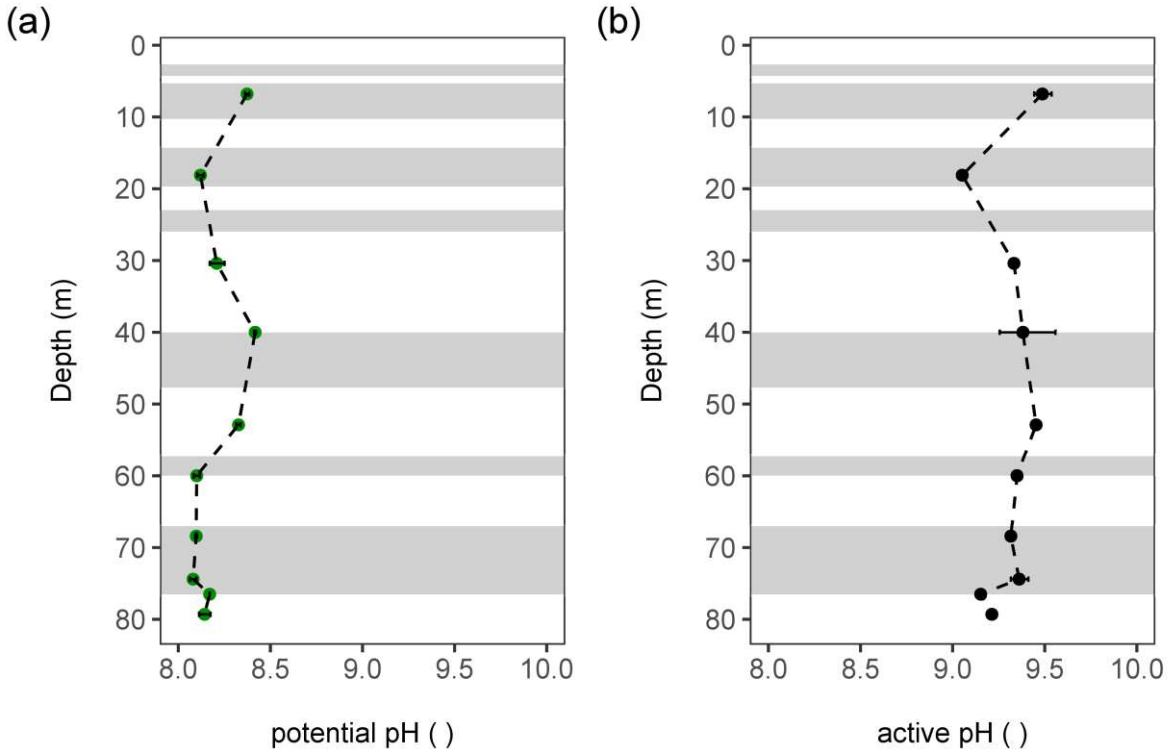

Fig. 2.S10. pH of Santa Gracia bulk drill core samples. Potential and active pH ( ) are plotted versus depth (m) (N = 10). Potential pH data were obtained by using 0.01 M $CaCl_2$ as leaching agent, whereas active pH data were acquired by addition of MilliQ water. Data points represent the average of three technical extraction replicates. Error bars denote mean ± standard deviation of the technical extraction replicates. Grey boxes denote the presence of prominent red zones and fracture zones (cf. Fig. 2.1).

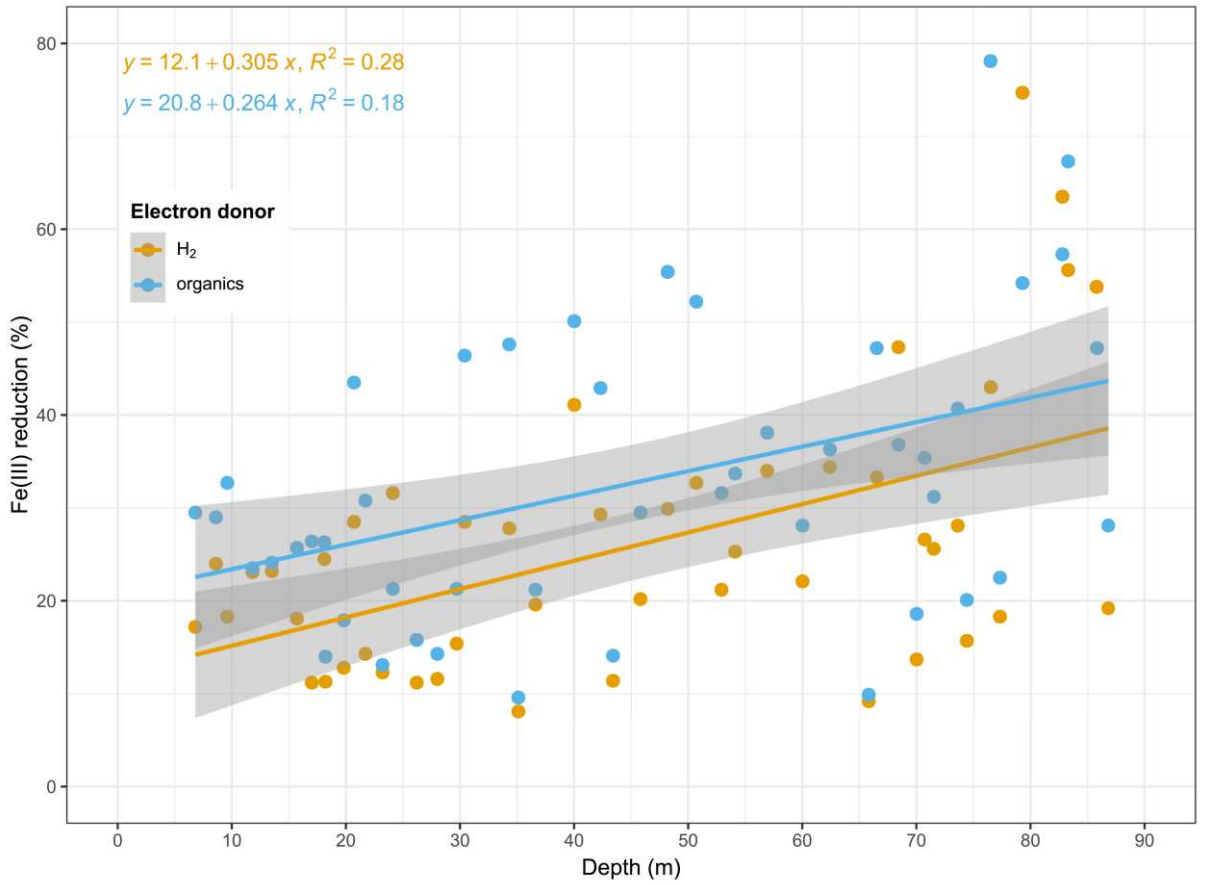

Fig. 2.S11. Fe(III) reduction shown as function of depth for two electron donor types. The amount of Fe(III) reduction (%) does significantly increase with depth (m), while having a weak correlation (H_2: R^2 = 0.28; organics: R^2 = 0.18). For each unit increase in depth, Fe(III) reduction increases by 0.28 % (slope = 0.28, t = 5.0, df = 92, $P < 0.001$). The grey ribbons in grey represent the 95% confidence intervals for H_2 (orange) and organics (blue), while the lines within show the linear regression lines.

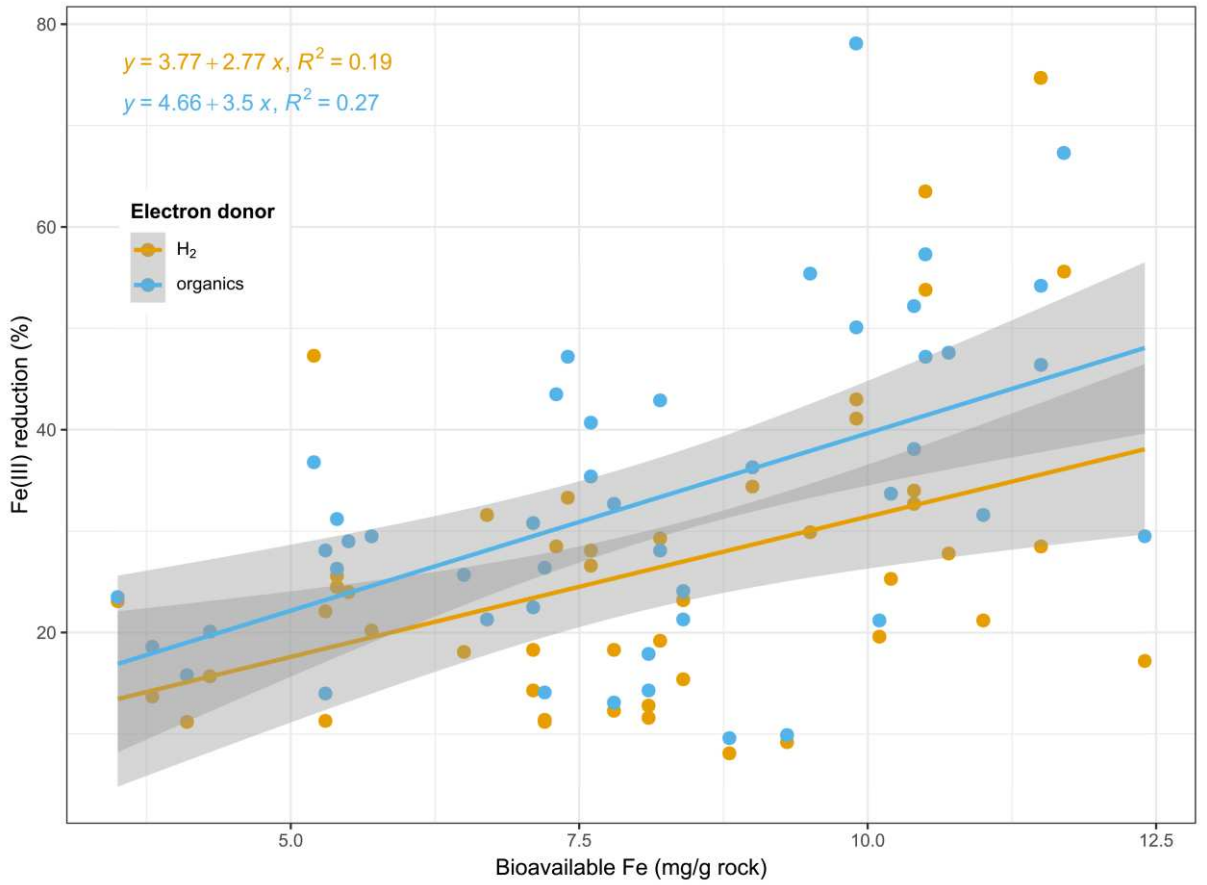

Fig. 2.S12. Fe(III) reduction shown as function of bioavailable Fe for two electron donor types. The amount of Fe(III) reduction (%) does significantly increase with the amount of bioavailable Fe (mg/g rock), while having a weak correlation (H_2: R^2 = 0.28; organics: R^2 = 0.18). For each unit increase in bioavailable Fe, Fe(III) reduction increases by 3.13 % (slope = 3.13, t = 5.1, df = 92, P < 0.001). The grey ribbons in grey represent the 95% confidence intervals for H_2 (orange) and organics (blue), while the lines within show the linear regression lines.

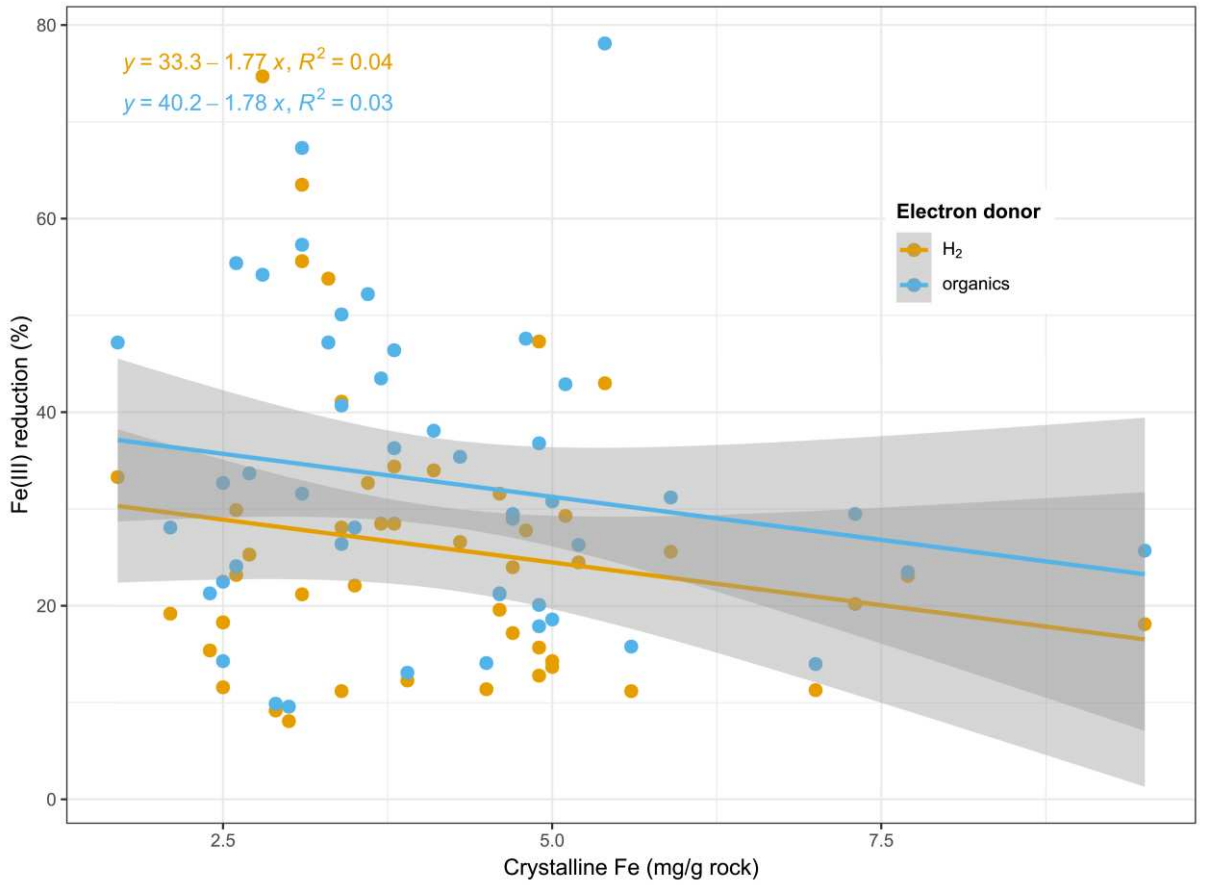

Fig. 2.S13. Fe(III) reduction shown as function of crystalline Fe for two electron donor types. The amount of Fe(III) reduction (%) does not significantly decrease with the amount of crystalline Fe (mg/g rock), while having a very weak correlation (H_2: R^2 = 0.04; organics: R^2 = 0.03). For each unit increase in crystalline Fe, Fe(III) reduction decreases by 1.77 % (slope = -1.77, t = -1.8, df = 92, *P* = 0.08). The grey ribbons in grey represent the 95% confidence intervals for H_2 (orange) and organics (blue), while the lines within show the linear regression lines.

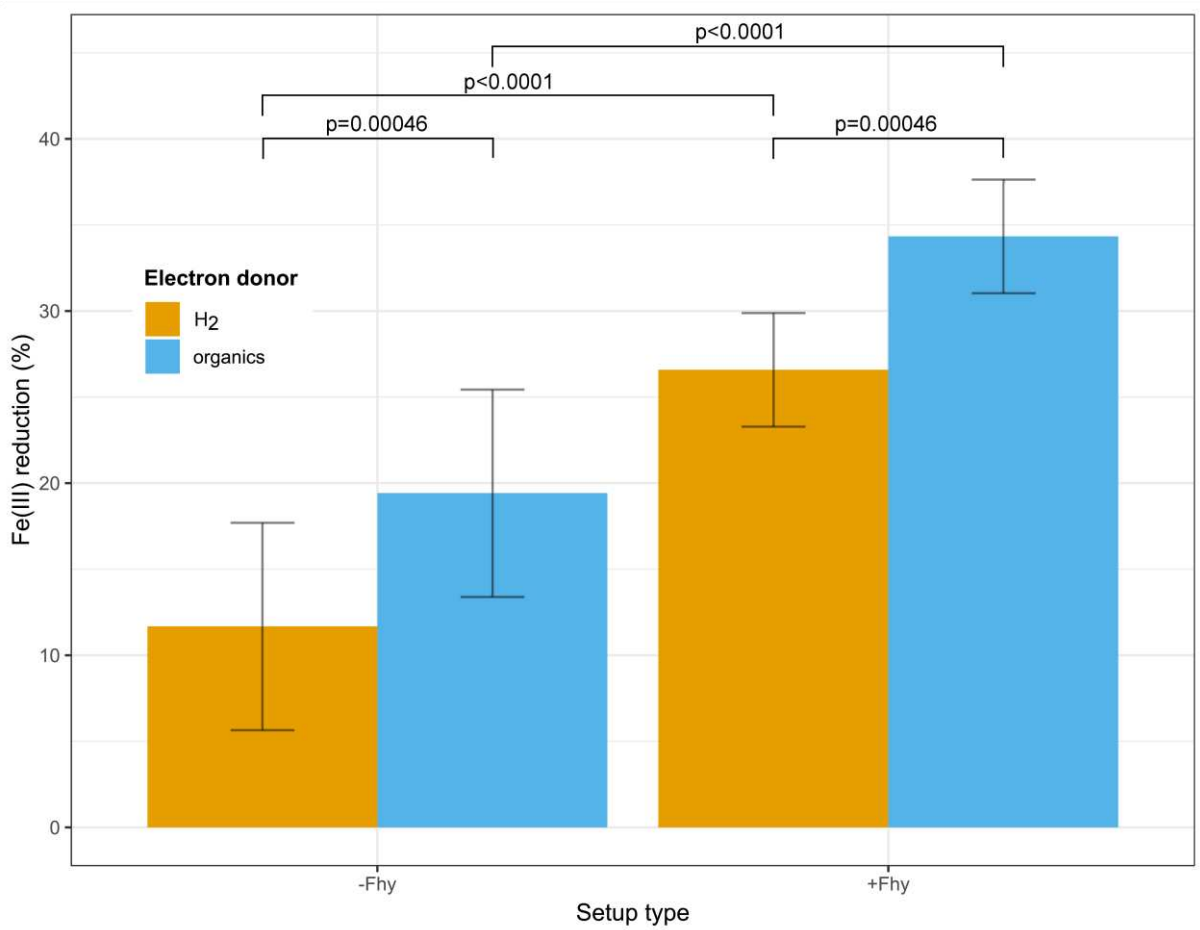

Fig. 2.S14. Fe(III) reduction shown as function of setup type. Fe(III) reduction was predicted by our linear multipredictor model, here indicated as bar charts. The bar charts in orange (H_2) and blue (organics) represent the predicted mean Fe(III) reduction (95% confidence interval). Control conditions ("-Fhy" = no ferrihydrite addition) are compared to experimental conditions ("+Fhy" = ferrihydrite addition). The amount of Fe(III) reduction (%) does significantly differ within groups (electron donor) and in between groups (setup type). More specifically, there is a significant increase in Fe(III) reduction for both electron donors when comparing control ("-Fhy") with experiment ("+Fhy") setups, as well as when comparing H_2 with organics within setup types ("-Fhy" and "+Fhy").

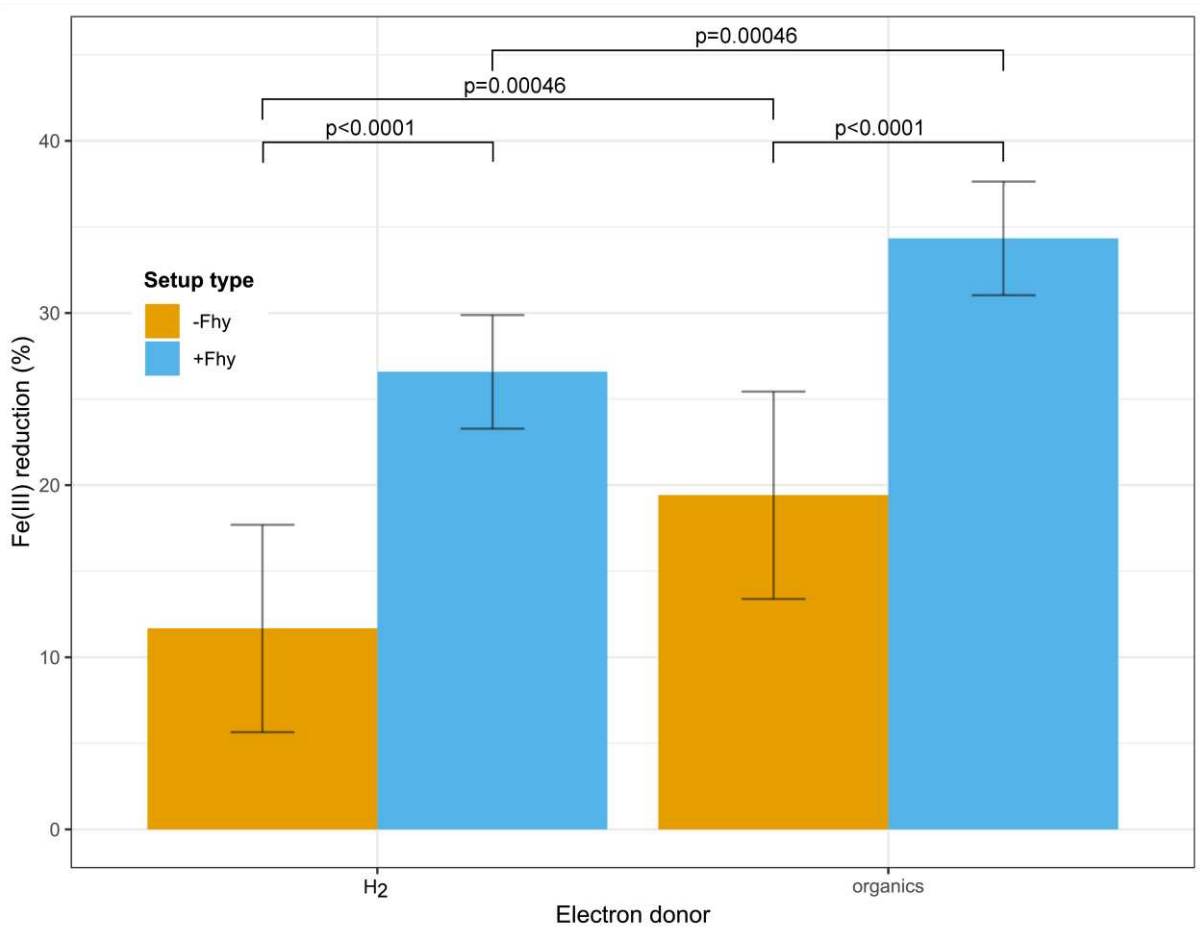

Fig. 2.S15. Fe(III) reduction shown as function of electron donor. Fe(III) reduction was predicted by our linear multipredictor model, here indicated as bar charts. The bar charts in orange (H_2) and blue (organics) represent the predicted mean Fe(III) reduction (95% confidence interval). H_2 as electron donor ("H_2") is compared to organic carbon ("organics"). The amount of Fe(III) reduction (%) does significantly differ within groups (setup type) and in between groups (electron donor). More specifically, there is a significant increase in Fe(III) reduction for both setup types when comparing H_2 with organic carbon setups, as well as when comparing setups without Fhy addition ("-Fhy") with setups with Fhy addition ("+Fhy") within electron donor types ("H_2" and "organics").

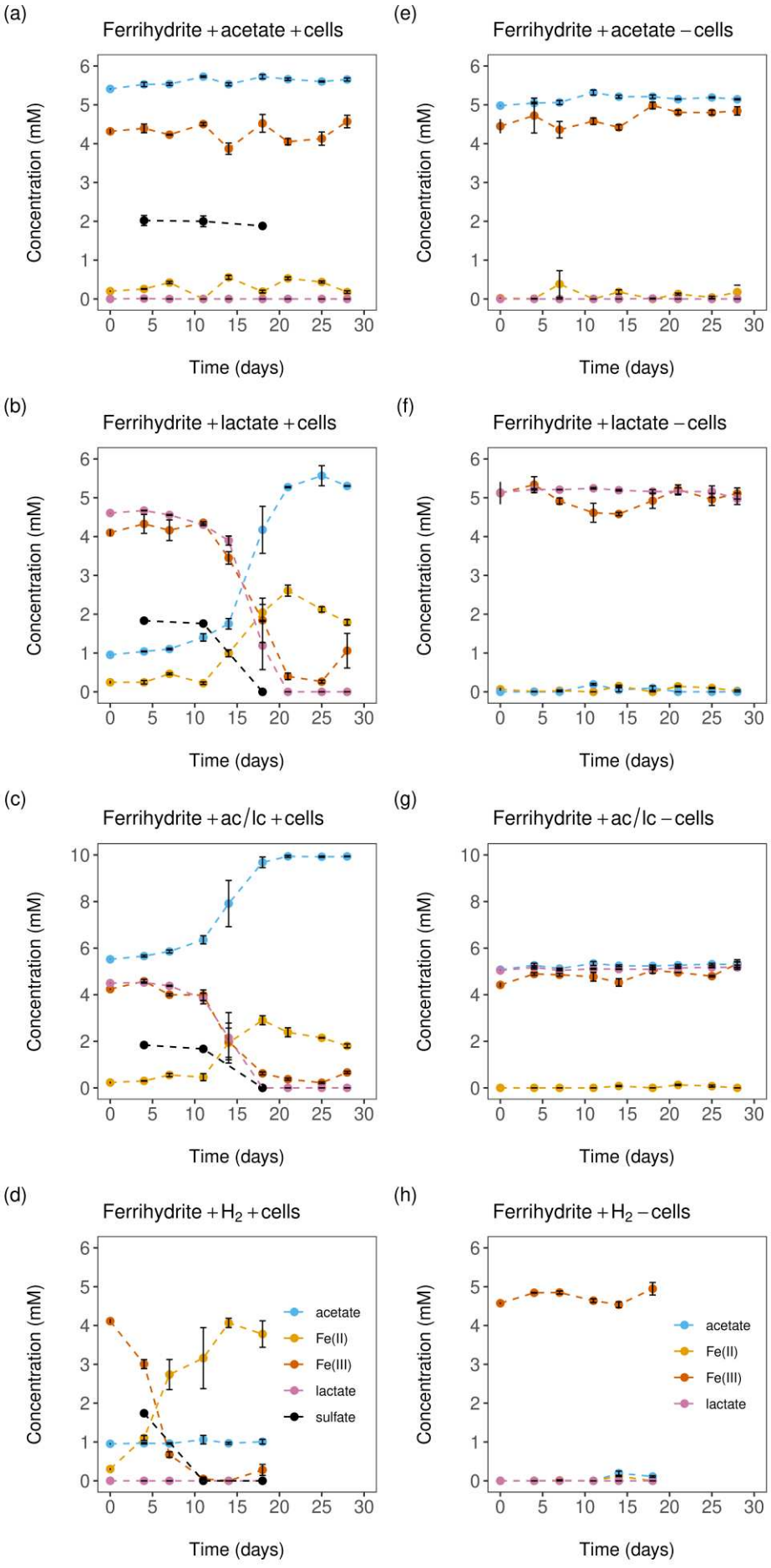
(a)
Ferrihydrite + acetate + cells
(e)
Ferrihydrite + acetate − cells
(b)
Ferrihydrite + lactate + cells
(f)
Ferrihydrite + lactate − cells
(c)
Ferrihydrite + ac/lc + cells
(g)
Ferrihydrite + ac/lc − cells
(d)
Ferrihydrite + H2 + cells
(h)
Ferrihydrite + H2 − cells
Concentration (mM)
Time (days)
acetate
Fe(II)
Fe(III)
lactate
sulfate

Fig. 2.S16. Microbially driven ferrihydrite reduction in microcosms by enrichment culture obtained from deepest weathering zone of Santa Gracia weathering profile versus abiotic control setups. An Fe(III)-reducing enrichment culture ("culture SG") obtained from the deepest weathering zone at ~77 m depth was inoculated into microcosm setups (a-d) (6^{th} transfer, 10 % (v/v)), while culture SG was not inoculated into microcosm control setups (e-h). Microcosms were set up with 5 mM ferrihydrite (Fhy) (= electron acceptor) and either 5 mM acetate (a,e), or 5 mM lactate (b,f), or 5 mM acetate/lactate (ac/lc) (c,g), or dihydrogen (H_2) in excess (d,h) (= electron donor), respectively. Successful microbially driven Fe(III) reduction is displayed in panels (b-d), while all abiotic control don`t show any Fe(III) reduction as expected. Data points represent the average of three biological replicates (a-d) or three abiotic control replicates (e-h), respectively. Data points equal to zero in Fig. 2.S16 (a-h) denote values below detection limit, but are plotted as "0" for better visualisation. Error bars denote standard error of the biological replicates or control replicates.

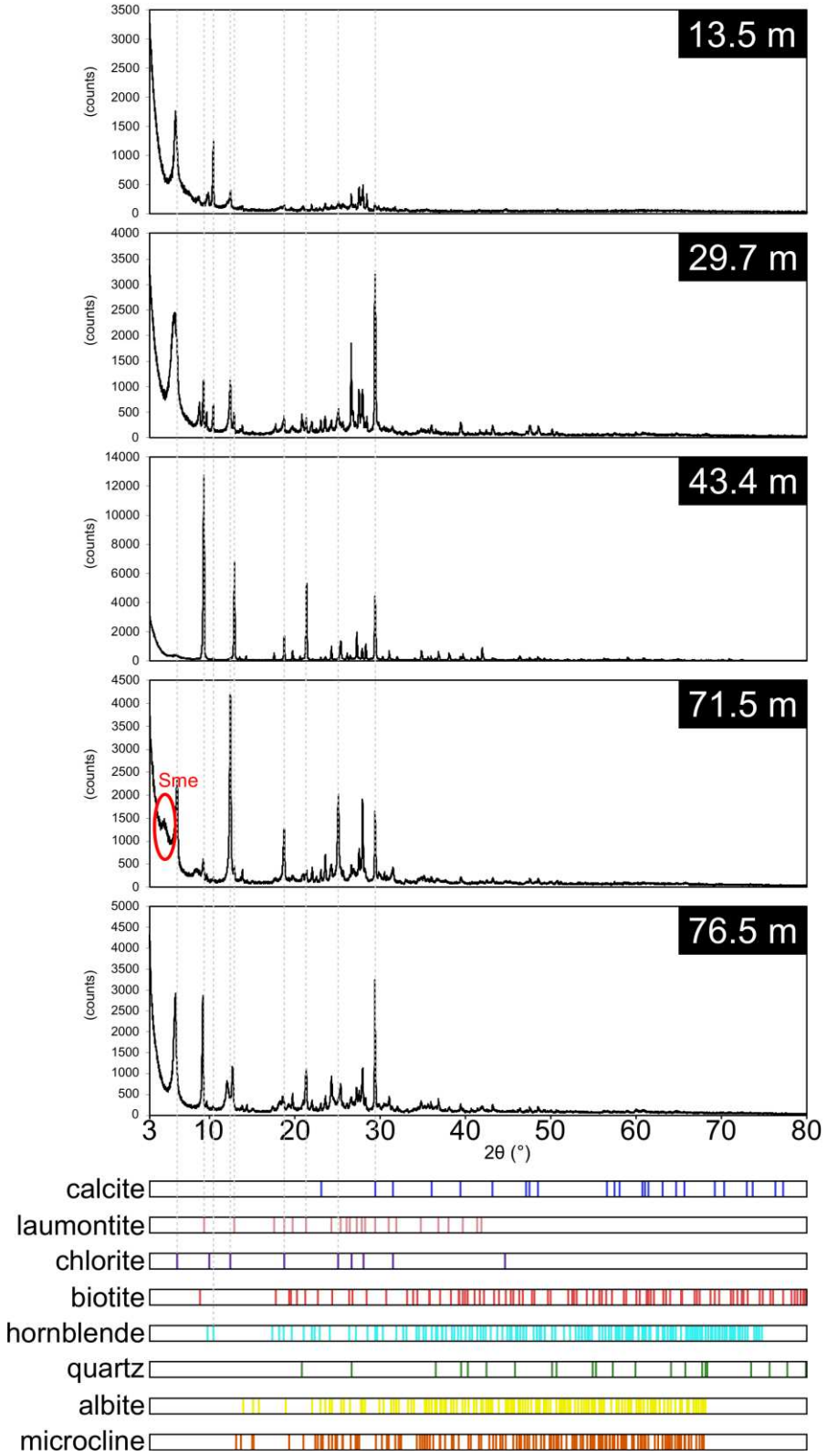

Fig. 2.S17. X-ray diffractograms of five representative fracture surface samples of Santa Gracia drill core profile. The diffractograms span from 3 to 80° 2θ to include granitoid lithology typical minerals like biotite and hornblende as well as hydrothermal alteration transformation products like chlorite. *Sme = smectite.*

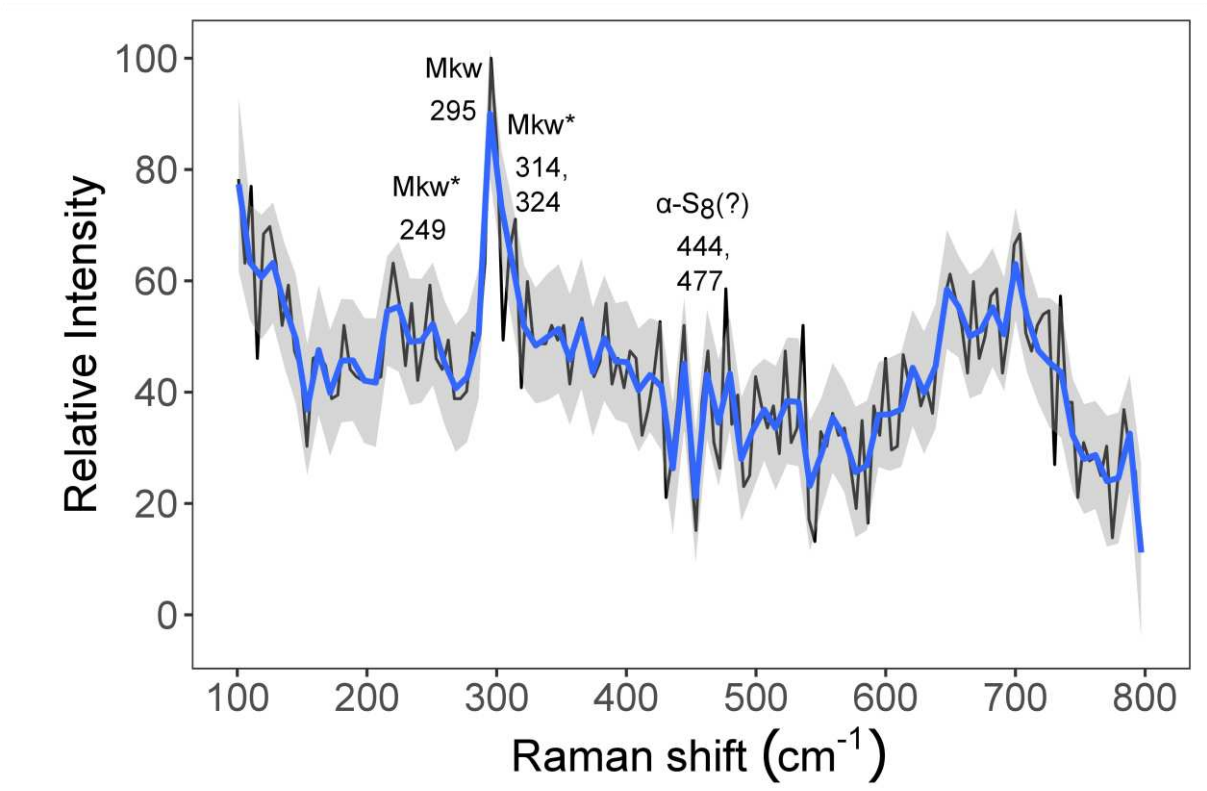

Fig. 2.S18. Raman spectroscopy spot analysis of biogenically reduced ferrihydrite sample. Raman spectrum of mineral products formed via microbially driven ferrihydrite reduction coupled to lactate oxidation by culture Santa Gracia. Characteristic peaks support formation of a visible blackish Fe-S mineral, here indicative for mackinawite (Mkw) and Fe(III)-mackinawite (Mkw*), as well as a potential presence of elemental sulfur (α-S_8). The blue line shows a smoothed line graph version of the Raman spectrum.

Chapter 3: Tectonic fracturing dictates the iron redox zonation of weathering profiles and potentially the microbial iron cycling along a climate gradient (Chilean Coastal Cordillera)

C. Schwerdhelm[a], *F. J. Hampl*[b], *L. V. Krone*[c], *L. Horstmann*[d], *K. Kaphegyi*[a], *B. Nisch*[e], *D. Buchner*[e], *N.A. Stroncik*[c], *T. Samuels*[a], *A. Kappler*[a,f], *C. Bryce*[g,*]

[a] Geomicrobiology, Department of Geosciences, University of Tuebingen, Schnarrenbergstrasse 94-96, 72076 Tuebingen, Germany

[b] Department of Applied Geochemistry, Technische Universität Berlin, Ernst-Reuter-Platz 1, 10587 Berlin, Germany; now: Chair of Resource Mineralogy, Montanuniversität Leoben, Peter-Tunner-Straße 5, 8700 Leoben, Austria

[c] Institute of Geological Sciences, Freie Universität Berlin, Malteserstrasse 74-100, 12249 Berlin, Germany

[d] GFZ German Research Centre for Geosciences, Section Geomicrobiology, 14473 Potsdam, Germany

[e] Department of Geosciences, University of Tuebingen, Schnarrenbergstrasse 94-96, 72076 Tuebingen, Germany

[f] Cluster of Excellence: EXC 2124: Controlling Microbes to Fight Infection, Tübingen, Germany

[g] School of Earth Sciences, University of Bristol, Wills Memorial Building, Queens Road, Bristol BS15N 1RJ, United Kingdom

*To whom correspondence should be sent:

Dr. Casey Bryce

In preparation for submission to AGU Geophysical Research Letters

3.1 Abstract

Microbial weathering of iron (Fe)-bearing minerals has been primarily studied in the shallow subsurface of humid and tropical environments. However, it is not well known how the activity of microorganisms in weathering of Fe-bearing minerals in the deep subsurface is related to differences in fracturing and partial alteration of granitoid bedrock. It is also not well constrained, if there are differences along a precipitation gradient or climate gradient, regarding microbial weathering activity. Investigating microbial weathering activity along a precipitation gradient is key, since an increase in the available amount of meteoric water results in both enhanced weathering intensity and enhanced nutrient and electron sources supply for microbial metabolisms.

To gain insights into the controlling factors of microbial weathering of Fe-bearing minerals, we recovered four weathering profiles in granitoid rock in arid (Pan de Azúcar), semi-arid (Santa Gracia), Mediterranean (La Campana) and humid (Nahuelbuta) regions of the Chilean Coastal Cordillera (26°-38° S) ranging from 41 to 94 m in depth. Combining Fe and C geochemical and petrophysical data with statistics, we found higher Fe(II)/Fe(tot)-ratios and poorly crystalline Fe contents at increased depth among all field sites. Contrastingly, weathering profile patterns regarding adsorbed and crystalline Fe mineral contents varied, since the extents of precipitation, fracturing and hydrothermal alteration differ along the gradient and bedrocks. We found more poorly crystalline Fe but less bioavailable organic carbon in fractures. Assessing our data in the context of the lithology, presence and intensity of fracturing and hydrothermal alteration, and surface inputs, we were able to reveal depth intervals of most probable *in situ* microbial Fe(II) oxidation and Fe(III) reduction along the climate gradient.

Our work demonstrates that fracturing and precipitation are key controls on microbial weathering of Fe-bearing minerals. This work highlights the need for a pairing of mineralogy, geochemistry, tectonics and hydrology with microbiology to adequately assess the role of Fe-metabolising microorganisms in subsurface weathering processes, especially in more complex geological environments.

Graphical abstract

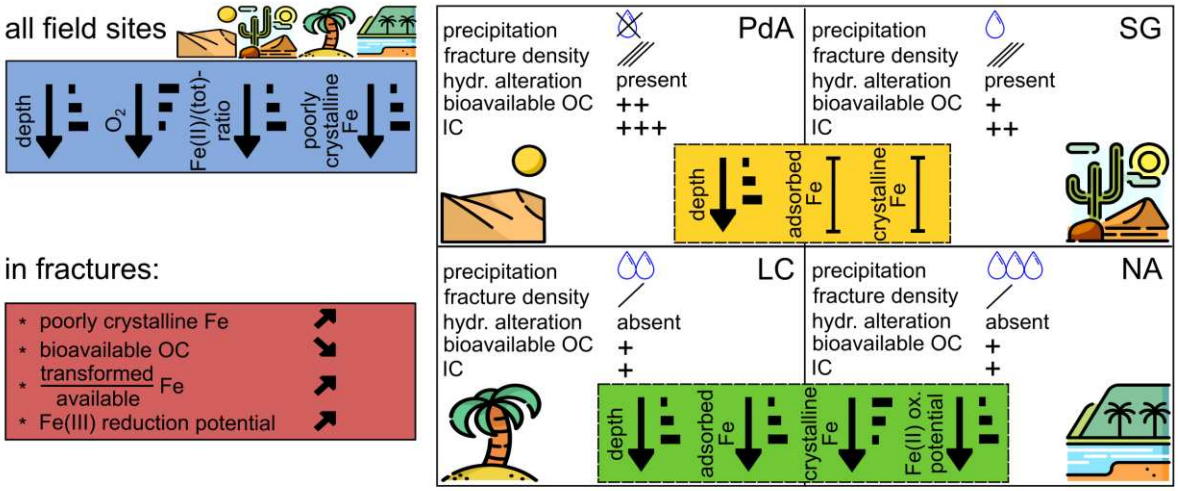

Keywords

Climate gradient, precipitation gradient, deep weathering, hydrothermal alteration, fracturing, Fe-metabolising bacteria, Fe(II) oxidation, Fe(III) reduction, Fe-cycling

3.2 Introduction

Multiple environmental parameters dictate the impact of microorganisms in weathering of iron (Fe)-bearing minerals in the deep subsurface. These environmental parameters include the availability of water, nutrients and electron sources and are dependent on bioavailable Fe minerals and organic carbon, lithological and mineralogical features such as fractures, fracture density, hydrothermal alteration, Fe mineral crystallinity and surface area as well as the Fe redox zonation (i.e. presence/absence of oxygen) (Pedersen, 1997; Buss et al., 2005; Cutting et al., 2009; Ginn et al., 2017; Samuels et al., 2020; Kappler et al., 2021; Hampl et al., 2022; Callahan et al., 2024). Among these proxies, the presence of fractures and availability of oxygen are of particular importance. They control the redox status of bioavailable Fe-bearing minerals in the subsurface and hence the potential of Fe-metabolising microorganisms to contribute to mineral weathering (Brantley et al., 2013; Bethencourt et al., 2020; Bochet et al., 2020; Ackerer et al., 2021).

The Fe redox status reflects the penetration depth of oxygen into the subsurface, which can be expressed as Fe(II)/Fe(tot)-ratio in depth profiles. High Fe(II)/Fe(tot)-ratios are correlated with the presence of Fe(II)-bearing minerals such as Fe(II) carbonates (i.e. ankerite and siderite), which have shown to be highly sensitive towards oxygen (Bachan and Kump, 2015; Swanner et al., 2018; Maisch et al., 2020). The amount of oxygen being transported into the deep subsurface primarily depends on the supply of water as a transporting fluid (i.e. climate) and the presence of fractures (i.e. tectonic deformation) (Gudmundsson, 2000; Berkowitz, 2002; Deng and Spycher, 2019). However, prior research on the impact of fractures on Fe-mineral bioavailability has been confined to individual field sites (Smith and Roychoudhury, 2013; Hampl et al., 2021; Krone et al., 2021a; Trichandi et al., 2022; Callahan et al., 2024), which limits our ability to understand confounding climatic effects. Besides that, it is unclear to which extent the fracture density, rather than simply the presence of fractures, is an important controlling factor (Tripp and Vearncombe, 2004).

To improve our knowledge on controlling factors of microbial weathering of Fe-bearing minerals, we conducted a systematic assessment of four weathering profiles along a climate gradient. We investigated four 41-94 m deep weathering profiles in granitoid rock in arid (Pan de Azúcar), semi-arid (Santa Gracia), Mediterranean (La Campana) and humid (Nahuelbuta) regions of the Chilean Coastal Cordillera. We examined how climate, fracturing, and mineralogical and geochemical conditions (bioavailable Fe mineral and C pools) effect a potential microbial weathering activity on Fe-bearing minerals in the deep subsurface. Eventually, we assessed whether Fe and C geochemistry paired with fracture analysis (type, density) is a sufficient tool to predict depth intervals/zones of potential microbial activity.

3.3 Material and methods

3.3.1 Study sites

The four EarthShape study sites Pan de Azúcar (PdA), Santa Gracia (SG), La Campana (LC) and Nahuelbuta (NA) span a climatic gradient from North to South between 26° and 38° S. The four study sites can be summarised as following:

Pan de Azúcar. Pan de Azúcar is situated in an arid climate zone of the Coastal Cordillera in Chile, ca. 17 km northeast of Chañaral. The bedrock of the drilling location (-26.302717°N, -70.457350°E, [WGS84]) is composed of monzo- to syenogranitic intrusions of Triassic age (240-205 Ma) (Parada et al., 2007). It is heavily fractured by the Atacama Fault Zone and has been hydrothermally overprinted to varying degrees (Trichandi et al., 2024). The study area is characterised by gently dipping hillslopes, mean annual precipitation of 10 mm yr^{-1}, mean annual temperature of 18°C, very sparse vegetation cover of lichens and UV-degraded shrubs, and a Holocene net primary production (NPP) of 30 g m^{-2} yr^{-1} C (Bernhard et al., 2018; Oeser et al., 2018; Werner et al., 2018; Oeser and von Blanckenburg, 2020; Übernickel et al., 2020).

Santa Gracia. Santa Gracia is located in a semi-arid climate zone of the Coastal Cordillera in Chile, ca. 18 km northeast of La Serena (Coquimbo) within the Santa Gracia National Reserve. The bedrock of the drilling location (-29.759414°N, -71.160322°E [WGS84]) is a quartz monzodiorite containing biotite, chlorite, hornblende, magnetite and hematite (Krone et al., 2021b). It is part of granitic to dioritic intrusions of the early Cretaceous (144-124 Ma), fractured by the Atacama Fault Zone and hydrothermally overprinted (Cembrano et al., 2005; Hampl et al., 2022; Trichandi et al., 2022). The study area is characterised by gently dipping hillslopes, mean annual precipitation of <100 mm yr^{-1}, mean annual temperature of 16°C, a sparse vegetation coverage of 30-40% dominated by shrubs and cacti, and a Holocene NPP of 150 g m^{-2} yr^{-1} C (Ministerio de Obras Públicas de Chile, 2016; Bernhard et al., 2018; Oeser et al., 2018; Werner et al., 2018; Oeser and von Blanckenburg, 2020; Übernickel et al., 2020).

La Campana. La Campana is situated in a Mediterranean climate zone, ca. 60 km northwest of Santiago de Chile, within the La Campana National Park. The bedrock of the drilling location (-33.02833°N, -71.04354°E [WGS84]) is granodiorite (Hampl et al., 2023) which is part of Upper Cretaceous intrusions of mainly granodiorites and tonalites with subordinate quartz monzodiorites (Gana et al., 1996). The study area is characterised by steep slope dip angles of 20–30°, mean annual precipitation of 346 mm yr^{-1}, mean annual temperature of 15°C, a native Mediterranean sclerophyllous forest with Cryptocarya alba and Lithraea caustica as dominant plants as well as shrubland, and a Holocene NPP of 280 g m^{-2} yr^{-1} C (Luebert and Pliscoff, 2006; Bernhard et al., 2018; Oeser et al., 2018; Werner et al., 2018; Oeser and von Blanckenburg, 2020; Übernickel et al., 2020).

Nahuelbuta. Nahuelbuta is located in a temperate rainforest climate zone, ca. 20 km west of Angol in southern Chile. The basement of the drilling location (-37.79381°N, -72.95043°E [WGS84]) is granite (Hampl et al., 2023) of the Nahuelbuta Batholith which mostly consists of tonalites and granodiorites. The Nahuelbuta Batholith is part of the Late Carboniferous (328-299 Ma) Chilean Coastal Batholith and situated on top of the Nahuelbuta central pluton (Herve, 1974; Deckart et al., 2013; Steenken et al., 2016). The study area is characterised by a plateau-like ridge with gently dipping slopes (ca. 10°), mean annual precipitation of 1927 mm yr^{-1}, mean annual temperature of 14°C, and a temperate forest with *Araucaria araucana* as the dominant tree, which has been replaced by a sparse forest due to pastoral farming (cow grazing) and fires, with a Holocene NPP of 520 g m^{-2} yr^{-1} C (Luebert and Pliscoff, 2006; Bernhard et al., 2018; Oeser et al., 2018; Werner et al., 2018; Oeser and von Blanckenburg, 2020; Übernickel et al., 2020).

3.3.2 Drilling procedure and sample preparation

The weathering profiles comprise 93.5 m (PdA), 87.2 m (SG), 88.3 m (LC) and 40.8 m (NA1) of drilled core material consisting of soil, saprolite and rock. The uppermost 2-6 m are additionally recovered by a manually dug soil pit adjacent to the drill hole. Drill core material was obtained by wireline diamond drilling, using a PQ3-sized crown and potable water as drill fluid (including contamination control) (Friese et al., 2017; Krone et al., 2021b; Hampl et al., 2023). After retrieving the drill cores (up to 1.5 m length), bulk core sample intervals with a length of ca. 20 cm were aseptically taken using a hammer, a chisel and an angle grinder in the field. Afterwards, the samples were anoxically stored at 4°C. The samples were aseptically split with a rock trimmer and separated into an outer (for geochemical and mineralogical analyses of this study) and an inner part (for microbiological analyses) in the laboratory. The outer part was further milled to a grain size of <10 µm with a planetary ball mill.

3.3.3 Sequential Fe extractions

Sequential Fe extractions using sodium acetate (1 M NaAc), hydrochloric acid (0.5 M HCl) and concentrated hydrochloric acid (6 M HCl) were performed on 15 samples of each weathering profile to quantify biogenic Fe pools available for microbial Fe redox reactions (N = 60, technical extraction triplicates) (Heron et al., 1994; Cornell and Schwertmann, 2003; Lueder et al., 2020; Grimm et al., 2024). Suspensions were centrifuged after each extraction step to remove the supernatant for quantification of the respective Fe pools and solids resuspended in the subsequent solvent. After extraction, Fe(II) and total Fe (Fe(tot); i.e. Fe(II) plus Fe(III)) were spectrophotometrically quantified using the ferrozine assay (Hegler et al., 2008). Details of the extractions were as follows:

1 M NaAc. 1 M NaAc targets surface-adsorbed Fe. Fe minerals dissolved are ankerite, calcite/aragonite and siderite (amorphous FeS (moderate extent) and mackinawite (marginal

extent)) (Voelz et al., 2019). We extracted surface-adsorbed Fe with 1 M NaAc at pH 5 and room temperature under anoxic conditions in the dark for 24 h (solid:liquid = 1:20) (Raiswell et al., 1994; Roden and Zachara, 1996).

0.5 M HCl. 0.5 M HCl targets poorly crystalline Fe. Fe minerals dissolved are ferrihydrite, lepidocrocite and partly magnetite, maghemite, hematite, goethite, biotite and chlorite via dissolution by protonation (Sidhu et al., 1981; Raiswell et al., 1994; Voelz et al., 2019). We extracted poorly crystalline Fe with 0.5 M HCl at room temperature under anoxic conditions in the dark for 2 h (solid:liquid = 1:20) (Raiswell et al., 1994; Roden and Zachara, 1996).

6 M HCl. 6 M HCl targets crystalline Fe. Fe minerals dissolved are goethite, hematite, magnetite, amorphous FeS and mackinawite (Voelz et al., 2019). We extracted crystalline Fe with 6 M HCl in the dark under anoxic conditions for 24 h (solid:liquid = 1:20) (Raiswell et al., 1994; Roden and Zachara, 1996).

3.3.4 Carbon analysis

Carbon concentrations of organic (OC) and inorganic (IC) carbon were quantified by using the single-run dual temperature combustion (SRDTC) method of Bisutti et al. (2007). The method provides data on bioavailable organic carbon ("TOC400"), residual organic carbon ("ROC") and inorganic carbon ("TIC900") in a single analysis run. 1g dry soil/rock powder of each sample was measured on a soli TOC® cube analyser (Elementar, Germany) (N = 127, technical extraction duplicates). The targeted carbon pools are more specifically:

TOC400. TOC400 is the bioavailable, total organic carbon released between 150 and 400°C in the presence of oxygen. It is called "BOC" in the following for clarification.

ROC. ROC comprises the residual oxidisable carbon pool, e.g. black carbon and soot, released between 400 and 600° C in the presence of oxygen. TOC400 and ROC represent TOC after acidification.

TIC900. TIC900 is the total inorganic carbon released between 600 and 900 °C in the presence of oxygen. It is called "IC" in the following for clarification.

3.3.5 Data and statistical analysis

Data analyses were performed in the R statistical environment (R Core Team, 2024) and plots were produced with the package ggplot2 (Wickham, 2016). Fe and C pools were analysed using general linear models (LM). We tested the combined effect of (a) fracture type and field site and (b) fracture density and field site (predictor variables) on quantified concentrations of either adsorbed Fe or poorly crystalline Fe or crystalline Fe or BOC or IC (response variable). We also ran a nonlinear model to check for the effect of the Fe(II)/Fe(tot)-ratio on the adsorbed Fe concentration of each field site. Model assumptions were checked for all selected models

and found not to have been violated. As the general linear models were partly found to be significant, we ran Tukey *post hoc* paired-samples t-tests of these models to determine the difference between the mean of all possible pairs using a studentised range distribution, i.e. testing every possible pair of all groups (Tukey, 1949).

3.4 Results

3.4.1 Drill core Fe mineralogy of the weathering profiles

Sequential Fe extractions were performed to quantify biogenic Fe pools available for microbial Fe redox reactions, corresponding to potentials for microbial *in situ* weathering of Fe-bearing minerals. Extractions targeted (1) the Fe that is adsorbed to minerals and easily bioavailable to microorganisms (via 0.5 M NaAc), (2) the poorly crystalline Fe, which is also bioavailable (0.5 M HCl), and (3) the crystalline Fe that is present as Fe(III) (oxyhydr)oxides and Fe-sulfides (via 6 M HCl). Total Fe concentrations vary between approximately 5 and 32 mg g^{-1} soil/rock powder (Fig. 3.1).

The Fe mineralogy of Pan de Azúcar in the upper 1.5 m is mostly comprised of crystalline Fe, while below sorbed and poorly crystalline Fe are relatively more abundant (>1.5 m: up to 25%; 1.6 and 87.5 m: up to 55%) with Fe concentrations of approximately 5-23 mg g^{-1} soil/rock. (Fig. 3.1a). Sorbed Fe(II) concentrations at 1.6 and 87.5 m are strikingly high (up to 5 mg Fe g^{-1} rock). The weathering profile can be divided into an oxidised and a reduced zone, which is clearly visible in the Fe(II)/Fe(tot)-ratios (Table 3.S1).

Comparable to Pan de Azúcar, extractable amounts of biogenic Fe are smaller in soil than in rock (8-15 mg g^{-1} soil vs 18-32 mg g^{-1} rock) in Santa Gracia (Fig. 3.1b). Soil and rock samples are rich in crystalline Fe (crystalline Fe pool: 80-95%). Sorbed Fe can be found throughout the weathering profile, but is not abundant (<1 mg g^{-1}). The zone of particularly intense weathering and hydrothermal alteration in the deepest weathering zone (67-77 m depth) (see Chapter 2) shows less extractable Fe. Like PdA, the weathering profile of SG consists of an oxidised and a transition/reduced zone.

Absolute Fe concentrations range from 12-31 mg g^{-1} soil/rock in La Campana, while the amount of extractable biogenic Fe increases with depth (soil < saprolite < bedrock) (Fig. 3.1c). There is also an increase in sorbed and poorly crystalline Fe with depth, while being almost entirely expressed as Fe(II). Interestingly, the pool of sorbed Fe is clearly visible at a depth of 48.9 m and below. The amount of crystalline Fe increases, too. Fe(II)/Fe(tot)-ratios suggest a 3 zone-redox zonation, i.e. an oxidised top part (0-1.6 m), a transitioning middle part (1.6-43.3 m) and a reduced bottom part (≥48.7 m).

Nahuelbuta is characterised by 13-31 mg Fe g^{-1} soil/rock, while the amount of extractable Fe in soil is smaller than in rock (Fig. 3.1d). There is a clear soil-rock boundary with sudden appearance of adsorbed and poorly crystalline Fe, which make up to 4 mg g^{-1} (adsorbed Fe) and 9 mg g^{-1} (poorly crystalline Fe), respectively. Overall, there is a high amount of Fe(II) through-

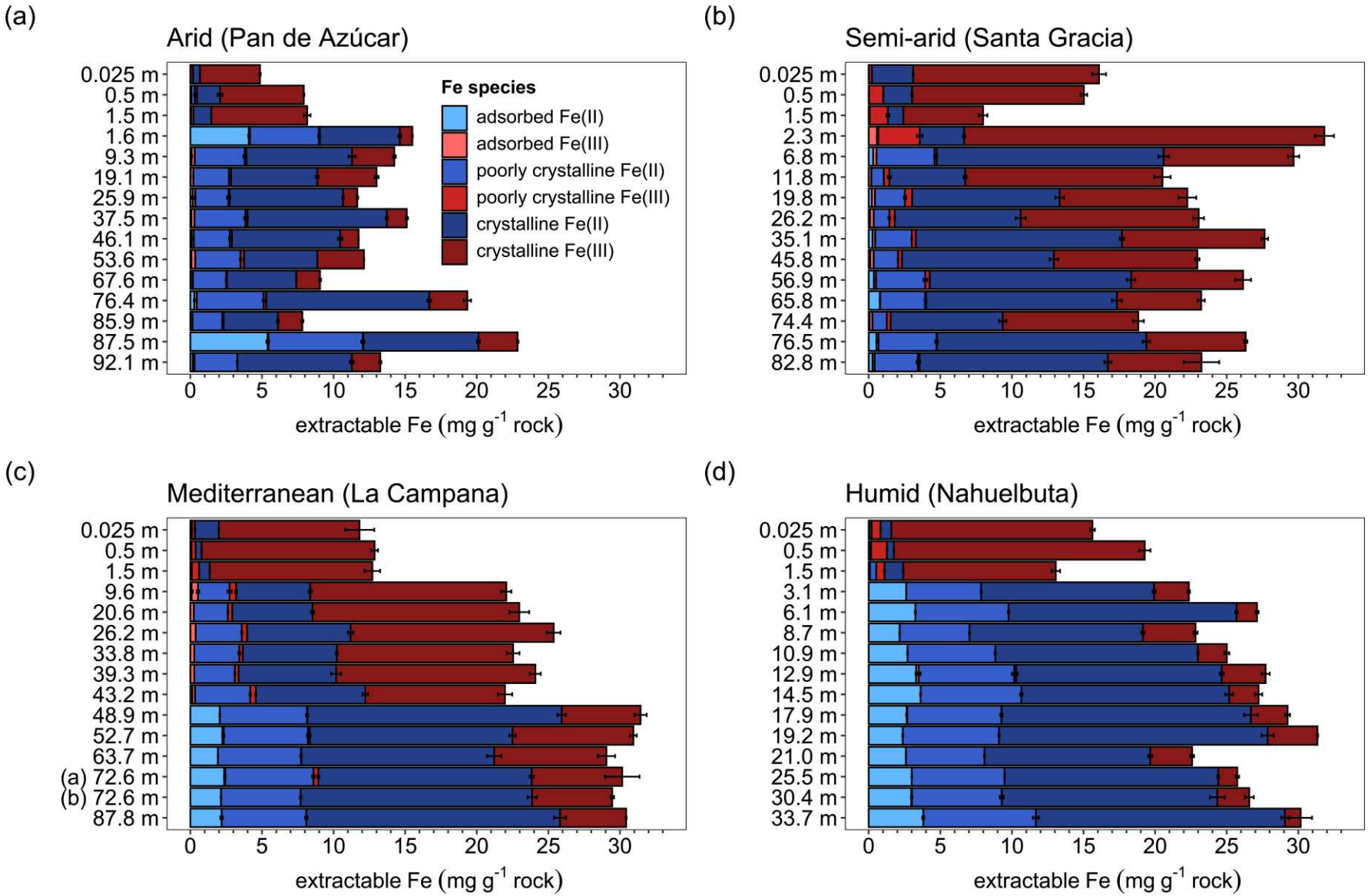
(a)
Arid (Pan de Azúcar)
0.025 m
0.5 m
1.5 m
1.6 m
9.3 m
19.1 m
25.9 m
37.5 m
46.1 m
53.6 m
67.6 m
76.4 m
85.9 m
87.5 m
92.1 m
Fe species
adsorbed Fe(II)
adsorbed Fe(III)
poorly crystalline Fe(II)
poorly crystalline Fe(III)
crystalline Fe(II)
crystalline Fe(III)
0 5 10 15 20 25 30
extractable Fe (mg g-1 rock)
(b)
Semi-arid (Santa Gracia)
0.025 m
0.5 m
1.5 m
2.3 m
6.8 m
11.8 m
19.8 m
26.2 m
35.1 m
45.8 m
56.9 m
65.8 m
74.4 m
76.5 m
82.8 m
0 5 10 15 20 25 30
extractable Fe (mg g-1 rock)
(c)
Mediterranean (La Campana)
0.025 m
0.5 m
1.5 m
9.6 m
20.6 m
26.2 m
33.8 m
39.3 m
43.2 m
48.9 m
52.7 m
63.7 m
(a) 72.6 m
(b) 72.6 m
87.8 m
0 5 10 15 20 25 30
extractable Fe (mg g-1 rock)
(d)
Humid (Nahuelbuta)
0.025 m
0.5 m
1.5 m
3.1 m
6.1 m
8.7 m
10.9 m
12.9 m
14.5 m
17.9 m
19.2 m
21.0 m
25.5 m
30.4 m
33.7 m
0 5 10 15 20 25 30
extractable Fe (mg g-1 rock)

Figure 3.1: Biogenic Fe species (mg g^{-1} rock) as function of depth (m) for the four field sites. The six Fe species are adsorbed Fe(II) and Fe(III), poorly crystalline Fe(II) and Fe(III), and crystalline Fe(II) and Fe(III) (*N* = 60). The four field sites (a) Pan de Azúcar, (b) Santa Gracia, (c) La Campana, and (d) Nahuelbuta cover an extreme climate gradient from arid to humid (North to South) along the Coastal Chilean Cordillera. Bars in (a) to (d) represent the average of technical extraction triplicates. Error bars denote standard error of the technical extraction replicates.

out the whole profile. Comparable to PdA and SG, the soil is oxidised, while saprolite and bedrock are reduced.

Regarding the correlation between the Fe pools, adsorbed Fe and poorly crystalline Fe are positively correlated (Fig. 3.S1). More specifically, the degree of correlation increases the more South the field site is located (PdA<SG<LC<NA). Adsorbed Fe and crystalline Fe are negatively correlated (Fig. 3.S2). The more crystalline Fe is present, the less adsorbed Fe (= easily bioavailable Fe) is present, while the degree of correlation is moderate to strong (SG< PdA<LC<NA). Poorly crystalline Fe and crystalline Fe are negatively correlated (Fig. 3.S3). The more crystalline Fe, the less poorly crystalline Fe is present. Correlation for all field sites is very strong (R^2 = 0.96-0.99), except for PdA (R^2 = 0.77).

3.4.2 Organic and inorganic carbon contents of the weathering profiles

Organic and inorganic carbon pools were quantified to assess how much bioavailable organic carbon (BOC) and inorganic carbon (IC) are available as C sources for microbial Fe(III) reduction and Fe(II) oxidation. SRDTC provided data on (1) the C that is bioavailable for heterotrophic microorganisms (BOC), (2) the C that is organic but not bioavailable for microorganisms (residual organic carbon = ROC), and (3) the C that is inorganic and bioavailable for autotrophic microorganisms (IC). Total C concentrations vary between approximately 0.05 and 20 mg Fe g^{-1} soil/rock powder (Fig. 3.2). Overall, PdA and SG are IC-dominated, while LC and NA have relatively more BOC compared to ROC and IC pool sizes. There is no clear indication of depth trends for the four field sites, but rather peaks of IC.

The total carbon pool size ranges from <1 to 20 mg C g^{-1} soil/rock in Pan de Azúcar (Fig. 3.2a). BOC concentrations range from 0.06-0.24 mg g^{-1} soil/rock (Fig. 3.S4), but are dominated by IC concentrations. The latter are most pronounced at 7.1, 7.2, 18.9, 19.1, 19.5, 51.5, 53.6, 54.8, 67.6, 79.6 and 87.5 m depth (*n* = 11).

In Santa Gracia, the total carbon pool size ranges from 0.1 to ~ 3 mg g^{-1} soil/rock (Fig. 3.2b). BOC is consistently present throughout the profile with a concentration range of 0.03-0.53 mg

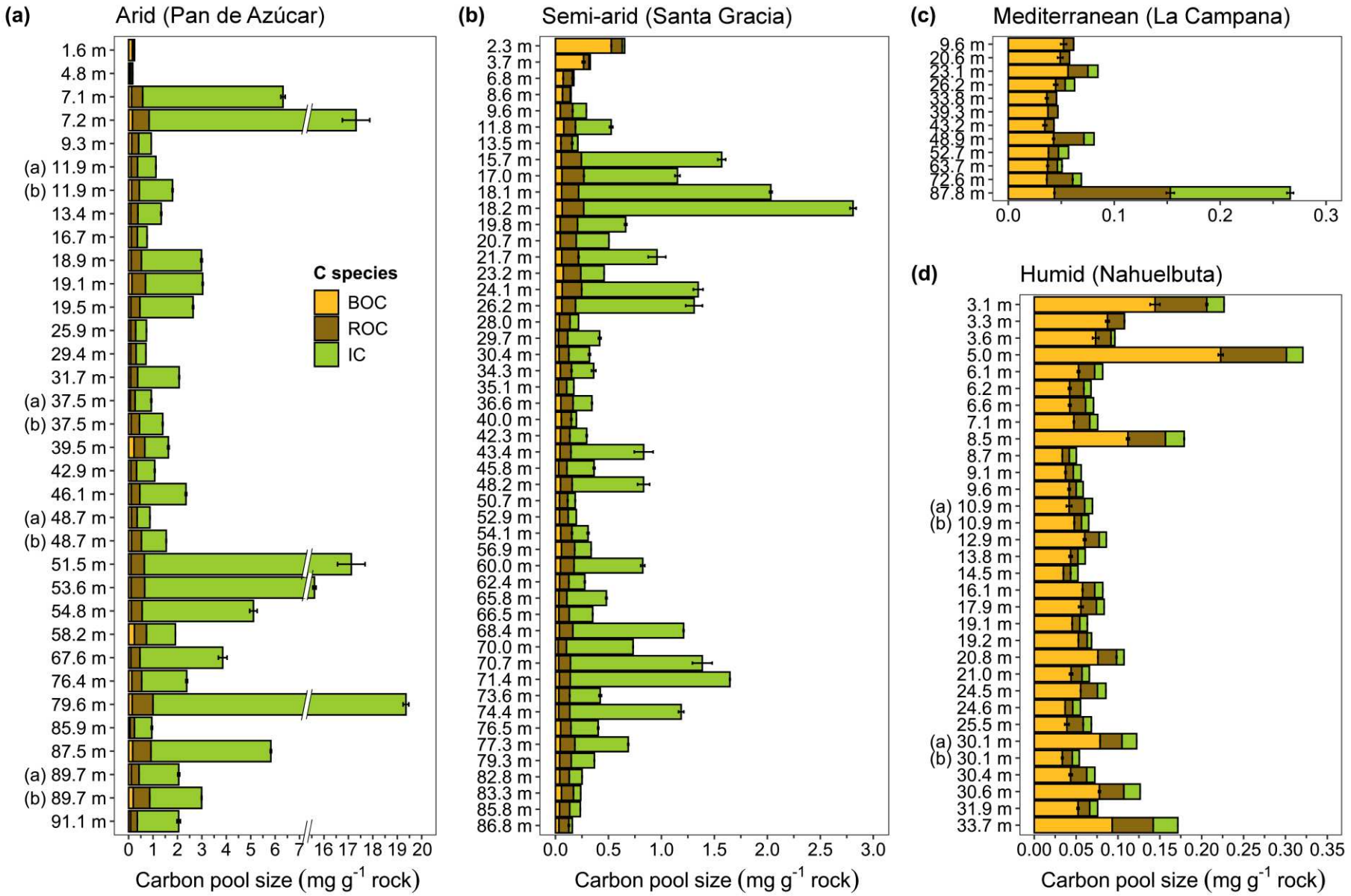
(a)
Arid (Pan de Azúcar)
1.6 m
4.8 m
7.1 m
7.2 m
9.3 m
(a) 11.9 m
(b) 11.9 m
13.4 m
16.7 m
18.9 m
19.1 m
19.5 m
25.9 m
29.4 m
31.7 m
(a) 37.5 m
(b) 37.5 m
39.5 m
42.9 m
46.1 m
(a) 48.7 m
(b) 48.7 m
51.5 m
53.6 m
54.8 m
58.2 m
67.6 m
76.4 m
79.6 m
85.9 m
87.5 m
(a) 89.7 m
(b) 89.7 m
91.1 m
C species
BOC
ROC
IC
0 1 2 3 4 5 6 7 16 17 18 19 20
Carbon pool size (mg g-1 rock)
(b)
Semi-arid (Santa Gracia)
2.3 m
3.7 m
6.8 m
8.6 m
9.6 m
11.8 m
13.5 m
15.7 m
17.0 m
18.1 m
18.2 m
19.8 m
20.7 m
21.7 m
23.2 m
24.1 m
26.2 m
28.0 m
29.7 m
30.4 m
34.3 m
35.1 m
36.6 m
40.0 m
42.3 m
43.4 m
45.8 m
48.2 m
50.7 m
52.9 m
54.1 m
56.9 m
60.0 m
62.4 m
65.8 m
66.5 m
68.4 m
70.0 m
70.7 m
71.4 m
73.6 m
74.4 m
76.5 m
77.3 m
79.3 m
82.8 m
83.3 m
85.8 m
86.8 m
0.0 0.5 1.0 1.5 2.0 2.5 3.0
Carbon pool size (mg g-1 rock)
(c)
Mediterranean (La Campana)
9.6 m
20.6 m
23.1 m
26.2 m
33.8 m
39.3 m
43.2 m
48.9 m
52.7 m
63.7 m
72.6 m
87.8 m
0.0 0.1 0.2 0.3
(d)
Humid (Nahuelbuta)
3.1 m
3.3 m
3.6 m
5.0 m
6.1 m
6.2 m
6.6 m
7.1 m
8.5 m
8.7 m
9.1 m
9.6 m
(a) 10.9 m
(b) 10.9 m
12.9 m
13.8 m
14.5 m
16.1 m
17.9 m
19.1 m
19.2 m
20.8 m
21.0 m
24.5 m
24.6 m
25.5 m
(a) 30.1 m
(b) 30.1 m
30.4 m
30.6 m
31.9 m
33.7 m
0.00 0.05 0.10 0.15 0.20 0.25 0.30 0.35
Carbon pool size (mg g-1 rock)

Figure 3.2: Carbon species (mg g^{-1} rock) as function of depth (m) for the four field sites. The three C species are bioavailable organic carbon (BOC), residual organic carbon (ROC) and total inorganic carbon (IC) (*N* = 127). The four field sites (a) Pan de Azúcar, (b) Santa Gracia, (c) La Campana, and (d) Nahuelbuta cover an extreme climate gradient from arid to humid (North to South). Bars in (a) to (d) represent the average of technical measurement duplicates. Error bars denote standard error of the technical measurement replicates. Note the differences in x-axis range of the four subplots.

C g^{-1} with high values in the soil. IC concentrations peak at some depths, comparable to PdA. Depths with high IC concentrations are 15.7-26.2, 43.4-48.2, 60.0, 68.4-77.3 m (*n* = 22). The IC data also complement previously identified zones of hydrothermal alteration in the SG weathering profile as elaborated in Chapter 2, Krone et al. (2021a); Hampl et al. (2022).

In La Campana, the total carbon pool size ranges from 0.05 to 0.3 mg C g^{-1} soil/rock, which is less quantified carbon than in PdA and SG (Fig. 3.2c). The BOC pool size is about 0.03-0.06 mg C g^{-1}, while representing 15-85% of the total carbon pool. IC carbon is present at 23.1, 26.2, 48.9, 52.7, 63.7, 72.6 and 87.8 m depth.

In Nahuelbuta, the total carbon pool size ranges from 0.05 to 0.35 mg C g^{-1} soil/rock, which represents a similar concentration range as in LC (Fig. 3.2d). The BOC pool size is approximately 0.03-0.22 mg g^{-1}, while being most pronounced in 5 and 8.5 m depth. ROC (0.01-0.08 mg C g^{-1}) and IC (0-0.03 mg C g^{-1}) concentrations are low compared to BOC concentrations.

Regarding the correlation between the C pools, BOC and ROC show a very weak (SG: R^2 = 0.12), weak (PdA: R^2 = 0.35), moderate (NA: R^2 = 0.59) to high correlation (LC: R^2 = 0.78) (Fig. 3.S5). The correlation between BOC and ROC for PdA and SG is negative, while positive for LC and NA. BOC and IC show a strong correlation (PdA, SG and LC: R^2 = 0.72-0.87) with one exception (NA: R^2 = 0.39) (Fig. 3.S6). The correlation is negative for all four field sites, i.e. the more IC the less BOC is present. Finally, ROC and IC show a strong (PdA, SG: R^2 = 0.76, 0.62), moderate (LC: R^2 = 0.43) or no correlation (NA: R^2 < 0.01) (Fig. 3.S7). The correlation is negative in the cases where it is strong (PdA, SG), and is positive, in the case where the strength of correlation is moderate (LC).

3.4.3 Fe-C pool interconnections

Overall, correlations between Fe and C pools are non-existent to moderate among the four field sites (R^2 = <0.01-0.52) (Figs 3.S8-3.S13). The correlation is strongest for LC (R^2 = 0.36-0.52) and decreases over NA (R^2 = 0.19-0.39) to PdA (R^2 = 0.05-0.22) and SG (R^2 = <0.01-0.12). In LC, the correlation between BOC and adsorbed Fe is slightly negative, i.e. the more BOC, the less adsorbed Fe is present. The trend is opposite between IC and adsorbed Fe. For poorly crystalline Fe and BOC, there is also a negative correlation, while it is hard to identify a

clear trend for the plot of poorly crystalline Fe vs IC. Finally, the scenario for crystalline Fe is different. If correlated with BOC, it is positive, if correlated with IC, it is negative.

3.4.4 Fe-fracture interconnections

Based on the findings of this study, we systemically investigated, if there are interconnections between fractures (type and density) and Fe minerals, we have defined the following four working hypothesis (*H1* - *H4*):

H1: Fe(II)/Fe(tot)-ratio is a good indicator for the penetration depth of oxygen, with high Fe(II)/Fe(tot)-ratios representing the presence of adsorbed Fe. (see Chapter 3.4.5)
H2: Fracture density controls the Fe redox zonation of the weathering profile. (see Chapter 3.4.6)
H3: Poorly crystalline Fe is a good indicator for predicting the presence of fractures. (see Chapter 3.4.7)
H4: The amount of BOC is higher in open fractures than in closed fractures. (see Chapter 3.4.7)

3.4.5 Fe(II)/Fe(tot)-ratio as proxy for the penetration depth of oxygen

We found a redox zonation comprised of two to three zones (see Chapter 3.1.1) in all four weathering profiles (Fig. 3.1; Table 3.S1). To determine, if there is an effect of penetration depth of oxygen on the Fe redox status, i.e. the Fe(II)/Fe(tot)-ratio, we plotted Fe(II)/Fe(tot)-ratios against adsorbed Fe concentrations for 15 samples of each of the four field sites (Fig. 3.3) (hypothesis *H1*).

Overall, there was a moderate to very strong positive correlation between Fe(II)/Fe(tot)-ratio and adsorbed Fe, which increased from North to South (nonlinear least squares fit equation: $y=a*e^{bx}$, R^2 = 0.42-0.93). These results suggest that Fe(II)/Fe(tot)-ratios are indicative for the oxygen penetration depth of each of the four weathering profiles (Table 3.S1), which is reflected in the adsorbed Fe concentrations (Fig. 3.1). Hence, the presence of adsorbed Fe marks depth zones, which oxygen does not reach and in which Fe(II) is preserved.

3.4.6 Does fracture density impact the Fe redox zonation of the weathering profiles?

The Fe(II)/Fe(tot)-ratio was found to be a good indicator for the penetration depth of oxygen (see Chapter 3.4.5). As oxygen is transported into the subsurface via fractures, we tested, if fracture density controlled the Fe redox zonation of the weathering profiles (Fig. 3.4) (hypothesis *H2*). An overview of the fracture density distribution of the four field sites can be found in the SI (Table 3.S2). The amount of fractures (x) was counted for 5m intervals and

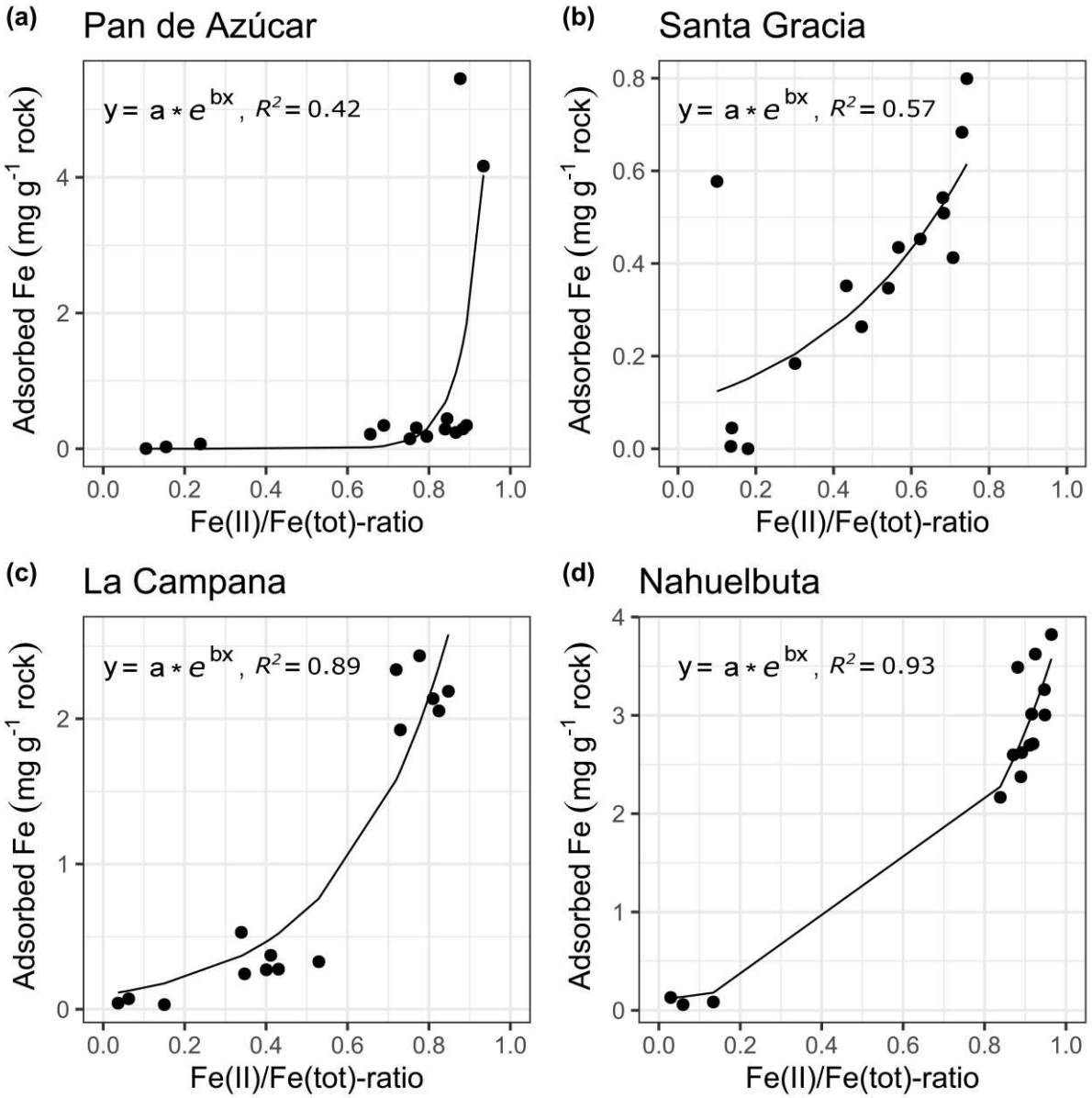

Figure 3.3: Adsorbed Fe concentration (mg g^{-1} rock) as function of the Fe(II)/Fe(tot)-ratio for the four field sites. The equation displays the function of the nonlinear least squares fit, accompanied by the adjusted R^2, which increases from North to South (R^2 = 0.42-0.93).

assigned to the categories (a) “low”, if x<=10, (b) “medium”, if 10<x>25, and (c) “high”, if x>=25. We found an indication for a statistically significant difference in the Fe(II)/Fe(tot)-ratio according to fracture density (F(2)=4.39, *P*<0.05) and a strong indication for a statistically significant difference in the Fe-ratio according to field site (F(3)=4.50, *P*<0.001) (Table 3.S3). A Tukey *post-hoc* test revealed a significant pairwise difference between fracture density types low and medium (*P*<0.01), but none for the fracture density type pairs low-high and medium-high (Table 3.S4). It also revealed significant pairwise differences between field sites NA and

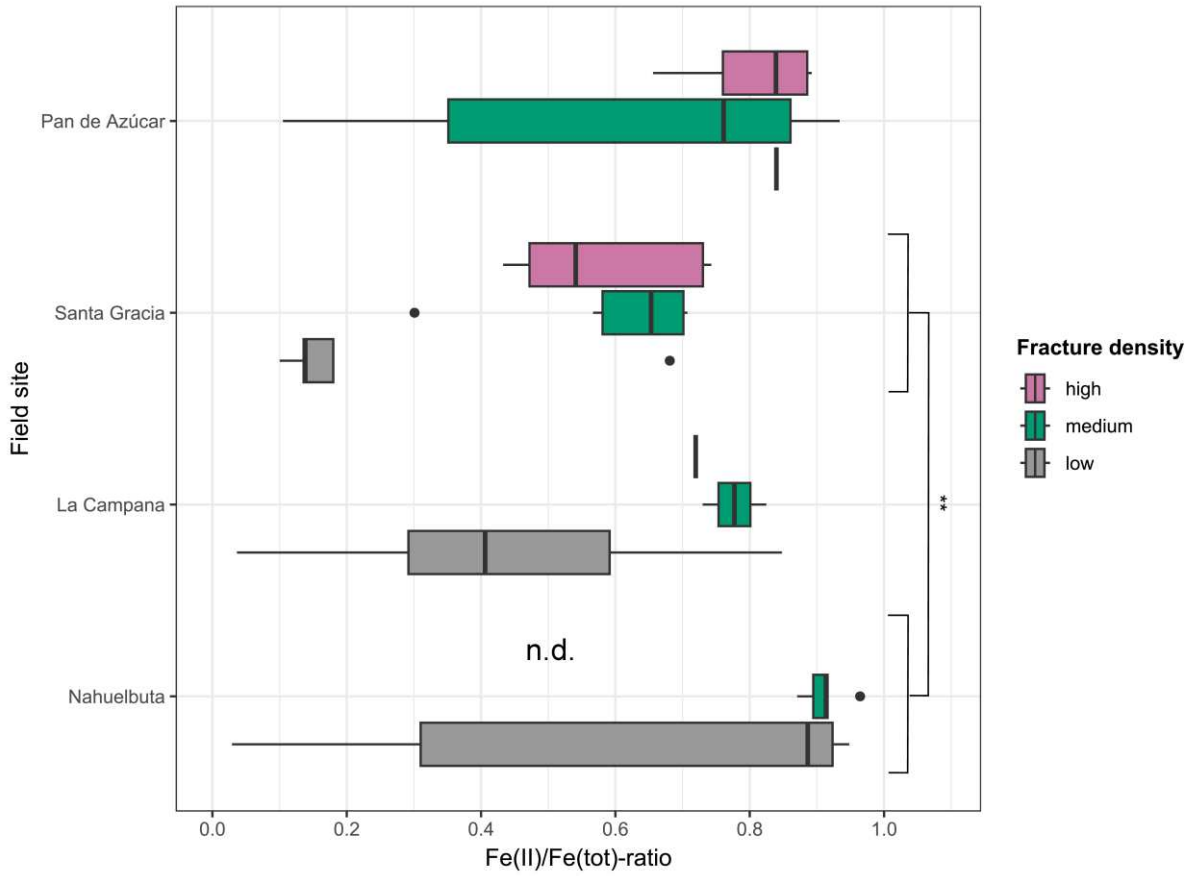

Figure 3.4: Fe(II)/Fe(tot)-ratio as function of fracture density (low, medium, high) for the four field sites. The three fracture density types are “low” (grey, *n*=28), “medium” (green, *n*=24) and “high” (purple, *n*=10). The amount of fractures (x) was counted for 5m intervals and assigned to the categories (a) “low”, if x<=10, (b) “medium”, if 10<x>25, and (c) “high”, if x>=25. The four field sites are displayed top-down from North to South. Significant differences in treatment contrasts revealed by a Tukey *post-hoc* test are highlighted as respective significance level (***: *P*<0.001, **: *P*<0.01, *: *P*<0.05, n.s.= not significant). ”n.d.” denotes no data.

SG (diff=0.329, *P*<0.01). These findings suggest that a low fracture density is associated with a moderate mean Fe(II)/Fe(tot)-ratio (*n*=28, mean=0.49), while a medium fracture density is associated with an on average 0.21 units higher Fe(II)/Fe(tot)-ratio (*n*=24, mean=0.70). In summary, fracture density can be used to predict an expected Fe(II)/Fe(tot)- ratio, if “low” and “medium” fracture density samples are referred to, while it fails to clearly distinguish Fe(II)/(tot)-ratios, if fracture density intervals are “high”.

Similarly to the Fe(II)/Fe(tot)-ratios, we systemically determined, if there is an effect of fracture density on adsorbed Fe (F=2.16, *P*=0.12) (Fig. 3.S14), poorly crystalline (F=1.62, *P*=0.21) (Fig. 3.S15), crystalline Fe (F=1.89, *P*=0.16) (Fig. 3.S16) and BOC (F=0.18, *P*=0.83) (Fig. 3.S17) or IC (F=4.87, *P*<0.01) (Fig. 3.S18) in the weathering profiles. In short, there were no significant effects of fracture density on any of these, but IC.

Regarding IC, there were indications for (a) an effect of fracture density (F=4.87, *P*<0.01), (b) an effect of site (F=12.3, *P*<0.001), and (c) an interaction effect (F=2.56, *P*<0.001). Fracture

density difference between levels medium-low was found to be significant (diff=1.64, *P*<0.01). We also found significant pairwise differences between sites NA-PdA (diff=-2.82, *P*<0.01), LC-PdA (diff=-2.45, *P*<0.05) and NA-PdA (diff=-2.85, *P*<0.001). These findings suggest an overall significant difference in IC between medium and low fracture density, but not for the pairs "high-low" and "high-medium".

In summary, fracture density can be potentially used as a proxy for the Fe(II)/Fe(tot)-ratio and IC concentrations, if only low and medium densely fractured depth intervals are considered.

3.4.7 Is there more poorly crystalline Fe and BOC in fractures compared to non-fractured zones?

As Fe(III) (oxyhydr)oxides were found to be abundant in fracture zones of Santa Gracia (Chapter 2), we followed up on this finding by assessing if this is true for all four field sites (hypothesis *H3*). Therefore, we plotted the four fracture types “none”, “open” (including weak zones), “closed” and “vein” against poorly crystalline Fe concentration for all field sites and tested, if there was a significant difference between the absence and presence of fractures (Fig. 3.5).

We found that poorly crystalline Fe concentrations were significantly higher for the three fracture types ("open", "closed" and "vein") compared to their absence ("none") (i.e. in between group means: "open-none" (diff=1.51, *P*<0.05), "closed-none" (diff=1.69, *P*<0.01), and "vein-none" (diff=1.96, *P*<0.05) (Tables 3.S5,3.S6). More detailed statistical analysis revealed three significant treatment contrasts for fracture type, four for field site and three for the interactions of fracture type and field site. Regarding the amount of poorly crystalline Fe found at the different field sites, there is significantly more Fe in LC and NA than in PdA, and significantly more Fe in LC and NA than in SG. Besides that, we found significantly more Fe in closed fractures in NA compared to closed fractures of PdA and SG. In summary, these results suggest that the amount of poorly crystalline Fe is a good indicator to predict the presence of fractures.

Based on our finding that poorly crystalline Fe is a good indicator to predict the presence of fractures, we further investigated its importance in fractured vs non-fractured zones (Table 3.1). We could identify that there is more poorly crystalline Fe in fractures compared to non-fractured zones for field sites PdA (5.7-fold), SG (1.6-fold) and NA (3.3-fold), but an almost identical amount in LC (1.0-fold).

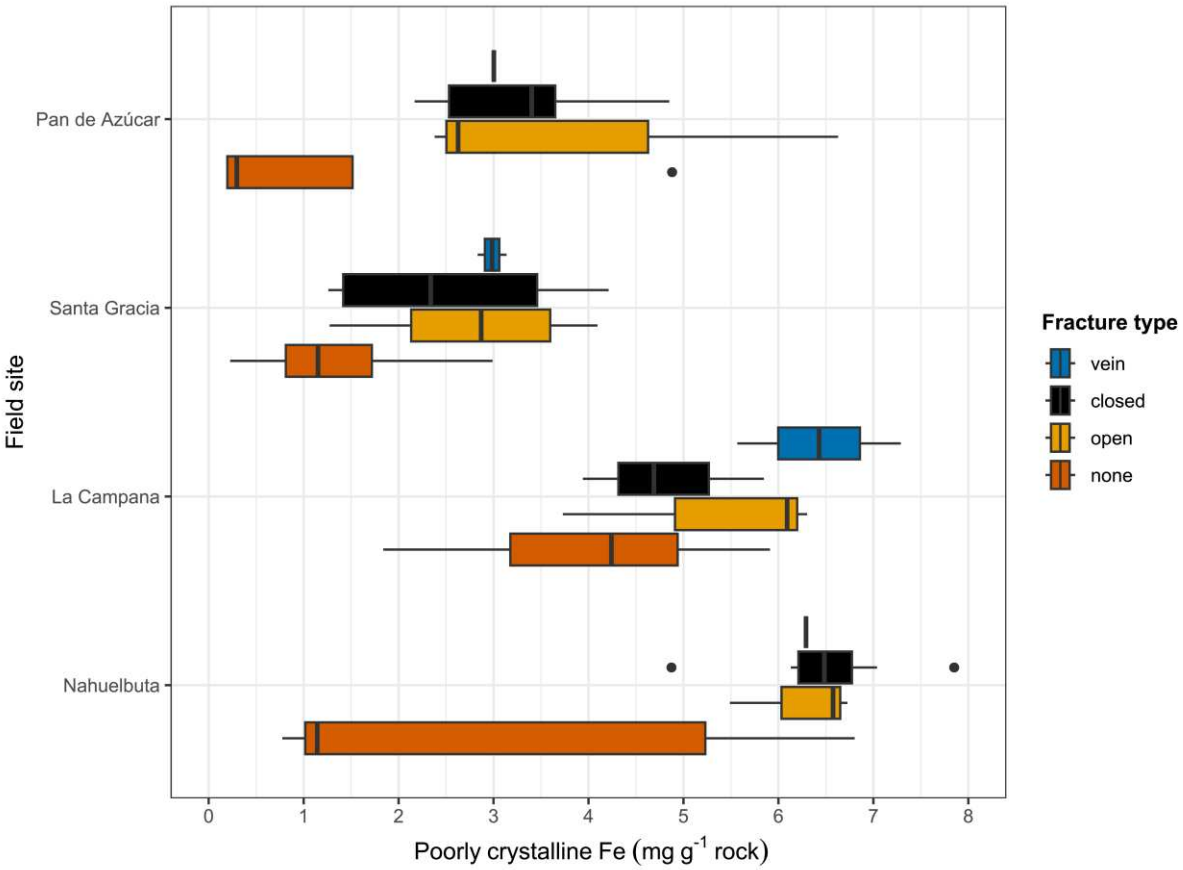

Figure 3.5: Poorly crystalline Fe concentration (mg g^{-1} rock) as function of fracture type for the four field sites. The four fractures types are “none” (orange, *n*=20), “open” (yellow, *n*=15), “closed” (black, *n*=21) and “vein” (blue, *n*=6), with “none” serving as reference for the absence of fractures. The four field sites are displayed top-down from North to South.

Table 3.1. Relative proportion of poorly crystalline Fe (P) of total bioavailable Fe pool (unitless), i.e. the sum of adsorbed (A), poorly crystalline (P) and crystalline (C) Fe (P/(A+P+C)) based on mean values, comparing non-fractured with fractured zones of the four field sites. For the mean, the median was used, since the mean will be distorted by outliers.

Field site	**Fracture type**					**Factor (fractured / non-fractured)**
	“none”	“open” (o)	“closed” (c)	“vein” (v)	**(o+c+v) / 3**	
PdA	**0.04**	0.20	0.27	0.23	**0.23**	**5.7**
SG	**0.07**	0.12	0.10	0.12	**0.11**	**1.6**
LC	**0.19**	0.20	0.18	0.20	**0.20**	**1.0**
NA	**0.07**	0.23	0.25	0.24	**0.24**	**3.3**
average	*0.09*	*0.19*	*0.20*	*0.19*	*0.19*	*2.1*

As crystalline Fe is abundant in all of four field sites, we investigated, if it served as a proxy for the presence of fractures, too. We found that the amount of crystalline Fe significantly differs between the absence of fractures (“none”) and “open”/”vein” fractures, but not between the absence of fractures and “closed” fractures (Fig. 3.S19). More specifically, the differences in treatment contrasts were "open-none" (diff=3.94, *P*<0.01), "vein-none" (diff=1.77, *P*=0.34),

"closed-none" (diff=4.97, *P*<0.05). These findings suggest that the type of fracture needs to be known to make use of crystalline Fe as indicator for the presence fractures.

Eventually, we statistically tested, if the amount of BOC found in open fractures is higher than in closed fractures (Fig. 3.6) (hypothesis *H4*). This is interesting to know, since we found poorly crystalline Fe to be significantly higher in open fractures (Fig. 3.5), which functions as electron acceptor for microbial Fe(III) reduction, while BOC functions as electron donor. Therefore, we further assumed that elevated BOC concentrations in open fractures required (a) an ongoing transport of BOC into the subsurface and (b) a preservation mechanism of BOC at depth.

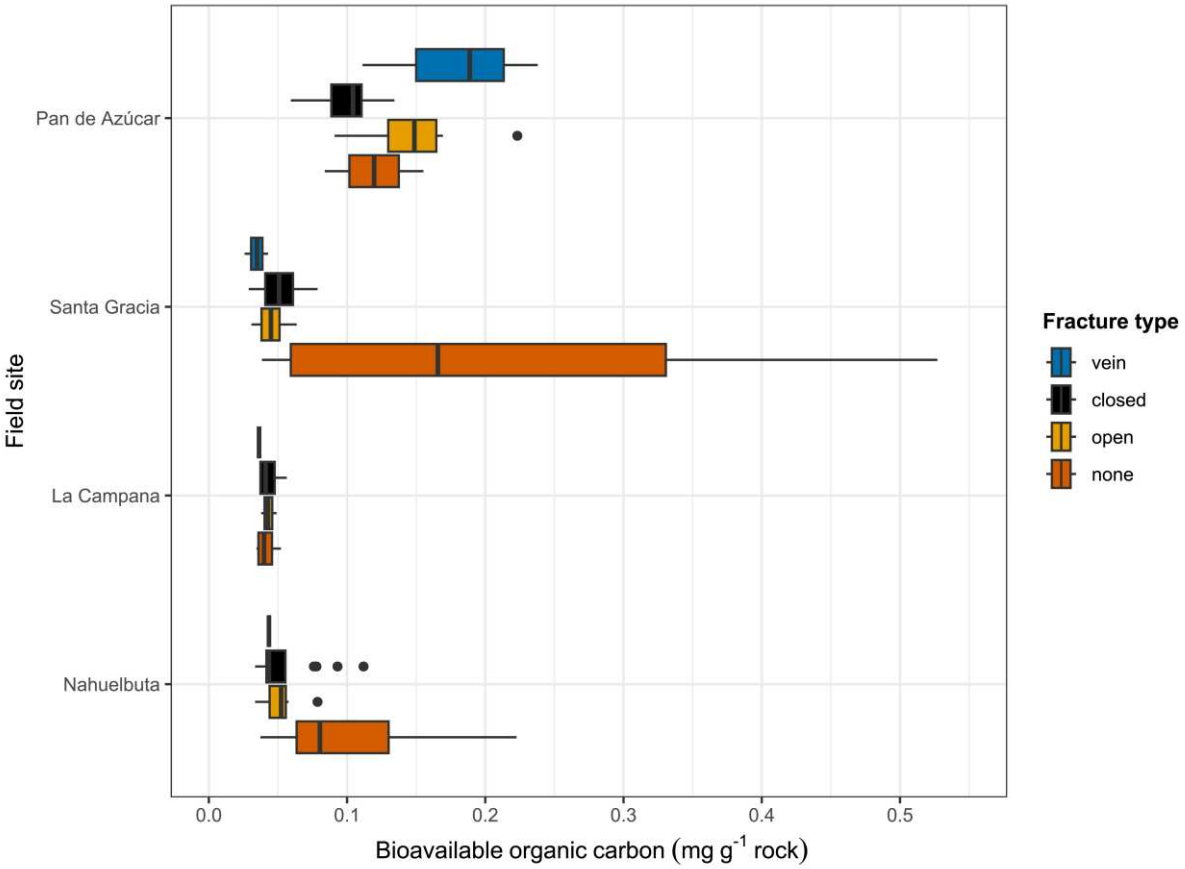

Figure 3.6: Bioavailable organic carbon concentration (mg g^{-1} rock) as function of fracture type for the four field sites. The four fractures types are “none” (orange, *n*=16), “open” (yellow, *n*=39), “closed” (black, *n*=61) and “vein” (blue, *n*=13), with “none” serving as reference for the absence of fractures. The four field sites are displayed top-down from North to South.

Overall, there was significantly less BOC in fractures compared to non-fractured depth intervals (F=6.67, *P*<0.001) (Table 3.S7). Differences between treatment levels were significant for the pairs “open-none” (diff=-0.06, *P*<0.001), “closed-none” (diff=-0.05, *P*<0.001) and “vein-none” (diff=-0.05, *P*<0.05) (Table 3.S8). The amount of BOC in open fractures is not significantly higher than in closed fractures (“closed-open”: diff=0.004, *P*=0.97). Hence, we could not prove that the amount of BOC in open fractures is significantly higher than in closed fractures.

Furthermore, we found a statistically significant difference in BOC concentration according to field site for the presence of fractures vs their absence (F=20.4, *P*<0.001). A Tukey *post-hoc* test revealed strong significant pairwise differences between PdA and each of the other field sites (SG, LC and NA) for open fractures (PdA-SG: diff=-0.06, *P*<0.001; PdA-LC: diff=-0.09, *P*<0.001; and PdA-NA: diff=-0.06, *P*<0.001), but not among other field site pairings.

Regarding interactions of fracture type and field site, a Tukey post-hoc test revealed that there is significantly more BOC in (a) open fractures of PdA than in open fractures of the other field sites SG (*P*<0.001), LC (*P*<0.05) and NA (*P*<0.01), and (b) non-fractured zones compared to fractured zones of SG (*P*<0.001) (Table 3.S8).

Further statistical tests revealed that there was no significant difference in the mean (a) adsorbed Fe concentration (F=1.62, *P*=0.20) (Fig. 3.S20), and (b) the mean IC concentration (F(3)=1.44, *P*=0.24) (Fig. 3.S21) when comparing the absence of fractures (“none”) with the presence of fractures (i.e. “open”, “closed”, “vein”). In summary, we found evidence that the presence of fractures can be predicted by poorly crystalline Fe, while this is only partially true for crystalline Fe and BOC.

3.5 Discussion

3.5.1 Drivers of Fe and C geochemistry in the deep subsurface along a climate gradient

The Fe and C geochemistry depth profile patterns of the field sites may be driven by differences in lithology, presence of fractures, hydrothermal alteration, surface inputs such as water, oxygen, acids and OC, and activity of microorganisms (Samuels et al., 2019; 2020; Krone et al., 2021b; 2024; Hampl et al., 2022; 2023; Trichandi et al., 2022; 2023; 2024). The granitoid lithology differs with depth and among field sites, since quartz, alkali feldspar and plagioclase contents of the bedrocks vary (see Chapter 3.3.1). Besides that, there are differences in the amount (wt.-%) of Fe-bearing minerals biotite, chlorite, hornblende, magnetite, hematite and accessory minerals such as pyrite and chalcopyrite. Consequences are a distinction in the degree of resistance to weathering as well as in the extractable crystalline Fe pools of the field sites, as, for example, magnetite being abundant in the SG weathering profile (Fig. 3.1) (see Hampl et al., 2022).

Tectonic activity creates fractures on a µm to km scale which play a vital role in weathering processes, since they are pathways for fluids to depth and hence control the weathering depth (Berkowitz, 2002; Deng and Spycher, 2019; Andrews et al., 2023). A feature of fracture zones in the study sites investigated in this dissertation is the accumulation of poorly crystalline Fe(III) (oxyhydr)oxides, which have proven to be a robust proxy (Fig. 3.5, Table 3.1). The same is conditionally true for crystalline Fe minerals (i.e. for open and closed fractures, but not for veins) (Fig. 3.S3). However, adsorbed Fe(II) concentrations were not significantly higher in fracture zones compared to unfractured zones, suggesting that this Fe pool is not stable enough to prevail, since easily oxidisable by oxygen (Fig. 3.S20) (Byrne et al., 2015; Schad et al., 2022).

Hydrothermal alteration alters the mineral composition of the bedrock. Typical features associated with hydrothermal alteration are the (a) chloritisation of biotite, (b) formation of expandable inter-stratified chlorite-smectite, (c) formation of zeolites, (d) partial transformation of magnetite to hematite (martitisation), and (e) Al and C depletion in fractures due to feldspar breakdown and related porosity increase (Eliasson, 1993; Drake et al., 2008; Nishimoto and Yoshida, 2010; Sandström et al., 2010; Kralj, 2016; Hampl et al., 2022). In PdA and SG, the impact of hydrothermal alteration is evident by the crystallinity of the Fe pool, high degrees of Fe(II) oxidation, fracture fillings (i.e. carbonates (= IC) and poorly crystalline Fe(III) (oxyhyr)oxides) and other features listed above, while it is virtually absent in LC and NA (Figs 3.1,3.2) (see Hampl et al., 2022; Krone et al., 2024).

Fe and C geochemistry patterns have also been linked to surface inputs such as water, oxygen, acids and OC (Eppes and Keanini, 2017). The amount of meteoric water introduced into the

subsurface depends on the climate zone which controls the weathering intensity of a system (Übernickel et al., 2020; Deng et al., 2022). Additionally, water can also be supplied via deep aquifers, which have not been investigated in depth at the four study sites (see Herrera et al., 2018; Taucare et al., 2020a; Taucare et al., 2020b). O_2 entering the subsurface is rapidly consumed by abiotic oxidation of Fe(II)-bearing silicates in the upper zone of weathering profiles resulting in the formation of secondary Fe minerals (White and Yee, 1985; Perez et al., 2005). Acid and OC patterns are primarily controlled by the net primary production (NPP) of a system with more nutrient cycling the wetter the climate (Oeser and von Blanckenburg, 2020; Koester et al., 2021; Stock et al., 2021). Hence, the NPP varies as a function of the climate zone (Werner et al., 2018). However, the bioavailable organic carbon contents in the deep subsurface of the four study sites are comparably high (0.03-0.53 mg C g^{-1} rock) (Fig 3.S4). This implies that (a) there is a transport of OC to depth but no accumulation (Fig. 3.6), and that (b) the type and quantity of biogenic Fe pool are the primary controls whether microbial weathering of Fe-bearing minerals occurred.

Finally, Fe-metabolising microorganisms play a role in weathering of Fe-bearing minerals (Chapter 2) (Cockell et al., 2011; Napieralski et al., 2019). Microbial weathering of Fe-bearing minerals has been investigated among others in shale (Samuels et al., 2019; Napieralski et al., 2022), limestone (Jakus et al., 2021a; 2021b), diorite (Buss et al., 2005) and granite (Napieralski et al., 2019; Bethencourt et al., 2020; Bochet et al., 2020). In presence of water, essential elements (e.g. C, N, P, S) and suitable electron sources, Fe-metabolising microorganisms impact the weathering process by Fe(II) oxidation and Fe(III) reduction resulting in the (trans)formation of biogenic Fe minerals. In the context of characterisation of the Fe and C geochemistry (Figs 3.1,3.2), depth intervals with bioavailable Fe minerals (i.e. Fe carbonates, ferrihydrite and magnetite) and BOC are probable zones of microbial weathering activity.

3.5.2 Tectonic control on Fe geochemistry

The subsurface weathering structure along the Chilean Coastal Cordillera is influenced by active fault systems such as the Atacama Fault System, Central Coastal Forarc and Southern Chile Forarc (Riquelme et al., 2003; Cembrano et al., 2005; Rehak et al., 2008; Melnick et al., 2019; Maldonado et al., 2021). Active fault systems create fractures (µm to km scale) and hence open pathways for water, O_2, CO_2 and nutrients to enter the subsurface (Brantley et al., 2017). These fractures promote the propagation of the weathering front to depth. The advancement of this front can either be connected to ‘bottom-up’ or ‘top-down’ systems. ‘Bottom-up’ systems are controlled by groundwater (GW) level and surface topography (Rempe and Dietrich, 2014), whereas ‘top-down’ systems are driven by infiltration of meteoric water and oxygen into the bedrock (Brantley and White, 2009; Eppes et al., 2018). Regarding the study sites of this thesis, there are three scenarios. Firstly, we can assign PdA to the

‘bottom-up’ type, since GW and surface topography are more relevant than the limited precipitation rate of this site. Secondly, LC can be classified as ‘top-down’ system, since it has a higher precipitation rate than PdA and lacks a groundwater table according to seismic investigations (Trichandi et al., 2023). Thirdly, we have a less distinct situation in SG and NA, which may be best explained by a mixture of a ‘bottom-up’ and ‘top-down’ system. In SG, combined seismic and borehole investigation suggest the presence of a major fault zone functioning as a fluid pathway, while signs for a potentially groundwater-influenced zone at depth (approx. 67-77 m) have been determined too (Krone et al., 2021b; Trichandi et al., 2022). In NA, we have a combination of high precipitation and presence of a groundwater table.

This classification of the four study systems helps us to explain the observed Fe geochemistry patterns (Figs 3.1,3.3). Since open fractures are pathways for the infiltration of fluids, they control how deep water and oxygen can be transported into the subsurface. Contrastingly, closed fractures will hamper the fluid transport to depth. This is confirmed by the positive correlation between Fe redox status (i.e. Fe(II)/Fe(tot)-ratio) and adsorbed Fe concentration, assuming higher Fe(II)/Fe(tot)-ratios (i.e. less oxygen) with increasing depth (Fig. 3.3).

Fracture density is another relevant parameter controlling the Fe(II)/Fe(tot)-ratio (Ehlen, 1999). Using statistics, we found a significant pairwise difference in the Fe(II)/Fe(tot)-ratio between fracture density types “low” and “medium” (P<0.01; mean(low)= 0.49, mean(medium)= 0.70), but no significant pairwise differences related to a “high” fracture density (Fig. 3.4). Andrews et al. (2023) found that a higher fracture density is related to more weathering and a slower mineral dissolution rate, while a lower fracture density is connected to less weathering and a higher mineral dissolution rate. More weathering implies more water infiltration and oxygen transport to depth resulting in Fe(II) oxidation of Fe-bearing minerals (Hampl et al., 2023; Trichandi et al., 2023). Hence, a high fracture density disrupts the preservation of the redox-sensitive Fe(II)/Fe(tot)-ratio, since the supply of oxygen is higher at a high fracture density, while the Fe(II)/Fe(tot)-ratio is preserved at a low and medium fracture density.

3.5.3 Implications for potential subsurface microbial Fe cycling along the climate gradient

Together the site-specific observations of lithology, fracturing, hydrothermal alteration and surface inputs suggest that fracturing, water availability and secondary Fe mineral formation are the key factors driving Fe cycling in the deep subsurface of the four study sites. More specifically, there are several key features of each site:

- ***PdA*:** very low precipitation (Übernickel et al., 2020), high fracture density (Stroncik et al., in prep.), hydrothermal alteration (Krone, 2024), no major change in amount of extractable adsorbed and crystalline Fe with depth (this thesis), high IC content (this thesis) and signs for a deep aquifer (Houston, 2002; Herrera et al., 2018; Gamboa et al., 2019; 2022);

- ***SG*:** low precipitation (Übernickel et al., 2020), high fracture density (Stroncik et al., in prep.), hydrothermal alteration (Hampl et al., 2022), no major change in amount of extractable adsorbed and crystalline Fe with depth (this thesis), high IC content (this thesis) and signs for a deep aquifer (Weckmann et al., 2020; Krone et al., 2021b; Trichandi et al., 2022);
- ***LC*:** moderate precipitation (Übernickel et al., 2020), low fracture density (Stroncik et al., in prep.), no hydrothermal alteration (Krone, 2024), increase in amount of extractable adsorbed and crystalline Fe with depth (this thesis), low IC content (this thesis), no deep aquifer (Trichandi et al., 2023);
- ***NA*:** high precipitation (Übernickel et al., 2020), low fracture density (Stroncik et al., in prep.), no hydrothermal alteration (Krone, 2024), increase in amount of extractable adsorbed and crystalline Fe with depth (this thesis), low IC content (this thesis), and implications for a deep aquifer (Rehak et al., 2008).

Systematic assessment of the observations and site-specific key features reveals depth intervals of most probable *in situ* microbial Fe(II) oxidation and Fe(III) reduction along the climate gradient (Table 3.2). Generally, depth intervals with a potential microbial activity classified as “excellent”, “high” or “moderate” are considered to realistically host Fe-cycling microorganisms. These depth intervals can deviate for Fe(II)-oxidising and Fe(III)-reducing microorganisms, since the required electron and C sources needed for redox reactions differ. The highest probability for a potential *in situ* microbial weathering activity of Fe-bearing minerals across all sites is linked to the presence of open fractures (Table 3.2; Figs 3.5,3.S20,3.S21). These findings demonstrate that a pairing of Fe and C geochemistry with lithology and fracturing is a powerful tool to identify hotspots of potential microbial *in situ* weathering activity.

Table 3.2. Heatmap highlighting depths of potential hotspots of microbial weathering activity. The ranking is based on the weighted assessment of fracture density, fracture type, concentrations of adsorbed Fe(II), inorganic carbon, poorly crystalline Fe(III) and bioavailable organic carbon, and Fe(II)/Fe(tot)-ratio (i.e. Fe redox state) (see Supplementary Methods for more information on criteria definition and ranking determination). It results in a potential for microbial Fe(II) oxidation and Fe(III) reduction (levels: very low, low, moderate, high and excellent). Columns fracture type, Fe(II)/Fe(tot)-ratio and potential for microbial Fe(II) ox./Fe(III) red. are colour-coded to highlight key features.

field site	depth (m)	fracture density	fracture type	Fe_ad_II (mg/g)	IC (mg/g)	Fe_p_III (mg/g)	BOC (mg/g)	Fe(II)/Fe(tot)-ratio	Fe redox state	potential for microbial Fe(II) ox.	potential for microbial Fe(III) red.
PdA	9.3	medium	closed	0.09	0.51	0.12	0.13	0.77	red	low	low
PdA	19.1	high	open	0.02	2.34	0.14	0.14	0.66	red	moderate	moderate
PdA	25.9	high	closed	0.17	0.44	0.09	0.09	0.89	red	low	low
PdA	37.5	high	closed	0.07	0.95	0.14	0.10	0.88	red	low	low
PdA	46.1	medium	closed	0.10	1.89	0.14	0.11	0.87	red	low	low
PdA	53.6	medium	closed	0.07	14.95	0.24	0.10	0.69	red	moderate	low
PdA	67.6	high	open	0.05	3.39	0.07	0.09	0.79	red	moderate	moderate
PdA	76.4	medium	closed	0.28	1.84	0.18	0.13	0.84	red	low	low
PdA	85.9	medium	closed	0.01	0.71	0.09	0.06	0.75	red	low	low
PdA	87.5	medium	open	5.39	4.91	0.04	0.17	0.88	red	excellent	moderate
SG	2.3	low	none	0.00	0.02	2.90	0.53	0.10	ox	low	high
SG	6.8	low	closed	0.31	0.01	0.16	0.07	0.68	red	low	low
SG	11.8	medium	closed	0.00	0.34	0.39	0.08	0.30	ox	low	low
SG	19.8	medium	open	0.22	0.45	0.50	0.04	0.57	trans	moderate	moderate
SG	26.2	high	closed	0.09	1.12	0.38	0.06	0.43	trans	moderate	low
SG	35.1	medium	vein	0.27	0.07	0.28	0.03	0.62	red	moderate	low
SG	45.8	high	open	0.11	0.26	0.28	0.03	0.54	trans	moderate	moderate
SG	56.9	medium	open	0.36	0.16	0.31	0.06	0.68	red	moderate	moderate
SG	65.8	high	closed	0.77	0.37	0.07	0.03	0.74	red	moderate	low
SG	74.4	high	open	0.06	1.05	0.27	0.03	0.47	trans	moderate	moderate
SG	76.5	high	open	0.55	0.26	0.04	0.05	0.73	red	moderate	moderate
SG	82.8	medium	open	0.27	0.12	0.12	0.04	0.71	red	moderate	moderate
SG	82.8	medium	vein	0.27	0.12	0.12	0.04	0.71	red	low	low
LC	9.6	low	none	0.09	0.00	2.04	0.05	0.34	ox	very low	moderate
LC	20.6	low	open	0.00	0.00	1.35	0.05	0.35	ox	low	high
LC	33.8	low	none	0.00	0.00	1.10	0.04	0.43	trans	very low	low
LC	39.2	low	closed	0.01	0.00	1.11	0.04	0.40	trans	low	moderate
LC	43.2	low	none	0.13	0.00	1.78	0.03	0.53	trans	low	moderate
LC	48.9	medium	open	2.05	0.01	0.00	0.04	0.82	red	high	moderate
LC	52.7	high	open	2.23	0.01	0.44	0.04	0.72	red	high	moderate
LC	63.7	medium	closed	1.92	0.00	0.04	0.04	0.73	red	moderate	low
LC	72.6	low	vein	2.37	0.01	1.12	0.04	0.78	red	moderate	moderate
LC	87.8	low	none	2.18	0.11	0.00	0.04	0.85	red	moderate	very low
NA	3.1	low	none	2.62	0.02	0.00	0.14	0.89	red	moderate	low
NA	6.1	low	closed	3.26	0.01	0.00	0.05	0.95	red	high	low
NA	8.7	low	closed	2.16	0.01	0.00	0.03	0.84	red	moderate	low
NA	12.9	low	none	3.31	0.01	0.13	0.06	0.88	red	high	low
NA	14.5	low	closed	3.62	0.01	0.00	0.03	0.92	red	high	low
NA	17.9	medium	open	2.66	0.01	0.00	0.06	0.91	red	excellent	moderate
NA	19.2	medium	open	2.38	0.01	0.00	0.05	0.89	red	excellent	moderate
NA	21.0	medium	open	2.60	0.01	0.00	0.04	0.87	red	excellent	moderate
NA	25.5	low	closed	3.00	0.01	0.00	0.04	0.95	red	high	low
NA	30.4	medium	closed	2.97	0.01	0.01	0.04	0.92	red	high	moderate
NA	30.4	medium	vein	2.97	0.01	0.01	0.04	0.92	red	high	moderate
NA	33.7	medium	closed	3.81	0.03	0.00	0.09	0.96	red	high	low

3.6 Conclusion

In this study we characterised four granitoid weathering profiles along the Chilean Coastal Cordillera, which span a climatic gradient from arid desert to temperate rain forest between 26° and 38° S. We combined geochemical and petrophysical data with statistics to assess potential microbial *in situ* weathering of Fe-bearing minerals in the deep subsurface along the gradient.

While there is an increase in precipitation from North to South (PdA < SG < LC < NA), the four field sites are divided into two groups regarding fracturing and hydrothermal alteration. PdA and SG are characterised by a high fracture density (i.e. intensity), hydrothermally overprinted weathering profiles and high IC concentrations. In contrast, weathering profiles of LC and NA show a low fracture density, absence of hydrothermal alteration and low IC concentrations. Our analysis shows that precipitation and fracturing are the two major controls on subsurface Fe and C geochemistry. Firstly, there is no major change in the amount of extractable adsorbed and crystalline Fe with depth in PdA and SG. Conversely, there is an increase with depth in LC and NA. Secondly, high Fe(II)/Fe(tot)-ratios positively correlate with low and medium fracture density zones. Thirdly, fractures were identified as locations of more poorly crystalline Fe compared to unfractured zones in all four sites. Fourthly, there is less BOC in fractures compared to unfractured zones in SG, LC and NA, while the opposite is the case for PdA.

Together these findings enable the identification of locations of potential microbial *in situ* weathering of Fe-bearing minerals within the four weathering profiles. Apparently, the highest probability of microbial *in situ* weathering of Fe-bearing minerals is linked to open fractures. This work highlights the need for a pairing of mineralogy, geochemistry, tectonics and hydrology with microbiology to adequately assess the role of Fe-metabolising microorganisms in subsurface weathering processes, especially in more complex geologic environments.

3.7 References

Ackerer J., Ranchoux C., Lucas Y., Viville D., Clément A., Fritz B., Lerouge C., Schäfer G. and Chabaux F. (2021) Investigating the role of deep weathering in critical zone evolution by reactive transport modeling of the geochemical composition of deep fracture water. *Geochimica et Cosmochimica Acta* **312,** 257-278. https://doi.org/https://doi.org/10.1016/j.gca.2021.07.017.

Andrews E.M., Hyman J.D., Sweeney M.R., Karra S., Moulton J.D. and Navarre-Sitchler A. (2023) Fracture Intensity Impacts on Reaction Front Propagation and Mineral Weathering in Three-Dimensional Fractured Media. *Water Resources Research* **59**(2)**,** e2022WR032121. https://doi.org/https://doi.org/10.1029/2022WR032121.

Bachan A. and Kump L.R. (2015) The rise of oxygen and siderite oxidation during the Lomagundi Event. *Proceedings of the National Academy of Sciences* **112**(21)**,** 6562-6567. https://doi.org/doi:10.1073/pnas.1422319112.

Berkowitz B. (2002) Characterizing flow and transport in fractured geological media: A review. *Advances in water resources* **25**(8-12)**,** 861-884.

Bernhard N., Moskwa L.-M., Schmidt K., Oeser R.A., Aburto F., Bader M.Y., Baumann K., von Blanckenburg F., Boy J. and van den Brink L. (2018) Pedogenic and microbial interrelations to regional climate and local topography: new insights from a climate gradient (arid to humid) along the Coastal Cordillera of Chile. *Catena* **170,** 335-355.

Bethencourt L., Bochet O., Farasin J., Aquilina L., Borgne T.L., Quaiser A., Biget M., Michon-Coudouel S., Labasque T. and Dufresne A. (2020) Genome reconstruction reveals distinct assemblages of Gallionellaceae in surface and subsurface redox transition zones. *FEMS Microbiology Ecology*. https://doi.org/10.1093/femsec/fiaa036.

Bisutti I., Hilke I., Schumacher J. and Raessler M. (2007) A novel single-run dual temperature combustion (SRDTC) method for the determination of organic, in-organic and total carbon in soil samples. *Talanta* **71**(2)**,** 521-528.

Bochet O., Bethencourt L., Dufresne A., Farasin J., Pédrot M., Labasque T., Chatton E., Lavenant N., Petton C., Abbott B.W., Aquilina L. and Le Borgne T. (2020) Iron-oxidizer hotspots formed by intermittent oxic–anoxic fluid mixing in fractured rocks. *Nature Geoscience*. https://doi.org/10.1038/s41561-019-0509-1.

Brantley S.L., Holleran M.E., Jin L. and Bazilevskaya E. (2013) Probing deep weathering in the Shale Hills Critical Zone Observatory, Pennsylvania (USA): the hypothesis of nested chemical reaction fronts in the subsurface. *Earth Surface Processes and Landforms* **38**(11)**,** 1280-1298.

Brantley S.L., Lebedeva M.I., Balashov V.N., Singha K., Sullivan P.L. and Stinchcomb G. (2017) Toward a conceptual model relating chemical reaction fronts to water flow paths in hills. *Geomorphology* **277,** 100-117.

Brantley S.L. and White A.F. (2009) 10. Approaches to Modeling Weathered Regolith. In Eric H.O. and Jacques S. (eds.), *Thermodynamics and Kinetics of Water-Rock Interaction.* Berlin, Boston: De Gruyter, 435-484.

Buss H., Bruns M., Schultz M., Moore J., Mathur C. and Brantley S. (2005) The coupling of biological iron cycling and mineral weathering during saprolite formation, Luquillo Mountains, Puerto Rico. *Geobiology* **3**(4)**,** 247-260.

Byrne J.M., Klueglein N., Pearce C., Rosso K.M., Appel E. and Kappler A. (2015) Redox cycling of Fe(II) and Fe(III) in magnetite by Fe-metabolizing bacteria. *Science* **347**(6229)**,** 1473-1476. https://doi.org/10.1126/science.aaa4834.

Callahan R.P., Huang M.-H., Donaldson A., Hudson-Rasmussen B. and Zimmer M. (2024) Geologic and Tectonic Controls on Deep Fracturing, Weathering, and Water Flow in the Central California Coast Range. *Geophysical Research Letters* **51**(13)**,** e2024GL109129. https://doi.org/https://doi.org/10.1029/2024GL109129.

Cembrano J., González G., Arancibia G., Ahumada I., Olivares V. and Herrera V. (2005) Fault zone development and strain partitioning in an extensional strike-slip duplex: A case study from the Mesozoic Atacama fault system, Northern Chile. *Tectonophysics* **400**(1)**,** 105-125. https://doi.org/https://doi.org/10.1016/j.tecto.2005.02.012.

Cockell C.S., Pybus D., Olsson-Francis K., Kelly L., Petley D., Rosser N., Howard K. and Mosselmans F. (2011) Molecular characterization and geological microenvironment of

a microbial community inhabiting weathered receding shale cliffs. *Microbial ecology* **61,** 166-181.

Cornell R.M. and Schwertmann U. (2003) *The iron oxides: structure, properties, reactions, occurrences, and uses*. Wiley-vch Verlag GmbH & Co. KGaA.

Cutting R.S., Coker V.S., Fellowes J.W., Lloyd J.R. and Vaughan D.J. (2009) Mineralogical and morphological constraints on the reduction of Fe(III) minerals by Geobacter sulfurreducens. *Geochimica et Cosmochimica Acta* **73**(14)**,** 4004-4022. https://doi.org/https://doi.org/10.1016/j.gca.2009.04.009.

Deckart K., Hervé F., Fanning C.M., Ramírez V., Calderón M. and Godoy E. (2013) U-Pb geochronology and Hf-O isotopes of zircons from the Pennsylvanian Coastal Batholith, south-central Chile. *Andean Geology* **41**(1)**,** 49-82.

Deng H. and Spycher N. (2019) Modeling reactive transport processes in fractures. *Reviews in Mineralogy and Geochemistry* **85**(1)**,** 49-74.

Deng K., Yang S. and Guo Y. (2022) A global temperature control of silicate weathering intensity. *Nature Communications* **13**(1)**,** 1781. https://doi.org/10.1038/s41467-022-29415-0.

Drake H., Tullborg E.-L. and Annersten H. (2008) Red-staining of the wall rock and its influence on the reducing capacity around water conducting fractures. *Applied Geochemistry* **23**(7)**,** 1898-1920. https://doi.org/https://doi.org/10.1016/j.apgeochem.2008.02.017.

Ehlen J. (1999) Fracture characteristics in weathered granites. *Geomorphology* **31**(1)**,** 29-45. https://doi.org/https://doi.org/10.1016/S0169-555X(99)00071-9.

Eliasson T. (1993) Mineralogy, geochemistry and petrophysics of red coloured granite adjacent to fractures. Swedish Nuclear Fuel and Waste Management Co.

Eppes M.C., Hancock G.S., Chen X., Arey J., Dewers T., Huettenmoser J., Kiessling S., Moser F., Tannu N., Weiserbs B. and Whitten J. (2018) Rates of subcritical cracking and long-term rock erosion. *Geology* **46**(11)**,** 951-954. https://doi.org/10.1130/g45256.1.

Eppes M.C. and Keanini R. (2017) Mechanical weathering and rock erosion by climate-dependent subcritical cracking. *Reviews of Geophysics* **55**(2)**,** 470-508.

Friese A., Kallmeyer J., Axel Kitte J., Montaño Martínez I., Bijaksana S., Wagner D., Team I.L.C.D.S. and Team t.I.T.D.S. (2017) A simple and inexpensive technique for assessing contamination during drilling operations. *Limnology and Oceanography: Methods* **15**(2)**,** 200-211.

Gamboa C., Godfrey L., Herrera C., Custodio E. and Soler A. (2019) The origin of solutes in groundwater in a hyper-arid environment: A chemical and multi-isotope approach in the Atacama Desert, Chile. *Science of The Total Environment* **690,** 329-351. https://doi.org/https://doi.org/10.1016/j.scitotenv.2019.06.356.

Gamboa C., Godfrey L., Urrutia J., Herrera C., Lu X. and Jordan T. (2022) Conditions of groundwater recharge in the hyperarid southern Atacama Desert. *Global and Planetary Change* **217,** 103931. https://doi.org/https://doi.org/10.1016/j.gloplacha.2022.103931.

Gana P., Wall R. and Gutiérrez A. (1996) Mapa geológico del área de Valparaíso-Curacaví, regiones de Valparaíso y Metropolitana.

Ginn B., Meile C., Wilmoth J., Tang Y. and Thompson A. (2017) Rapid Iron Reduction Rates Are Stimulated by High-Amplitude Redox Fluctuations in a Tropical Forest Soil. *Environmental science & technology* **51**(6)**,** 3250-3259. https://doi.org/10.1021/acs.est.6b05709.

Grimm H., Drabesch S., Nicol A., Straub D., Joshi P., Zarfl C., Planer-Friedrich B., Muehe E.M. and Kappler A. (2024) Arsenic immobilization and greenhouse gas emission depend on quantity and frequency of nitrogen fertilization in paddy soil. *Heliyon* **10**(16). https://doi.org/10.1016/j.heliyon.2024.e35706.

Gudmundsson A. (2000) Fracture dimensions, displacements and fluid transport. *Journal of Structural Geology* **22**(9)**,** 1221-1231.

Hampl F.J., Schiperski F., Byrne J.M., Schwerdhelm C., Kappler A., Bryce C., von Blanckenburg F. and Neumann T. (2021) Mineralogical, geochemical and magnetic

susceptibility data from a deep hydrothermally altered profile in a semi-arid region (Chilean Coastal Cordillera).

Hampl F.J., Schiperski F., Byrne J.M., Schwerdhelm C., Kappler A., Bryce C., von Blanckenburg F. and Neumann T. (2022) The role of iron-bearing minerals for the deep weathering of a hydrothermally altered plutonic rock in semi-arid climate (Chilean Coastal Cordillera). *Chemical Geology* **604,** 120922. https://doi.org/https://doi.org/10.1016/j.chemgeo.2022.120922.

Hampl F.J., Schiperski F., Schwerdhelm C., Stroncik N., Bryce C., von Blanckenburg F. and Neumann T. (2023) Feedbacks between the formation of secondary minerals and the infiltration of fluids into the regolith of granitic rocks in different climatic zones (Chilean Coastal Cordillera). *Earth Surf. Dynam.* **11**(3)**,** 511-528. https://doi.org/10.5194/esurf-11-511-2023.

Hegler F., Posth N.R., Jiang J. and Kappler A. (2008) Physiology of phototrophic iron (II)-oxidizing bacteria: implications for modern and ancient environments. *FEMS Microbiology Ecology* **66**(2)**,** 250-260.

Heron G., Crouzet C., Bourg A.C. and Christensen T.H. (1994) Speciation of Fe (II) and Fe (III) in contaminated aquifer sediments using chemical extraction techniques. *Environmental science & technology* **28**(9)**,** 1698-1705.

Herrera C., Gamboa C., Custodio E., Jordan T., Godfrey L., Jódar J., Luque J.A., Vargas J. and Sáez A. (2018) Groundwater origin and recharge in the hyperarid Cordillera de la Costa, Atacama Desert, northern Chile. *Science of The Total Environment* **624,** 114-132.

Herve F. (1974) Petrology of the crystalline basement of the Nahuelbuta Mountains, south-central Chile. 北海道大学.

Houston J. (2002) Groundwater recharge through an alluvial fan in the Atacama Desert, northern Chile: mechanisms, magnitudes and causes. *Hydrological Processes* **16**(15)**,** 3019-3035. https://doi.org/https://doi.org/10.1002/hyp.1086.

Jakus N., Blackwell N., Osenbrück K., Straub D., Byrne J.M., Wang Z., Glöckler D., Elsner M., Lueders T., Grathwohl P., Kleindienst S. and Kappler A. (2021a) Nitrate Removal by a Novel Lithoautotrophic Nitrate-Reducing, Iron(II)-Oxidizing Culture Enriched from a Pyrite-Rich Limestone Aquifer. *Applied and Environmental Microbiology* **87**(16)**,** e00460-00421. https://doi.org/doi:10.1128/AEM.00460-21.

Jakus N., Blackwell N., Straub D., Kappler A. and Kleindienst S. (2021b) Presence of Fe(II) and nitrate shapes aquifer-originating communities leading to an autotrophic enrichment dominated by an Fe(II)-oxidizing Gallionellaceae sp. *FEMS Microbiology Ecology* **97**(11). https://doi.org/10.1093/femsec/fiab145.

Kappler A., Bryce C., Mansor M., Lueder U., Byrne J.M. and Swanner E.D. (2021) An evolving view on biogeochemical cycling of iron. *Nature Reviews Microbiology* **19**(6)**,** 360-374.

Koester M., Stock S.C., Nájera F., Abdallah K., Gorbushina A., Prietzel J., Matus F., Klysubun W., Boy J., Kuzyakov Y., Dippold M.A. and Spielvogel S. (2021) From rock eating to vegetarian ecosystems — Disentangling processes of phosphorus acquisition across biomes. *Geoderma* **388,** 114827. https://doi.org/https://doi.org/10.1016/j.geoderma.2020.114827.

Kralj P. (2016) Hydrothermal alteration of chlorite to randomly interstratified corrensite-chlorite: Geological evidence from the Oligocene Smrekovec Volcanic Complex, Slovenia. *Applied Clay Science* **134,** 235-245. https://doi.org/https://doi.org/10.1016/j.clay.2016.10.025.

Krone L.V. (2024) Exploring the climate dependence of deep weathering in the Chilean Coastal Cordillera. *FU Berlin,* **PhD Thesis,** 189 pages. https://doi.org/http://dx.doi.org/10.17169/refubium-43418.

Krone L.V., Hampl F.J., Schwerdhelm C., Bryce C., Ganzert L., Kitte A., Übernickel K., Dielforder A., Aldaz Cifuentes S.R. and Oses-Pedraza R. (2021a) Physical and geochemical data on a drill core from the semi-arid Coastal Cordillera, Chile.

Krone L.V., Hampl F.J., Schwerdhelm C., Bryce C., Ganzert L., Kitte A., Übernickel K., Dielforder A., Aldaz S., Oses-Pedraza R., Perez J.P.H., Sanchez-Alfaro P., Wagner

D., Weckmann U. and von Blanckenburg F. (2021b) Deep weathering in the semi-arid Coastal Cordillera, Chile. *Scientific Reports* **11**(1), 13057. https://doi.org/10.1038/s41598-021-90267-7.

Krone L.V., Wittmann H. and von Blanckenburg F. (2024) Precipitation Control on Weathering Intensity and Depositional Flux of Meteoric 10Be Revealed From Soil Profiles Along a Climate Gradient (Chile). *Geophysical Research Letters* **51**(15), e2024GL108825. https://doi.org/https://doi.org/10.1029/2024GL108825.

Luebert F. and Pliscoff P. (2006) *Sinopsis bioclimática y vegetacional de Chile*. Editorial universitaria.

Lueder U., Maisch M., Laufer K., Jorgensen B.B., Kappler A. and Schmidt C. (2020) Influence of Physical Perturbation on Fe(II) Supply in Coastal Marine Sediments. *Environmental science & technology* **54**(6), 3209-3218. https://doi.org/10.1021/acs.est.9b06278.

Maisch M., Lueder U., Kappler A. and Schmidt C. (2020) From plant to paddy—how rice root iron plaque can affect the paddy field iron cycling. *Soil Systems* **4**(2), 28.

Maldonado V., Contreras M. and Melnick D. (2021) A comprehensive database of active and potentially-active continental faults in Chile at 1:25,000 scale. *Scientific Data* **8**(1), 20. https://doi.org/10.1038/s41597-021-00802-4.

Melnick D., Hillemann C., Jara-Muñoz J., Garrett E., Cortés-Aranda J., Molina D., Tassara A. and Strecker M.R. (2019) Hidden Holocene Slip Along the Coastal El Yolki Fault in Central Chile and Its Possible Link With Megathrust Earthquakes. *Journal of Geophysical Research: Solid Earth* **124**(7), 7280-7302. https://doi.org/https://doi.org/10.1029/2018JB017188.

Ministerio de Obras Públicas de Chile D. (2016) Información oficial hidrometeorológica y de calidad de aguas en línea. In.: DGA (Dirección General de Aguas), Ministerio de Obras Públicas de Chile.

Mitchell T.M. and Faulkner D.R. (2009) The nature and origin of off-fault damage surrounding strike-slip fault zones with a wide range of displacements: A field study from the Atacama fault system, northern Chile. *Journal of Structural Geology* **31**(8), 802-816. https://doi.org/https://doi.org/10.1016/j.jsg.2009.05.002.

Napieralski S.A., Buss H.L., Brantley S.L., Lee S., Xu H. and Roden E.E. (2019) Microbial chemolithotrophy mediates oxidative weathering of granitic bedrock. *Proceedings of the National Academy of Sciences* **116**(52), 26394-26401.

Napieralski S.A., Fang Y., Marcon V., Forsythe B., Brantley S.L., Xu H. and Roden E.E. (2022) Microbial chemolithotrophic oxidation of pyrite in a subsurface shale weathering environment: Geologic considerations and potential mechanisms. *Geobiology* **20**(2), 271-291.

Nishimoto S. and Yoshida H. (2010) Hydrothermal alteration of deep fractured granite: Effects of dissolution and precipitation. *Lithos* **115**(1), 153-162. https://doi.org/https://doi.org/10.1016/j.lithos.2009.11.015.

Oeser R.A., Stroncik N., Moskwa L.-M., Bernhard N., Schaller M., Canessa R., van den Brink L., Köster M., Brucker E. and Stock S. (2018) Chemistry and microbiology of the Critical Zone along a steep climate and vegetation gradient in the Chilean Coastal Cordillera. *Catena* **170**, 183-203.

Oeser R.A. and von Blanckenburg F. (2020) Do degree and rate of silicate weathering depend on plant productivity? *Biogeosciences* **17**(19), 4883-4917. https://doi.org/10.5194/bg-17-4883-2020.

Parada M.A., López-Escobar L., Oliveros V., Fuentes F., Morata D., Calderón M., Aguirre L., Féraud G., Espinoza F. and Moreno H. (2007) Andean magmatism.

Pedersen K. (1997) Microbial life in deep granitic rock. *FEMS microbiology reviews* **20**(3-4), 399-414.

Perez J.R., Banwart S.A. and Puigdomenech I. (2005) The kinetics of O2 (aq) reduction by structural ferrous iron in naturally occurring ferrous silicate minerals. *Applied Geochemistry* **20**(11), 2003-2016.

Raiswell R., Canfield D.E. and Berner R.A. (1994) A comparison of iron extraction methods for the determination of degree of pyritisation and the recognition of iron-limited pyrite

formation. *Chemical Geology* **111**(1), 101-110. https://doi.org/https://doi.org/10.1016/0009-2541(94)90084-1.

Rehak K., Strecker M.R. and Echtler H.P. (2008) Morphotectonic segmentation of an active forearc, 37°–41°S, Chile. *Geomorphology* **94**(1), 98-116. https://doi.org/https://doi.org/10.1016/j.geomorph.2007.05.002.

Rempe D.M. and Dietrich W.E. (2014) A bottom-up control on fresh-bedrock topography under landscapes. *Proceedings of the National Academy of Sciences* **111**(18), 6576-6581.

Riquelme R., Martinod J., Hérail G., Darrozes J. and Charrier R. (2003) A geomorphological approach to determining the Neogene to Recent tectonic deformation in the Coastal Cordillera of northern Chile (Atacama). *Tectonophysics* **361**(3-4), 255-275.

Roden E.E. and Zachara J.M. (1996) Microbial Reduction of Crystalline Iron(III) Oxides: Influence of Oxide Surface Area and Potential for Cell Growth. *Environmental science & technology* **30**(5), 1618-1628. https://doi.org/10.1021/es9506216.

Samuels T., Bryce C., Landenmark H., Marie-Loudon C., Nicholson N., Stevens A.H. and Cockell C. (2020) Microbial weathering of minerals and rocks in natural environments. In *Biogeochemical cycles: Ecological drivers and environmental impact.* 59-79.

Samuels T., Pybus D., Wilkinson M. and Cockell C.S. (2019) pH Influences the Distribution of Microbial Rock-Weathering Phenotypes in Weathered Shale Environments. *Geomicrobiology Journal* **36**(8), 752-763. https://doi.org/10.1080/01490451.2019.1620381.

Sandström B., Annersten H. and Tullborg E.-L. (2010) Fracture-related hydrothermal alteration of metagranitic rock and associated changes in mineralogy, geochemistry and degree of oxidation: a case study at Forsmark, central Sweden. *International Journal of Earth Sciences* **99**(1), 1-25. https://doi.org/10.1007/s00531-008-0369-1.

Schad M., Byrne J.M., ThomasArrigo L.K., Kretzschmar R., Konhauser K.O. and Kappler A. (2022) Microbial Fe cycling in a simulated Precambrian ocean environment: Implications for secondary mineral (trans)formation and deposition during BIF genesis. *Geochimica et Cosmochimica Acta* **331**, 165-191. https://doi.org/https://doi.org/10.1016/j.gca.2022.05.016.

Sidhu P., Gilkes R., Cornell R., Posner A. and Quirk J. (1981) Dissolution of iron oxides and oxyhydroxides in hydrochloric and perchloric acids. *Clays and Clay Minerals* **29**, 269-276.

Smith M. and Roychoudhury A.N. (2013) Mobilisation of Iron from rocks in a fractured aquifer: Lithological and geochemical controls. *Applied Geochemistry* **31**, 171-186.

Steenken A., Rabbia O. and Hernández L. (2016) The Emplacement of the Nahuelbuta Batholith in an Active Continental Margin (Central Chile). In: *XVIII Congreso Peruano de Geología, Lima, Peru.*

Stock S.C., Koester M., Boy J., Godoy R., Nájera F., Matus F., Merino C., Abdallah K., Leuschner C., Spielvogel S., Gorbushina A.A., Kuzyakov Y. and Dippold M.A. (2021) Plant carbon investment in fine roots and arbuscular mycorrhizal fungi: A cross-biome study on nutrient acquisition strategies. *Science of The Total Environment* **781**, 146748. https://doi.org/https://doi.org/10.1016/j.scitotenv.2021.146748.

Stroncik N.A., Krone L.V., Pierdominici S., Kummerow J., Blukis R. and von Blanckenburg F. (in prep.) Geochemical, mineralogical, and petrophysical characteristics of DeepEarthshape drill cores from the Chilean Coastal Cordillera. *GFZ Data Services*.

Swanner E.D., Maisch M., Wu W. and Kappler A. (2018) Oxic Fe(III) reduction could have generated Fe(II) in the photic zone of Precambrian seawater. *Scientific Reports* **8**(1), 4238. https://doi.org/10.1038/s41598-018-22694-y.

Taucare M., Daniele L., Viguier B., Vallejos A. and Arancibia G. (2020a) Groundwater resources and recharge processes in the Western Andean Front of Central Chile. *Science of The Total Environment* **722**, 137824.

Taucare M., Viguier B., Daniele L., Heuser G., Arancibia G. and Leonardi V. (2020b) Connectivity of fractures and groundwater flows analyses into the Western Andean Front by means of a topological approach (Aconcagua Basin, Central Chile).

Team R.C. (2024) R: A language and environment for statistical computing. R Foundation for Statistical Computing. *(No Title)*.

Trichandi R., Bauer K., Ryberg T., Heit B., Araya Vargas J., von Blanckenburg F. and Krawczyk C.M. (2024) 3D shear wave velocity imaging of the subsurface structure of granite rocks in the arid climate of Pan de Azúcar, Chile, revealed by Bayesian inversion of HVSR curves. *Earth Surf. Dynam.* **12**(3)**,** 747-763. https://doi.org/10.5194/esurf-12-747-2024.

Trichandi R., Bauer K., Ryberg T., Scherler D., Bataille K. and Krawczyk C.M. (2022) Combined seismic and borehole investigation of the deep granite weathering structure—Santa Gracia Reserve case in Chile. *Earth Surface Processes and Landforms* **n/a**(n/a). https://doi.org/https://doi.org/10.1002/esp.5457.

Trichandi R., Bauer K., Ryberg T., Wawerzinek B., Araya Vargas J., von Blanckenburg F. and Krawczyk C.M. (2023) Shear-wave velocity imaging of weathered granite in La Campana (Chile) from Bayesian inversion of micro-tremor H/V spectral ratios. *Journal of Applied Geophysics* **217,** 105191. https://doi.org/https://doi.org/10.1016/j.jappgeo.2023.105191.

Tripp G.I. and Vearncombe J.R. (2004) Fault/fracture density and mineralization: a contouring method for targeting in gold exploration. *Journal of Structural Geology* **26**(6-7)**,** 1087-1108.

Tukey J.W. (1949) Comparing individual means in the analysis of variance. *Biometrics***,** 99-114.

Übernickel K., Ehlers T.A., Ershadi M.R., Paulino L., Fuentes Espoz J.-P., Maldonado A., Oses-Pedraza R. and von Blanckenburg F. (2020) Time series of meteorological station data in the EarthShape study areas in the Coastal Cordillera, Chile.

Voelz J.L., Johnson N.W., Chun C.L., Arnold W.A. and Penn R.L. (2019) Quantitative Dissolution of Environmentally Accessible Iron Residing in Iron-Rich Minerals: A Review. *ACS Earth and Space Chemistry* **3**(8)**,** 1371-1392.

Weckmann U., Bauer K., Krawczyk C., Kück J., Übernickel K. and von Blanckenburg F. (2020) Geophysical borehole logging data from Santa Gracia, Chile.

Werner C., Schmid M., Ehlers T.A., Fuentes-Espoz J.P., Steinkamp J., Forrest M., Liakka J., Maldonado A. and Hickler T. (2018) Effect of changing vegetation and precipitation on denudation – Part 1: Predicted vegetation composition and cover over the last 21 thousand years along the Coastal Cordillera of Chile. *Earth Surf. Dynam.* **6**(4)**,** 829-858. https://doi.org/10.5194/esurf-6-829-2018.

White A.F. and Yee A. (1985) Aqueous oxidation-reduction kinetics associated with coupled electron-cation transfer from iron-containing silicates at 25 C. *Geochimica et Cosmochimica Acta* **49**(5)**,** 1263-1275.

Wickham H. (2016) Programming with ggplot2. In Wickham H. (ed.), *ggplot2: Elegant Graphics for Data Analysis.* Cham: Springer International Publishing, 241-253.

3.8 Supplementary Information

Supplementary Methods

Microbial weathering activity heatmap. Columns displayed in the heatmap of potential hotspots of microbial weathering activity within the four weathering profiles are: field site (PdA, SG, LC and NA), fracture density (= fracture intensity), fracture type (vein, closed, open, none), adsorbed Fe(II) (mg g^{-1} rock), inorganic carbon (IC) (mg g^{-1} rock), poorly crystalline Fe(III) (mg g^{-1} rock), bioavailable organic carbon (BOC) (mg g^{-1} rock), Fe(II)/Fe(tot)-ratio, Fe redox state (oxidised (ox), transition (trans), reduced (red)), and potential for microbial Fe(II) oxidation and Fe(III) reduction. The weighted ranking is based on these columns. A maximum of 17 points could be reached for each of the two microorganism categories, i.e. Fe(II)-oxidising and Fe(III)-reducing microorganisms. Points for each depth / site were summed up, expressed as rel. % and binned into five categories regarding *in situ* weathering potential: very low = 0-25%, low = 25-40%, moderate = 40-55%, high = 55-70% or excellent = 70-100%. Points achievable in the respective categories were:

- fracture density (0-1 point): high = 1 point, medium = 0.5 point, low = 0 points
- fracture type (1-3 points): open fracture (including weak zones) = 3 points, closed fracture/vein = 1 point, none = 0 points
- field site (representing precipitation, i.e. amount of available water) (1-4 points): PdA = 1, SG = 2, LC = 3, NA = 4
- Fe redox state (depending on favourability for Fe(II)-oxidising and Fe(III)-reducing microorganisms) (0-1 point) (see also Table S1):
    - (a) Fe(II)-oxidising microorganisms: oxidised (i.e. Fe(II)/(tot)-ratio = 0-0.35) = 0 points, transition (i.e. Fe(II)/(tot)-ratio = 0.35-0.60) = 0.5 point, reduced = 1 point (i.e. Fe(II)/(tot)-ratio = 0.60-1)
    - (b) Fe(III)-reducing microorganisms: oxidised (i.e. Fe(II)/(tot)-ratio = 0-0.35) = 1 point, transition (i.e. Fe(II)/(tot)-ratio = 0.35-0.60) = 0.5 point, reduced = 0 points (i.e. Fe(II)/(tot)-ratio = 0.60-1)
- Fe and C source (0-8 points):
    - (a) Fe(II)-oxidising microorganisms: Fe(Fe(II) ox) = 0-5 points, quantitatively, points given for relative amount of adsorbed Fe(II) regarding all depths / sites; C(Fe(II) ox) = 0-3 points, quantitatively, points given for relative amount of IC regarding all depths / sites
    - (b) Fe(III)-reducing microorganisms: Fe(Fe(III) red) = 0-5 points, quantitatively, points given for relative amount of poorly crystalline Fe(III) regarding all depths / sites; C(Fe(III) red) = 0-3 points, quantitatively, points given for relative amount of BOC regarding all depths / sites

Supplementary Tables

Table 3.S1. Fe redox zonation of the four EarthShape field sites. 15 samples of each site were analysed (*N* = 60). The column “ratio” displays Fe(II)/Fe(tot)-ratios of bioavailable Fe, while the column “redox” indicates oxidised (ox), transition (trans) or reduced (red) zones.

Pan de Azúcar			**Santa Gracia**			**La Campana**			**Nahuelbuta**		
depth (m)	ratio	redox	depth (m)	ratio	redox	depth (m)	ratio	redox	depth (m)	ratio	redox
0.025	0.11	ox	0.025	0.18	ox	0.025	0.15	ox	0.025	0.06	ox
0.5	0.24	ox	0.5	0.14	ox	0.5	0.04	ox	0.5	0.03	ox
1.5	0.15	red	1.5	0.14	ox	1.5	0.06	ox	1.5	0.13	ox
1.6	0.93	red	2.3	0.10	ox	9.6	0.34	ox	3.1	0.89	red
9.3	0.77	red	6.8	0.68	red	20.6	0.35	ox	6.1	0.95	red
19.1	0.66	red	11.8	0.30	ox	26.2	0.41	trans	8.7	0.84	red
25.9	0.89	red	19.8	0.57	trans	33.8	0.43	trans	11.9	0.92	red
37.5	0.88	red	26.2	0.43	trans	39.3	0.40	trans	12.9	0.88	red
46.1	0.87	red	35.1	0.62	red	43.2	0.53	trans	14.5	0.92	red
53.6	0.69	red	45.8	0.54	trans	48.9	0.82	red	17.9	0.91	red
67.6	0.79	red	56.9	0.68	red	52.7	0.72	red	19.2	0.89	red
76.4	0.84	red	65.8	0.74	red	63.7	0.73	red	21.0	0.87	red
85.9	0.75	red	74.4	0.47	trans	72.6	0.78	red	25.5	0.95	red
87.5	0.88	red	76.5	0.73	red	72.6	0.81	red	30.4	0.92	red
92.5	0.84	red	82.8	0.71	red	87.8	0.85	red	33.7	0.96	red

Table 3.S2. Fracture density distribution of the four weathering profiles investigated in this study. The fracture density (= intensity) distribution has been divided into three categories. Therefore, the amount of fractures (x) was counted for 5m intervals and assigned to the categories (a) “low”, if x<=10, (b) “medium”, if 10<x>25, and (c) “high”, if x>=25. Overall, sample sizes of the three categories were: “low” (red, *n*=22), “medium” (yellow, *n*=29) and “high” (green, *n*=13). “n.d.” denotes “not determined”.

Δ 5m	PdA	SG	LC	NA
0-5 m	11	NA	NA	NA
5-10 m	23	4	0	0
10-15 m	26	20	1	3
15-20 m	32	22	4	17
20-25 m	18	17	4	12
25-30 m	28	25	1	9
30-35 m	30	16	2	22
35-40 m	37	17	1	9
40-45 m	26	16	0	1
45-50 m	21	27	12	n.d.
50-55 m	21	22	25	n.d.
55-60 m	21	13	21	n.d.
60-65 m	22	17	19	n.d.
65-70 m	26	26	17	n.d.
70-75 m	21	28	7	n.d.
75-80 m	16	27	7	n.d.
80-85 m	18	14	12	n.d.
85-90 m	13	10	9	n.d.
90-95 m	5	n.d.	n.d.	n.d.

Table 3.S3. Analysis of Variance Table for Fe(II)/Fe(tot)-ratio as function of fracture density (frac_dens), field site (site) and their interaction. Model terms, degrees of freedom (df), sum of squares (Sum Sq), mean of squares (Mean Sq), effect sizes (F values), and significance (*P* values) within the statistical model (Fe_ratio ~ frac_dens * site) to explain variation in Fe(II)/Fe(tot)-ratios. Terms in bold were statistically significant at $P < 0.05$.

Model term	df	Sum Sq	Mean Sq	F value	*P* value
frac_dens	2	0.6451	0.32256	4.39	**0.017340**
site	3	0.9913	0.33042	4.50	**0.007062**
frac_dens:site	5	0.2637	0.05273	0.72	0.612550
Residuals	51	3.7431	0.07339	NA	NA

Table 3.S4. *post hoc* paired-samples t-tests, corrected with Tukey`s procedure, were run for comparing within-group means of the two factorial variables frac_dens' and 'site'. Note that negative values for 'diff' indicate that the Fe(II)/Fe(tot)-ratio is greater for the second frac_dens/site-term within the pair. lwr and upr denote the lower and upper range of data, while 'p adj' represents the adjusted significance value *P*. Pairwise comparisons that were significant at $P < 0.05$ are highlighted in bold. To focus on scientifically relevant comparisons, not all pairs are listed below and regarding interaction effects only, if viable.

type	comparison	diff	lwr	upr	p adj
frac_dens	**medium-low**	0.209	0.027	0.391	**0.020630**
frac_dens	high-low	0.194	-0.047	0.435	0.136976
frac_dens	high-medium	-0.015	-0.261	0.231	0.987813
site	SG-PdA	-0.150	-0.409	0.108	0.418791
site	LC-PdA	-0.042	-0.304	0.221	0.974594
site	NA-PdA	0.179	-0.080	0.437	0.268640
site	LC-SG	0.109	-0.150	0.367	0.680806
site	**NA-SG**	0.329	0.075	0.584	**0.006282**
site	NA-LC	0.220	-0.038	0.479	0.120144

Table 3.S5. Analysis of Variance Table for poorly crystalline Fe as function of fracture type (frac_type), field site (site) and their interaction. Model terms, degrees of freedom (df), sum of squares (Sum Sq), mean of squares (Mean Sq), effect sizes (F values), and significance (*P* values) within the statistical model (Fe_pc ~ frac_type * site) to explain variation in Fe(II)/Fe(tot)-ratios. Terms in bold were statistically significant at $P < 0.05$.

Model term	df	Sum Sq	Mean Sq	F value	*P* value
frac_type	3	38.479	12.826	5.50	**0.002591**
site	3	112.589	37.530	16.09	**< 0.0001**
frac_type:site	9	13.106	1.456	0.62	0.770244
Residuals	46	107.310	2.333	NA	NA

Table 3.S6. *post hoc* paired-samples t-tests, corrected with Tukey`s procedure, were run for comparing within-group means of the two factorial variables frac_type' and 'site'. Note that negative values for 'diff' indicate that the amount of poorly crystalline Fe is greater for the second frac_type/site-term within the pair. lwr and upr denote the lower and upper range of data, while 'p adj' represents the adjusted significance value *P*. Pairwise comparisons that were significant at $P < 0.05$ are highlighted in bold. To focus on scientifically relevant comparisons, not all pairs are listed below and regarding interaction effects only, if viable.

type	comparison	diff	lwr	upr	p adj
frac_type	**open-none**	1.507	0.116	2.898	**0.028978**
frac_type	**closed-none**	1.690	0.418	2.962	**0.004939**
frac_type	**vein-none**	1.968	0.073	3.863	**0.039056**
frac_type	closed-open	0.183	-1.193	1.560	0.984472
frac_type	vein-open	0.461	-1.505	2.428	0.923534
frac_type	vein-closed	0.278	-1.607	2.162	0.979173
site	SG-PdA	-0.480	-1.943	0.983	0.817826
site	**LC-PdA**	2.226	0.739	3.712	**0.001299**
site	**NA-PdA**	2.531	1.068	3.994	**0.000183**
site	**LC-SG**	2.706	1.243	4.169	**<0.0001**
site	**NA-SG**	3.011	1.572	4.450	**<0.0001**
site	NA-LC	0.305	-1.158	1.768	0.944509
frac_type:site	**closed:NA-closed:PdA**	3.199	0.243	6.155	**0.022582**
frac_type:site	**closed:NA-closed:SG**	3.917	0.451	7.383	**0.013860**
frac_type:site	**closed:NA-none:NA**	3.460	0.222	6.698	**0.025872**

Table 3.S7. Analysis of Variance Table for bioavailable organic carbon (BOC) as function of fracture type (frac_type), field site (site) and their interaction. Model terms, degrees of freedom (df), sum of squares (Sum Sq), mean of squares (Mean Sq), effect sizes (F values), and significance (*P* values) within the statistical model (BOC ~ frac_type * site) to explain variation in Fe(II)/Fe(tot)-ratios. Terms in bold were statistically significant at $P < 0.05$.

Model term	df	Sum Sq	Mean Sq	F value	*P* value
frac_type	3	0.039087	0.013029	6.67	**0.000344**
site	3	0.119432	0.039811	20.39	**< 0.0001**
frac_type:site	9	0.092961	0.010329	5.29	**< 0.0001**
Residuals	113	0.220584	0.001952	NA	NA

Table 3.S8. *post hoc* paired-samples t-tests, corrected with Tukey`s procedure, were run for comparing within-group means of the two factorial variables frac_type' and 'site'. Note that negative values for 'diff' indicate that the amount of BOC is greater for the second frac_type/site-term within the pair. lwr and upr denote the lower and upper range of data, while 'p adj' represents the adjusted significance value *P*. Pairwise comparisons that were significant at $P < 0.05$ are highlighted in bold. To focus on scientifically relevant comparisons, not all pairs are listed below and regarding interaction effects only, if viable.

type	comparison	diff	lwr	upr	p adj
frac_type	**open-none**	-0.055	-0.089	-0.021	**0.000307**
frac_type	**closed-none**	-0.051	-0.083	-0.019	**0.000423**
frac_type	**vein-none**	-0.052	-0.095	-0.008	**0.011706**
frac_type	closed-open	0.004	-0.020	0.028	0.970478
frac_type	vein-open	0.003	-0.033	0.040	0.994906
frac_type	vein-closed	-0.001	-0.036	0.035	0.999970
site	**SG-PdA**	-0.059	-0.084	-0.033	**<0.0001**
site	**LC-PdA**	-0.090	-0.129	-0.052	**<0.0001**
site	**NA-PdA**	-0.063	-0.091	-0.035	**<0.0001**
site	LC-SG	-0.031	-0.068	0.006	0.126007
site	NA-SG	-0.004	-0.030	0.022	0.980001
site	NA-LC	0.028	-0.011	0.066	0.254962
frac_type:site	**open:SG-open:PdA**	-0.105	-0.173	-0.037	**<0.0001**
frac_type:site	**open:LC-open:PdA**	-0.107	-0.214	-0.0001	**0.049315**
frac_type:site	**open:NA-open:PdA**	-0.099	-0.177	-0.021	**0.002180**
frac_type:site	**vein:SG-vein:PdA**	-0.145	-0.250	-0.040	**0.000452**
frac_type:site	**open:SG-none:SG**	-0.179	-0.264	-0.094	**<0.0001**
frac_type:site	**closed:SG-none:SG**	-0.173	-0.258	-0.870	**<0.0001**
frac_type:site	**vein:SG-none:SG**	-0.190	-0.284	-0.095	**<0.0001**
frac_type:site	**none:LC-none:SG**	-0.183	-0.292	-0.073	**<0.0001**
frac_type:site	**none:NA-none:SG**	-0.120	-0.220	-0.020	**0.005021**

Supplementary Figures

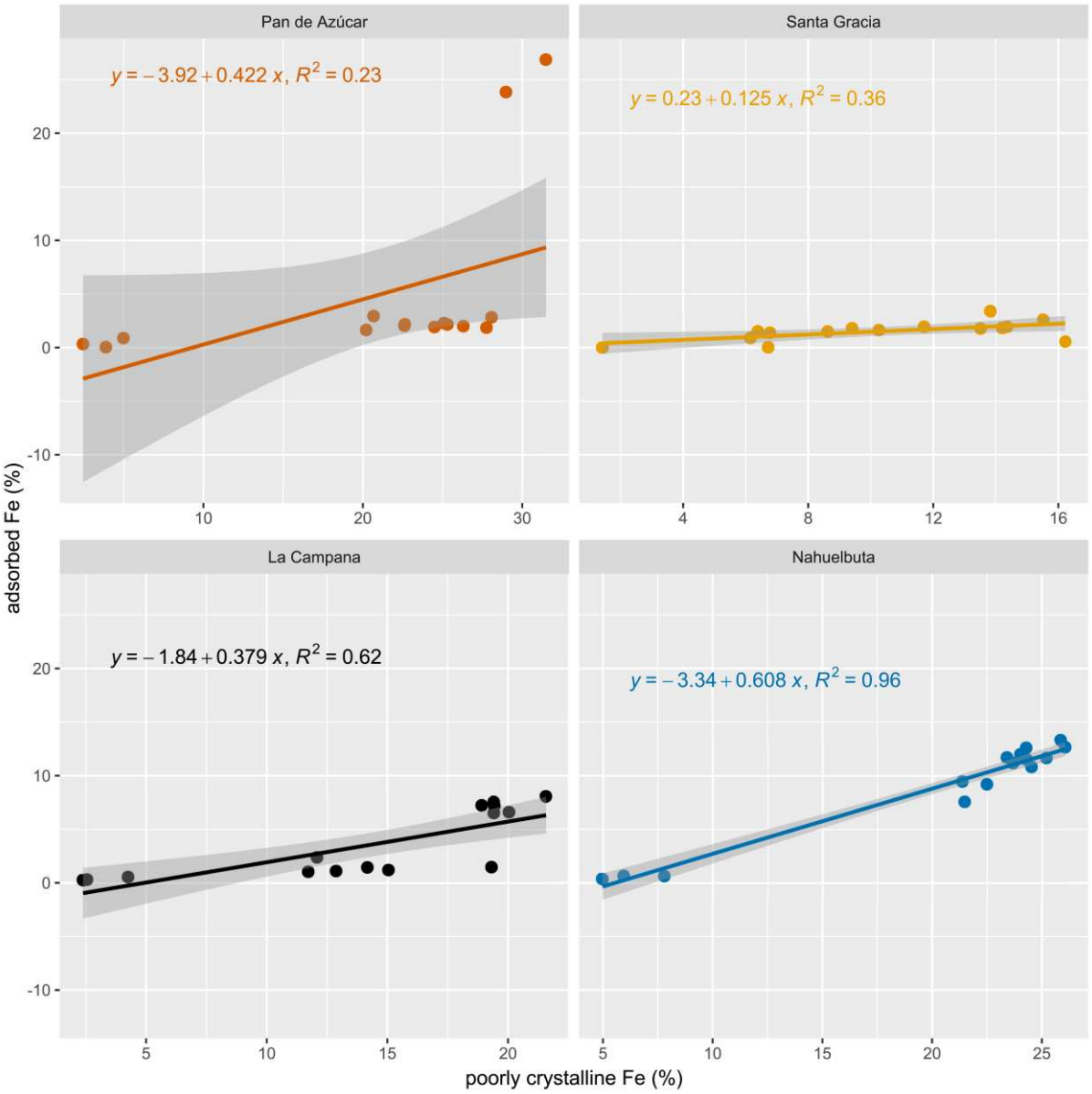

Figure 3.S1: Relative adsorbed Fe concentration (%) as function of the poorly crystalline concentration (%) for the four field sites. The equations display the function of the linear fit, accompanied by the adjusted R^2. The correlation between the two Fe pools is weak to very strong and positive, while the adjusted R^2 increases from North to South (Pan de Azúcar < Santa Gracia < La Campana < Nahuelbuta).

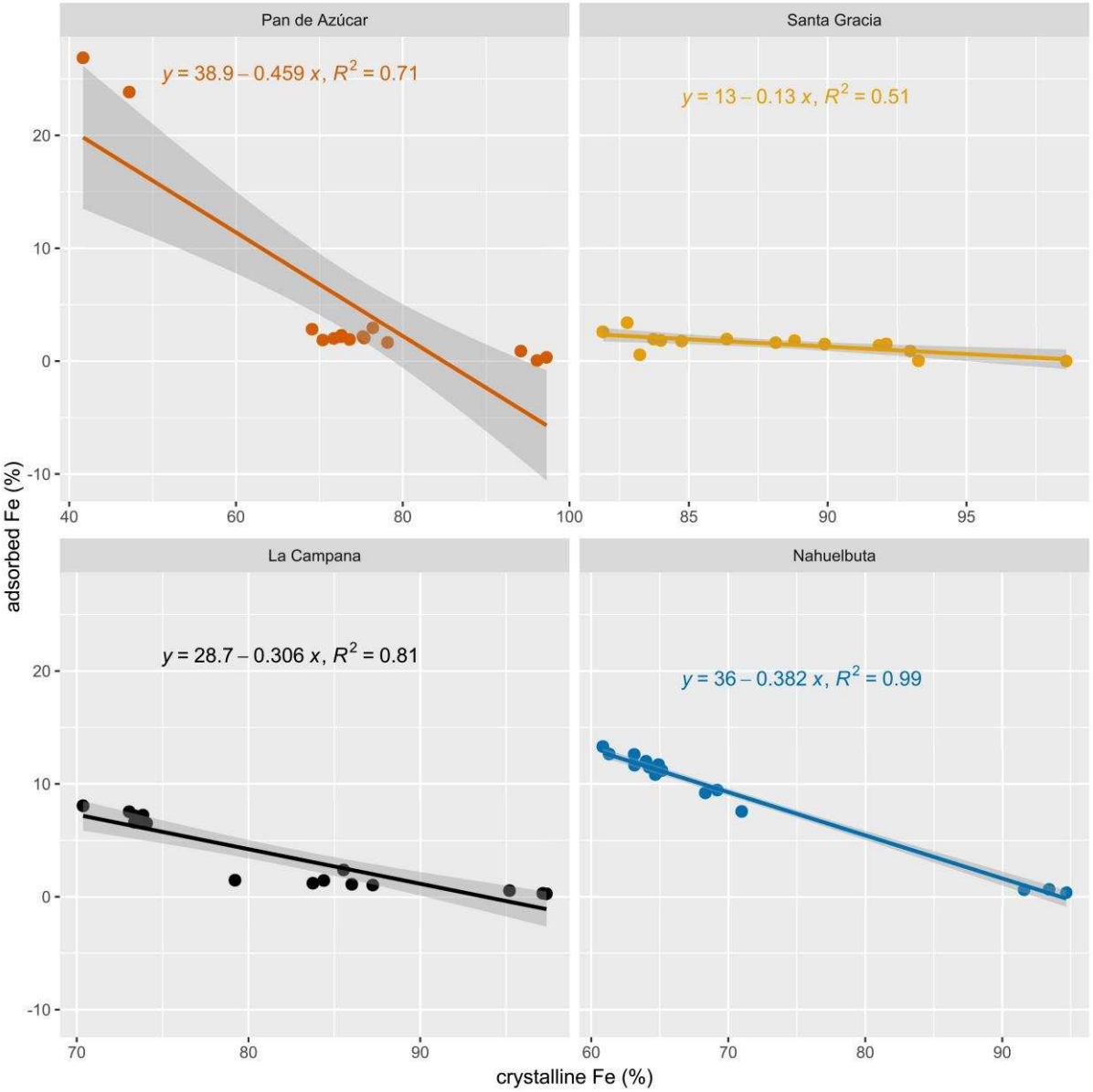

Figure 3.S2: Relative adsorbed Fe concentration (%) as function of the crystalline concentration (%) for the four field sites. The equations display the function of the linear fit, accompanied by the adjusted R^2. The correlation between the two Fe pools is decent to very strong and negative, while the adjusted R^2 generally increases from North to South apart from Santa Gracia (Santa Gracia < Pan de Azúcar < La Campana < Nahuelbuta).

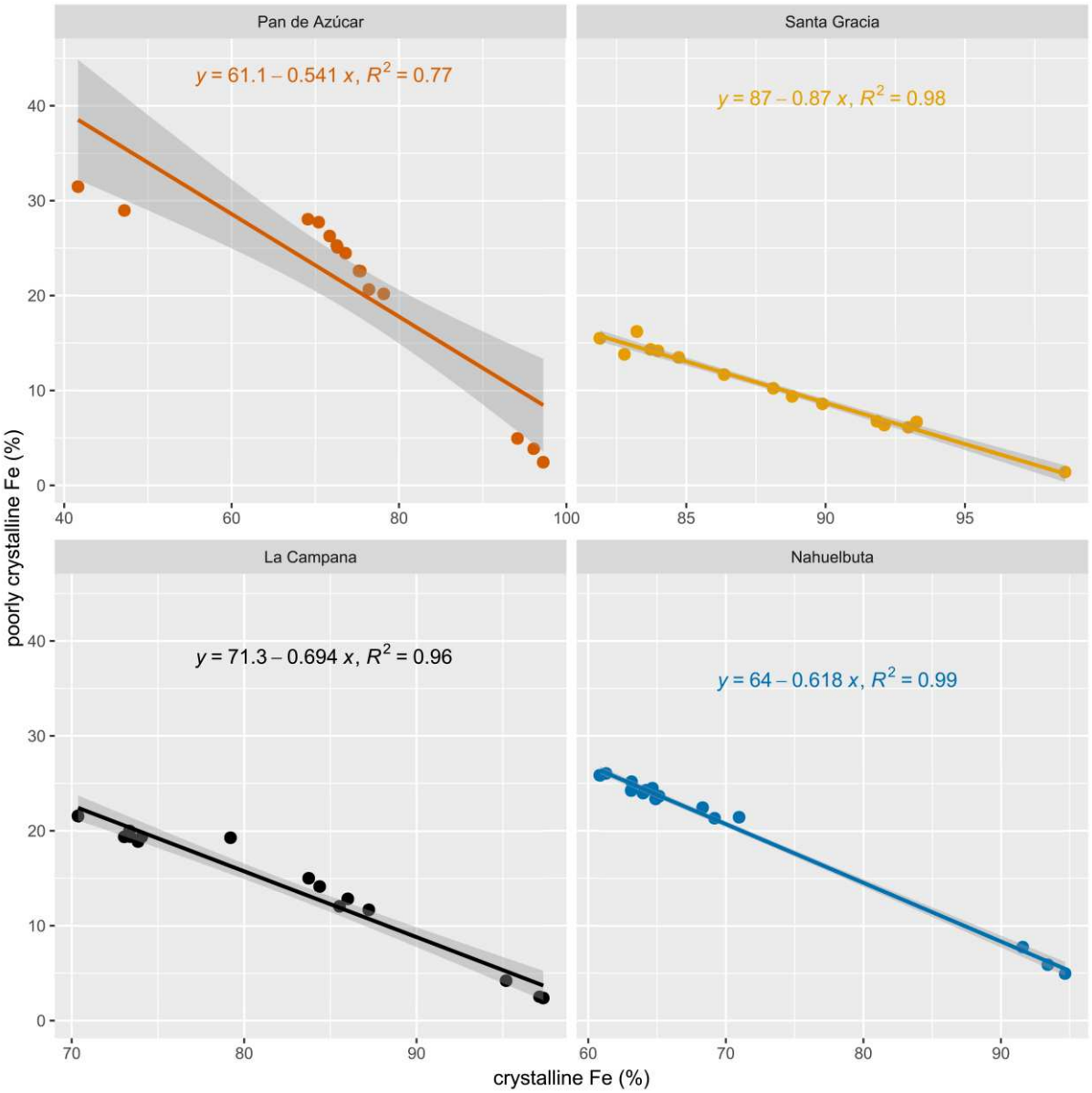

Figure 3.S3: Relative poorly crystalline Fe concentration (%) as function of the crystalline concentration (%) for the four field sites. The equations display the function of the linear fit, accompanied by the adjusted R^2. The correlation between the two Fe pools is very strong and negative, while the adjusted R^2 generally increases from North to South (Pan de Azúcar < La Campana < Santa Gracia < Nahuelbuta).

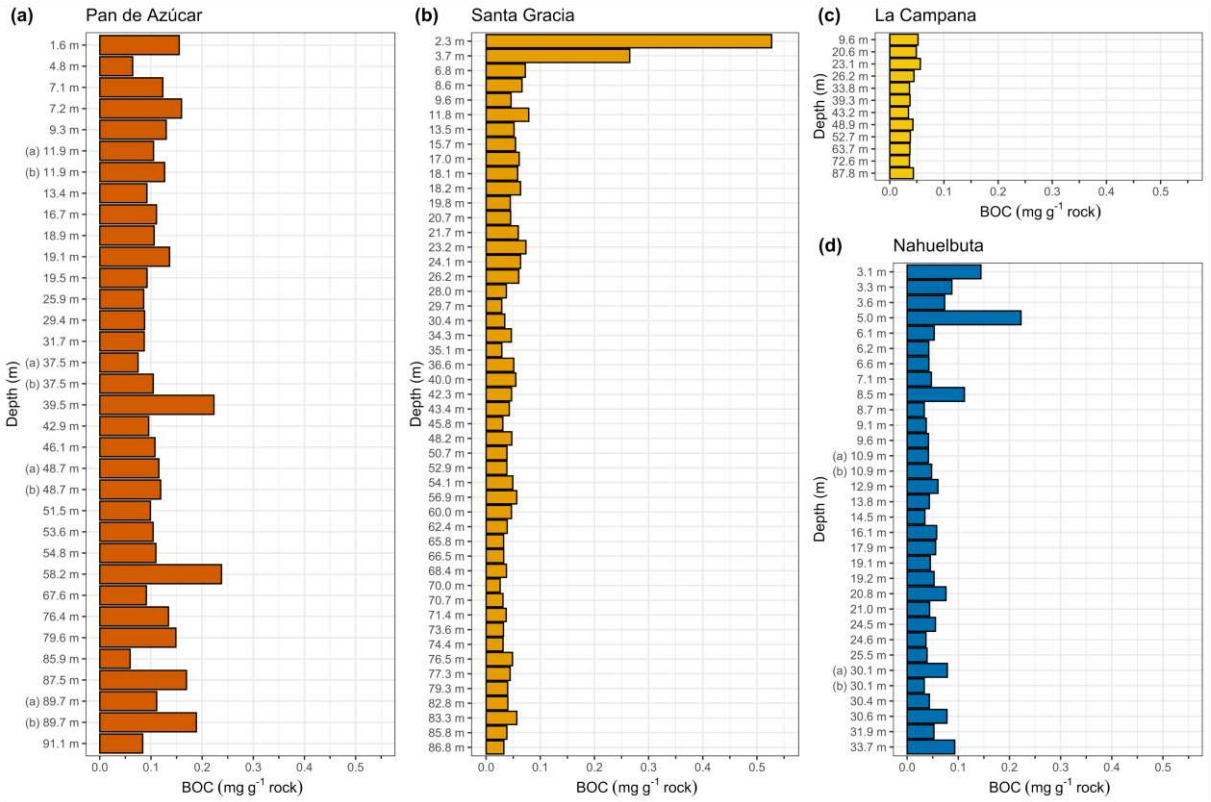

Figure 3.S4: Bioavailable organic carbon (BOC) (mg g^{-1} rock) as function of depth (m) for the four study field sites (*N* = 127). The four field sites (a) Pan de Azúcar, (b) Santa Gracia, (c) La Campana, and (d) Nahuelbuta cover an extreme climate gradient from North to South. Bars in (a) to (d) represent the average of technical measurement duplicates.

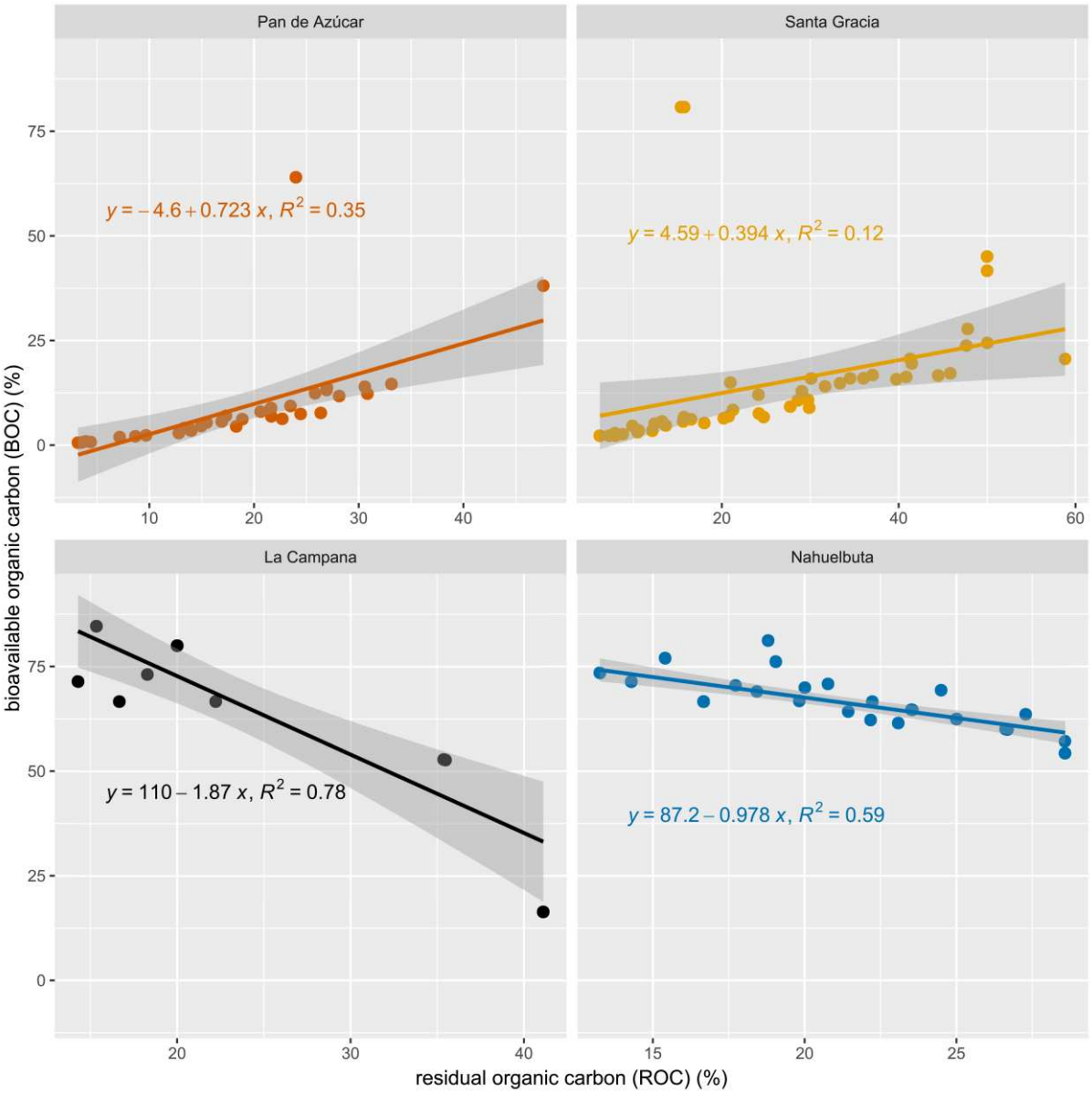

Figure 3.S5: Relative amount of bioavailable organic carbon (BOC) (%) as function of residual organic carbon (ROC) (%) for the four field sites. The equations display the function of the linear fit, accompanied by the adjusted R^2. The correlation between the two C pools is weak and negative or strong and positive, while the adjusted R^2 does not generally increase from North to South (Santa Gracia < Pan de Azúcar < Nahuelbuta < La Campana).

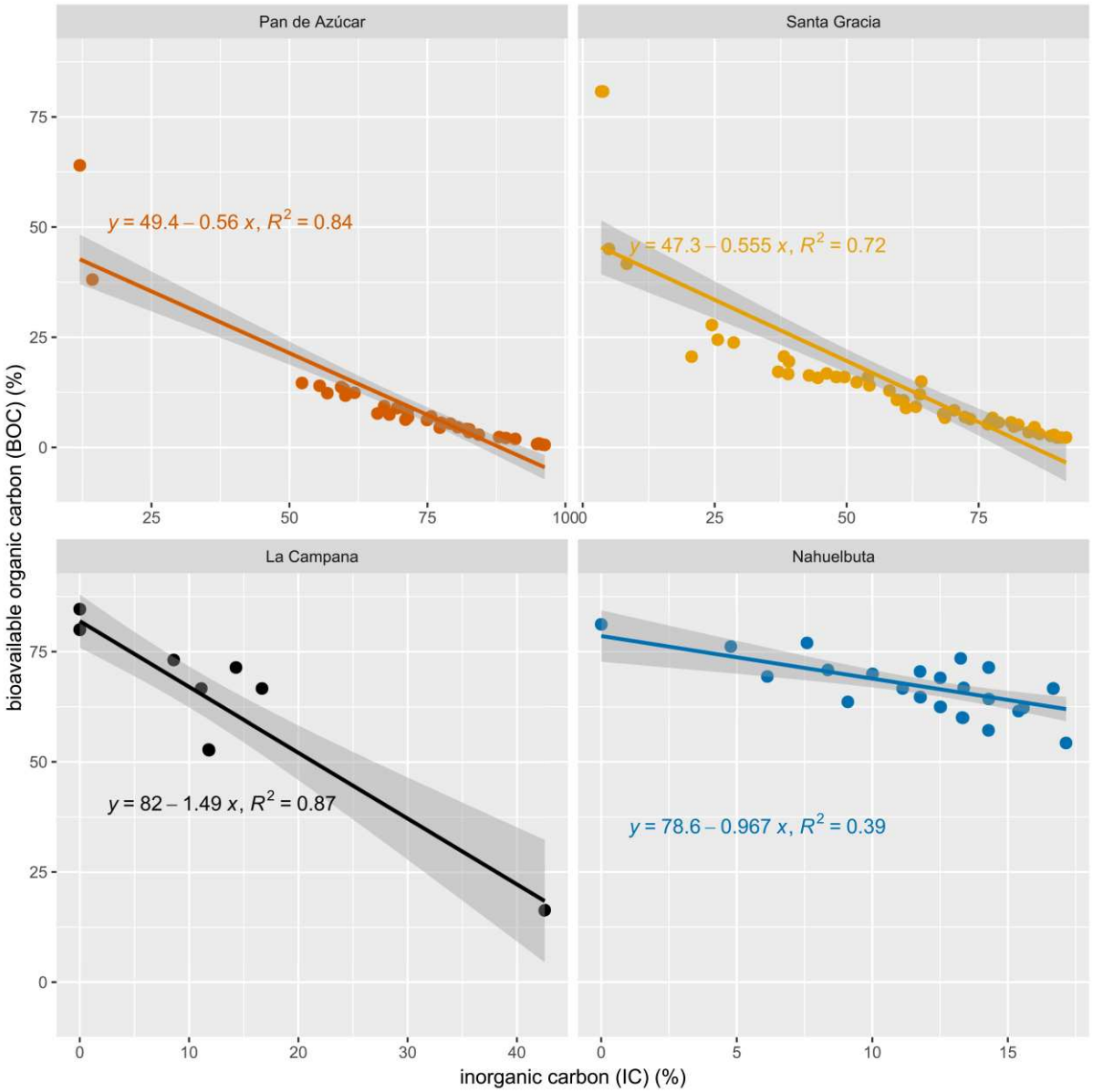

Figure 3.S6: Relative amount of bioavailable organic carbon (BOC) (%) as function of inorganic carbon (IC) (%) for the four field sites. The equations display the function of the linear fit, accompanied by the adjusted R^2. The correlation between the two C pools is moderate to strong and negative, while the adjusted R^2 is smaller in NA than in the other field sites (Nahuelbuta < Santa Gracia < Pan de Azúcar < La Campana).

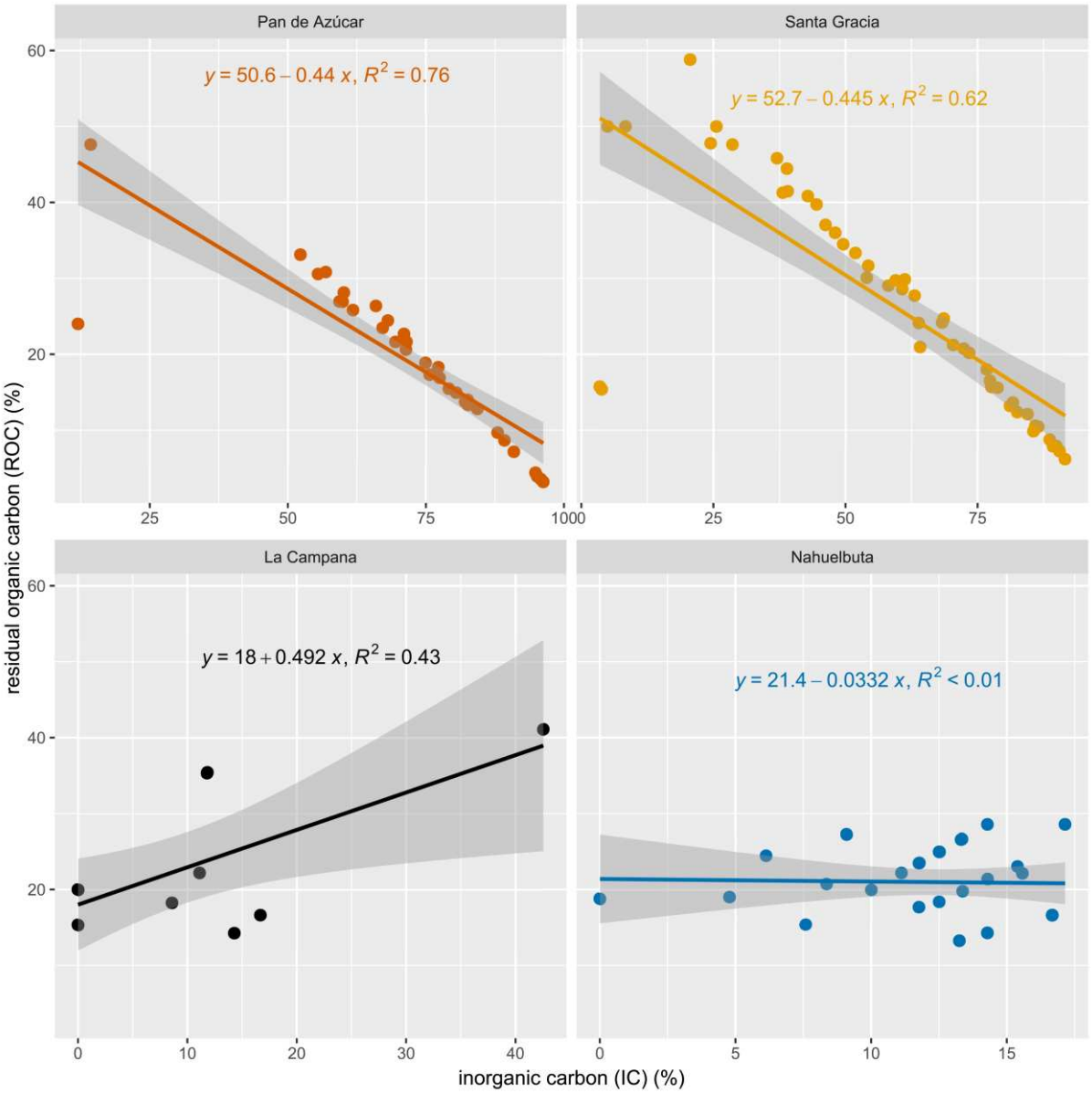

Figure 3.S7: Relative amount of residual organic carbon (ROC) (%) as function of inorganic carbon (IC) (%) for the four field sites. The equations display the function of the linear fit, accompanied by the adjusted R^2. The correlation between the two C pools is decently strong and negative for PdA and SG, while moderate in LC and not existing in NA. The adjusted R^2 decreases from North to South (Nahuelbuta < La Campana < Santa Gracia < Pan de Azúcar).

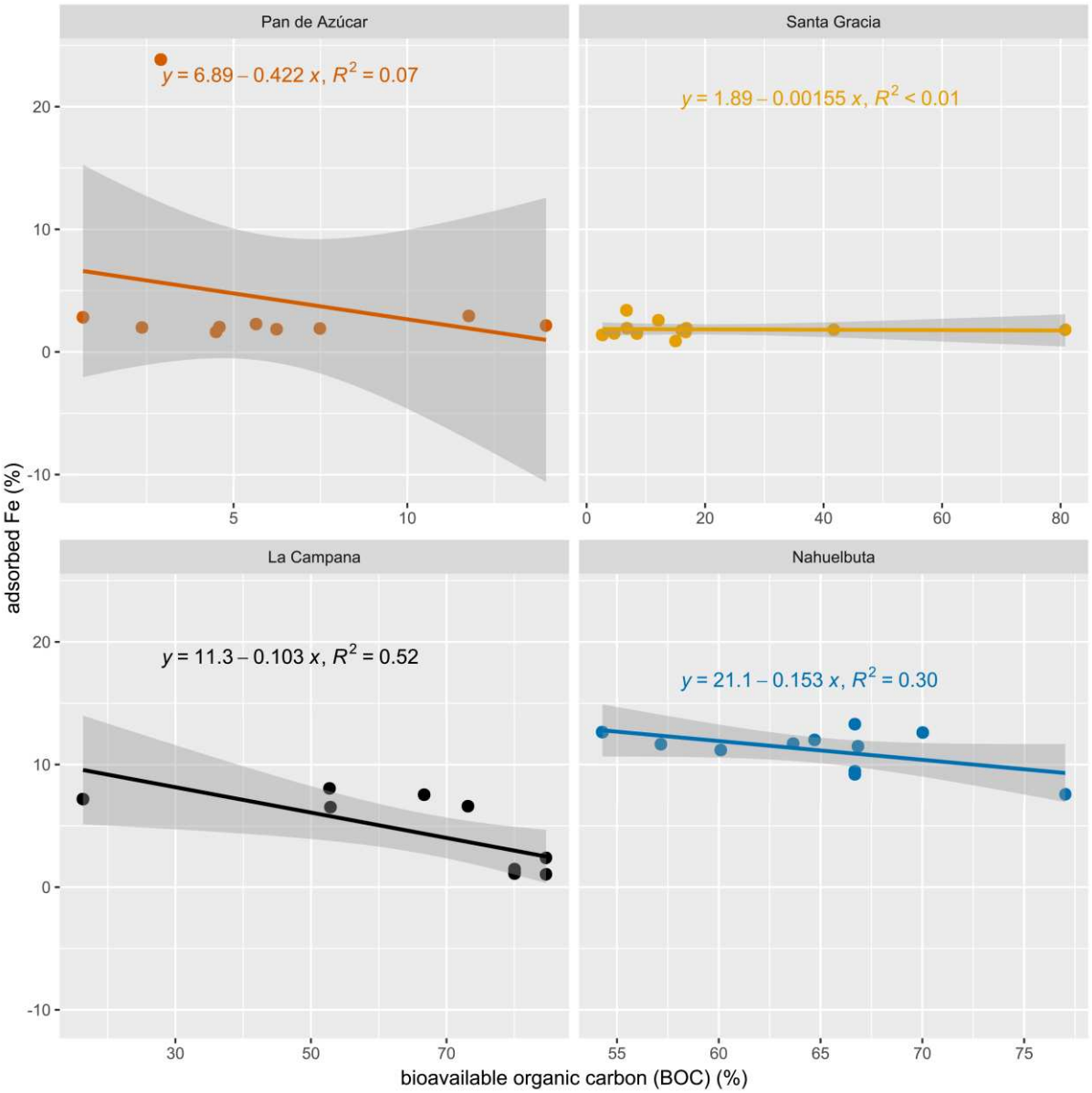

Figure 3.S8: Relative amount of adsorbed Fe (%) as function of bioavailable organic carbon (BOC) (%) for the four field sites. The equations display the function of the linear fit, accompanied by the adjusted R^2. The correlation between the C and Fe pools ranges from non-existent to moderate and is negative, if present. There is no clear trend in the adjusted R^2 from North to South (Santa Gracia < Pan de Azúcar < Nahuelbuta < La Campana).

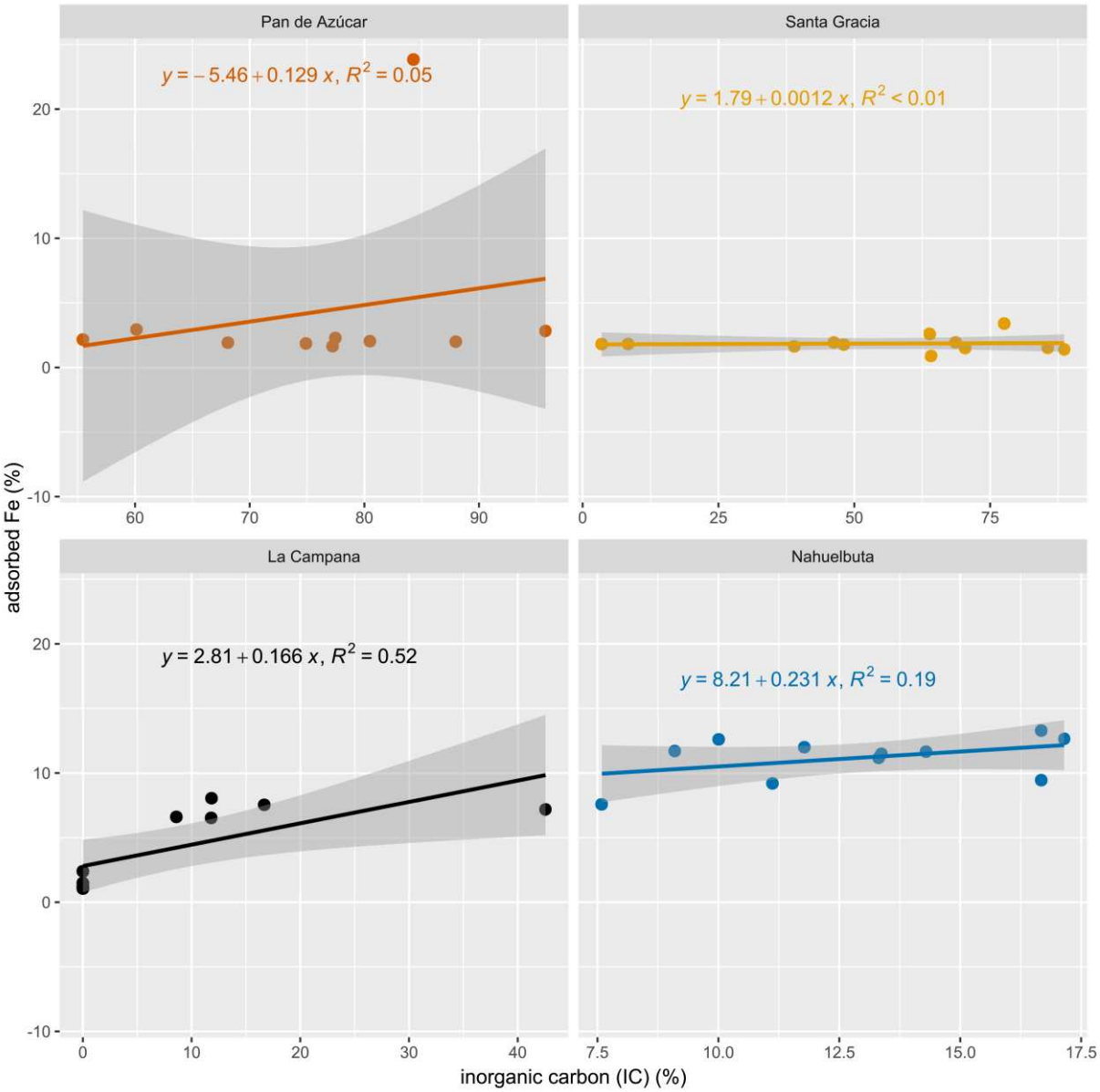

Figure 3.S9: Relative amount of adsorbed Fe (%) as function of inorganic carbon (IC) (%) for the four field sites. The equations display the function of the linear fit, accompanied by the adjusted R^2. The correlation between the C and Fe pools ranges from non-existent to moderate and is positive, if present. There is no clear trend in the adjusted R^2 from North to South (Santa Gracia < Pan de Azúcar < Nahuelbuta < La Campana).

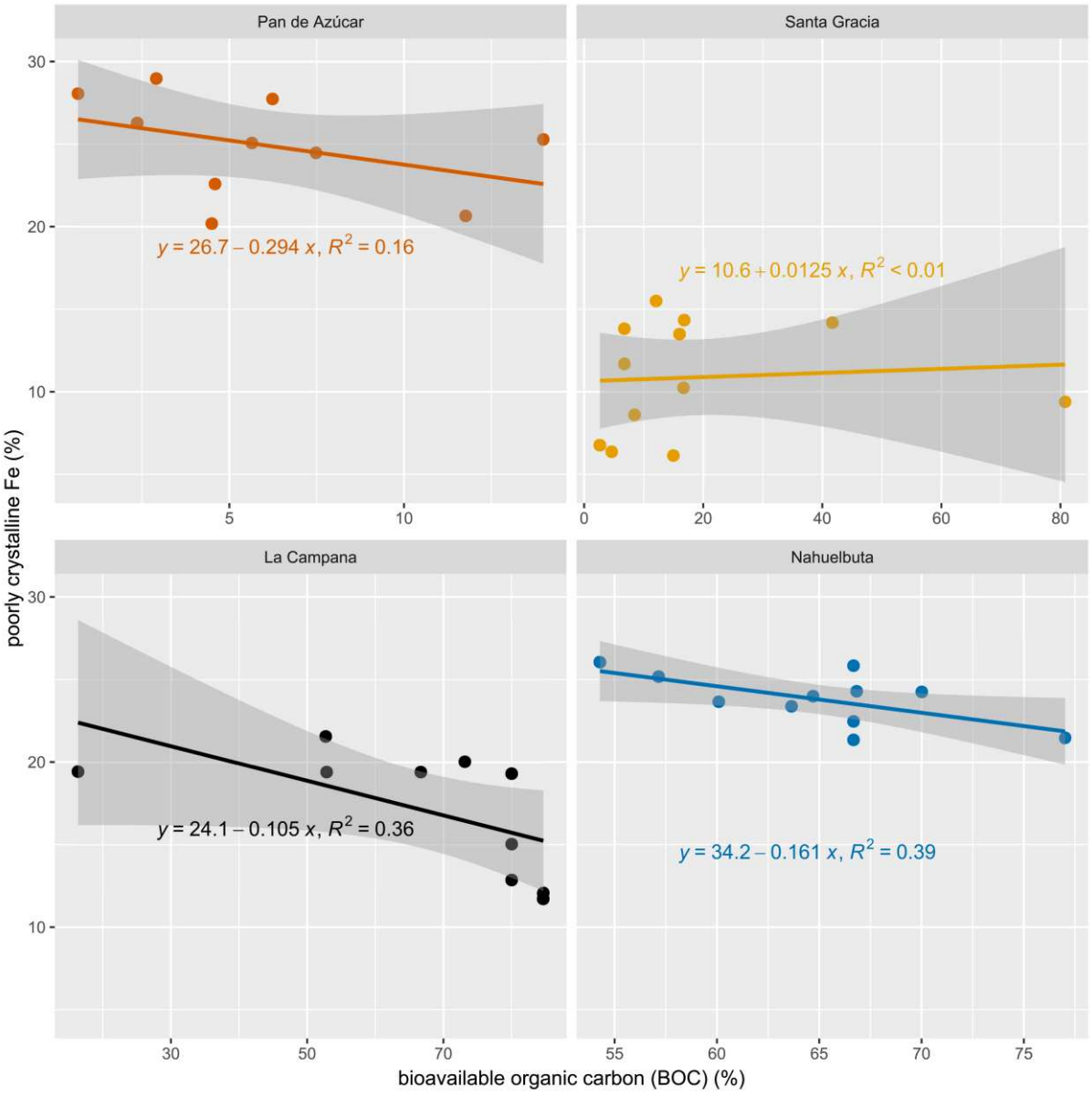

Figure 3.S10: Relative amount of poorly crystalline Fe (%) as function of bioavailable organic carbon (BOC) (%) for the four field sites. The equations display the function of the linear fit, accompanied by the adjusted R^2. The correlation between the C and Fe pools ranges from non-existent to weak and is negative, if present. The adjusted R^2 generally decreases from North to South (Santa Gracia < Pan de Azúcar < La Campana < Nahuelbuta).

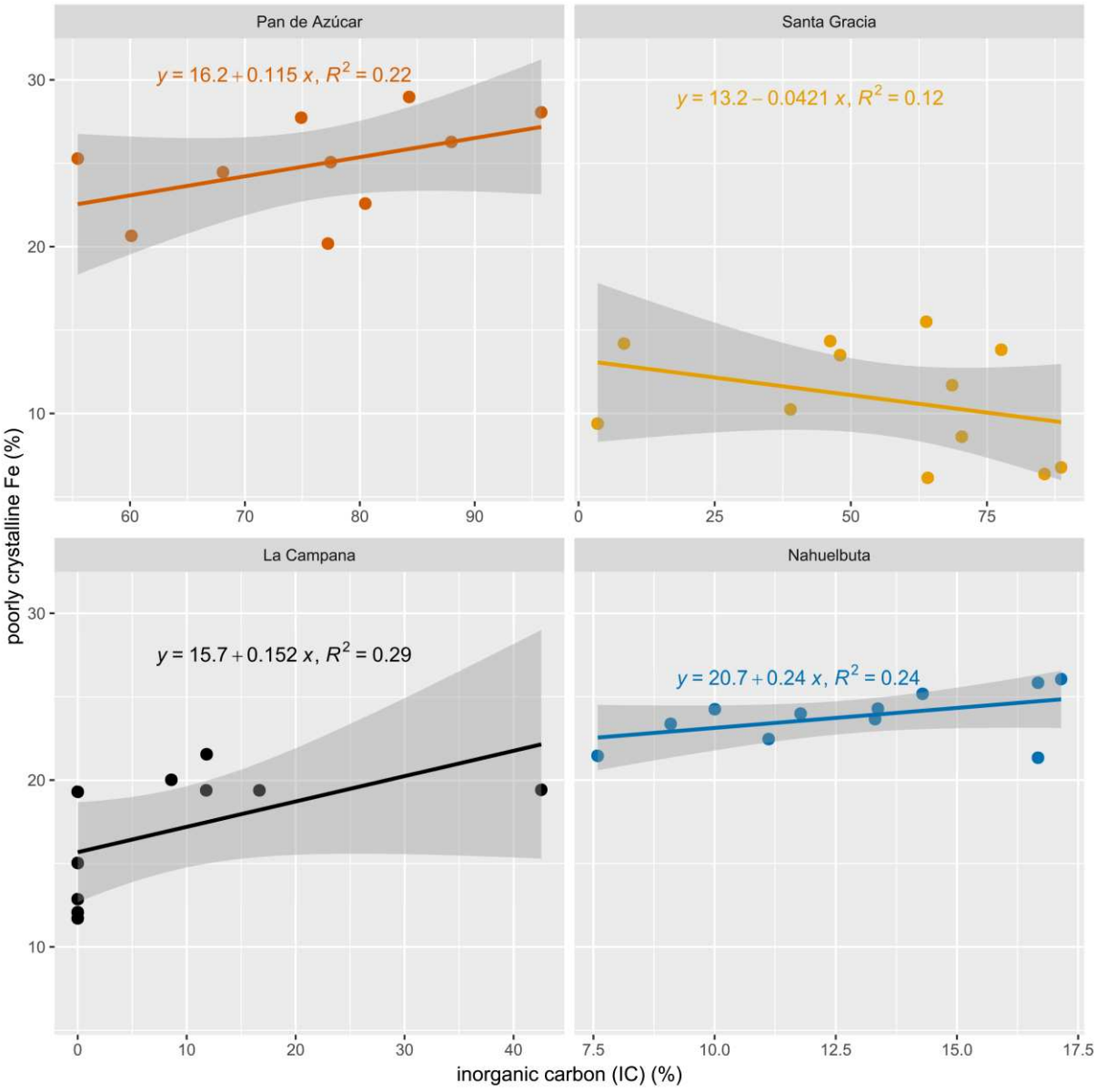

Figure 3.S11: Relative amount of poorly crystalline Fe (%) as function of inorganic carbon (IC) (%) for the four field sites. The equations display the function of the linear fit, accompanied by the adjusted R^2. The correlation between the C and Fe pools ranges from very weak to weak and is positive for PdA, LC and NA while negative for SG. There is no clear trend in the adjusted R^2 from North to South (Santa Gracia < Pan de Azúcar < Nahuelbuta < La Campana).

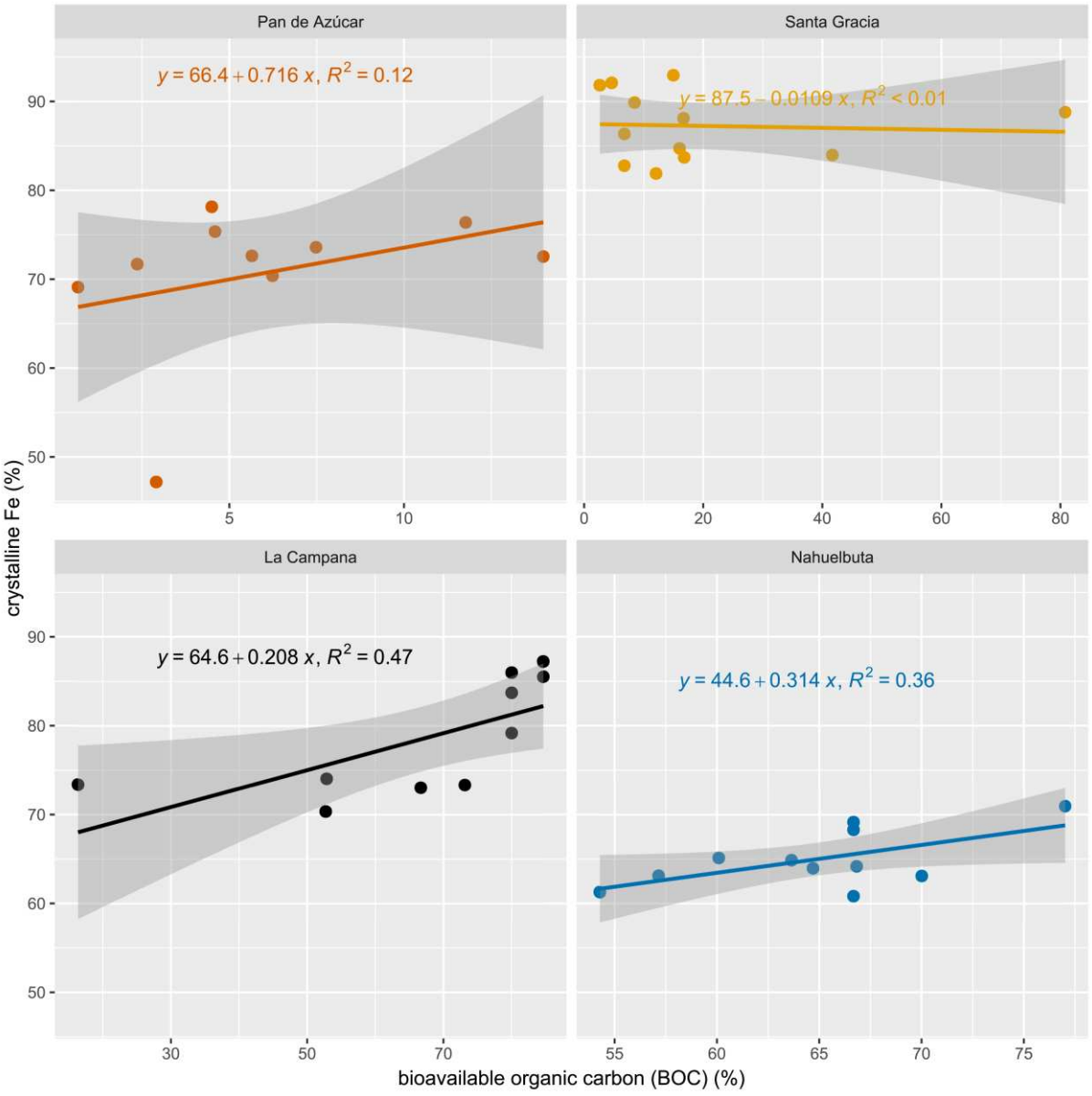

Figure 3.S12: Relative amount of crystalline Fe (%) as function of bioavailable organic carbon (BOC) (%) for the four field sites. The equations display the function of the linear fit, accompanied by the adjusted R^2. The correlation between the C and Fe pools ranges from non-existent to moderate and is positive, if present. The adjusted R^2 is lower for the two field sites in the North compared to the two field sites in the South (Santa Gracia < Pan de Azúcar < Nahuelbuta < La Campana).

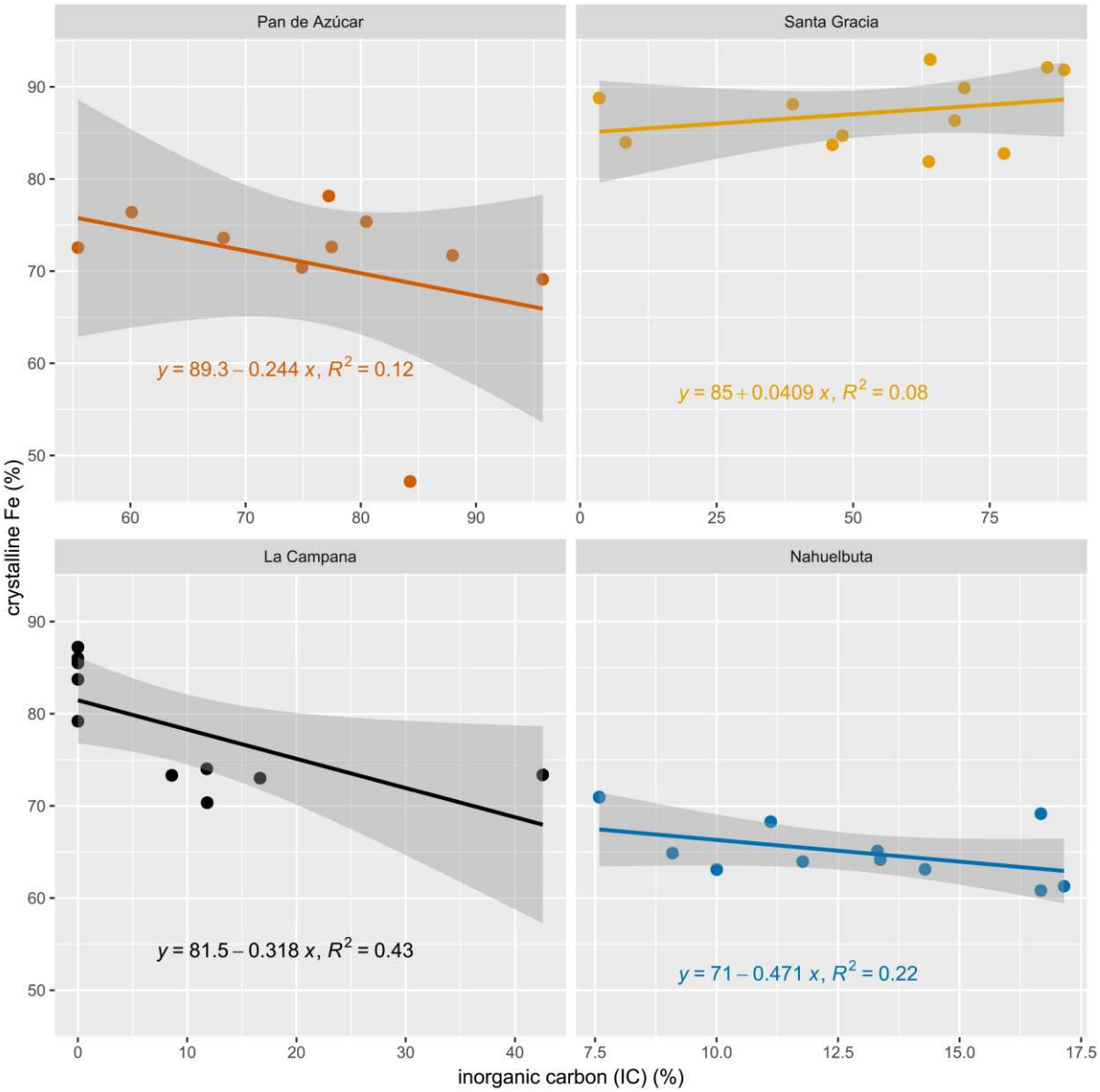

Figure 3.S13: Relative amount of crystalline Fe (%) as function of inorganic carbon (IC) (%) for the four field sites. The equations display the function of the linear fit, accompanied by the adjusted R^2. The correlation between the C and Fe pools ranges from very weak to moderate and is negative except for SG. The adjusted R^2 is highest in LC (Santa Gracia < Pan de Azúcar < Nahuelbuta < La Campana).

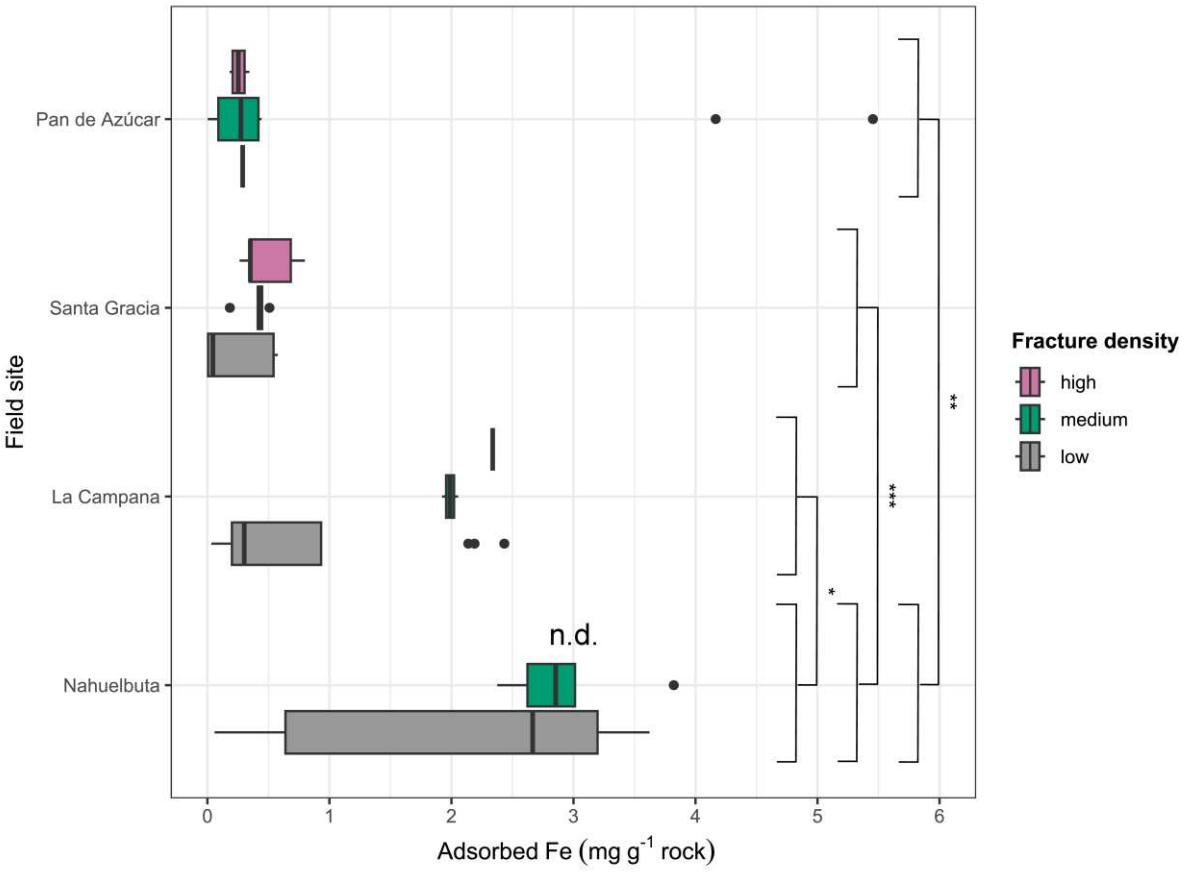

Figure 3.S14: Adsorbed Fe concentration (mg g^{-1} rock) as function of fracture density (low, medium, high) for the four field sites. The three fracture density types are “low” (grey, *n*=28), “medium” (green, *n*=24) and “high” (purple, *n*=10). The amount of fractures (x) was counted for 5m intervals and assigned to the categories (a) “low”, if x<=10, (b) “medium”, if 10<x>25, and (c) “high”, if x>=25. The four field sites are displayed top-down from North to South. Significant differences in treatment contrasts revealed by a Tukey *post-hoc* test are highlighted as respective significance level (***: *P*<0.001, **: *P*<0.01, *: *P*<0.05, n.s.= not significant). ”n.d.” denotes no data.

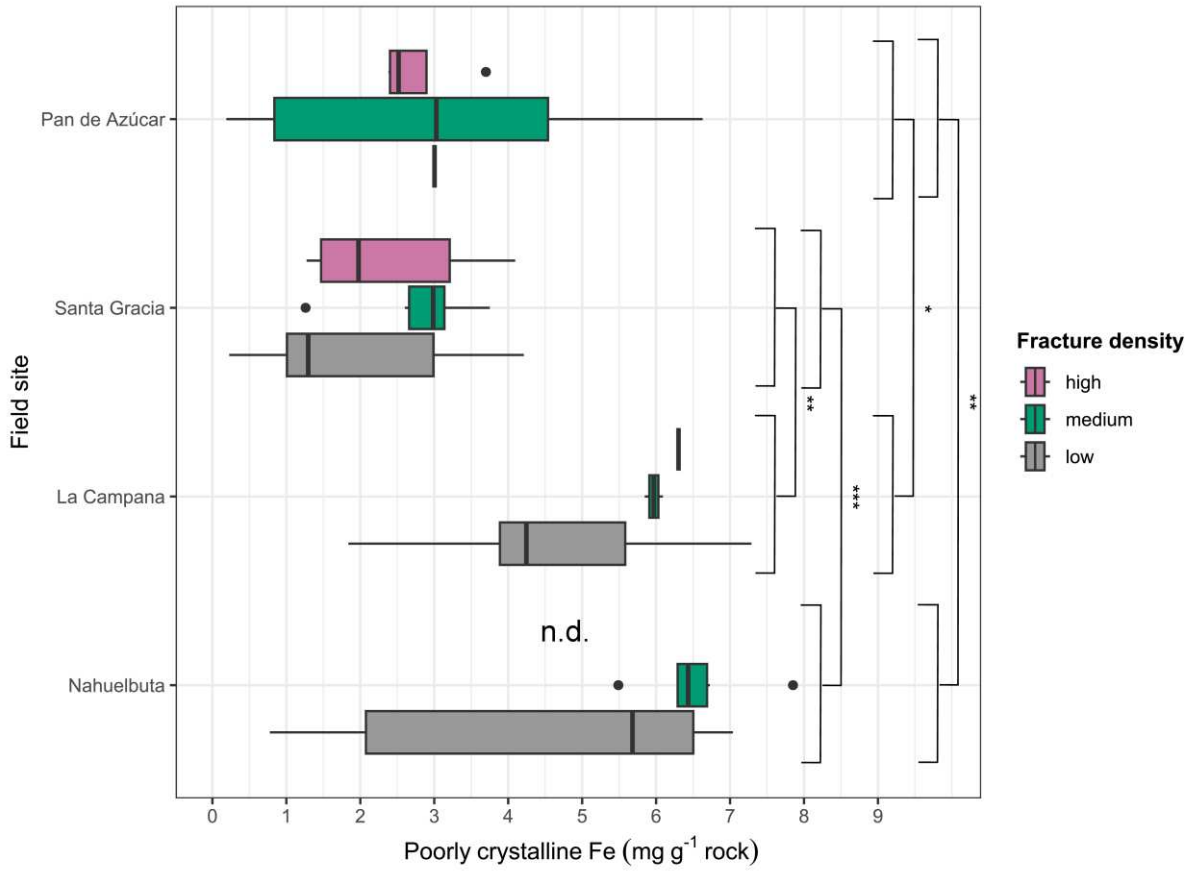

Figure 3.S15: Poorly crystalline Fe concentration (mg g^{-1} rock) as function of fracture density (low, medium, high) for the four field sites. The three fracture density types are “low” (grey, *n*=28), “medium” (green, *n*=24) and “high” (purple, *n*=10). The amount of fractures (x) was counted for 5m intervals and assigned to the categories (a) “low”, if x<=10, (b) “medium”, if 10<x>25, and (c) “high”, if x>=25. The four field sites are displayed top-down from North to South. Significant differences in treatment contrasts revealed by a Tukey *post-hoc* test are highlighted as respective significance level (***: *P*<0.001, **: *P*<0.01, *: *P*<0.05, n.s.= not significant). ”n.d.” denotes no data.

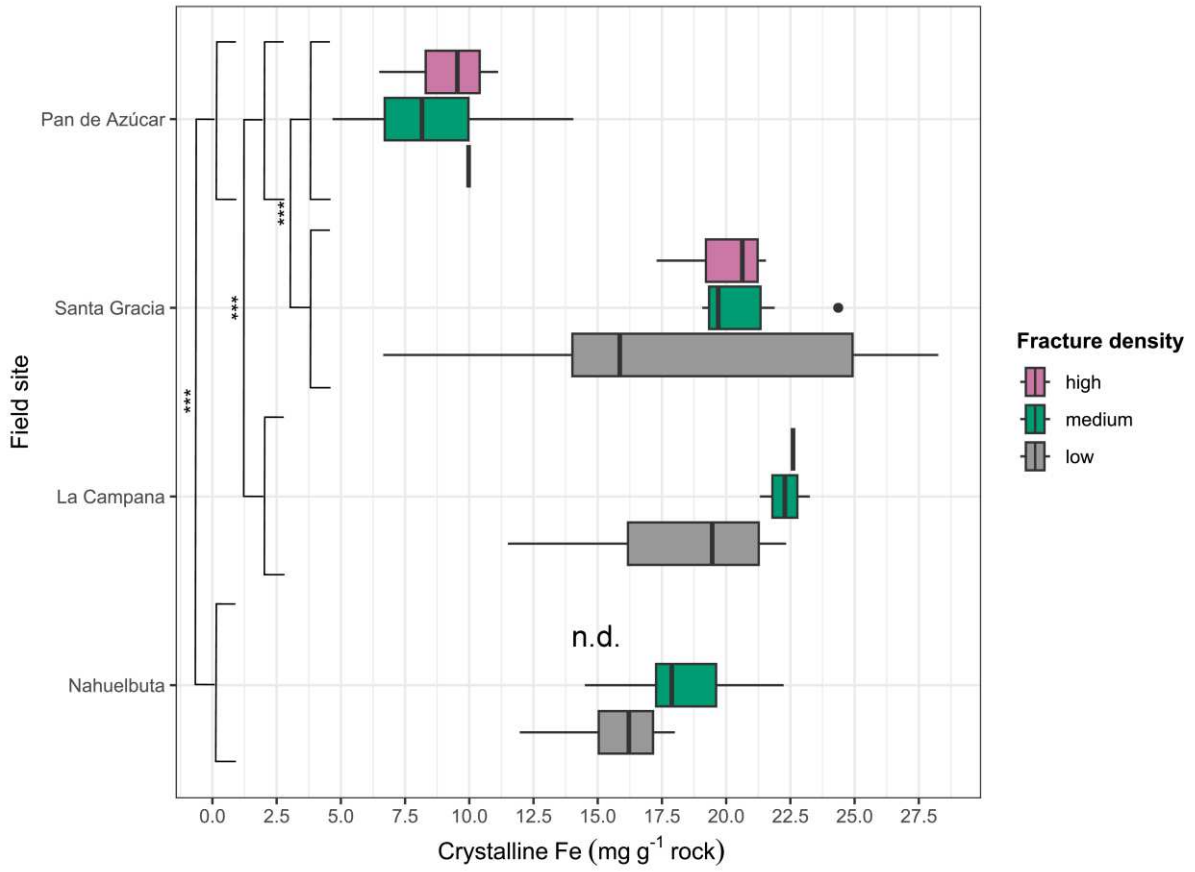

Figure 3.S16: Crystalline Fe concentration (mg g^{-1} rock) as function of fracture density (low, medium, high) for the four field sites. The three fracture density types are “low” (grey, *n*=28), “medium” (green, *n*=24) and “high” (purple, *n*=10). The amount of fractures (x) was counted for 5m intervals and assigned to the categories (a) “low”, if x<=10, (b) “medium”, if 10<x>25, and (c) “high”, if x>=25. The four field sites are displayed top-down from North to South. Significant differences in treatment contrasts revealed by a Tukey *post-hoc* test are highlighted as respective significance level (***: *P*<0.001, **: *P*<0.01, *: *P*<0.05, n.s.= not significant). ”n.d.” denotes no data.

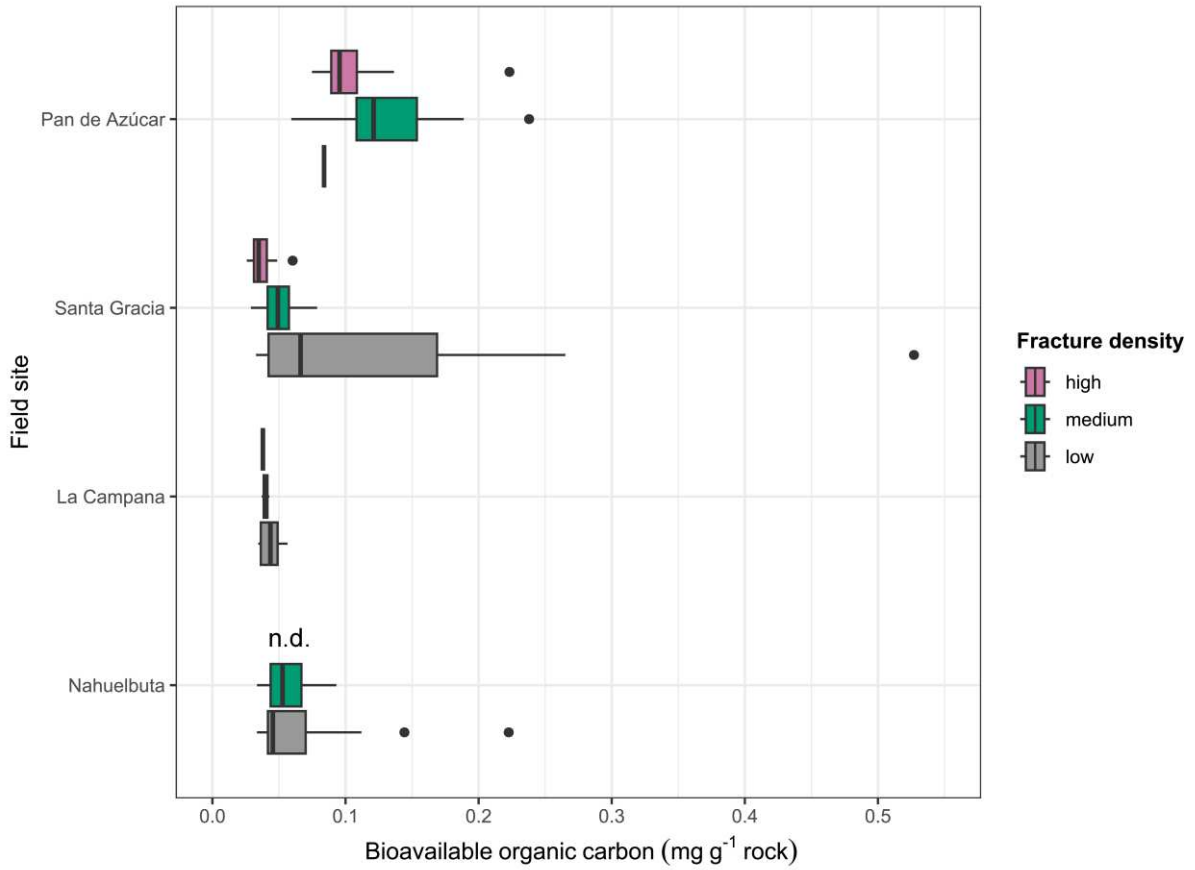

Figure 3.S17: Bioavailable organic carbon concentration (mg g^{-1} rock) as function of fracture density (low, medium, high) for the four field sites. The three fracture density types are “low” (grey, *n*=28), “medium” (green, *n*=24) and “high” (purple, *n*=10). The amount of fractures (x) was counted for 5m intervals and assigned to the categories (a) “low”, if x<=10, (b) “medium”, if 10<x>25, and (c) “high”, if x>=25. The four field sites are displayed top-down from North to South. Significant differences in treatment contrasts revealed by a Tukey *post-hoc* test are highlighted as respective significance level (***: *P*<0.001, **: *P*<0.01, *: *P*<0.05, n.s.= not significant). ”n.d.” denotes no data.

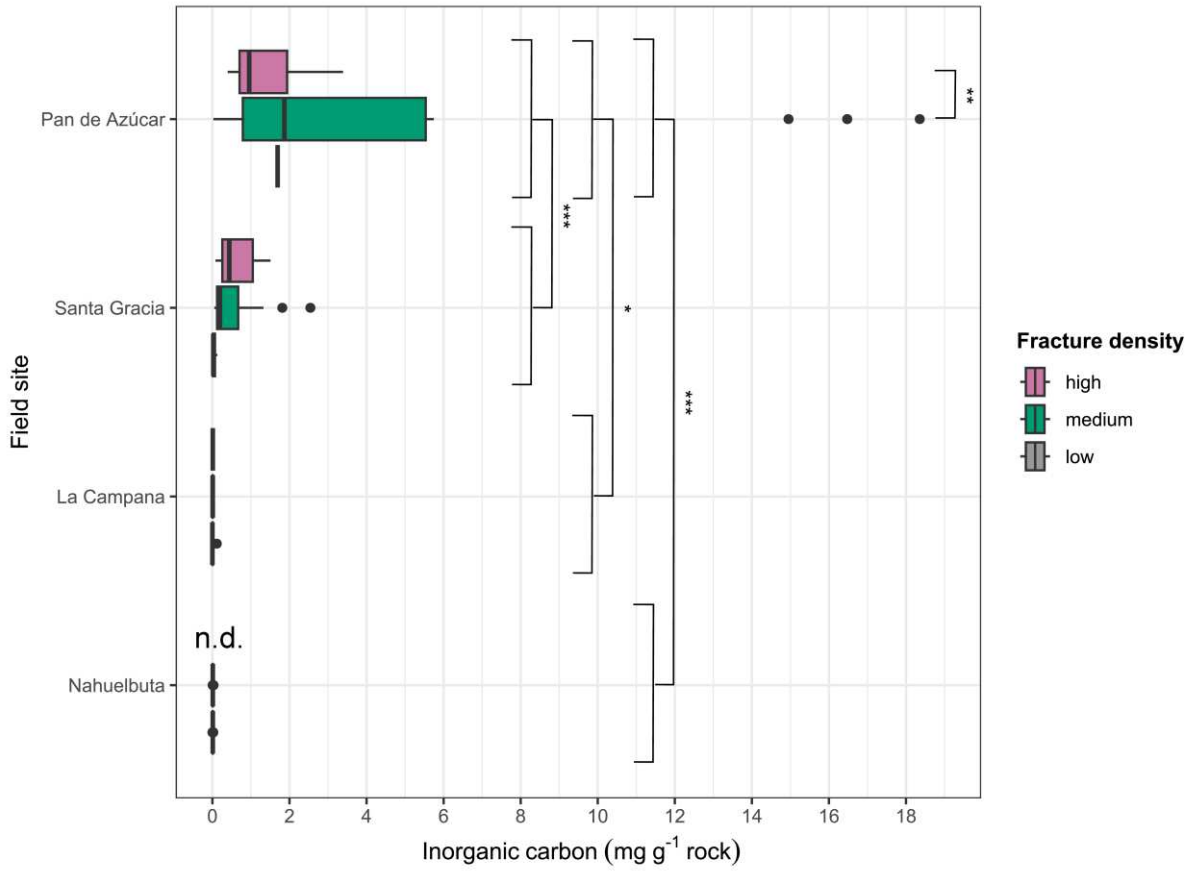

Figure 3.S18: Inorganic carbon concentration (mg g^{-1} rock) as function of fracture density (low, medium, high) for the four field sites. The three fracture density types are “low” (grey, *n*=28), “medium” (green, *n*=24) and “high” (purple, *n*=10). The amount of fractures (x) was counted for 5m intervals and assigned to the categories (a) “low”, if x<=10, (b) “medium”, if 10<x>25, and (c) “high”, if x>=25. The four field sites are displayed top-down from North to South. Significant differences in treatment contrasts revealed by a Tukey *post-hoc* test are highlighted as respective significance level (***: *P*<0.001, **: *P*<0.01, *: *P*<0.05, n.s.= not significant). ”n.d.” denotes no data.

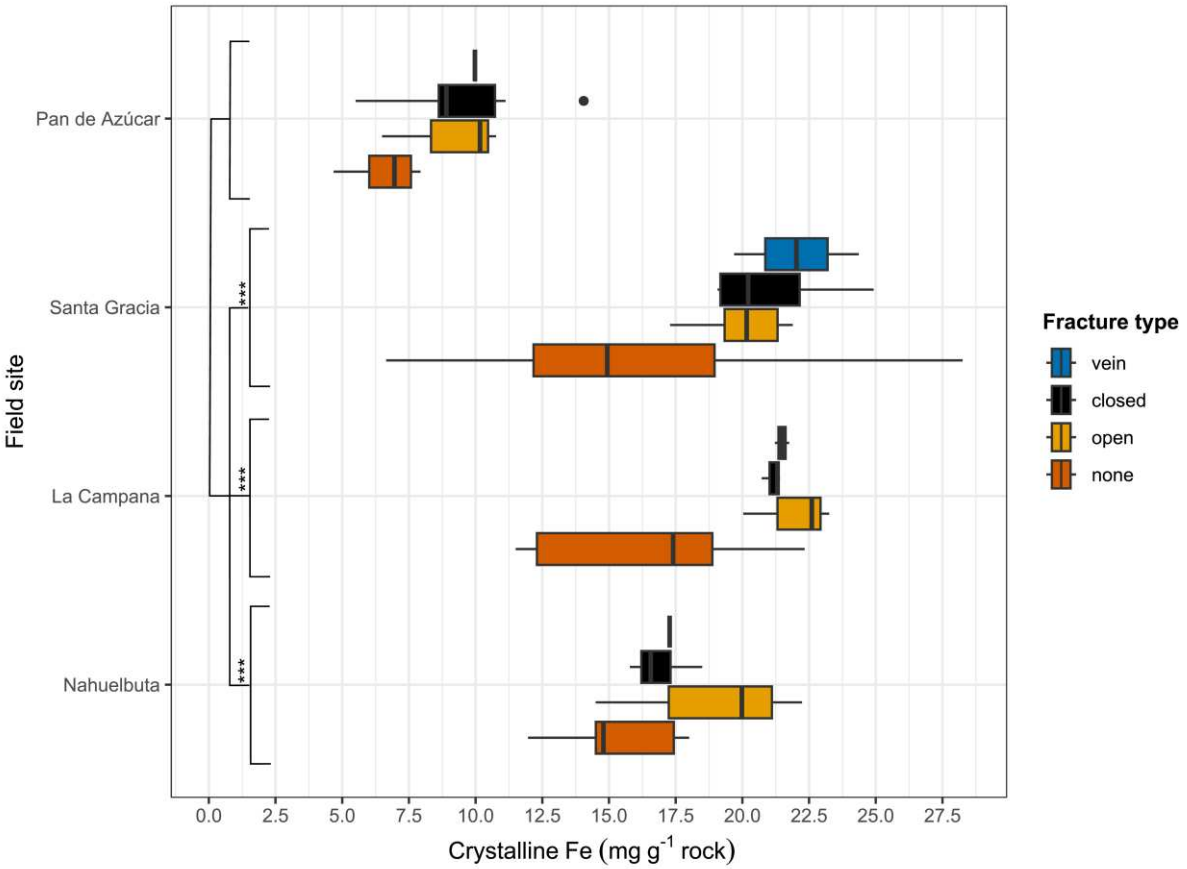

Figure 3.S19: Crystalline Fe concentration (mg g^{-1} rock) as function of fracture type for the four field sites. The four fractures types are “none” (orange, *n*=20), “open” (yellow, *n*=15), “closed” (black, *n*=21) and “vein” (blue, *n*=6), with “none” serving as reference for the absence of fractures. The four field sites are displayed top-down from North to South. Significant differences in treatment contrasts revealed by a Tukey *post-hoc* test are highlighted as respective significance level (***: *P*<0.001, **: *P*<0.01, *: *P*<0.05, n.s.= not significant).

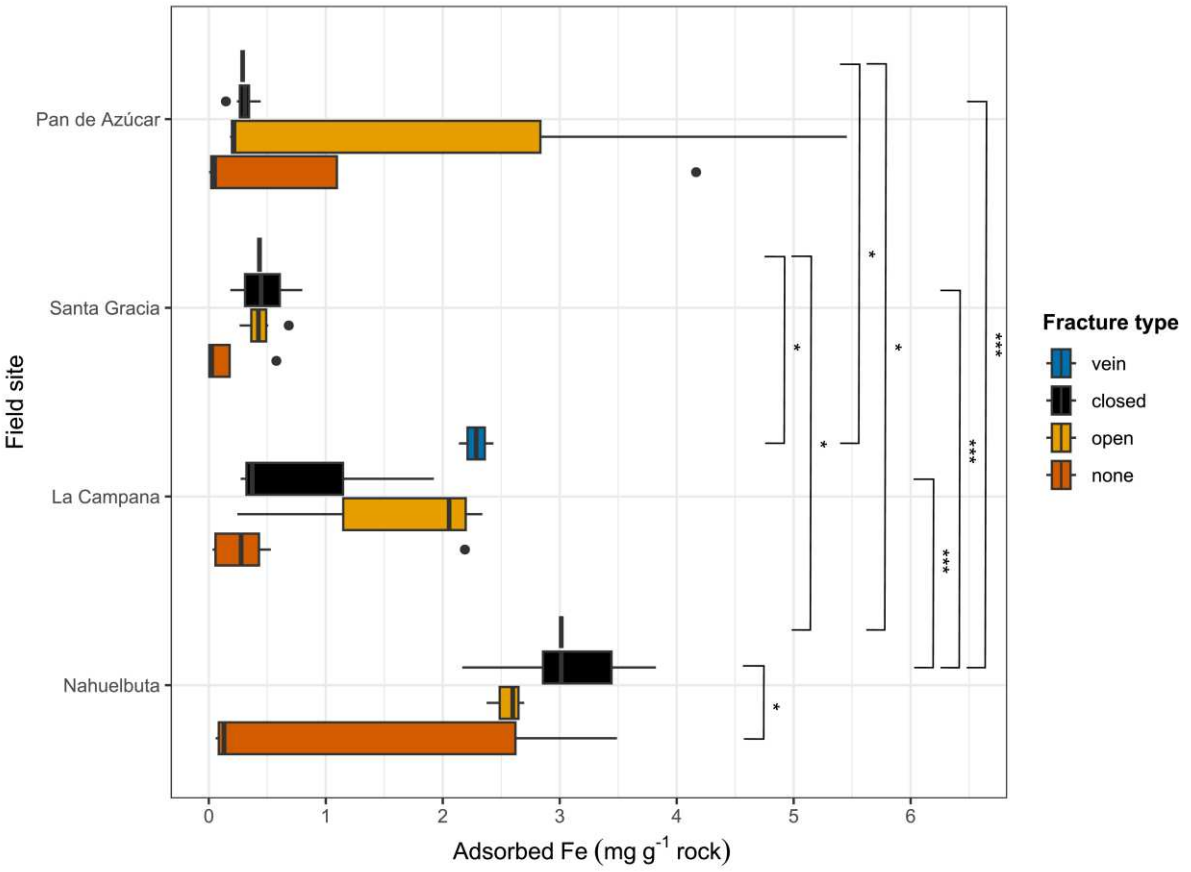

Figure 3.S20: Adsorbed Fe concentration (mg g^{-1} rock) as function of fracture type for the four field sites. The four fractures types are “none” (orange, *n*=20), “open” (yellow, *n*=15), “closed” (black, *n*=21) and “vein” (blue, *n*=6), with “none” serving as reference for the absence of fractures. The four field sites are displayed top-down from North to South. Significant differences in treatment contrasts revealed by a Tukey *post-hoc* test are highlighted as respective significance level (***: *P*<0.001, **: *P*<0.01, *: *P*<0.05, n.s.= not significant).

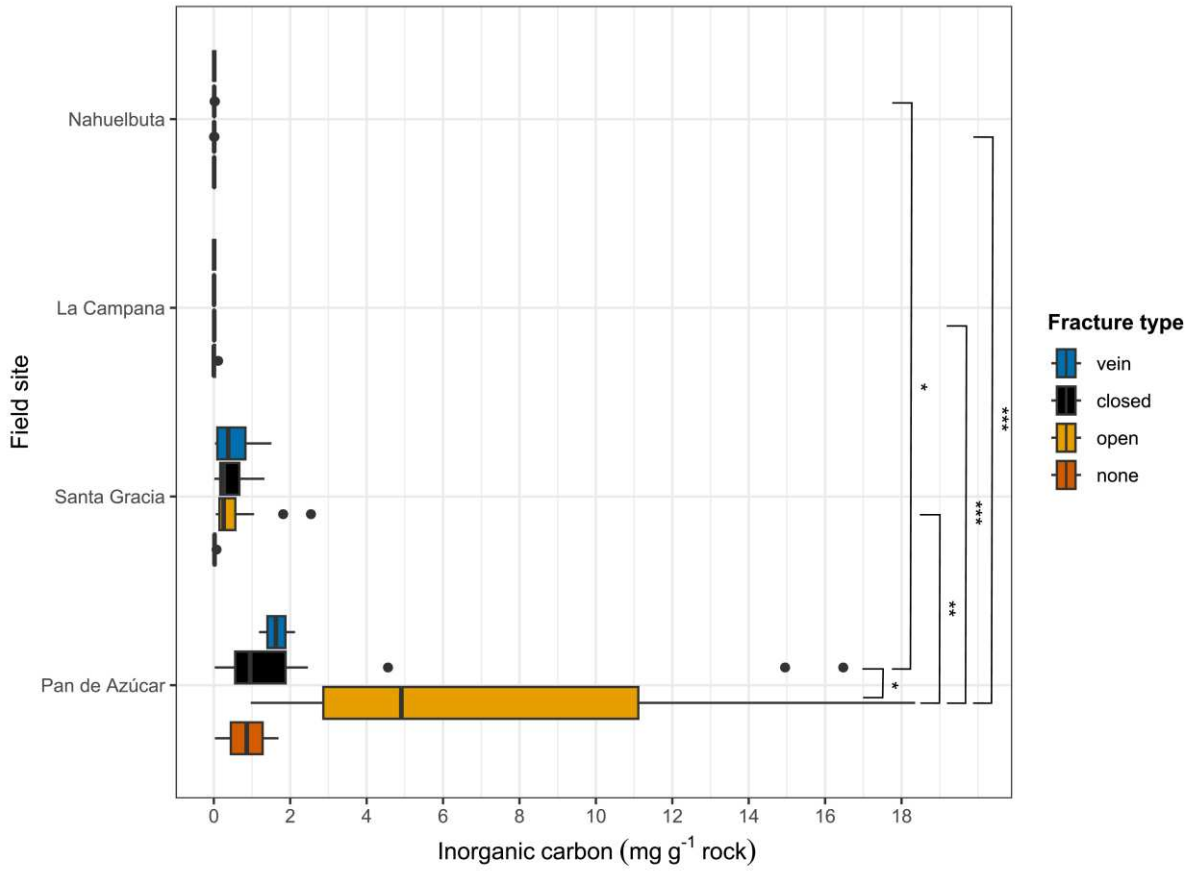

Figure 3.S21: Inorganic carbon concentration (mg g^{-1} rock) as function of fracture type for the four field sites. The four fractures types are “none” (orange, *n*=16), “open” (yellow, *n*=39), “closed” (black, *n*=61) and “vein” (blue, *n*=13), with “none” serving as reference for the absence of fractures. The four field sites are displayed top-down from North to South. Significant differences in treatment contrasts revealed by a Tukey *post-hoc* test are highlighted as respective significance level (***: *P*<0.001, **: *P*<0.01, *: *P*<0.05, n.s.= not significant).

Chapter 4: Discussion and Outlook

Microbial weathering occurs during all stages of rock-soil transformation such as rock colonisation, rock breakdown, saprolite formation and element cycling (Melton et al., 2014; Banwart et al., 2019). It has been primarily investigated at shallow depths in humid and tropical environments (Buss et al., 2005; Minyard et al., 2012; Brantley et al., 2013; Napieralski et al., 2019). Until now, there are not many studies deciphering the role of microorganisms in weathering processes occurring in the deep (10s to 100s of metres) CZ especially in (semi-)arid climates where rocks are less intensely weathered (Moser et al., 2003; Fredrickson and Balkwill, 2006; Onstott et al., 2019; Takamiya et al., 2021). Even more, we might currently underestimate how quantitatively important and widespread microbial weathering may be. Besides that, there is a knowledge gap in understanding the impact of microorganisms on rock and mineral weathering in the deep subsurface along climate gradients. Hence, this thesis contributes to overcoming these knowledge gaps by studying the role of Fe-metabolising microorganisms in weathering of Fe-bearing minerals in granitoid lithology in the deep terrestrial subsurface along a climate gradient (Chilean Coastal Cordillera).

Firstly, we identified mineralogical and geochemical conditions in the deep subsurface of hydrothermally altered granitoid lithology in semi-arid climate, in which Fe-metabolising microorganisms would thrive in most by performing Fe extractions, XRD and μXRD analyses. Secondly, we investigated the suitability of Fe-bearing minerals for microbial Fe-mineral weathering in the deep subsurface of semi-arid climate, i.e. in a water- and nutrient deprived system, via thermodynamic calculations. Based on a profound characterisation of the mineralogical, geochemical and thermodynamic conditions, we thirdly elucidated the role and impact of Fe-metabolising bacteria in weathering of Fe-bearing minerals in a semi-arid climate by (1) exploring whether they actively induce major weathering by fostering alteration of solids (i.e. via demonstrating active Fe(III) reduction by the *in situ* community), and (2) investigating the *in situ* microbial community composition in the deepest weathering zone via 16S rRNA sequencing (**Chapter 2**).

Next, we zoomed out from our hydrothermally altered granitoid weathering profile in semi-arid climate to the whole weathering gradient covering granitoid lithology in arid, semi-arid, Mediterranean and humid climate (from North to South). To assess the potential role of Fe-metabolising microorganisms in weathering of Fe-bearing minerals, we quantified bioavailable Fe and C pools by performing sequential Fe and C extractions for all four field sites. Subsequently, we identified controlling factors of microbial deep subsurface weathering of Fe-bearing minerals by evaluating the relative importance of climate (field sites), tectonic activity (presence/absence of fractures, fracture density), and mineralogical and geochemical

conditions (bioavailable Fe mineral and C pools) for each field site along the climate gradient. Eventually, we assessed whether Fe and C geochemistry paired with fracture analysis (type and density) is a sufficient tool to predict depth intervals/zones of potential microbial activity (**Chapter 3**).

In the following, the findings of this thesis and its subprojects, cultivation efforts, “lessons learned” (troubleshooting) and potential future experiments are discussed.

4.1 Microorganisms are agents of weathering of Fe-bearing minerals

Microbial weathering comprises growth and activity of both prokaryotes and eukaryotes (Brantley et al., 2012; Ehrlich et al., 2015). It is a key process for microorganisms to adapt and survive in oligotrophic (i.e. nutrient depleted) environments such as the deep biosphere, since it facilitates nutrient access and energy production (autolithotrophy) (Tebo et al., 2015). Among the four main mechanisms for microorganisms to break down minerals and rocks (**Chapter 1**), microbial weathering via redox reactions comprehends the main focus of this work.

Research investigating the role of microorganisms in weathering processes occurring in the deep (10s to 100s of metres) CZ especially in (semi-)arid climates where rocks are less intensely weathered is scarce. Schwerdhelm et al. (2025) is the first study that investigated the role of Fe-metabolising microorganisms in a hydrothermally altered granitoid weathering profile in a semi-arid climate (Santa Gracia). Intense investigations of our study site Santa Gracia (Weckmann et al., 2020; Krone et al., 2021b; Trichandi et al., 2022), especially the disentanglement of hydrothermal alteration and weathering features (Hampl et al., 2022), allowed us to use it as a model site to study microbial contributions to weathering of Fe-bearing minerals under water- and nutrient-limiting conditions. Due to the lack of *in situ* fluid data, observations made in previous studies are not conclusive evidence for a potential water table in the deepest weathering zone (Krone et al., 2021b; Hampl et al., 2022).

Regarding Fe-bearing minerals, it depends on their nature, whether Fe-metabolising microorganisms can use them as an energy source. Granitoid lithology found in SG mainly consists of hornblende, biotite and chlorite, which are primary Fe(II)-bearing silicates (**Chapter 2**). Microbial Fe(II) oxidation of these silicates under *in situ* conditions is energetically not feasible. Since Fe(II) is strongly bound in the crystal structure of poorly soluble, highly crystalline silicates, it is less accessible for microbial redox reactions (Shelobolina et al., 2012; Napieralski et al., 2019; Fan et al., 2023). Still, we observed microbial Fe(II) oxidation in our microaerophilic Fe(II)-oxidising SG enrichments, which is proof for their *in situ* existence but does not provide information on their *in situ* activity in weathering of Fe(II)-bearing minerals (**Chapter 2**). Microniches with micromolar concentrations of oxygen as electron acceptor are a potential environment, in which microaerophiles might thrive in. Eventually, primary Fe-bearing minerals could be rather accessible to microorganisms excreting acids, i.e. by proton-

promoted dissolution. Contrastingly, we could demonstrate that secondary Fe-bearing minerals (= Fe(III) (oxyhydr)oxides) can be used as feasible energy source by microbial Fe(III) reduction throughout the whole weathering profile (Schwerdhelm et al., 2025).

Fe(II)-bearing silicates are often oxidised abiotically by O_2 in meteoric water, limiting O_2 supply for microbial metabolisms at greater depths (White and Yee, 1985; Perez et al., 2005). Hence, overall weathering rates in SG might depend on seasonal fluctuations in O_2 concentrations in the deep subsurface. In this context, the work of Frey et al. (2010) should be highlighted. They grew several strains isolated from granitic rock material of an Alpine Glacier forefield. In granite dissolution experiments, more specifically cell suspension experiments (approx. $5x10^8$ cells ml^{-1}), they quantified strain-specific 0-140 µM Fe in solution after 4 or 8 days of incubation. Hence, microbial metabolisation of fresh Fe(II) silicates may occur to a minor extent under ideal conditions. Regarding our field site SG, weathering induced fracturing generates secondary Fe(III) (oxyhydr)oxides, but also consumes water and O_2 during Fe(II)-bearing silicate transformation. The weathering rates of secondary Fe(III) (oxyhydr)oxides by microbial reduction would probably be further increased by this, if enough water for microbial metabolisms was available. However, the amount of cells (ml^{-1}) *in situ* is lower than in cell suspension experiments and the amount of available meteoric water being transported into the (deep) subsurface (= precipitation (mm)) of SG even in the wettest months is limited (10-30 mm $month^{-1}$) compared to wetter field sites like the Shale Hills catchment (Gu et al., 2020a), the Alpine Damme Glacier forefield (Frey et al., 2010) or also the other EarthShape field sites La Campana and Nahuelbuta (Oeser et al., 2018). This suggests that there might be seasonally dependent and locally limited accelerated weathering by microbes in fracture zones with pockets of water (e.g. a potential water table in approx. 68-70 m depth). In summary, we can conclude that the impact of Fe-metabolising microorganisms in the SG weathering profile is higher regarding Fe(III) reduction than Fe(II) oxidation and that Fe(III) (oxyhydr)oxides are preferentially used for microbial metabolisms.

4.2 Impact of microorganisms on weathering of Fe-bearing minerals along a climate gradient

Assuming that our findings from SG (**Chapter 2**) are generally applicable for the whole climate gradient, we can formulate two working hypotheses. Firstly, Fe-metabolising microorganisms are probably not the main driving force for weathering of primary Fe(II)-bearing silicates, since energetically not feasible with regard to activation energy needed. Secondly, Fe(III) reduction of minerals such as magnetite and Fe(III) (oxyhydr)oxides like hematite, goethite or ferrihydrite is energetically feasible for microbes, as demonstrated for Fe(III)-reducing microorganisms in SG. To this end, we are limited to a data set consisting of geochemical, mineralogical, thermodynamic and fracture data when discussing microbial weathering of Fe-bearing

minerals in the context of deep subsurface. Hence, a comprehensive overview of the four field sites and its main controlling factors is given below.

4.2.1 Role of aridification for microbial Fe-cycling

The four EarthShape field sites are located along a climate gradient, which is expressed as differences in solar radiation, mean annual temperature and precipitation. As water is key for microbial metabolisms, the role of aridification along the climate gradient has to be considered (Gaviria-Lugo et al., 2023). The amount of meteoric water introduced into the subsurface depends on the climate zone while controlling the weathering intensity of a system (Übernickel et al., 2020; Deng et al., 2022). It has to be noted that the role of groundwater has not been investigated in the EarthShape projects, which would be a valuable addition to the data set.

Water is limiting. In arid Pan de Azúcar and semi-arid Santa Gracia, there is a high fracture density (Stroncik et al., in prep.). Importantly, the amount of available water for microbial redox reactions is very low (10 mm yr^{-1}) and low (<100 mm yr^{-1}) and hence the rate limiting factor (Übernickel et al., 2020). However, there are implications for a deep aquifer (Houston, 2002; Herrera et al., 2018; Krone et al., 2021b; Gamboa et al., 2022; Trichandi et al., 2022). Microbial redox reactions are primarily bound to the presence of secondary Fe(III) minerals or a potential aquifer at depth (Schwerdhelm et al., 2025).

Water is potentially limiting. The fracture density in mediterranean La Campana is low, while the MAP is higher (346 mm yr^{-1}) (Übernickel et al., 2020; Stroncik et al., in prep.). There was no clear evidence for a deep aquifer (Trichandi et al., 2023). An increase in amount of extractable adsorbed and crystalline Fe could be observed with depth. In summary, the amount of water is potentially one factor, fracture density and type another factor (**Chapter 3**).

Water is not limiting. The fracture density in humid Nahuelbuta is low, while NA has the by far highest MAP among the four field sites (1927 mm yr^{-1}) (Übernickel et al., 2020; Stroncik et al., in prep.). There is an increase in amount of extractable adsorbed and crystalline Fe with depth (**Chapter 3**). Interestingly, weathering was not found to be intense below the upper few metres of the weathering profile (Hampl et al., 2023). The authors explained this feature by a hampering via clay minerals, which seal of the subsurface from the input of meteoric water. In short, water is not the primary control for microbial weathering in NA, but mineralogy.

4.2.2 Role of geochemistry, mineralogy, thermodynamics and fractures for predicting the impact of Fe-metabolising microorganisms on weathering of Fe-bearing minerals

In the absence of a robust microbiological dataset regarding the activity of Fe-metabolising microorganisms, the pairing of mineralogy, geochemistry, fracturing and hydrology helps to identify locations of potential microbial *in situ* weathering of Fe-bearing minerals within the four weathering profiles. Site-specific observations of lithology, fracturing, hydrothermal alteration and surface inputs suggest that fracturing, water availability and secondary Fe mineral formation are the key factors driving Fe cycling in the deep subsurface of the four study sites.

The highest probability of microbial *in situ* weathering of Fe-bearing minerals is linked to open fractures (**Chapter 3**). Fe-metabolising microorganisms thrive most in zones of unaltered and altered rock with increased concentrations of bioavailable and accessible Fe. Thereby, they can even further enhance abiotically produced secondary Fe(III) (oxyhydr)oxides mineral weathering. Interconnections of Fe and S cycles also foster the probability of microbiomes to adapt and survive at great depth in water- and nutrient -deprived systems (**Chapter 2**).

The investigation of groundwater and gas data during and after the conducted drilling campaigns would have been highly beneficial for an in-depth understanding of the deep subsurface microbial weathering processes along the climate gradient. Especially with regard to running thermodynamic calculations, identified amounts of soluble gases and ions help to identify reaction limiting steps (Amend and Shock, 2001; Amend et al., 2019; LaRowe and Amend, 2019; Schwerdhelm et al., 2025).

4.2.3 Microbial Fe-cycling in the shallow subsurface (< 2m) along the climate gradient

Unless for the deep subsurface, there is data on microbial weathering of Fe-bearing minerals in the shallow subsurface (< 2m) along the EarthShape gradient. Two master theses investigated the changes in Fe(III) mineral bioavailability along the climate gradient within the framework of this PhD project. The first study utilised microcosms to quantify the effect of Fe-metabolising bacteria on weathering rates of Fe(III)-minerals and mineral transformation along a precipitation gradient, i.e. the EarthShape field sites (Sauter et al., in prep.). Therefore, the role of the model strain *Shewanella oneidensis MR-1* in Fe(III) reduction was investigated by performing cell suspension experiments for a set of shallow (< 2m) soil samples. As a result, two key findings were made. Firstly, there is a clear order of bioavailability of Fe(III)-minerals for the model strain as function of the field site: SG > LC > NA > PdA. Secondly, the bioavailability of Fe(III)-minerals was independent from Fe(III)-mineral abundances. This suggests mineral bioavailability to be rather related to mineral reactivity, which is controlled by crystallinity.

The second study quantified the effect of Fe-metabolising bacteria on weathering rates of Fe(III)-minerals and mineral transformation along a precipitation gradient, too. However, enrichment cultures obtained soil samples from the EarthShape gradient were used in this follow-up study (Tian et al., in prep.). Fe(III)-reducing microorganisms could be successfully enriched from SG, LC and NA, but not from PdA. The most active enrichment culture from LC was used as microbial strain for the Fe(III)-microcosms. In contrast to the previous study, the order of observed Fe(III) reduction was SG > NA > LC > PdA. Hence, the absolute amounts of Fe(III) reduction by enriched native Fe(III)-reducing microorganisms can completely differ from laboratory model strains such as *Shewanella oneidensis MR-1*.

4.3 Enrichment culture efforts, outcome and improvement ideas for future approaches

Fe-metabolising microorganisms have been shown to contribute to deep (> 7m) subsurface rock weathering of various granitoid lithology in different climatic conditions (Lehman et al., 2001; Buss et al., 2005; Osburn et al., 2014; Napieralski et al., 2019; Bethencourt et al., 2020; Bochet et al., 2020; Napieralski and Roden, 2020; Jakus et al., 2021a; 2021b). Obtaining enrichment cultures and isolates from the investigated field site allows to unravel microbial *in situ* interactions. It is noteworthy that the obtainment of an Fe-metabolising enrichment culture is proof for its *in situ* existence but does not provide information on its *in situ* activity in weathering of Fe(II)-bearing minerals. However, in order to study the potential role of Fe-metabolising microorganisms under conditions as close to the natural setting as possible, microbial enrichment cultures shed light on key metabolisms within a subsurface microbiome.

In granitoid lithology as present for our field site Santa Gracia, lithotrophic Fe(II)-oxidising and Fe(III)-reducing microorganisms were expected to be found. Hence, we set up gradient tubes for the enrichment of microaerophilic Fe(II)-oxidising microorganisms as well as hungate tubes and deep-well plates for the enrichment of Fe(III)-reducing microorganisms at circumneutral pH (**Chapter 2**). Enrichments of microaerophilic Fe(II) oxidisers were successful for eight out of 47 samples (~17%) from 30.4, 34.3, 35.1, 40.0, 43.3, 50.7, 70.7 and 73.6 m depth. We identified growth in FeS tubes by the formation of distinct orange Fe(III) mineral accumulations within or below the orange-coloured top layer. Subsequent cultivation and isolation attempts were not successful. One possible explanation for unsuccessful subsequent cultivation and isolation attempts might have been low cell numbers, as we only observed growth in gradient tubes with a dilution of 10^{-1} and 10^{-2}. Other explanations might be missing co-cultures or energy sources. A few enrichments got affected by contamination, which might have been introduced by access of too high oxygen concentrations when alternating between gradient tubes and ZVI plates in order to obtain a robust enrichment culture.

Fe(III)-reduction could be quantified throughout the whole weathering profile. However, a robust Fe(III)-reducing enrichment culture could only be obtained from the deepest weathering zone in ~ 77 m depth. The novel obligately anaerobic culture SG reduces Fe(III) and sulfate. It grows chemoheterotrophically with lactate as well as autotrophically with dihydrogen as an electron donor but cannot oxidise acetate. Culture SG is capable of reducing ferrihydrite (up to 0.6 mM d^{-1}) and dominated by the spore-forming *Desulfotomaculum ruminis* (abundance of 98.5%) as revealed by 16S rRNA gene amplicon sequencing. In the following, we aimed for obtaining an isolate by using agar shakes and picking single colonies. To this end, the outcome of the isolation effort is unclear, since the enrichment has not been sequenced yet. Besides that, we did metagenomics on the enrichment culture, but struggled to get sufficient quality DNA for sequencing. In order to obtain enough biomass during DNA extraction, pooling of material obtained enough biomass but accumulated inhibiting compounds of the culture media.

Hence, a library generation could not be achieved. Prior to our Fhy reduction experiments we tried to wash the cells in order to minimise a carry-over of substrates, but observed the death of cells expressed as a net Fe(III) reduction of 0 mM. Cell death might have been caused by washing with buffer solution itself and/or the subsequent centrifugation step. Therefore, we run the Fhy experiments without a cell washing step. Encouraged by the reproducibility of the growth of culture SG, there is a couple of interesting research questions:

1. Can culture SG reduce ferrihydrite (Fhy) in sulfate-free medium, while adding lactate or dihydrogen as electron donors?
2. How do Fhy reduction rates compare, if sulfate is added in different concentrations?
3. Which other Fe(III) minerals besides ferrihydrite can culture SG reduce?
4. What are the Fe(III) reduction rates of the (potential) Fe(III) minerals culture SG can reduce?
5. Which preparation steps would be needed to get sufficient quality DNA for sequencing (metagenomics), i.e. enough biomass, but less inhibiting compounds from culture media accumulated?

Besides enriching Fe(II)-oxidising and Fe(III)-reducing microorganisms at circumneutral pH, we tried to enrich acidophilic Fe-metabolising microorganisms. Preparing the growth medium for acidophilic microaerophilic Fe(II)-oxidising microbes (pH 4) was a major challenge. We used the growth medium of the acidophilic, heterotrophic strain *Acidophilum SJH* (DSMZ 269) (Johnson and McGinness, 1991). Unless for the enrichments at circumneutral pH, bicarbonate buffer could not be used due to its lower end of buffer range being > pH 4. pH of the medium was adjusted to 4 with 1N sulfuric acid, but did not buffer the system. Enriching Fe(III)-reducing microorganisms at pH 3 did not succeed either. This time, we did not manage to modify the agar recipe in the way that the agar would solidify. Hence, it was impossible to streak out the agar plates for cell counts and isolation. Eventually, we dropped our cultivation efforts. Another approach for trying to enrich acidophilic Fe(II)-oxidisers could be by using phosphate buffer, while an alternative approach to enriching heterotrophic Fe(III)-reducers could be using liquid media, more specifically DSMZ 269 medium. Finally, setting up less enrichments at the same time might be an improvement to keep track of all of them.

4.4 Can Fe(II)-oxidising microorganisms oxidise structural Fe(II) in biotite and chlorite?

Granitoid lithology found in SG mainly consists of the primary Fe(II)-bearing silicate minerals hornblende, biotite and chlorite, as well as magnetite and hematite (**Chapter 2**). Besides that, chloritisation is common at all four Deep EarthShape drill sites. Hence, the key question is: Can Fe(II)-oxidising microorganisms use structural Fe(II) of Fe(II)-bearing silicates such as biotite and chlorite as sole energy source? If not, does microbial Fe(II) oxidation require prior mineral dissolution? Microbial Fe(II) oxidation of Fe(II)-bearing silicates under SG *in situ* conditions is energetically not feasible. Interestingly, Shelobolina et al. (2012) demonstrated

microbial oxidation of structural Fe(II) in very fine-grained (<5 µm) biotite (stock suspension concentration of 15 to 20 g L^{-1}) by nitrate-reducing, Fe(II)-oxidising (NRFeOx) culture KS. Therefore, we aimed for replicating this observation by adapting our experimental setup so that we accounted for (a) the chloritisation feature found at all four Deep EarthShape drill sites, and (b) coarser grain size ranges reflecting *in situ* conditions. More specifically, we quantified microbial oxidation of structural Fe(II) in biotite and chlorite for three NRFeOx cultures (Schwerdhelm et al., in prep.).

In Schwerdhelm et al. (in prep.), six batch experiments were set up, one for each NRFeOx culture (culture KS, AG, BoFeN1) and mineral (biotite, chlorite) combination with respective controls. The three NRFeOx cultures originate in case of (a) lithoautotrophic culture KS from a freshwater sediment, (b) chemolithoautotrophic culture AG from a fractured, anoxic, pyrite-rich limestone aquifer, and (c) mixotrophic culture BoFeN1 from lake sediments (Straub et al., 1996; Kappler et al., 2005; Klueglein and Kappler, 2013; Jakus et al., 2021a; Huang et al., 2022). We run experiments with powdered biotite and chlorite with a grain size of 63-25 µM and < 25 µM and a Fe(II) concentration of 20 mM.

Overall, NRFeOx microcosms did not show clear evidence for microbial oxidation of structural Fe(II) in biotite and chlorite. Hence, it is crucial to consider how bioavailable structural Fe(II) in Fe(II)-bearing silicates is. We argue that grain size and dissolution degree of Fe(II) in biotite and chlorite control the extent of microbial Fe(II) oxidation. The smaller the grain size and the higher the amount of dissolution structural Fe(II) from the mineral matrix, the higher the amount of quantifiable microbial Fe(II) oxidation. If we assume our mineral grains have a cube shape, the difference in available surface area will become obvious. 125 cubes of 5 µM side length fit into one cube of 25 µm side length, which equals respective surface areas of 18650 μm^2 versus 3750 μm^2. Hence, the expected amount of microbial Fe(II) oxidation is five times higher in the setup for biotite with a grain size < 5 µm. Shelobolina et al. (2012) further suggest microbial oxidation of structural Fe(II) to take place in subsurface environments such as deep granitic aquifers. This is an interesting possibility, although not probable in (semi-)arid field sites such as Pan de Azúcar and Santa Gracia due to the lack of water. Mineral dissolution is clearly a factor to consider in *in situ* systems, but was negligible in our setups. In summary, our results suggest microorganisms to most probably not being the main driving force for oxidation of structural Fe(II) in Fe(II)-bearing silicates in the deep subsurface of (semi-)arid terrestrial granitoid systems.

4.5 Future research projects

Open fractures were identified as locations with the highest probability of microbial *in situ* weathering of Fe-bearing minerals (**Chapter 3**). We characterised the mineralogy of SG fracture surface samples with µXRD (**Chapter 2**). However, attempts to screen our fracture

surface samples for microbe-mineral interactions with a SEM were not sufficient. Therefore, it might be a valuable attempt to characterise promising fracture surface samples on a nanometer scale. X-ray photoelectron spectroscopy (XPS) is a surface sensitive technique, which irradiates the sample surface with a beam of X-rays. These X-rays have known wavelength corresponding to a known photon energy. This photon energy allows for measuring the top 10-12 nm of the surface. High-speed atomic force microscopy (HS-AFM) maps the sample topography with nanometre lateral and sub-atomic height resolution over mm-sized areas. This technique can be used to observe nm- and mm-scale processes with millisecond temporal resolution. Applying these two techniques could answer the following open research questions:

1. Can we see a microtopography on our weathered SG fracture surface samples?
2. How does the elemental composition of the surfaces look like?
3. Are fracture surfaces coated?
4. How does coating affect weathering, i.e. the dissolution of fracture surfaces?

Nugent et al. (1998) showed a patchy coating of particles ranging from nm to mm in size and from 5mm to 1µm in thickness. Mineral coatings can be largely undetected under SEM, but visible under AFM. They do not only alter the surface chemistry but may also partially inhibit *in situ* dissolution, which includes microbial weathering activity.

Open fractures within the subsurface of our four Deep EarthShape field sites PdA, SG, LC and NA are fluid pathways. Hence, they are potent locations of quantifying geogenic gases linked to volcanic activity such as CO_2, H_2 and CH_4. Gas flow rates could be quantified with measuring sensors installed in regular intervals (e.g. 5 m) throughout the weathering profiles and would be a valuable addition to our data sets to assess which energy sources are available for microbial weathering activity.

The obtainment of our Fe(III)-reducing enrichment culture SG is proof for its *in situ* existence but does not provide information on its *in situ* activity in weathering of Fe(II)-bearing minerals. Hence, it would be interesting to carry out *in situ* Fe(III) reduction experiments. In a first experiment, Fhy mineral bags could be placed within the borehole at the depth from which culture SG was obtained. Fe(III) reduction rates could then be monitored in a sacrificial setup by sampling these bags to quantify Fe(III) reduction over time. In follow up experiments, the same setup could be repeated with goethite, hematite and magnetite to obtain a systematic overview about different Fe minerals. *In situ* Fe(III) reduction rates could then be compared with Fe(III) reduction rates predicted with thermodynamics to evaluate, whether our fluid concentration assumptions (**Chapter 2**) were correct.

4.6 References

Amend J.P., Aronson H.S., Macalady J. and LaRowe D.E. (2019) Another chemolithotrophic metabolism missing in nature—sulfur comproportionation. *bioRxiv*, 820597. https://doi.org/10.1101/820597.

Amend J.P. and Shock E.L. (2001) Energetics of overall metabolic reactions of thermophilic and hyperthermophilic Archaea and Bacteria. *FEMS microbiology reviews* **25**(2), 175-243.

Banwart S.A., Nikolaidis N.P., Zhu Y.-G., Peacock C.L. and Sparks D.L. (2019) Soil Functions: Connecting Earth's Critical Zone. *Annual Review of Earth and Planetary Sciences* **47**, 333-359.

Bethencourt L., Bochet O., Farasin J., Aquilina L., Borgne T.L., Quaiser A., Biget M., Michon-Coudouel S., Labasque T. and Dufresne A. (2020) Genome reconstruction reveals distinct assemblages of Gallionellaceae in surface and subsurface redox transition zones. *FEMS Microbiology Ecology*. https://doi.org/10.1093/femsec/fiaa036.

Bochet O., Bethencourt L., Dufresne A., Farasin J., Pédrot M., Labasque T., Chatton E., Lavenant N., Petton C., Abbott B.W., Aquilina L. and Le Borgne T. (2020) Iron-oxidizer hotspots formed by intermittent oxic–anoxic fluid mixing in fractured rocks. *Nature Geoscience*. https://doi.org/10.1038/s41561-019-0509-1.

Brantley S.L., Holleran M.E., Jin L. and Bazilevskaya E. (2013) Probing deep weathering in the Shale Hills Critical Zone Observatory, Pennsylvania (USA): the hypothesis of nested chemical reaction fronts in the subsurface. *Earth Surface Processes and Landforms* **38**(11), 1280-1298.

Brantley S.L., Lebedeva M. and Hausrath E.M. (2012) A geobiological view of weathering and erosion. *Fundamentals of geobiology*, 205-227.

Buss H., Bruns M., Schultz M., Moore J., Mathur C. and Brantley S. (2005) The coupling of biological iron cycling and mineral weathering during saprolite formation, Luquillo Mountains, Puerto Rico. *Geobiology* **3**(4), 247-260.

Deng K., Yang S. and Guo Y. (2022) A global temperature control of silicate weathering intensity. *Nature Communications* **13**(1), 1781. https://doi.org/10.1038/s41467-022-29415-0.

Ehrlich H.L., Newman D.K. and Kappler A. (2015) *Ehrlich's Geomicrobiology*, 6th Edition edn.: CRC Press.

Fan Q., Wang L., Fu Y., Li Q., Liu Y., Wang Z. and Zhu H. (2023) Iron redox cycling in layered clay minerals and its impact on contaminant dynamics: A review. *Science of The Total Environment* **855**, 159003. https://doi.org/https://doi.org/10.1016/j.scitotenv.2022.159003.

Fredrickson J.K. and Balkwill D.L. (2006) Geomicrobial Processes and Biodiversity in the Deep Terrestrial Subsurface. *Geomicrobiology Journal* **23**(6), 345-356. https://doi.org/10.1080/01490450600875571.

Frey B., Rieder S.R., Brunner I., Plötze M., Koetzsch S., Lapanje A., Brandl H. and Furrer G. (2010) Weathering-associated bacteria from the Damma glacier forefield: physiological capabilities and impact on granite dissolution. *Applied and Environmental Microbiology* **76**(14), 4788-4796.

Gamboa C., Godfrey L., Urrutia J., Herrera C., Lu X. and Jordan T. (2022) Conditions of groundwater recharge in the hyperarid southern Atacama Desert. *Global and Planetary Change* **217**, 103931. https://doi.org/https://doi.org/10.1016/j.gloplacha.2022.103931.

Gaviria-Lugo N., Läuchli C., Wittmann H., Bernhardt A., Frings P., Mohtadi M., Rach O. and Sachse D. (2023) Climatic controls on leaf wax hydrogen isotope ratios in terrestrial and marine sediments along a hyperarid-to-humid gradient. *Biogeosciences* **20**(21), 4433-4453.

Gu X., Heaney P.J., Reis F.D.A. and Brantley S.L. (2020) Deep abiotic weathering of pyrite. *Science* **370**(6515), eabb8092.

Hampl F.J., Schiperski F., Byrne J.M., Schwerdhelm C., Kappler A., Bryce C., von Blanckenburg F. and Neumann T. (2022) The role of iron-bearing minerals for the deep weathering of a hydrothermally altered plutonic rock in semi-arid climate (Chilean

Coastal Cordillera). *Chemical Geology* **604,** 120922. https://doi.org/https://doi.org/10.1016/j.chemgeo.2022.120922.

Hampl F.J., Schiperski F., Schwerdhelm C., Stroncik N., Bryce C., von Blanckenburg F. and Neumann T. (2023) Feedbacks between the formation of secondary minerals and the infiltration of fluids into the regolith of granitic rocks in different climatic zones (Chilean Coastal Cordillera). *Earth Surf. Dynam.* **11**(3)**,** 511-528. https://doi.org/10.5194/esurf-11-511-2023.

Herrera C., Gamboa C., Custodio E., Jordan T., Godfrey L., Jódar J., Luque J.A., Vargas J. and Sáez A. (2018) Groundwater origin and recharge in the hyperarid Cordillera de la Costa, Atacama Desert, northern Chile. *Science of The Total Environment* **624,** 114-132.

Houston J. (2002) Groundwater recharge through an alluvial fan in the Atacama Desert, northern Chile: mechanisms, magnitudes and causes. *Hydrological Processes* **16**(15)**,** 3019-3035. https://doi.org/https://doi.org/10.1002/hyp.1086.

Huang Y.-M., Jakus N., Straub D., Konstantinidis K.T., Blackwell N., Kappler A. and Kleindienst S. (2022) 'Candidatus ferrigenium straubiae' sp. nov., 'Candidatus ferrigenium bremense' sp. nov., 'Candidatus ferrigenium altingense' sp. nov., are autotrophic Fe(II)-oxidizing bacteria of the family Gallionellaceae. *Systematic and Applied Microbiology* **45**(3)**,** 126306. https://doi.org/https://doi.org/10.1016/j.syapm.2022.126306.

Jakus N., Blackwell N., Osenbrück K., Straub D., Byrne J.M., Wang Z., Glöckler D., Elsner M., Lueders T., Grathwohl P., Kleindienst S. and Kappler A. (2021a) Nitrate Removal by a Novel Lithoautotrophic Nitrate-Reducing, Iron(II)-Oxidizing Culture Enriched from a Pyrite-Rich Limestone Aquifer. *Applied and Environmental Microbiology* **87**(16)**,** e00460-00421. https://doi.org/doi:10.1128/AEM.00460-21.

Jakus N., Blackwell N., Straub D., Kappler A. and Kleindienst S. (2021b) Presence of Fe(II) and nitrate shapes aquifer-originating communities leading to an autotrophic enrichment dominated by an Fe(II)-oxidizing Gallionellaceae sp. *FEMS Microbiology Ecology* **97**(11). https://doi.org/10.1093/femsec/fiab145.

Johnson D.B. and McGinness S. (1991) Ferric Iron Reduction by Acidophilic Heterotrophic Bacteria. *Applied and Environmental Microbiology* **57**(1)**,** 207-211. https://doi.org/doi:10.1128/aem.57.1.207-211.1991.

Kappler A., Schink B. and Newman D.K. (2005) Fe(III) mineral formation and cell encrustation by the nitrate-dependent Fe(II)-oxidizer strain BoFeN1. *Geobiology* **3**(4)**,** 235-245. https://doi.org/https://doi.org/10.1111/j.1472-4669.2006.00056.x.

Klueglein N. and Kappler A. (2013) Abiotic oxidation of Fe (II) by reactive nitrogen species in cultures of the nitrate-reducing Fe (II) oxidizer A cidovorax sp. BoFeN1–questioning the existence of enzymatic Fe (II) oxidation. *Geobiology* **11**(2)**,** 180-190.

Krone L.V., Hampl F.J., Schwerdhelm C., Bryce C., Ganzert L., Kitte A., Übernickel K., Dielforder A., Aldaz S., Oses-Pedraza R., Perez J.P.H., Sanchez-Alfaro P., Wagner D., Weckmann U. and von Blanckenburg F. (2021b) Deep weathering in the semi-arid Coastal Cordillera, Chile. *Scientific Reports* **11**(1)**,** 13057. https://doi.org/10.1038/s41598-021-90267-7.

LaRowe D. and Amend J. (2019) Energy Limits for Life in the Subsurface. In Orcutt B.N., Daniel I. and Dasgupta R. (eds.), *Deep Carbon: Past to Present.* Cambridge: Cambridge University Press, 585-619.

Lehman R.M., Roberto F.F., Earley D., Bruhn D.F., Brink S.E., O'Connell S.P., Delwiche M.E. and Colwell F.S. (2001) Attached and unattached bacterial communities in a 120-meter corehole in an acidic, crystalline rock aquifer. *Applied and Environmental Microbiology* **67**(5)**,** 2095-2106.

Melton E.D., Swanner E.D., Behrens S., Schmidt C. and Kappler A. (2014) The interplay of microbially mediated and abiotic reactions in the biogeochemical Fe cycle. *Nature Reviews Microbiology* **12**(12)**,** 797.

Minyard M.L., Bruns M.A., Liermann L.J., Buss H.L. and Brantley S.L. (2012) Bacterial associations with weathering minerals at the regolith-bedrock interface, Luquillo Experimental Forest, Puerto Rico. *Geomicrobiology Journal* **29**(9)**,** 792-803.

Moser D.P., Onstott T.C., Fredrickson J.K., Brockman F.J., Balkwill D.L., Drake G.R., Pfiffner S.M., White D.C., Takai K., Pratt L.M., Fong J., Lollar B.S., Slater G., Phelps T.J., Spoelstra N., Deflaun M., Southam G., Welty A.T., Baker B.J. and Hoek J. (2003) Temporal Shifts in the Geochemistry and Microbial Community Structure of an Ultradeep Mine Borehole Following Isolation. *Geomicrobiology Journal* **20**(6)**,** 517-548. https://doi.org/10.1080/713851170.

Napieralski S.A., Buss H.L., Brantley S.L., Lee S., Xu H. and Roden E.E. (2019) Microbial chemolithotrophy mediates oxidative weathering of granitic bedrock. *Proceedings of the National Academy of Sciences* **116**(52)**,** 26394-26401.

Napieralski S.A. and Roden E.E. (2020) The weathering microbiome of an outcropping granodiorite. *Frontiers in Microbiology* **11,** 601907.

Nugent M.A., Brantley S.L., Pantano C.G. and Maurice P.A. (1998) The influence of natural mineral coatings on feldspar weathering. *Nature* **395**(6702)**,** 588-591. https://doi.org/10.1038/26951.

Oeser R.A., Stroncik N., Moskwa L.-M., Bernhard N., Schaller M., Canessa R., van den Brink L., Köster M., Brucker E. and Stock S. (2018) Chemistry and microbiology of the Critical Zone along a steep climate and vegetation gradient in the Chilean Coastal Cordillera. *Catena* **170,** 183-203.

Onstott T.C., Ehlmann B.L., Sapers H., Coleman M., Ivarsson M., Marlow J.J., Neubeck A. and Niles P. (2019) Paleo-rock-hosted life on Earth and the search on Mars: a review and strategy for exploration. *Astrobiology* **19**(10)**,** 1230-1262.

Osburn M.R., LaRowe D.E., Momper L.M. and Amend J.P. (2014) Chemolithotrophy in the continental deep subsurface: Sanford Underground Research Facility (SURF), USA. *Frontiers in Microbiology* **5**(610). https://doi.org/10.3389/fmicb.2014.00610.

Perez J.R., Banwart S.A. and Puigdomenech I. (2005) The kinetics of O2 (aq) reduction by structural ferrous iron in naturally occurring ferrous silicate minerals. *Applied Geochemistry* **20**(11)**,** 2003-2016.

Sauter L., Schwerdhelm C., Samuels T., Bayer T., Witzgall K., Hampl F.J., Müller C.W., Riveras-Muñoz N., Scholten T., Wagner D., Merino C., Matus F., Neumann T., Kappler A. and Bryce C. (in prep.) Microbial iron(III) reduction in soils along a precipitation gradient on the Chilean Coastal Cordillera.

Schwerdhelm C., Hampl F.J., Keldenich S., Grimm L., Schädler F., Shuster J., Bayer T., Joshi P., Neumann T., Kappler A. and Bryce C. (in prep.) Microbial oxidation of structural Fe(II) in biotite and chlorite.

Schwerdhelm C., Hampl F.J., Krone L.V., Sauter L., Kaphegyi K., Horstmann L., Straub D., Samuels T., Mansor M., Merino C., Matus F., v. Blanckenburg F., Wagner D., Neumann T., Kappler A. and Bryce C. (2025) Microbial weathering of iron-bearing minerals in deep hydrothermally altered granitic rock of a semi-arid environment (Chilean Coastal Cordillera). *Geo-Bio Interfaces* **2,** e8. https://doi.org/10.1180/gbi.2025.2.

Shelobolina E., Xu H., Konishi H., Kukkadapu R., Wu T., Blöthe M. and Roden E. (2012) Microbial Lithotrophic Oxidation of Structural Fe(II) in Biotite. *Applied and Environmental Microbiology* **78**(16)**,** 5746-5752. https://doi.org/10.1128/aem.01034-12.

Straub K.L., Benz M., Schink B. and Widdel F. (1996) Anaerobic, nitrate-dependent microbial oxidation of ferrous iron. *Applied and Environmental Microbiology* **62**(4)**,** 1458-1460. https://doi.org/doi:10.1128/aem.62.4.1458-1460.1996.

Stroncik N.A., Krone L.V., Pierdominici S., Kummerow J., Blukis R. and von Blanckenburg F. (in prep.) Geochemical, mineralogical, and petrophysical characteristics of DeepEarthshape drill cores from the Chilean Coastal Cordillera. *GFZ Data Services*.

Takamiya H., Kouduka M. and Suzuki Y. (2021) The deep rocky biosphere: new geomicrobiological insights and prospects. *Frontiers in Microbiology* **12,** 785743.

Tebo B.M., Davis R.E., Anitori R.P., Connell L.B., Schiffman P. and Staudigel H. (2015) Microbial communities in dark oligotrophic volcanic ice cave ecosystems of Mt. Erebus, Antarctica. *Frontiers in Microbiology* **6,** 179.

Tian R., Schwerdhelm C., Samuels T., Kappler A. and Bryce C. (in prep.) Change in microbial bioavailability of iron across a climatic gradient.

Trichandi R., Bauer K., Ryberg T., Scherler D., Bataille K. and Krawczyk C.M. (2022) Combined seismic and borehole investigation of the deep granite weathering structure—Santa Gracia Reserve case in Chile. *Earth Surface Processes and Landforms* **n/a**(n/a). https://doi.org/https://doi.org/10.1002/esp.5457.

Trichandi R., Bauer K., Ryberg T., Wawerzinek B., Araya Vargas J., von Blanckenburg F. and Krawczyk C.M. (2023) Shear-wave velocity imaging of weathered granite in La Campana (Chile) from Bayesian inversion of micro-tremor H/V spectral ratios. *Journal of Applied Geophysics* **217,** 105191. https://doi.org/https://doi.org/10.1016/j.jappgeo.2023.105191.

Übernickel K., Ehlers T.A., Ershadi M.R., Paulino L., Fuentes Espoz J.-P., Maldonado A., Oses-Pedraza R. and von Blanckenburg F. (2020) Time series of meteorological station data in the EarthShape study areas in the Coastal Cordillera, Chile.

Weckmann U., Bauer K., Krawczyk C., Kück J., Übernickel K. and von Blanckenburg F. (2020) Geophysical borehole logging data from Santa Gracia, Chile.

White A.F. and Yee A. (1985) Aqueous oxidation-reduction kinetics associated with coupled electron-cation transfer from iron-containing silicates at 25 C. *Geochimica et Cosmochimica Acta* **49**(5)**,** 1263-1275.

Statement of personal contribution

The work presented in this dissertation was funded by the German Research Foundation (DFG, Deutsche Forschungsgesellschaft) priority research program SPP 1803 “EarthShape: Earth Surface Shaping by Biota” (project no. 255469939, grant no. BR 5927/2-1, KA 1736/54-1) and the EarthShape coordination (grant no. EH 329/17-2, BL 562/20-1). The conceptual background of this PhD project was designed by Dr. Casey Bryce, Prof. Andreas Kappler and Prof. Thomas Neumann in cooperation with our Chilean research partners Dr. Carolina Merino and Dr. Francisco Matus. Dr. Casey Bryce was the first supervisor and Prof. Dr. Andreas Kappler the second supervisor throughout this PhD. Dr. Muammar Mansor co-supervised me during parts of my PhD and was involved in general discussion, thermodynamic calculations and discussion of results. Dr. Toby Samuels co-supervised me, too, and was involved in the design and discussion of statistical analyses, discussion of results and co-supervision of M.Sc. students. Unless stated otherwise, the experiments were conceptualised by me, Dr. Casey Bryce and Prof. Andreas Kappler and performed by myself. Data analysis, interpretation and discussion as well as manuscript writing were done my myself together with Dr. Casey Bryce and Prof. Andreas Kappler. The contributions of people to fieldwork and single chapters is listed in detail below.

Field work: This PhD project was part of the Deep EarthShape consortium, a collaboration of four projects. The coordinative organisation of field work, i.e. preparation and conduction of four drilling campaigns in Chile, was done by project coordinator Dr. Kirstin Übernickel and Prof. Friedhelm von Blanckenburg in cooperation with our Chilean partners Dixie Rivera, Dr. Ròmulo Oses, Dr. Carolina Merino, Dr. Francisco Matus, and Dr. Oscar Seguel. Access to the field sites during field excursions prior to the drilling campaigns was provided by the national park service of Chile (CONAF). The fieldwork of my own project was planned by me, Dr. Casey Bryce and Prof. Andreas Kappler. Field work sampling was prepared by me, Lea Sauter and Dr. Casey Bryce. Retrieving of drill core samples was conducted by the Chilean drilling company ARAOS. Sampling of geomicrobiological samples during fieldwork was done by me, Dr. Ferdinand Hampl, Dr. Laura Krone, Lea Sauter, Dr. Lars Ganzert, Prof. Friedhelm von Blanckenburg, Dr. Casey Brye and Chilean students of Dr. Carolina Merino and Dr. Francisco Matus. Axel Kitte and Oliver Burckhardt took contamination control samples during the drilling campaigns.

Chapter 2: The original hypothesis was formulated by Dr. Casey Bryce, Prof. Andreas Kappler and Prof. Thomas Neumann. Resources were provided by Dr. Casey Bryce and Prof. Andreas Kappler. Me and Dr. Casey Bryce designed the project together with input of Prof. Andreas Kappler and Dr. Muammar Mansor and Dr. Toby Samuels. Dixie Rivera, Dr. Kirstin Übernickel,

Dr. Lars Ganzert, Axel Kitte, Dr. Ròmulo Oses, Dr. Laura Krone, Dr. Ferdinand Hampl, Dr. Casey Bryce and Prof. Friedhelm von Blanckenburg supported the project during the drilling campaign. I conducted the analysis in the laboratory with assistance of Lea Sauter and Kari Kaphegyi. Dr. Hanna Grimm performed DOC measurements. Franziska Schädler performed FIA measurements and helped with the molecular microbiology sample preparation. Dr. D. Straub and Dr. L. Horstmann performed the molecular microbiological analyses. Dr. Natalia Jakus performed µXRD measurements. Dr. Ferdinand Hampl helped with the µXRD data analysis and visualisation and provided mineralogical data. Dr. Eric Runge performed Raman spectroscopy measurements. Dr. Laura Krone provided geochemical data. Dr. Toby Samuels and I did the statistical data analysis. I wrote the manuscript. All co-authors contributed to the manuscript revisions and/or wrote parts of the manuscript.

Chapter 3: The original hypothesis was formulated by Dr. Casey Bryce, Prof. Andreas Kappler and Prof. Thomas Neumann. Resources were provided by Dr. Casey Bryce, Prof. Andreas Kappler and Dr. Daniel Buchner. Me, Dr. Casey Bryce and Prof. Andreas Kappler designed the project with input from Dr. Toby Samuels. Drill core samples were processed/provided by me, Dr. Ferdinand Hampl, Dr. Laura Krone and Dr. Lukas Horstmann. I conducted the Fe analysis in the laboratory with assistance of Kari Kaphegyi. Bernice Nisch performed carbon quantification measurements. Dr. Nicole Stroncik obtained fracture data. Dr. Nicole Stroncik, Dr. Laura Krone and Prof. Friedhelm von Blanckenburg provided fracture data. I did the fracture data analysis. Dr. Toby Samuels and I did the statistical data analysis. I wrote the manuscript. Dr. Casey Bryce and Prof. Andreas Kappler contributed to the manuscript revisions and/or wrote parts of the manuscript.

I hereby state that I have neither plagiarised nor copied any of the text. Chapter 2 has been published in Geo-Bio Interfaces (Schwerdhelm et al., 2025). Chapter 3 will be submitted to a scientific journal and might be published in a modified version elsewhere in the future. Schwerdhelm et al. (in prep.) (Chapter 4.4) has to be written still, and will be submitted to a scientific journal.

Publications and conference contributions

Paper and data publications

2025	**Schwerdhelm, C.**, Hampl, F. J., Krone, L. V., Sauter, L., Kaphegyi, K., Horstmann, L., … Bryce, C. (2025). Microbial weathering of iron-bearing minerals in deep hydrothermally altered granitic rock of a semi-arid environment (Chilean Coastal Cordillera). Geo-Bio Interfaces, 2, e8. https://doi.org/10.1180/gbi.2025.2
2025	**Schwerdhelm, C.**, Hampl, F. J., Krone, L. V., Sauter, L., Kaphegyi, K., Horstmann, L., … Bryce, C. (2025)**:** Mineralogical, geochemical, microbiological and thermodynamic data from a deep hydrothermally altered profile of a semi-arid environment (Chilean Coastal Cordillera). GFZ Data Services. https://doi.org/10.5880/fidgeo.2024.027
2023	Hampl, F. J., Schiperski, F., **Schwerdhelm, C.**, Stroncik, N., Bryce, C., von Blanckenburg, F., and Neumann, T. (2023). Feedbacks between the formation of secondary minerals and the infiltration of fluids into the regolith of granitic rocks in different climatic zones (Chilean Coastal Cordillera), Earth Surf. Dynam., 11, 511–528, 2023. https://doi.org/10.5194/esurf-11-511-2023
2023	Hampl, F. J.; Schiperski, F.; **Schwerdhelm, C.**; Stroncik, N.; Bryce, C.; von Blanckenburg, F.; Neumann, T. (2022): Mineralogical and geochemical data of two weathering profiles in a Mediterranean and a humid climate region of the Chilean Coastal Cordillera. GFZ Data Services. https://doi.org/10.5880/fidgeo.2022.035
2022	Hampl, F. J., Schiperski, F., Byrne, J. M., **Schwerdhelm, C.**, Kappler, A., Bryce, C., ... & Neumann, T. (2022). The role of iron-bearing minerals for the deep weathering of a hydrothermally altered plutonic rock in semi-arid climate (Chilean Coastal Cordillera). *Chemical Geology*, *604*, 120922. https://doi.org/10.1016/j.chemgeo.2022.120922
2021	Hampl, F. J.; Schiperski, F.; Byrne, J. M.; **Schwerdhelm, C.**; Kappler, A.; Bryce, C.; ... & Neumann, T. (2021): Mineralogical, geochemical and magnetic susceptibility data from a deep hydrothermally altered profile in a semi-arid region (Chilean Coastal Cordillera). GFZ Data Services. https://doi.org/10.5880/fidgeo.2021.037
2021	Krone, L. V., Hampl, F. J., **Schwerdhelm, C.**, Bryce, C., Ganzert, L., Kitte, A., ... & von Blanckenburg, F. (2021). Deep weathering in the semi-arid Coastal Cordillera, Chile. *Scientific Reports*, *11*(1), 1-15. https://doi.org/10.1038/s41598-021-90267-7
2021	Krone, L. V., Hampl, F. J., **Schwerdhelm, C.**, Bryce, C., Ganzert, L., Kitte, A., ... & von Blanckenburg, F. (2021): Physical and geochemical data on a drill core from the semi-arid Coastal Cordillera, Chile. GFZ Data Services. https://doi.org/10.5880/GFZ.3.3.2021.002

Conference contributions

2023	Biosignatures workshop (University of Tübingen) - poster presentation: Schwerdhelm et al. (2023). Evidence for microbial mineral weathering in deep biosphere of semi-arid environments. *Tübingen• 27-28 March*.
2022	Final EarthShape meeting & DFG review (Austria) - poster presentation: Deep EarthShape: Geomicrobiology - Iron-metabolizing bacteria as driving force in weathering of silicate minerals. *Obergurgl• 17-22 September*.
2022	**Schwerdhelm, C.**, Hampl, F. J., Sauter, L., Mansor, M., Merino, C., Matus, F. J., von Blanckenburg, F. Neumann, T. Kappler, A. and Bryce, C., 2022. Evidence for microbial mineral weathering in semi-arid environments. GES12, Zurich, 24-29 July, poster presentation. https://doi.org/10.5281/zenodo.6829020
2022	Hampl, F. J., Schiperski, F., **Schwerdhelm, C.**, Stroncik, N., von Blanckenburg, F. and Neumann, T., 2022. Weathering-intensifying and -mitigating processes in granitic rock along a climate gradient of the Chilean Coastal Cordillera. Goldschmidt 2022, online oral presentation. https://doi.org/10.46427/gold2022.12029
2022	Krone, L., Hampl, F. J., **Schwerdhelm, C.**, Bryce, C., Ganzert, L., Kitte, A., Übernickel, K., Dielforder, A., Aldaz, S., Oses-Pedraza, R., Perez, J. P. H., Sanchez-Alfaro, P., Wagner, D., Weckmann, U., and von Blanckenburg, F., 2022. Deep weathering in the semi-arid Coastal Cordillera, Chile. EGU General Assembly 2022, Vienna, Austria, 23-27 May 2022, EGU22-8025, oral presentation. https://doi.org/10.5194/egusphere-egu22-8025
2021	**Schwerdhelm, C.**, Hampl, F., Sauter, L., Merino, C., Matus, F., von Blanckenburg, F., Neumann, T., Kappler, A. and Bryce, C., 2021. Deep Weathering of Subsurface Fe-Bearing Minerals by Fe-Metabolizing Microorganisms in a Semi-Arid Climate. Goldschmidt 2021, online oral presentation. https://doi.org/10.7185/gold2021.6102
2021	Sauter, L., **Schwerdhelm, C.**, Samuels, T., Witzgall, K., Hampl, F., Mueller, C. W., Riveras, N.-A., Scholten, T., Wagner, D., Merino, C., Matus, F., Neumann, T., Kappler, A. and Bryce C., 2021. Changes in the Bioavailability of iron(III) for Microbial Reduction along a Precipitation Gradient. Goldschmidt 2021, online oral presentation. https://doi.org/10.7185/gold2021.6053
2020	**Schwerdhelm, C.**, Hampl, F., Merino, C., Matus, F., Neumann, T., Kappler, A. and Bryce, C., 2020. Could Fe-metabolizing microbes weather sub-surface minerals in a semi-arid climate? EGU General Assembly 2020, 4-8 May 2020, EGU2020-6037, online oral presentation. https://doi.org/10.5194/egusphere-egu2020-6037